C-O-N-F-I-D-E-N-T-I-A-L [redacted] SEE BOTTOM OF PAGE FOR SPECIAL CONTROLS, IF ANY

INFORMATION REPORT

PREPARED AND DISSEMINATED BY
CENTRAL INTELLIGENCE AGENCY

25X1

COUNTRY
USSR

SUBJECT
Soviet Metallurgical Research and Experiments

DATE DISTRIBUTED
6 Jan 58

25X1

NO. OF PAGES
1

NO. OF ENCLS.

SUPPLEMENT TO REPORT #

25X1

25X1

25X1

THIS IS UNEVALUATED INFORMATION

This report was obtained by the Department of the Air Force, and is disseminated by CIA in accordance with paragraph 3.d of NSCID #7.

25X1

USAF review completed.

Folder 1

C-O-N-F-I-D-E-N-T-I-A-L

DISTRIBUTION	STATE	ARMY	NAVY	AIR

NOFORN NO DISSEM ABROAD LIMITED

LIMITED: Dissemination limited to full-time employees of CIA, AEC and FBI; and, within State and Defense, to the intelligence components, other offices producing NIS elements, and higher echlons with their immediate supporting staffs. Not to be disseminated to consultants, external projects or reserve personnel on short term active duty (excepting individuals who are normally full-time employees of CIA, AEC, FBI, State or Defense) unless the written permission of the originating office has been obtained through the Assistant Director for Central Reference, CIA.

Batelle # 1-10-49

C-O-N-F-I-D-E-N-T-I-A-L | SEE BOTTOM OF PAGE FOR SPECIAL CONTROLS, IF ANY

INFORMATION REPORT

PREPARED AND DISSEMINATED BY
CENTRAL INTELLIGENCE AGENCY

25X1

COUNTRY
USSR

SUBJECT
Soviet Metallurgical Research and Experiments

DATE DISTRIBUTED
25X1

NO. OF PAGES
1

NO. OF ENCLS.
25X1

SUPPLEMENT TO REPORT #

25X1

25X1

THIS IS UNEVALUATED INFORMATION

This report was obtained by the Department of the Air Force, and is disseminated by CIA in accordance with paragraph 3.d of HMCID #7.

25X1

C-O-N-F-I-D-E-N-T-I-A-L

DISTRIBUTION	STATE	ARMY	NAVY	AIR

NOFORN | NO DISSEM ABROAD | LIMITED

LIMITED: Dissemination limited to full-time employees of CIA, AEC and FBI; and, within State and Defense, to the intelligence components, other offices producing NIS elements, and higher echlons with their immediate supporting staffs. Not to be disseminated to consultants, external projects or reserve personnel on short term active duty (excepting individuals who are normally full-time employees of CIA, AEC, FBI, State or Defense) unless the written permission of the originating office has been obtained through the Assistant Director for Central Reference, CIA.

25X1

Next 61 Page(s) In Document Denied

APPENDIX 2

A New Method of Investigation of the Chemical Composition in the Micro Volume of An Alloy

By I. B. Borovskii and N. P. Ilyin

(From ACADEMY OF SCIENCES USSR REPORTS 106, (4) 655-657 (1956))

The development of the theory of solids as well as practical problems for producing alloys with special properties require the development of special investigation methods as well as analysis of the atomic and electronic structure and of the micro composition of metals, alloys, compounds. The existing physical methods of investigation were directed in the majority to the study of atomic and electronic structures of solids.

In 1951, a new method was suggested by one of the authors (1) in the USSR and simultaneously in France (2), consisting in an X-ray-spectral quantitative analysis of the composition at a "point" which permits to carry out quantitative determination of the majority of elements of the Mendeleev periodic system in the region of the size of a few microns.

In the following, we developed an apparatus and the method of investigation permitting determination of the chemical composition in the micro volume of the sample based on the characteristic X-ray radiation, excited by a focused electron beam in a volume of $10\mu^3$ with the sensitivity of .1%. The developed method gives a possibility of determining the content of various elements at a given spot of the sample, as well as the distribution of a given element in various parts of the sample.

For analyzing the composition at the "point", one of the procedures of the regular X-ray spectroscopy is used (3). A schematic presentation of the arrangement worked out by us is shown in Figure 1. The electron beam (Э. П. = electronic "cannon" or tube) is focused by one or two electromagnetic lenses Л on the polished anode of the X-ray tube A, which is arranged on a special plate serving as a holder for the samples. By means of microscrews the anode can be moved horizontally; a motor with a reducing gear is attached to one of the handles permitting a continuous motion of the anode-sample in the chosen direction at a speed of 10 to 20 μ/minute keeping it under the electron beam. The holder is arranged to carry simultaneously 3 samples, a fluorescent screen and a frame with a net for control pictures of the focus size. The following items are mounted into the X-ray tube: A small mirror З and a metallographic microscope M of special construction with a long focus lens; the microscope itself is arranged outside the vacuum. Its rigid mounting ensures superposition of the objective cross hair with the mirror image of the focal spot on the sample-anode. For measuring the electron current passing the tube, a Faraday cylinder is used, which is connected to constant current amplifier. For resolving the X-ray into a spectrum, a spectrograph with a bent crystal was constructed using the reflection

method. The rigid crystal is bent along a cylindrical surface with the radius of 300mm. 2 movable arms of the spectrograph which are connected with each other, carry the microfocus tube and the photon counter. The kinematic and vacuum arrangement permit simultaneous moving of the 2 arms toward each other along equal angles. The turning is achieved by hand or by means of a motor with a reducing and reverse gear.

All leading devices from the low voltage as well as high voltage side, are stabilized, the stabilization percent being not lower than .05%. High voltage for the tube can be changed from 30 to 50 kilowatt. The electron current within the tube reaches 1 μ ampere. The diameter of the focal point on the anode is 2-4 μ (determined by the method of the shadow image of the wire mesh having 5 μ diameter). The average specific charge of the sample anode equals 1 kilowatt/mm^2.

For recording intensities of characteristic lines the block appratus URS-50-I is used, permitting determination of the intensities by direct or conversion method, or by recording the spectrum on self-registering electronic potentiometer. Varying speeds of the sample motion and of the chart permit to vary widely the "enlargement" of the observed recording of the element distribution in the sample. Maximum "enlargement" is 2.10^4.

At optimum conditions the intensity of the line K_α, of a pure element is 10^4-10^5 pulses per second. Therefore, at higher contents of the element to be determined at a given spot of the sample it is necessary to work with smaller specific charges (weaker currents through the tube). The accuracy of this analysis, determined by the stability of leading devices and recording arrangement, when checked experimentally was found to be 2-5%.

In Figure 2 a point spectrogram of a multi-component alloy is shown illustrating the work of the invented apparatus.

In Figure 3 results of a "point" analysis of another multicomponent alloy are shown. Curve A shows the intensity changesof the line Ni $K_{\alpha 1}$ (RC = 4 seconds, the scale 1000 pulses per second) by moving the sample under an electron beam. Curve B - shows the intensity changes of the line tungsten $L_{\alpha 1}$ (RC=2 seconds, scale 200 pulses/second) in the same area of the sample. Comparing these results with a microphotograph of the sample, it is possible to draw conclusions, that the inclusions observed in the sample represent a phase enriched in W and with a decreased content of the Ni base.

Thus, the apparatus and method worked out permit not only a quantitative analysis of the composition at the "point" with an accuracy of .1% (which corresponds to 10^{-13}g of the element at the "point"), but also the distribution of the given element within the sample. Investigations were carried out with a series of multicomponent alloys of metals and of metal-ceramics, welds, diffusion layers, to determine distribution of elements Fe, Ni, Cu, Zn, Nv, Ms, W, Re in micro

samples and in given directions. Results of these investigations have shown large possibilities of this new method for solving problems which cannot be solved by other existing methods of physico-chemical analysis.

Bibliography:

1. I.B.Borovskii, Collective volume. "Problems in Metallurgy", dedicated to Acad. I.P.Bardin on his 70th birthday. Publisher Acad. Sciences USSR,1953.
2. R.Castaing, A.Guinier, Anal.Chem. 25,#5 724 (1953).
3. I.B.Borovskii, M.A.Blokhin, X-Ray Spectral Analysis, (1939).

Appendix 2

тонов. Кинематическое и вакуумное устройство позволяет перемещать плечи одновременно на равные углы навстречу друг другу. Вращение осуществляется вручную или мотором с редуктором и реверсом.

Все питающие устройства как с низковольтной, так и с высоковольтной стороны стабилизированы, процент стабилизации не ниже 0,05%. Высокое

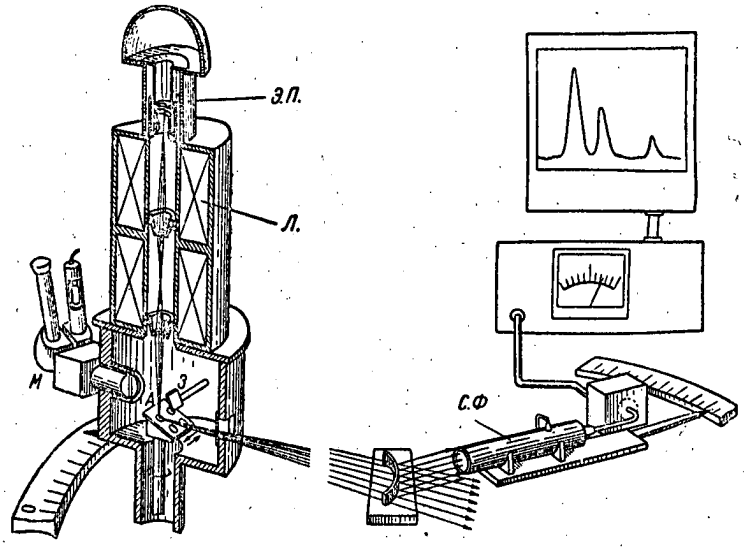

Рис. 1

напряжение, подаваемое на трубку, может меняться от 30 до 50 кв. Электронный ток через трубку достигает 1 μа. Диаметр фокального пятна на аноде составляет 2—4 μ (по определениям методом теневой съемки сетки

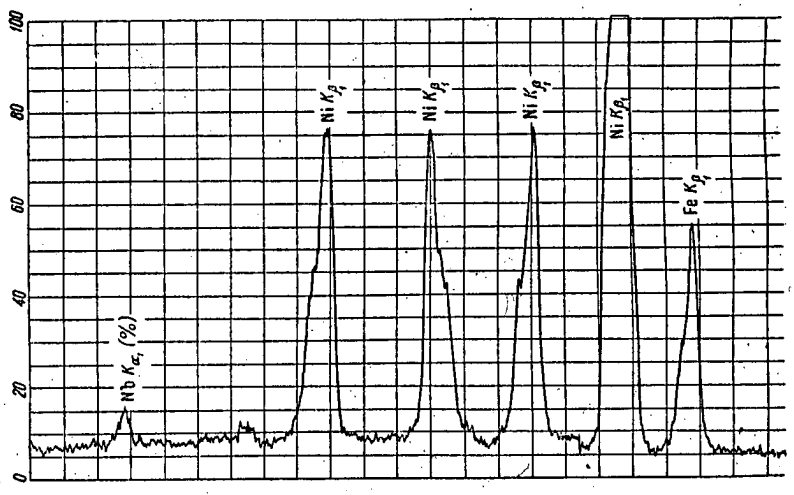

Рис. 2

из проволоки диаметром 5 μ). Удельная нагрузка на шлифе-аноде в среднем равна 1 квт/мм².

Для регистрации интенсивности характеристических линий использован блок аппарата УРС-50-И, позволяющий определять интенсивность по пересчетному или по прямопоказывающему прибору, а также записывать спектр на самопишущем электронном потенциометре. Различные скорости пере-

Appendix 2

движения образца и диаграммной ленты самописца позволяют широко варьировать «увеличение» получающейся на ленте картины распределения элемента по шлифу. Максимальное «увеличение» $\times 2 \cdot 10^4$.

При оптимальном режиме интенсивность линии $K\alpha_1$ чистого элемента составляет 10^4—10^5 имп/сек. Поэтому при значительных содержаниях определяемого элемента в данной точке шлифа приходится работать при меньших удельных нагрузках (меньших токах через трубку). Точность анализа, определяемая стабильностью питающих устройств и схемы регистрации, при опытной проверке оказалась равной 2—5%.

На рис. 2 представлена спектрограмма «в точке» многокомпонентного сплава, иллюстрирующая работу созданной аппаратуры.

На рис. 3 представлен результат анализа «по точкам» другого многокомпонентного сплава. Кривая A передает ход изменения интенсивности линии Ni $K\alpha_1$ ($RC = 4$ сек., шкала 1000 имп/сек) при перемещении шлифа под электронным пучком, кривая $Б$—ход изменения интенсивности линии W $L\alpha_1$ ($RC = 2$ сек., шкала 200 имп/сек) на том же участке шлифа. Сопоставление этих данных с микрофотографией шлифа позволяет сделать заключение о том, что наблюдающиеся на шлифе включения представляют собой фазу, значительно обогащенную W при уменьшенном содержании основы Ni.

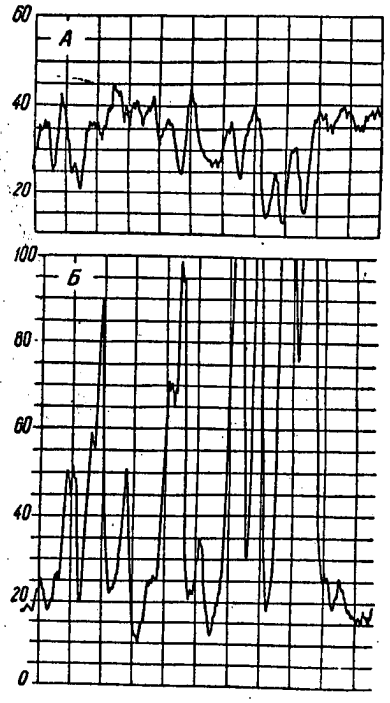

Рис. 3

Таким образом, разработанная аппаратура и методика позволяют проводить не только количественные анализы состава «в точке» с чувствительностью до 0,1% (что соответствует 10^{-13} г элемента «в точке»), но и исследовать распределение данного элемента по шлифу. Проведенные исследования ряда сложнолегированных металлических и металлкерамических сплавов, сварочных швов, диффузионных слоев на распределение элементов Fe, Ni, Cu, Zn, Nb, Mo, W, Re в микрообъемах и в заданных направлениях практически доказали большие возможности нового метода в решении с его помощью задач, которые не могут быть решены другими существующими методами физико-химического анализа.

Институт металлургии им. А. А. Байкова
Академии наук СССР

Поступило
14 VII 1955

ЦИТИРОВАННАЯ ЛИТЕРАТУРА

[1] И. Б. Боровский, Сборн. Проблемы металлургии, Акад. И. П. Бардину к 70-летию, Изд. АН СССР, 1953. [2] R. Castaing, A. Guinier, Anal. Chem., 25, No. 5, 724 (1953). [3] И. Б. Боровский, М. А. Блохин, Рентгено-спектральный анализ, 1939.

APPENDIX 3

CENTRIFUGAL METHOD FOR STUDYING METALS AND ALLOYS FOR HIGH TEMPERATURE STRENGTH

By I. I. Kornilov
Institute for General and Inorganic Chemistry
USSR Academy of Sciences

Machine for Testing by the Centrifugal Method

The centrifugal method of testing of alloys is based on the deformation of the specimens being tested at high temperatures under the continuous action of a centrifugal force.

The centrifugal force can be used for purposes of bend straining, tensile straining, and studies of creep. The method of studying deformation in bending of test specimens at high temperatures is very simple and may be used at any laboratory. Moreover, a large number of small specimens can be tested at the same time, and no complicated apparatus is needed.

Tension testing by the centrifugal method also is relatively simple and makes it possible to run creep tests on a large number of specimens simultaneously within wide ranges of temperature.

We have developed a testing machine suitable for the two tests just mentioned.

The machine for bend testing metallic specimens (see Figure 2) consists of a vertical shaft with a pulley and a revolution counter. The lower part of the shaft with a special holder and the specimens is arranged inside the furnace chamber and heated to the required temperature. The shaft is rotated by a motor and the speed of rotation is controlled by a rheostat, while the stress is kept constant by a stress stabilizer.

For study of the bending strength, vertical specimens are fastened by one end to a holder so as to be arranged around the end of the rotating shaft and are all rotated at a uniform, constant speed.

The bending stress acting on the specimens is a function of the length of the specimens, their mass, and the speed of rotation. Inasmuch as the speed of rotation is proportional to the square of the stress, higher stresses can be attained by increasing the speed of rotation. In order to increase the stress, moreover, supplementary weights may be applied to the free end of the specimens.

The strength of the material is determined by the angle of bend (in degrees) or by the deflection (in millimeters) after a given period of time. The degree of residual deformation is determined by periodic measurements of the deflection or angle of bend. In the tests, round-section bars, 3, 4, 5 ... mm (0.12, 0.16, 0.2") in diameter, are used. Sets of 12, 24, or more specimens may be tested simultaneously. The weight of the specimens is from 5 to 10 grams. They can be prepared easily by casting or in the form of forged, or rolled

Testing of Alloys by New Method

As the shaft together with the specimens fastened to it is rotated, the specimens undergo deformation. At given intervals of time, the amount of bend in linear units or degrees (or the elongation of the outer fiber in %) are determined and in this way, experimental data are obtained which are plotted in the form of amount of (bending) strain vs. time of straining curves.

Curves relating to the rate of straining as a function of the strength of the material being tested are presented in Figure 3. Under identical initial conditions, specimens differing in their strength undergo deformation at different rates.

The alloy having the highest strength of all of the materials tested under identical constant conditions of straining may not show any bending at all over a given period of testing (see curve 1 in Figure 3). On the other hand, the alloy of the lowest mechanical strength undergoes deformation under the same conditions at maximum speed, beginning at the instant the centrifugal force starts to act (Figure 3, curve 7). All of the other specimens of different strengths are found between curves 1 and 7, with respect to their rate of deformation.

When determining analytically the shape of the curves and computing the rate of straining as a function of time, $dv/d\tau$, we obtain a mathematical expression of the rate of straining of the specimens in bending. It makes it possible to express the strength of the different alloys in analytical form.

In addition to characterizing the strength of the alloys being tested by the rate of their straining, it is also possible to use as a relative index of strength the time at which the specimen starts to show deformation. The specimens having the lowest strength undergo deformation as soon as the centrifugal force begins to become active, or at least, mere minutes later, while the strongest specimens do not become deformed under the same conditions for hundreds of hours.

The start of plastic deformation is the "tentative creep limit" which determines the strength of alloys able to undergo straining. The start of the straining and the rate of initial straining of different alloys differing in strength are determined under strictly constant conditions of the stress state of the specimens.

However, this constancy of the state of stress exists only during the initial period of rotation of the specimens and with small amounts of straining. As the angle of bend or the deflection increase, the bending stress likewise undergoes a change.

It has been established by calculation that the bending stress increases as the angle of bend increases and that it reaches a maximum at an angle of 40-45 degrees. Upon further increase of the angle of bend, the stress again decreases. As a result, low strength materials are bound to be in a less favorable condition as the angle of bend increases.

In the initial stage of the development of the proposed method, this circumstance proved to be its principal drawback. However, a study of the experimental materials revealed the fact that in the process of straining, the specimens pass through the same course of bending and the same state of stress, only they do so at different times. For any intermediate position of the specimen in the process of bending, the same states of stress correspond to the same degrees of straining. Consequently, different specimens of different strength experience like bending stresses at like angles of bend. This affords a basis for the assumption that the differences in strength among the specimens manifest themselves in that the specimens pass through the same stress states at different times. The alloy of the lowest strength passes through this straining routine in the course of a few minutes or hours whereas the alloy of the highest strength does so in the course of hundreds or, possibly, thousands of hours (see curves 1 - 7 in Figure 3). This important circumstance offers a possibility of characterizing the relative strength by the time required for straining, provided that the conditions of the state of stress are maintained uniform for all of the alloys being studied.

In this way, it is possible to adopt the time required for the same amount of bending, expressed in degrees, a linear unit, or percent of the maximum amount of bending, to 90 degrees, or else the time required for the maximum bending strain of the specimens, as a characteristic of their high temperature strength.

Thus, the relative strength of different alloys may be characterized quantitatively as follows:

(1) by the time at which plastic deformation commences under conditions of an identical stress state of all of the specimens. This characteristic may well be designated as "tentative bending creep limit";

(2) by the rate of bend straining, expressed by the amount of bend $dv/d\tau$, per unit time (for the initial period of deformation);

(3) by the time required for the same amount of strain in a complex-stress state; and

(4) by the time required for the maximum bend straining of the specimens in a complex-stress state.

In our further work, attention was given to different metallic systems; thus, the bending strength of alloys of the aluminum-magnesium system at a temperature of 300° C (570°F) was investigated. The aluminum side of the phase diagram is shown in Figure 5a. It is characterized by a limited solubility of magnesium in aluminum in the solid state. The solubility of magnesium in aluminum along the isotherm of 300°C (570°F), which is of interest to us, is 6.2%. When selecting the compositions of the alloys, an attempt was made to obtain compositions corresponding to solid solutions, and alloys with

precipitation of the excess phase. In this connection, the dependence of the strength on the concentration of the solid solution and on the precipitation of the extra phase, i.e., on the physical-chemical nature of the alloy, was investigated. In all, six compositions of alloys of aluminum with 0, 2.5, 5, 7.5, 10, and 12.0% Mg were prepared. The specimens had the shape of small rods, 4 mm (0.16") in diameter and 100 mm (4") in length. Before they were tested for their mechanical strength, they were annealed at 400°C (750°F) for four hours and slowly furnace cooled to room temperature. The deflection was measured at first every 30 minutes, then every hour, and after twenty hours of testing, every two hours.

The tests showed that all six alloy compositions behaved differently with respect to the time of incipient bending, as well as the amount of bending, as a function of time. The tests showed that the alloys containing 10 and 12% Mg are the first to commence bending.

Ninety minutes after the start of the rotation, the straight aluminum specimen began to deflect, while the alloys containing 2-1/2, 5 and 7-1/2% Mg did not do so. After five hours, the alloy with 7.5% Mg started to deflect, and after ten hours, the 2.5% Mg alloy. At that time, the alloy containing 5% Mg was still unaffected. The curves relating to the rate of deformation of the alloys with time as a function of their composition are quite similar to the typical curves of the rate of deformation presented in Figure 3.

In Figure 5b, there is shown a series of curves relating to the deflection after a constant time of testing at 300°C (570°F) as a function of the magnesium content.

The values of the deflection after 5, 10, 15, 20, 30, and 45 hours of testing have been used to characterize the bending strength and variation in the amount of bending as a function of the magnesium content of the alloys.

These curves show a relative strength of the aluminum-magnesium alloys as a function of their composition and structure. The alloys having a clearly two-phase structure (with 10 and 12% Mg) undergo deflection at a higher rate than even straight Al. As the concentration of solid solution of the alloys increases, the deflection for one and the same period of time becomes smaller. With a magnesium content of the alloy of 5%, the alloy possesses the highest bending strength. An alloy of this composition corresponds to the maximum concentration (of the compositions studied here) of solid solution. All of the curves pass through minimum deflections corresponding to maximum concentrations of (a) solid solution of magnesium and aluminum.

Just as in the direction of a decreasing content of magnesium in the solid solution, so in the direction of an appearance of extra (β) phase, the deflection intensifies; in other words, the strength decreases.

Conclusions

(1) A machine for the bend testing of specimens by the centrifugal method has been designed and built, which is simple and compact, and can be used within the range of temperatures extending from room temperature to 1200°C (2190°F). The machine may be used for studies of the strength of various materials in the form of round-section rods weighing 5-10 grams each. The number of specimens which can be tested simultaneously, is 12, 24, or more. All of the specimens are tested under exactly the same conditions.

(2) As a criterion of the high temperature strength of alloys, there may be used the time required to attain the same degree of straining, or the time at which maximum straining takes place. These times reflect quantitatively the relative strength of specimens tested simultaneously. Bending straining is not limited as to time. It may continue for an indefinite time.

(3) At high temperatures, the proposed test may also be used in studies of the chemical stability of alloys with respect to oxidation. The fact that simultaneously information on the mechanical strength and chemical stability at high temperatures can be secured on a large number of specimens, enables the selection of a limited number of alloys possessing optimum properties.

(4) The conditions under which the specimens are tested in the centrifugal method approach the conditions of actual service.

References:

1. A.A.Bochvar, IZVESTIYA AKADEMII NAUK SSSR, Otd. Tekh. Nauk, 1947, No. 10, pp. 1369-1388;

2. I. A. Oding, VESTNIK MASHINOSTROENIYA, vol. 24, 1944, No. 5, p. 57 et seq.;

3. I. I. Kornilov and A. A. Azovskaya, "Review of Scientific Papers of the Division of Chemical Sciences, USRR Academy of Sciences for 1941-1943", page 31.

ITPPENDIX 5

I. I. Kornilov:

CENTRIFUGAL METHOD FOR STUDYING METALS AND ALLOYS FOR HIGH TEMPERATURE STRENGTH.

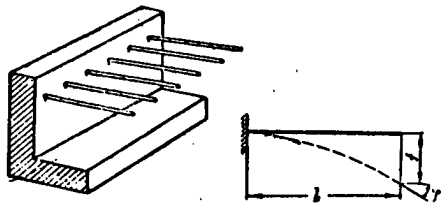

Fig. 1. Wire specimens tested for sagging.

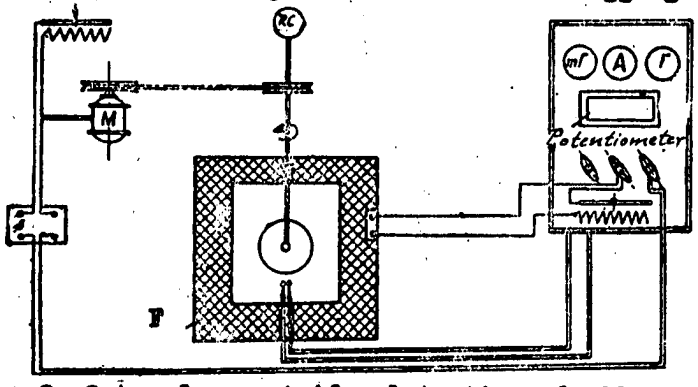

Fig. 2. Setup for centrifugal testing of alloys. M = motor; F = electric heating furnace; RC = revolution counter; S = stabilizer.

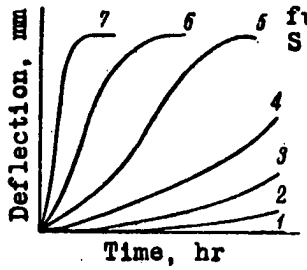

Fig. 3. Rate of bend straining of alloys having different strengths.

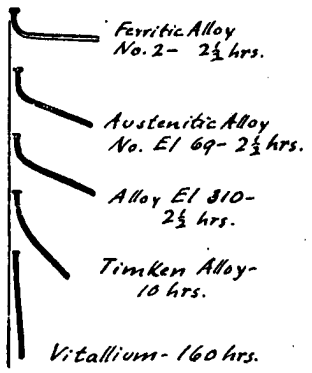

Fig. 4. Appearance of specimens after test for high-temperature strength (schematic).

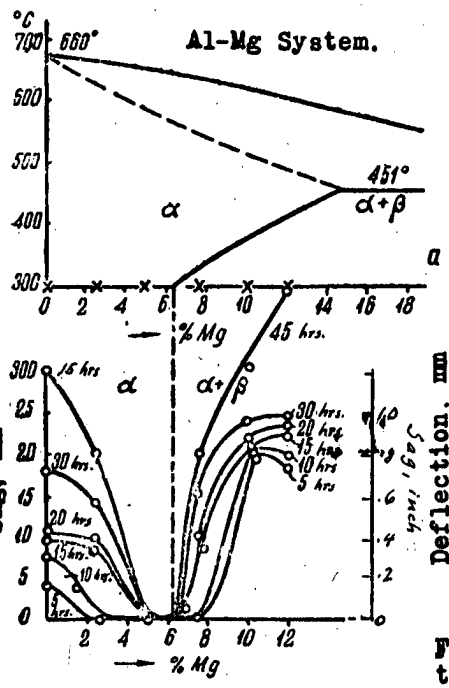

Fig. 5. Composition vs. high temperature strength diagram for alloys of Al-Mg system at 300° C (570° F).

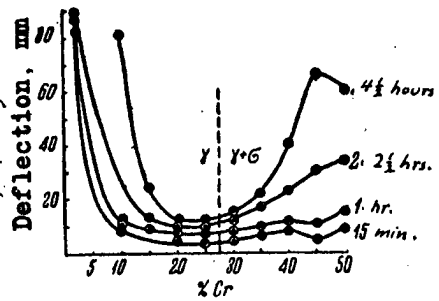

Fig. 6. Composition vs. high temperature strength diagram of alloys of ternary system Fe-Ni-Cr. Radial section of Fe/Ni = 3/1; temperature: 770° C (1420° F).

APPENDIX 4

The Phase Diagram of the Magnesium Corner of the Mg-Mn-Ce System

By D. A. Petrov and M. S. Mirgalovskaya
I. A. Strel'nikova and E. M. Komova

The investigation of the Mg-Ce-Mn has practical importance since the addition of Ce gives added improvement to Mg-Mn alloys. These alloys are particularly corrosion resistant and have good weldability.

The Mg-Mn-Ce system has not been studied intensively up till now -- the only investigation was carried out as graduate work at Mati (1).

This work was carried out at the Institute of Metallurgy of the Academy of Sciences imeni Baikov, in 1953.

The alloys were melted in a corundum crucible under a (LiCl + KCl) flux. The magnesium contained 0.031% Fe, 0.03% Si, 0.009% Al, 0.008% Cu. The cerium contained about 1.4% total rare earths and only .01% of iron silicon and alkaline metals. Mn was added in the form of anhydrous $MnCl_2$.

The methods of investigation for alloys which lie in the range of primary precipitation of α magnesium were thermal analysis and metallography of cast and annealed samples. The alloys were annealed at 300, 400, 500, 550, 570, 600 from 2 to 18 days, depending on the annealing temperature under an inert atmosphere.

Thermal analysis was not possible for alloys lying in the field of primary crystallization of magnesium.

For the location of the thermal variant curve, a method suggested by N. K. H. Abrikosov was used because thermal analysis was not possible in this area. This method is based on the following theoretical assumptions:

If the alloy is composed of components, one of which has greater density and if the data point lies in the field of primary crystallization of the heavy component (peritectic type diagram is considered). Then upon cooling, the precipitate crystallites of the heavy phase will settle to the bottom and the upper layer will be impoverished by this amount. At the end of the primary crystallization, the upper layer will correspond to the composition of the peritectic point. If the melt is binary, this composition will correspond to one of the points on the mono variant curve, i.e., the liquidus valley of the ternary. The composition of such a point can be determined by chemical analysis of the upper layer and the corresponding temperature can be determined by thermal analysis.

The tests were carried out in the following manner: The magnesium was melted at 850°C. Anhydrous $MnCl_2$(12%Mn) was introduced and the

melt stirred and held at 850°C for 2.5 hours. Then, cerium was introduced (150% of the amount required). The melt was stirred for another five minutes after which it was slowly cooled to the required temperature (over 2 hours). At the given temperature, the melt was held 30 minutes and the casting cooled rapidly. The casting (well cleaned of flux) was cut and the upper .8cms removed. This piece was cut in two -- one part analyzed chemically, the other part thermally.

Based on these experiments, the magnesium corner of this system was determined. The influence of Ce in the solubility of Mn in liquid magnesium was studied. The location of the mono varient curve in the partial system Mg-Mn-$CeMg_9$ was determined and finally the solubility of Mn and Ce in the magnesium solid solution was investigated.

Discussion of Results:

Figures 1 and 2 were constructed on the basis of the data as well as Figure 3. The Mg-Mn diagram was constructed from the data of reference 1.

Three mono variant lines of the ternary phase equilibria are located in the magnesium corner of the system -- L+Mg+Mn, L+Mg+$CeMg_9$, L+Mn+$CeMg_9$. These lines separate the three fields of primary crystallization -- α Mg, Mn, $CeMg_9$.

From the location of the isotherms on the surface of the liquidus on the field of the primary crystallization of Mn, it follows that with the change of Ce content from 0 to 1.5%, the solubility of Mn at high temperatures ($\approx$ 850°C) is reduced considerably (from $\approx$ 5% to 3.8%). A further increase of Ce (to 12%) decreases it slightly to 3.4% Mn. The solubility of Ce in Mg solid solution in the presence of Mn decreases slightly (more of a decrease at 550 than at 570). The solubility of Mn in Mg in the presence of Ce is almost unchanged.

The point of maximum solubility of magnesium by the two phases Mn and $CeMg_9$ is about 0.76 and 1.3% Mn.

The mono variant line (i.e., liquidus valley) of the three phase equilibrium L Mg+Mn starts on the Mg=Mn side at 2% Mn and in the ternary diagram it gradually comes close to the Mg-Ce side ending in the ternary point ($\approx$ 1.45%Mn, $\approx$ 585°C).

This line characterizes the peritectic process L+Mn$\leftrightarrows$Mg to the point which corresponds to the sample composition 97.7%Mg 2.0%Mn 0.3%Ce; further on this line characterizes the eutectic process L$\leftrightarrows$Mn+Mg.

The starting point of the mono variant line of the three phase equilibria L Mg+$CeMg_9$ is the point of the system corresponding to 21%Ce at 590°C and ends in the ternary point.

Appendix 4

в виде лигатуры магния с марганцем, содержавшей до 2,5% Mn. Лигатура бралась в колпчестве 130% (по марганцу) и вводилась при температуре 850°. Расплав перемешивался 20 мин., затем вводился церий и еще 5 мин. продолжалось перемешивание. После отстаивания в течение 10 мин. сплав отливался в плоскую холодную изложницу.

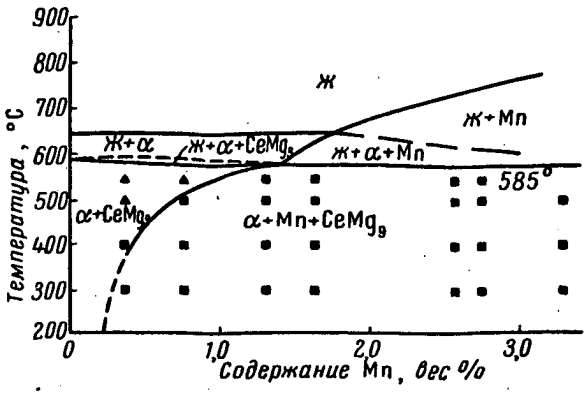

Рис. 1. Диаграмма вертикального разреза (~0,3% Ce)

Для определения положения моновариантной кривой вместо метода термического анализа, который в данном случае оказался неприменимым, была разработана подсказанная Н. Х. Абрикосовым методика, базирующаяся на следующих теоретических предпосылках.

Если сплав составлен из компонентов, один из которых резко отличается по удельному весу от другого, и если фигуративная точка сплава лежит в поле первичной кристаллизации тяжелого компонента (имеется в виду диаграмма перитектического типа), то при остывании сплава выпадающие первичные кристаллы тяжелой фазы будут садиться на дно тигля, а верхние слои расплава будут обедняться тяжелым компонентом. К концу первичной кристаллизации состав расплава в верхнем слое будет соответствовать составу, отвечающему перитектической точке, если сплав будет двойным, и одной из точек моновариантной кривой, если сплав состоит из трех компонентов. Состав, отвечающий такой точке, может быть определен химическим анализом верхнего слоя слитка, а соответствующая температура — методом термического анализа.

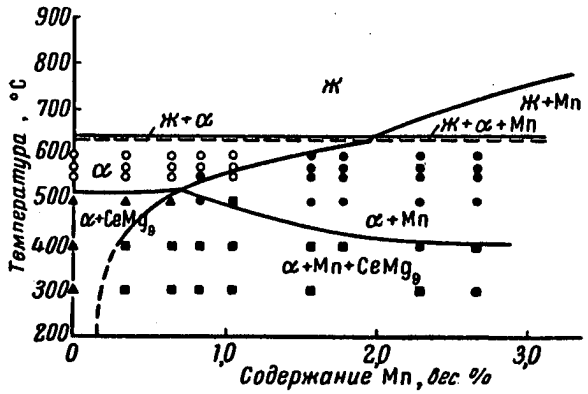

Рис. 2. Диаграмма вертикального разреза (~1,6% Ce)

Опыты проводились следующим образом. В расплавленный магний при температуре 850° вводился безводный хлористый марганец (12% Mn). Расплав перемешивался и выдерживался при температуре 850° 2,5 часа. Затем вводился церий (150% от требуемого количества). Расплав перемешивался еще 5 мин., после чего медленно (в течение 2 час.) охлаждался до нужной температуры. При заданной температуре расплав выдерживался еще 30 мин. и затем быстро охлаждался. У слитка, тщательно отмытого от флюса, срезалась верхняя часть (высотой около 0,8 *см*), которая затем разрезалась на куски. Часть из них передавалась на химический анализ, часть подвергалась термическому анализу.

Appendix 4

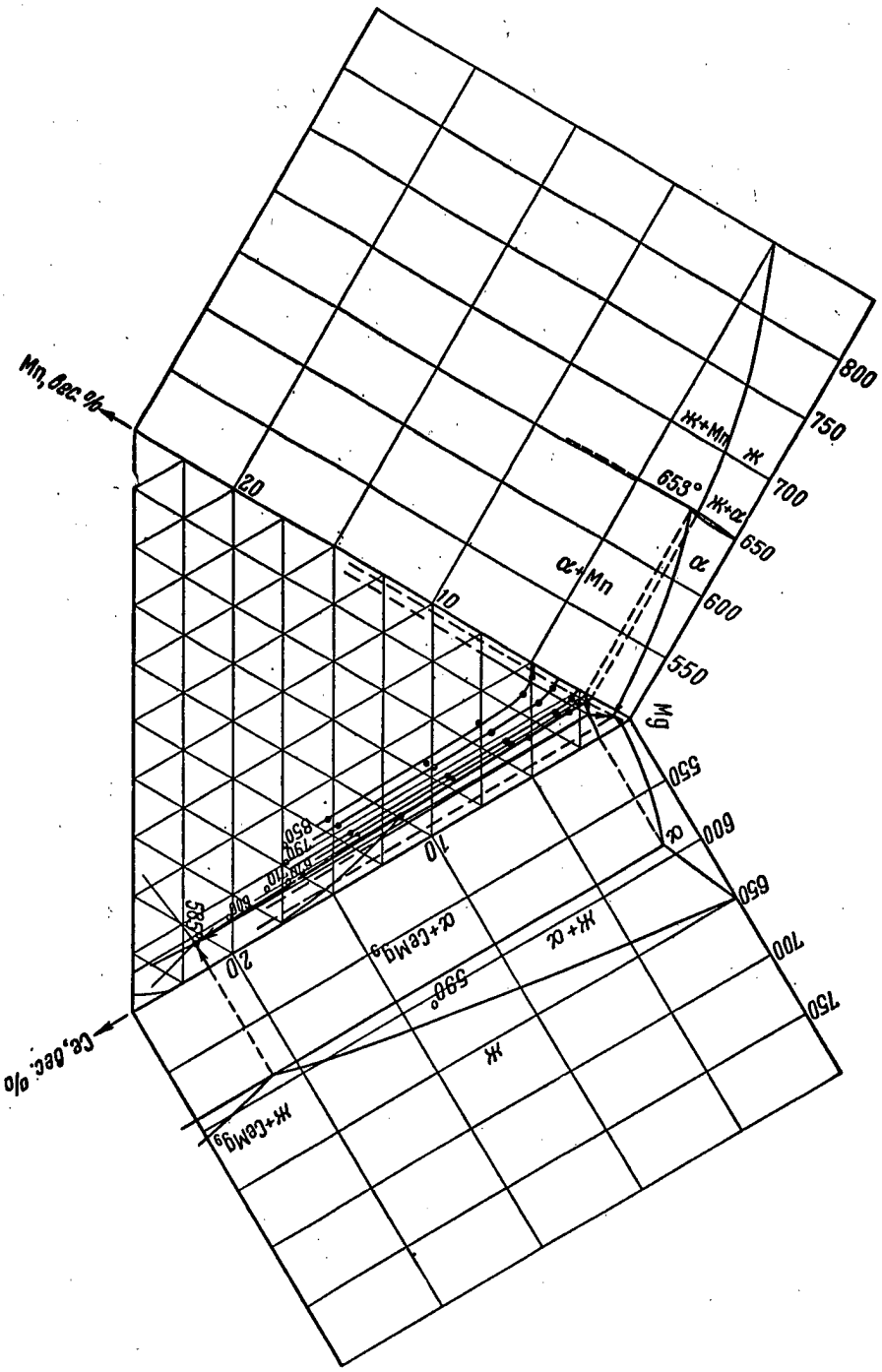

Рис. 3. Диаграмма состояния магниевого угла системы Mg — Mn — Ce

APPENDIX 5

Prof. Dr. A. I. BELYAEV

METALLURGY OF LIGHT METALS

(General Course)

Approved by the Ministry of Higher Education in the USSR as a textbook for the higher metallurgical schools.

FOURTH EDITION

State Scientific-Technical Press of Literature on Ferrous and Nonferrous Metallurgy

Moscow, 1954

30 Literature References, all Russian.

TABLE OF CONTENTS — PAGE

APPENDIX 6

Ministry of Higher Education of the USSR

MAIN ADMINISTRATION OF MINING, METALLURGICAL AND ARCHITECTURAL COLLEGES

Index GMS-444

Certified by the Main Administration of Mining, Metallurgical and Architectural Colleges

July 4, 1955

PROGRAM

Of The General Course

"METALLURGY OF LIGHT METALS"

particularly the "METALLURGY OF NONFERROUS METALS"

INTRODUCTION

Properties of aluminum, magnesium and other light metals. The importance of light metals for the national economy of the country. The role of the Communist party and Soviet government in the creation and development of the aluminum and magnesium industries in the USSR. The principal stages in the development of the metallurgy of aluminum and magnesium. The importance of the studies made by St. Claire Deville, N. N. Beketov, K. J. Bayer, P. Heroult, C. Hall, P. P. Fedot'ev, A. A. Yakovkin, A. N. Kuznetsov and others for the development of the metallurgy of aluminum and magnesium. The electrolysis of fused salts as the principal process in the metallurgy of these metals. The position of thermal processes. The connection between the development of the aluminum and magnesium industries and the electrification of the country. The principal schemes for the production of aluminum and magnesium. The contents of the course.

Section 1. METALLURGY OF ALUMINUM

Production of Alumina

Aluminum ores. Location of aluminum ores in the USSR and in foreign countries. The geochemistry of aluminum. The formation of aluminum ores. Specifications of aluminum ores. General survey of the methods for the preparation of alumina from aluminum ores. Alkaline, acid and electrothermal methods. The combination of these methods. Alumina as a material for electrolysis. Standards for alumina.

Bayer method. General scheme of the method and main reactions. The leaching of bauxites. The various forms of bauxites and their behavior during leaching. The detrimental effect of silica, titanium

oxide and other impurities on alumina extraction. The influence of various factors on the process for the leaching of bauxites. Autoclaves. Decomposition of the aluminate solution by centrifuging. Influence of various factors on this process. The centrifuging conditions. Apparatus: Decomposers with mechanical and air stirring. Calcination of aluminum hydroxide. Physiochemical transformations in the dehydration of aluminum hydroxide. Conditions for running the process in a rotary tube furnace. Evaporation of the recovered alkaline solutions and causticization of the soda. The technical and economic indices of the Bayer method. Soda-lime leaching.

Sintering method. General scheme of the sintering method. Physicochemical principles of the method. The behavior of the batch components during sintering. The principles of the batch composition. The preparation of the batch. The sintering of the batch in a rotary furnace. Leaching of the sintered mass. The principal reactions in the leaching of the sintered mass. Leaching by stirring and by diffusion. Apparatus for separating the red sludge. Silica in aluminate solutions. The practice of silicon-removal. The conditions for running the process. The theory of carbonization. The construction of carbonizers. The practice of carbonization. The separation of aluminum hydroxide from the soda solution and its washing. The technical and economical indices of the sintering method. Combination of the sintering method with the Bayer process. Parallel and consecutive schemes. The use of the sintering method to treat nepheline. Scheme for the complex treatment of nepheline to yield alumina, soda, potash and cement. Apparatus and technical-economic indices.

Production of alumina from slags. General scheme of the Kuznetsov-Zhukovskii method. Conditions for the smelting of slags, suitable for leaching. Behavior of the batch components during smelting. The possibility of preparing slags in blast-furnaces. The characteristics of slag leaching and the removal of silicon from aluminate solutions. The technical-economic indices.

The problem of using alunites. The ammoniacal-alkaline method of Labutin and Naumchik to obtain alumina and ammonium sulfate from alunites. The perspectives of using alunites as a complex ore.

General characterization of other methods for the production of alumina. The problem of extracting alumina from raw materials poor in aluminum: Clays, ashes, carbonaceous shales.

Safety rules in the production of alumina. Methods for the operation of new ideas in the alumina divisions of aluminum plants. Automatization of alumina production. Cost of alumina.

Production of Fluorides

Fluorite as the principal raw material for the production of cryolite and other fluorides. Location of fluorite beds and its

enrichment. The standards for cryolite, aluminum fluoride and sodium fluoride. The technological scheme for the production of cryolite by the acid method. The production of aluminum fluoride and sodium fluoride. The production of cryolite by the alkaline method. The technical-economic indices. Safety rules in the production of fluorides.

Production of Carbon Electrodes

The development of carbon electrode production in connection with the development of electrothermy and electrolytic processes. Carbon fabricates and electrodes in the aluminum and magnesium industries: Anodes, cathode blocks, electrodes for electric furnaces, carbon anode assembly, lining plates, graphitized electrodes. Solid carbon materials for the production of electrodes, their properties and evaluation. Binding (cementing) substances, their characterization and designation. The roasting, crushing, grinding and classification of solid carbon materials. Apparatus for accomplishing these processes. Composition of the batch for the production of various types of electrodes. Influence of the nature of the materials, grain size, and amount of binder. Mixing of the dry portion of the batch with the binder. The pressure molding of green electrodes. The influence of pressure. The types of processes and their operation. The roasting of electrodes and the conditions for running this process. The roasting temperature curve. The construction of furnaces for the roasting of electrodes. The principal technical-economic indices in the production of carbon electrodes. The technical conditions in electrode production. Graphitization of carbon electrodes. Properties of these electrodes and the scope of their use. Physiochemical essentials and practice of the process. Safety rules in the production of carbon and graphitized electrodes.

Production of Aluminum

Melts of the system: Aluminum fluoride-sodium fluoride-alumina-calcium fluoride as electrolytes for the electrolytic preparation of aluminum. The fusion diagram of the systems: Aluminum fluoride-sodium fluoride, cryolite-alumina and cryolite-calcium fluoride. Physicochemical properties of the electrolyte in an aluminum bath. The anode and cathode processes during electrolysis. The voltage on the bath. The current efficiency and the consumption of electrical energy. The influence of various factors: The current density, the interpolar distance, the temperature, and the composition of the electrolyte. The construction of aluminum cells. Multianode cells. Cells with continuous anodes. Cells with side and top leads for the current. Electrolysis section. Arrangement of the cells in the section. Direct current commutation. Transport of alumina, fluorides and the anodic mass. Starting up the cell. Operation of the aluminum cell. The anodic effect and its role in the operation of aluminum cells. The feeding of alumina and fluorides to the cell. The change in the electrolyte composition during cell operation. The

correcting of the electrolyte. The accumulation of carbon in the electrolyte. The removal and treatment of the carbon scum. The extraction of aluminum from the cell. The chlorination, fusion and casting of the original aluminum. The electrolytic refining of aluminum. The properties and uses of high-purity aluminum. The three-layer method for the electrolytic refining of aluminum. The organization of the work in the electrolysis section. Methods for the operation of new ideas. Mechanization of the aluminum cell. Technical-economic indices. Production cost of aluminum. Safety rules in the production of aluminum.

Production of Aluminum Alloys by Electrothermy

The problems of reducing alumina with carbon. The obtaining of silicoaluminum in electric furnaces. Starting materials. Preparation of the batch and conditions for running the fusion. The uses of silicoaluminum. Electrothermal silumin. Technical-economic indices. Methods for the extraction of pure aluminum from silicoaluminum.

Section II. METALLURGY OF MAGNESIUM AND OTHER LIGHT METALS

Preparation of the Starting Crude for the Production of Magnesium

The occurrence of magnesium in nature. Magnesite, dolomite, magnesium chloride and carnallite as basic raw materials. Other types of magnesium crude. Dehydration of magnesium chloride and carnallite. Production of magnesium chloride by the chlorination of magnesite. Conditions for running the process. Apparatus. Technical-economic indices in the production of anhydrous magnesium chloride and carnallite. Safety rules in the production of anhydrous magnesium chloride salts.

Production of Magnesium by Electrolysis and by Thermal Methods

Electrolysis of magnesium chloride. Composition and physicochemical properties of the electrolyte in a magnesium cell. The cathode and anode processes. Yield based on the current and on the energy. Cells with top and side anodes. Conditions for running the electrolysis. Extraction of the magnesium. Removal and utilization of the anodic chlorine. Technical-economic indices. The operation of new ideas. Safety rules for working in the electrolysis section of a magnesium plant. Thermal methods for the preparation of magnesium by the reduction of magnesite and dolomite with ferrosilicon and carbon. Technological schemes, apparatus, technical-economic data. The refining of magnesium. The fusion and casting of magnesium. The standards for magnesium. The cost of magnesium.

Metallurgy of Other Light Metals

Preparation of the starting materials for the construction of electrolyzers and the characteristics of electrolysis in the production of beryllium, calcium and lithium. Thermal methods for the preparation of these metals. The reduction of beryllium fluoride by magnesium. The vacuum-reduction of calcium and lithium oxides.

LITERATURE

a) Obligatory

Belyaev, A. I., Metallurgy of Light Metals, 4th Edition, Metallurgical Press, 1954.

b) Supplementary

Kuznetsov, S. I. and Epshtein, A. M., Electrolytic Production of Aluminum, Metallurgical Press, 1953.

Belyaev, A. I., Notes on the History of the Metallurgy of Light Metals, Metallurgical Press, 1950.

The program was approved by a conference of the professors and docents of the metallurgical institutes and faculties in May of 1955.

APPENDIX 7

PRODUCTION OF ALUMINA

Prof. Dr. V. A. Mazel

Approved by the Administration of Educational Institutions,
Ministry of Nonferrous Metallurgy in the USSR,
as a textbook for technical schools

State Scientific-Technical Press of Literature
on Ferrous and Nonferrous Metallurgy

Moscow 1955

TABLE OF CONTENTS

Page

Chapter VII. (Continued)

Page

Appendix (Continued)

APPENDIX 8

"ELECTROMETALLURGY OF ALUMINUM"

by

A. I. Belyaev, M. B. Rapoport and L. A. Firsanova

State Scientific-Technical Press of Literature
on Ferrous and Nonferrous Metallurgy
Moscow - 1953

(344 Literature References, of which 244 are Russian)

TABLE OF CONTENTS

SECTION TWO

ELECTROLYTIC REFINING OF ALUMINUM

SECTION THREE

ELECTROTHERMY OF ALUMINUM AND ITS ALLOYS

APPENDIX 9

MAGNESIUM METALLURGY

K. L. Strelets, A. J. Taits, and B. S. Guljanitskii

Published in Moscow in 1950

State Scientific-Technical Press of Literature on
on Ferrous and Nonferrous Metallurgy

63 Literature References, of which 55 are Russian.

TABLE OF CONTENTS

Page

Part 3

THERMAL MAGNESIUM PRODUCTION WITH CARBON FREE REDUCING AGENTS

APPENDIX 10

Ministry of Higher Education of the USSR

MAIN ADMINISTRATION OF MINING,
METALLURGICAL AND ARCHITECTURAL COLLEGES

Index GMS-452

Certified by the Main
Administration of Mining, Metallurgical
and Architectural Colleges

July 5, 1955

PROGRAM

Of the Special Course

"METALLURGY OF LIGHT METALS"
particularly the "METALLURGY OF NONFERROUS METALS"

INTRODUCTION

Subject and contents of the course. Place of the special course in the preparation of engineers specializing in the metallurgy of nonferrous metals. Special course on the metallurgy of light metals as one of the disciplines completing the theoretical preparation of metallurgical students.

Section 1. TECHNOLOGY OF THE PRODUCTION OF ALUMINA

1. Physicochemical properties of aluminate solutions. Existing theories on the nature of aluminate solutions based on the studies of Manoev, Lileev, Kurbatov, Pazukhin and others. The studies of Tsirlin, Magarshak, Wolf and others on the investigation of the isotherms of the system Na_2O-Al_2O_3-H_2O. The cycle of the Bayer process in the system Na_2O-Al_2O_3-H_2O. Possible ways of expanding the capacity of this cycle.

2. Leaching of bauxites. Theoretical possible yield of alumina. Materials balance formula for the leaching of bauxite. Comparison of the schemes for the periodic and continuous leaching of bauxites. The principles of selecting a leaching technology as a function of the type of bauxite. The principles of designing the autoclave and autoclave equipment. The material and heat balances of the autoclave equipment. Methods for reducing the steam consumption. Capacity of the autoclave equipment.

3. Dilution of the pulp. Change in the stability and viscosity of the solution on dilution. The behavior of silica. Separation of the solution from the sludge and its washing. Determination of the alumina yield based on the amount of alumina and iron oxide in the

sludge. Calculation of the amount of water and the number of washings of the red sludge in multistage concentrators.

4. Decomposition of aluminate solutions by the centrifuging method. Analysis of the centrifuging process in the light of the equilibrium states existing in the system Na_2O-Al_2O_3-H_2O and from the viewpoint of the equations for the crystallization of salts from supersaturated solutions. The yield obtained in the centrifuging process. The material and heat balances of the process. Comparison of the operation of periodic and continuous decomposers. Calculation of the necessary number of decomposers and hydroseparators.

5. Calcination of aluminum hydroxide. Phase transformations during calcination. The role of mineralizing agents. The temperature zones in the calcination furnace. The material and heat balances of a calcination furnace. Pneumatic transport in the calcination of alumina.

6. Evaporation of aluminate solutions. Water and soda balances in the cycle of the Bayer process. Behavior of soda and organic substances in the evaporation of alkaline solutions. Conditions for the crystallization of soda during evaporation.

Construction of evaporators suitable for the evaporation of recovered alkaline solutions. The influence of the composition and viscosity of recovered alkaline solutions on the capacity of evaporators. Principles of calculating multi-shelled evaporating equipment for the evaporation of alkaline solutions.

7. Causticization of soda. The system $NaOH$-Na_2CO_3-H_2O and the reaction $CaCO_3 + 2NaOH \rightleftarrows Na_2CO_3 + Ca(OH)_2$, based on the studies of Fedot'ev. Conditions for the causticization of soda. Soda-lime leaching of bauxites in the light of the equilibrium diagrams for the system Na_2O-Al_2O_3-CaO-CO_2-H_2O.

8. Reaction in the solid state in the sintering of the components of the bauxite charge, based on the studies of Yakovkin, Lileev, Mazel, Strokov and others. Calculation of the batch. Comparison of four- and five-component batches. Saturated and unsaturated batches. The first and second periods in the sintering of bauxite batches. Temperature zones in the sintering furnace. Material and heat balances of the sintering furnace. Capacity of the sintering furnace.

9. Leaching of the sintered mass. Reaction of the components in sintered masses with water, aluminate solutions, sodium hydroxide solutions and soda. Comparison of leaching by the stirring and diffusion methods. Efficiency of a diffusion battery and the principles of its calculation. Removal of silica from aluminate solutions. The curve for the equilibrium concentrations of SiO_2 in aluminate solutions. The conditions for silica removal in the presence and in the absence of lime. Comparison of the methods for the periodic and continuous removal of silica.

10. Carbonization of aluminate solutions. Carbonization curves. Behavior of silica during carbonization. Complete, incomplete and fractional carbonization and its place in various technological schemes. Periodic and continuous carbonization. The material and heat balances of carbonization.

11. Combination of the Bayer and sintering methods. Comparison of the technological schemes for consecutive and parallel operation. Calculation of the ratio between the output of the sintering process and that of the Bayer process using the two variations of consecutive and parallel operation.

12. The treatment of nepheline ores by the sintering method. Mechanism and technological aspects of the sintering of nepheline-limestone batches. Construction details of rotary furnaces for the sintering of nepheline-limestone batches. Necessity for the rapid separation of the liquid and solid phases in the leaching of the nepheline sintered mass. Scheme and regime for the separation of soda and potash by stepwise evaporation and fractional crystallization.

13. Production of alumina from alunites. Characteristics of the technology of various processes. The alkaline method of Kametsky. The ammoniacal-alkaline method of Labutin-Naumchik. The acid method of Vanyukov-Lisovskii. The conditions for the thermal treatment of alunite-containing rock and its subsequent leaching. The roasting of alunites in a boiling layer. Comparison of various methods.

14. Problems of safety practice in the various technological stages of alumina production. Organization of labor in the alumina industry. Operation of new ideas. Automatic controls and the direction of the more important trends in the alumina industry. A technical-economic comparison of various methods for the production of alumina on the basis of various types of raw material. Perspectives for the possible improvement in the technology, equipment and organization of the production and labor in the alumina industry. Calculation of the cost of alumina and methods for reducing it.

Section II. ELECTROMETALLURGY OF ALUMINUM

1. Physicochemical properties of the systems: $NaF-AlF_3$, $KF-AlF_3$, $LiF-AlF_3$ and $Na_3AlF_6-Al_2O_3$, based on the data of various investigators. The systems: Cryolite-fluorides of the alkaline earth metals. The systems: Cryolite-oxides. Fusion diagrams and properties of the ternary and reciprocal systems formed by fluorides and oxides, based on the studies of G. A. Abramov. The possibility of improving the properties of the electrolyte in an aluminum cell.

2. The theory for the electrolysis of cryolite-alumina melts. The structure of cryolite-alumina melts. The decomposition potential of alumina and the electrolyte components. Current transfer in the electrolysis of cryolite-alumina melts. Various theories on the

mechanism for the electrolysis of cryolite-alumina melts. The theory of Fedot'ev. Development of the Fedot'ev theory by Soviet scientists (Mashovts, Baimakov, Abramov). The application of the crystallochemical theories proposed by Pazukhin to the electrolysis of cryolite-alumina melts. The studies of French and Italian investigators on the theory of the electrolysis of cryolite-alumina melts.

3. Processes at the electrodes in an aluminum cell. Processes at the cathode. The possibility of liberating sodium. Cathodic depolarization. Solubility of aluminum and its losses in a cryolite-alumina melt. The nature of this phenomenon. The role of monovalent aluminum. The formation of aluminum carbide in an aluminum cell and various theories on the mechanism of this reaction. Selective absorption of the electrolyte components by the cathode and cell lining. Capillary phenomena in the carbon lining of aluminum cells. The reaction of carbonaceous materials with sodium and the influence of this phenomenon on the stability of the cathode blocks. Processes at the anode. Overvoltage on a carbon anode and its nature. Composition of the anodic gases. The anodic effect. The critical current density and the influence of various factors on it. Various theories on the nature of the anodic effect. Study of the mechanism for the anodic effect by Soviet scientists. The role of wetting in the phenomenon of the anodic effect.

4. The yield based on the current and on the energy in the electrolysis of cryolite-alumina melts. Principal mathemathical functions as outlined by Alabyshev, Drossbach, Abramov and Rotinyan. A comparison of these functions. The influence of various factors on the yield based on the current and on the energy.

The influence of the amount of aluminum and the shape of the working area of the cell on the yield based on the current and on the energy. Magnetic fields and their influence on the operation of the aluminum cell.

5. History of the construction of aluminum cells. Modern aluminum cells. Calculation principles of the aluminum cell. The voltage and heat balances of the cell. The starting up of aluminum cells. The starting up of the cells after overhauling. The starting up of a series of aluminum cells. The importance of the temperature regime in the starting up of the cells. The shutting down and starting up of the cells after prolonged interruption of the direct current. The influence of various factors on the length of service of the cells.

6. The feeding of alumina to the cell. Preventing the anodic effects and the economic practicality of this. Dependence of the voltage of the direct current source on the simultaneous arising of the anodic effects in several cells. The problem of continuously feeding alumina to the cell. The regulation of the anodes. The possibility of making this an automatic operation. The processes that take place in the coking of the anode. Methods for removal of the pins from anodes with side and top leads. Comparison of various methods for the extraction of aluminum from the cell. Correcting the composition

of the electrolyte. Methods for determining the cryolite ratio (crystalloptical, hot titration). Abnormalities in the operation of the cell and their elimination. Hot and cold operation of the cell. Accumulation of carbon and carbides in the electrolyte. Short-circuiting of the anode on the hearth incrustation. Recovery of fluorides from the gases liberated in aluminum cells. The sanitary-hygienic and economic advantages of such a measure.

The technical-economic indices for the electrolytic production of aluminum. Organization of the work in the electrolysis section. Organization of labor in the brigade of electrolysis operators. Generalization and distribution of primary instructions to electrolysis operators. Safety rules for work in the electrolysis section. Measures that should be taken to prevent injury by high-voltage direct current. Production control in the electrolysis section. Perspectives for possible improvement in the equipment technology and organization of the production and labor in the electrolytic production of aluminum. The cost of aluminum and methods for reducing it.

7. Electrolytic refining of aluminum. Development of the three-layer method for the electrolytic refining of aluminum. Mechanism of current transfer. The polarization e.m.f. and the voltage balance in the cell. The behavior of impurities in the anodic metal. The construction of electrolyzers. The physicochemical properties and composition of the electrolyte and anodic alloy. The preparation of the electrolyte and anodic alloy. The starting up and operation of the cells for the electrolytic refining of aluminum. Regulation of the voltage. Feeding of the electrolyte and starting metal. The removal of sludge and anodic deposits. Replacement of the anodic alloy. The casting of aluminum. Production control to give a high-purity aluminum. The use of electrolytic refining to extract aluminum from the secondary metal. Technical-economic indices of the process for the electrolytic refining of aluminum.

8. The electrothermy of aluminum and its alloys. The thermodynamics for the reduction of alumina by carbon.

The system $Al-Al_2O_3-Al_4-C_3$. The electrothermy of aluminum alloys. The conditions for the reduction of alumina in the presence of alloying metals. The mutual reduction of alumina and silica. The principal and secondary reactions. The technology for the electrothermal production of silicon and silicoaluminum. Types of silica-containing raw material and carbon-reduction. Batch requirements and the principles of its calculation. Preparation of the batch. Electric furnaces for the fusion of silicoaluminum. Regime for the operation of the furnaces. Fusion properties of aluminum-rich alloys. Technical-economic indices for the electrothermal production of silicoaluminum. Electrothermal silumin. The system Al-Si-Fe. Apparatus for the separation of silumin from silicoaluminum by filtration. The removal of iron from silumin. Methods for the extraction of pure aluminum from silicoaluminum. Extraction with zinc. The magnesium refining method. The mercury method. Sublimation through subcompounds. Perspectives for the development of these processes.

Section III. METALLURGY OF MAGNESIUM

1. Comparison of the technological schemes for the electrolytic production of magnesium. The carnallite scheme. The principal transformations and the flow of materials in this scheme. Possible methods involving the use of chlorine. The use of chlorine to chlorinate either titanium-containing raw materials or their intermediates, and for other chlorination processes, as one of the ways of consuming excess chlorine. The necessity of going to a mixed scheme of feeding carnallite and magnesium chloride to the cell. The flow of materials in the scheme of mixed feeding under the conditions of using the anodic chlorine to produce titanium.

2. The magnesium chloride scheme for the production of magnesium. Magnesite and magnesium oxide, obtained from brines, as possible sources of the basic starting material. Principal transformations and the flow of materials by this scheme. Possible ways to supply the chlorine deficiency. Combination with the carnallite scheme, with the feeding of partially dehydrated magnesium chloride, with the production of sodium hydroxide, or with the production of sodium. The coupling of magnesium production by the magnesium chloride scheme with the production of titanium. The flow of materials in such a coupling and the possible ratios of the recovered chloride to the original chloride.

3. Theoretical principles of the dehydration of magnesium chloride and carnallite. Evaporation of magnesium chloride brines and drying the crystallohydrate. Conditions under which the least amount of chloride hydrolysis occurs. Carnallite, enriched in heavy suspensions, and carnallite, isolated by recrystallization. The drying and dehydration of carnallite in the light of V. A. Il'ichev's data. Conditions preventing carnallite hydrolysis. The fusion of carnallite to obtain complete dehydration. Fusion in electric furnaces as the most rational method for the preparation of anhydrous fused carnallite. Automatic controls in the fusion of carnallite. The innovation of new ideas in the industry.

4. Theoretical principles of magnesium oxide chlorination. Equilibrium in the system $MgCl_2$-O_2 in the light of the studies made by Soviet scientists. The influence of dilution of the magnesium chloride by other chlorides and the influence of water vapors and carbon oxides on this equilibrium. The behavior of impurities during chlorination. Chlorination calculations.

5. Physicochemical properties of the melts fed to a magnesium electrolyzer. Impurities in the melts, including magnesium oxide. The physicochemical properties of the electrolytes in a magnesium cell. The choice of electrolyte and the conditions that determine this choice.

6. Phenomena at the anode and cathode in a magnesium cell. The behavior of impurities in the electrolyte in connection with the decomposition potential of the electrolyte components. Destruction of

the anode and passivation of the cathode in a magnesium cell as the main reasons for operation troubles. Conditions for obtaining the highest current efficiency and the least expenditure of electrical energy during electrolysis.

7. The starting and stopping of magnesium cells. Organization of the work around magnesium cells and in the electrolysis section. Instructions in the servicing and running of electrolysis in a magnesium cell. The extraction of magnesium and the removal of chlorine from the cell. The chlorine economy of an electrolytic magnesium plant. Purification of the gases allowed to escape up the stack, especially the gases from the cathode compartments. Electrolysis calculations. The technical-economic indices and possible ways of improving them.

8. Comparison of the principal types of electrolyzers used in modern magnesium plants. Electrolyzers without diaphrams and with external heating. The operation of this type of electrolyzer when fed partially dehydrated magnesium chloride. The possibility of feeding magnesium oxide to the cell (anode compartments). The utilization of spent electrolyte from the magnesium cell. The practice of safety in the electrolysis section of a magnesium plant.

9. The refining of magnesium. The separatory furnace. The use of the separatory furnace for the recovery of magnesium chloride and magnesium as sublimates from the production of titanium. Impurities in electrolytic magnesium. The role of fluxes in the purification of magnesium from salt impurities and suspended magnesium oxide. The purification of magnesium from impurities of the alkali metals and iron. The refining furnace and its operation. The casting of magnesium into pigs. The etching, washing and re-refining of magnesium. The technical-economic indices of refining magnesium by fusion with fluxes. The refining of magnesium by sublimation. Furnace for the refining of magnesium by vacuum-sublimation. Behavior of impurities during sublimation and the purity of the obtained magnesium. Conversion of the crystalline sublimate to the pig metal. Comparison of the methods for the refining of magnesium.

10. Schemes for the thermal production of magnesium. Theoretical principles of magnesium oxide reduction by carbon, carbide and ferrosilicon (silicon). The difficulties and impracticality of using vacuum in the carbon-thermal process and the important role of vacuum in the carbido- and silico-thermal processes. Explanation of the influence of vacuum in these processes from the thermodynamics and kinematics viewpoints.

Principles of calculating the vacuum system for vacuum furnaces and the selection of vacuum pumps for them.

Construction and operation of the furnace for the sublimation of magnesium from magnesium oxide by carbon-thermal reduction. Apparatus for the instantaneous cooling of the gas stream from the furnace and

for trapping the magnesium dust. Safety practices in the operation and servicing of the carbon-thermal furnace. Conversion of magnesium dust to pig metal by sublimation and remelting or pressing. Technical-economic indices for the carbon-thermal production of magnesium. The practice of the carbido- and silico-thermal processes. Furnaces with steel retorts, their operation and limitations. The conditions for magnesium condensation and the behavior of the alkali metals in this connection. Ideas on the construction of vacuum furnaces with a large production capacity. Soviet constructions of such furnaces. Technical-economic indices and calculations on the vacuum-thermal methods for the production of magnesium.

11. Comparison of the electrolytic and thermal methods for the production of magnesium and the perspectives for their future improvement and development. Methods for improving the production of magnesium. Cost of magnesium and methods for reducing it.

Section IV. BASIC EQUIPMENT AND THE ELEMENTS OF ALUMINUM AND MAGNESIUM PLANT DESIGN

Schemes of the apparatus used in the production of alumina, the electrometallurgy of aluminum and the metallurgy of magnesium. The basic principles and selection of apparatus-technological schemes and individual apparatus (equipment), incorporating the newest accomplishments of both domestic and foreign techniques. Calculation characteristics and the design of basic equipment for accomplishing the technological transformations involved in the production of alumina and in the metallurgy of aluminum and magnesium.

Understanding the three stages involved in the design of alumina, aluminum and magnesium plants: Design problem, technical design and working design. Selection of a plant site depending on the character of the technological process: The important role played by a close source of cheap electrical energy for the electrolysis plant and a close source of raw material for the alumina plant. Establishing the output (production capacity) of the plant. Selection of the proper power regime for the operation of a series of cells in the case of the electrolysis plants. Determination of the dimensions of the different sections. Arrangement of the equipment. Selection of ventilating means. Design of overall plant facilities (steam, water, transportation, electrical power). Skilled mechanics and repair men. Amount of space needed for warehouses and storage. The design of accessory partitions and installations. Typical general plans for alumina, aluminum and magnesium plants. Technical-economic calculations. Determination of capital expenditures, list of officials, fund for payments and expenditures for raw materials, fuel and electrical energy. Structure for the calculation of the production costs (alumina, aluminum, magnesium) of the designed plant.

Section V. COURSE PROJECT

The course project on the metallurgy of light metals is done by each student simultaneously with attending the lectures on the special

course. The problem assigned to each student taking the special course on design planning is a narrow technical problem on the technology of the production of alumina, the electrometallurgy of aluminum or the metallurgy of magnesium.

The course project consists in each student submitting a report on the individual problem assigned to him by the instructor, which report should contain the following: (1) Record of the calculations, and (2) two sheets of sketches, showing the designed apparatus (technological assembly) in 2-3 views on a scale of either 1/50 or 1/100. The calculation record (about 15-20 pages) should contain the following: (1) A short description of the essential details of the process operating in the designed apparatus, (2) computation of the principal dimensions of the apparatus, (3) the material and heat balances of the apparatus (assembly), (4) enumeration of the materials needed to build the apparatus, and (5) computation of the technical-economic benefits derived from the use of the designed apparatus (assembly) when compared with existing equipment.

After the course project has been accepted by the instructor, it is defended by the student at a meeting of the faculty on the metallurgy of light metals.

Section VI. LABORATORY EXERCISES

The laboratory exercises in the special course on the metallurgy of light metals consist in each student completing a short investigation, which will permit him to become familiar with the method and acquire practice in the running of experiments in one of the fields pertaining to the metallurgy of light metals.

The performed laboratory investigation is summarized in a report, in which is given a description of the apparatus, the conditions used in running the experiments, the obtained results, and the conclusions derived from them.

LITERATURE

Basic

Mazel, V. A., Production of Alumina, Metallurgical Press, 1955.

Belyaev, A. I., Rapoport, M. B., and Firsanova, L. A., Electrometallurgy of Aluminum, Metallurgical Press, 1953.

Strelets, Kh. L., Taits, A. J., and Guljanitskii, B. S., Metallurgy of Magnesium, Metallurgical Press, 1951.

Supplemental

Kasatkin, Processes and Apparatus of Chemical Technology, 1950.

Pavlov, K. F., and others, Examples for the Calculation of Chemical Apparatus, State Chemical Press, 1950.

Abramov, G. A., and others, Principles of the Electrometallurgy of Aluminum, Metallurgical Press, 1953.

Kuznetsov, S. I., and Epshtein, A. M., Electrolytic Production of Aluminum, Metallurgical Press, 1953.

Pazukhin, V. A., and Fisher, A. Ya., Vacuum Metallurgy, Metallurgical Press, 1955.

The program was approved by a conference of the professors and docents of the metallurgical institutes and faculties in May of 1955.

APPENDIX 11

THE INFLUENCE OF BORDER ZONES, CONTAINING LOW-MELTING COMPONENTS, ON THE RESULTS OF DETERMINING THE HEAT RESISTANCE OF ALLOYS WITH DIFFERENT DEFORMATION METHODS

Academician A. A. Bochvar, M. E. Dritz and E. S. Kadaner

(Izvest. Akad. Nauk SSSR, Otdel. Techn. Nauk, 1954, No. 2, pp. 42-45)

The important role played by the structure of alloys in creep processes at high temperatures has been indicated in a number of studies, published recently in both the Soviet and foreign literature.

Statements exist that the state of the boundaries and border grain layers exerts great influence on the creep resistance shown by alloys at high temperatures.

A rapid accumulation of experimental material for the development of a heat-resistance theory and the seeking of new heat-resistant alloys became possible due to the use of a number of accelerated heat-resistance test methods. Included in this number is the prolonged hardness method. With the aid of this method various investigators ran a large number of heat-resistance tests, which showed in the vast majority of cases a qualitative analogy with the results of determining the heat resistance by the tension method. However, in studying the heat-resistance of some alloys based on magnesium we found cases where the results of determining the heat-resistance by the prolonged hardness and tension methods showed a divergence. It was revealed that magnesium alloys, containing cadmium, are equal to known heat-resistant alloys with a magnesium base in the value of the prolonged hardness, but on checking the heat-resistance of these alloys by the tension method it was found that they show exceedingly large creep.

To determine the reasons for the observed discrepancy we selected for study, in addition to the cadmium-containing alloys, the magnesium-manganese alloys with tin and lead as additions, and having a structure similar to the structure of the Mg-Cd-Mn alloys. The microstructure of these alloys is shown in Figs. 1-3.

As can be seen from the presented microphotographs, the investigated alloys show a coarse dendritic structure of solid solution with a well-defined intracrystalline heterogeneity. In all cases the periphery of the grains and the branches of the dendrites are rich in the low-melting component.

It was interesting to determine whether the alloys, containing tin and lead, would show a behavior similar to that of the cadmium-containing alloys when tested for their heat-resistance.

In Tables 1 and 2 we give the compositions of the investigated alloys, the test conditions used, and the results of testing these alloys for their heat-resistance by the methods of prolonged hardness and tension.

These results show that the magnesium-tin-manganese and magnesium-lead-manganese alloys, similar to the magnesium-cadmium-manganese alloy, show a prolonged hardness that is in no way inferior to the prolonged hardness value of the heat-resistant magnesium alloy M7 (Figure 4). However, when the alloys containing the low-melting components, and the M7 alloy were tested for heat resistance by the tension method (with a load of 4.5 kg./sq. mm.) it was found that the M7 alloy shows a pronounced advantage in that its heat resistance is ten times that of the other investigated alloys.

TABLE I

PROLONGED HARDNESS OF MG ALLOYS

Alloy Composition, %	H_B (Kg/mm²), P = 100 Kg, D_{Ball} = 10mm					
	As Cast			S.H.T. or Aged		
	20°C 30 sec	300°C 30 sec	300°C 60 min	20°C 30 sec	300°C 30 sec	300°C 60 min
M7 (Base Mg Alloy)	36.7	17.1	10.0	38.3	17.2	10.25
Mg-10Cd-1.5Mn	29.7	12.9	8.7	25.2	14.3	9.7
Mg-2Sn-2.0Mn	24.8	14.8	10.7	29.0	13.8	11.55
Mg-1Pb-2.0Mn	26.0	12.7	8.8	26.4	15.9	11.0

TABLE II

HEAT RESISTANCE OF MG ALLOYS,
DETERMINED BY THE TENSION METHOD

Alloy Composition, %	Time Before Failure τ (hours); T_{Test} = 250°C	
	σ = 4.5 Kg/mm²	σ = 3.5 Kg/mm²
M7 (Base Mg Alloy)	100.0	-
Mg-1.5Mn	-	120.0
Mg-10Cd-1.5Mn	12.0	54.0
Mg-2Sn-2Mn	1.25	27.0
Mg-1Pb-2Mn	2.5	17.0

FIGURES 1 and 2

(1) Microstructure of Mg-10% Cd-1.5% Mn alloy (cast in sand).

Etchant 1% HNO_3, in alcohol, X 200

(2) Microstructure of Mg-2% Sn-2% Mn alloy (cast in sand).

Etchant 1% HNO_3 in alcohol, X 200

FIGURES 3, 4 and 5

(1) Microstructure of Mg-1% Pb-2% Mn alloy (cast in sand).

Etchant 1% HNO_3 in alcohol, X 200

(2) $\tau_{hrs.}$, 250°C
σ = 4.5 kg./sq. mm.

(3) H_B, kg./sq. mm., 300°C
P = 100 kg.

(4) T_{test} = 250°C
σ = 3.5 kg./sq. mm.

The influence of the low-melting elements cadmium, tin and lead on the heat-resistance of the binary magnesium-manganese alloy was studied at a load of 3.5 kg./sq. mm. (Figure 5). The results of these tests also quite convincingly show the negative effect of low-melting components on the heat-resistance of a binary alloy.

When the experimental data of the heat-resistance tests and the structure character of the investigated alloys are compared the following explanations of the reasons for the observed discrepancy in the results of determining the heat-resistance by the prolonged hardness and tension methods in the presence of low-melting components in the alloy can be given.

In the processes where the prolonged hardness of an alloy is tested the resistance offered by the alloy to imprint by the indenting agent is, evidently, mainly a function of the hardness of the base metal in the alloy, and to a lesser degree a function of the condition of the grain boundaries.

A completely different picture is observed when the specimen is exposed to prolonged stress at high temperatures. In this case the destruction of the specimen occurs predominantly along the grain boundaries.

The presence of intracrystalline heterogeneity in a solid solution can lead to a weakening of the grain border zones or of the dendrite

seams due to enrichment of these portions with the low-melting component and, as a result, can be the reason for the large creep shown by alloys when they are subjected to stress at high temperatures. At the same time the presence of thin low-melting interlayers in the alloy structure may not exert significant influence on the hardness.

The present investigation showed that alloys, containing low-melting elements in their composition and possessing a cast structure with well-defined intracrystalline liquation, are inclined to show a large creep, although this is not revealed by the prolonged hardness method.

Consequently, in seeking heat-resistant alloys it is out of the question to be limited only to the prolonged hardness method, which appears as a method for the preliminary qualitative selection of alloys.

It is impractical to use the tension method for testing the heat resistance of alloys having low prolonged hardness values; the alloys, showing excellent results when tested for heat resistance by the prolonged hardness method, should of necessity be checked by the tension method.

Paper received by the editor February 11, 1954

Appendix II

Таблица 1

Длительная твердость магниевых сплавов

Состав сплава, %	H_B, кг/мм², P = 100 кг, $Д_ш$ = 10 мм					
	литые			стабилизированные		
	20° 30 сек.	300° 30 сек.	300° 60 мин.	20° 30 сек.	300° 30 сек.	300° 60 мин.
М7	36,7	17,1	10,0	38,3	17,2	10,25
Mg — 10Cd — 1,5Mn	29,7	12,9	8,7	25,2	14,3	9,7
Mg — 2Sn — 2Mn	24,8	14,8	10,7	29,0	13,8	11,55
Mg — 1Pb — 2Mn	26,0	12,7	8,8	26,4	15,9	11,0

Таблица 2

Жаропрочность магниевых сплавов, определенная методом растяжения

Состав сплава, %	Время до разрыва τ, час, $T_{исп}$ = 250° С	
	σ = 4,5 кг/мм²	σ = 3,5 кг/мм²
М7	100	—
Mg — 1,5 Mn	—	120,0
Mg — 10 Cd — 1,5 Mn	12,0	54,0
Mg — 2 Sn — 2 Mn	1,25	27,0
Mg — 1 Pb — 2 Mn	2,5	17,0

марганец, обладают длительной твердостью, не уступающей по величине длительной твердости жаропрочного магниевого сплава М7 (фиг. 4). Однако испытания на жаропрочность (методом растяжения при напряже-

Фиг. 1. Микроструктура сплава Mg — 10% Cd — 1,5% Mn (отливка в землю).
Травитель 1% HNO_3 в спирте, × 200

Фиг. 2. Микроструктура сплава Mg — 2% Sn — 2% Mn (отливка в землю).
Травитель 1% HNO_3 в спирте, × 200

нии 4,5 кг/мм²) сплавов, содержащих легкоплавкие компоненты, и сплава М7 указывают на явное преимущество последнего, который оказался в десятки раз более жаропрочным.

Appendix II

Влияние легкоплавких элементов кадмия, олова и свинца на жаропрочность двойного сплава магний — марганец исследовалось при напряжении 3,5 кг/мм² (фиг. 5). Результаты этих испытаний также достаточно убедительно показывают отрицательное действие легкоплавких компонентов на жаропрочность двойного сплава.

Фиг. 3. Микроструктура сплава Mg — 1% Pb — 2% Mn (отливка в землю)
Травитель 1% HNO_3 в спирте, × 200

Сопоставляя экспериментальные данные испытаний на жаропрочность и характер структуры исследованных сплавов, можно дать следующее объяснение причины наблюдаемого несоответствия в результатах определения жаропрочности методами длительной твердости и растяжения при наличии в сплаве легкоплавких компонентов.

В процессах испытания сплава на длительную твердость сопротивление, которое оказывает сплав при вдавливании в него индентора, очевидно, зависит главным образом от прочности металлической основы сплава и в меньшей степени — от состояния границ зерен.

Совершенно иная картина наблюдается в условиях длительного растяжения образца при повышенных температурах. Разрушение образца в этом случае преимущественно происходит по границам зерен.

Наличие внутрикристаллической неоднородности твердого раствора может привести к ослаблению пограничных зон зерен или стыков дендритов вследствие обогащения этих участков легкоплавкой составляющей и, таким образом, может явиться причиной сильной ползучести сплавов в условиях растяжения их при повышенных температурах. В то же время наличие тонких легкоплавких прослоек в структуре сплавов может не оказать существенного влияния на величину твердости.

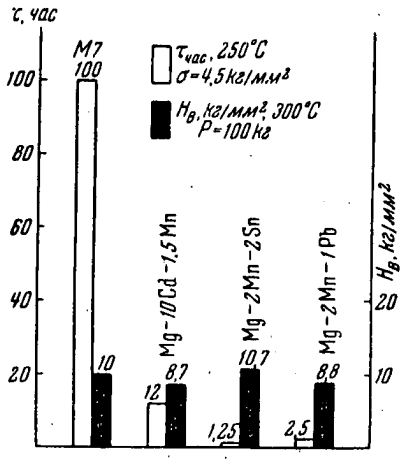

Фиг. 4

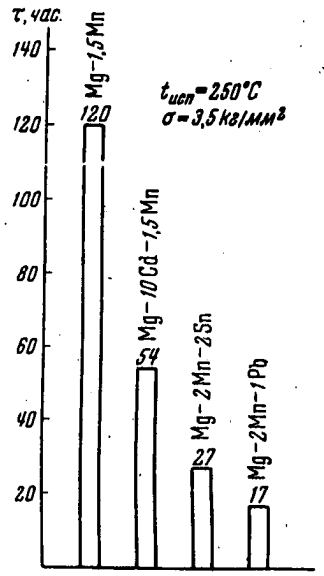

Фиг. 5

Проведенное исследование показало, что сплавы, имеющие в своем составе легкоплавкие элементы и обладающие литой структурой с явно

Appendix 12

THE INFLUENCE OF TEMPERATURE ON THE MECHANICAL PROPERTIES OF METALS AND ALLOYS

by E. M. Savitskii

Academy of Sciences of the USSR
The A.A. Baikov Institute of Metallurgy

Academy of Sciences of the USSR Press
Moscow 1957

454 Literature References, of which 369 are Russian

TABLE OF CONTENTS

Part II. Apparatus and methods of operation

2. Development of the apparatus and micromechanical test methods

In addition to establishing equipment for testing macro samples, a special apparatus for micro mechanical testing was developed, appropriated and utilized. Many efforts have been spent in this direction and a sufficiently good solution of the problem has been found. In the beginning work has been carried out only for substitution of tensile strength tests by shearing tests, as the latter require samples that are smaller and easier to prepare. A special device was developed by LFTI at the Academy of Sciences of the USSR for cutting out holes of 2 mm. diameter from a sheet 0.5 mm. thick. The idea of this device consisted in making a work diagram of shearing, based on registration of the punch (or stamp) movement as a function of load; from data of this diagram basic tensile strength characteristics can be calculated.

The first step of our work was investigating the possibility to use the LFTI device for physico-chemical analysis. Some experiments were carried out with copper-nickel alloys and magnesium alloys giving positive results (107). However, work with the LFTI apparatus has some substantial disadvantages, such as:

1. the necessity to have a special, fairly complex device in addition to the testing device, which can be adjusted only for one type of tests,
2. a very small surface of the tested sample (3 mm^2), due to which a slight variation of the composition, size of grain and amount of inclusions can give deviating results,
3. the necessity to interrupt the testing procedure for calculating the load.

Therefore it has been decided to carry out shearing tests with the "Gagarin" press, whereby several advantages were achieved: the special complex device became superfluous, the sample had a large surface (50 mm^2) and a large work diagram was recorded automatically (107). The device used for shearing tests is shown in Fig. 34.

Fig. 34. Adaptation of the Gagarin press for shearing tests. a. assembled, taken apart.

Sample 1 (thickness - 2 mm.) is placed on matrix 2 and pressed down by nut 3, which has an 8 mm. diameter opening serving as a guide for stamp 4. The assembled device is placed on a special table for the Gagarin press and the stamping of a 8 mm. hole 5 is carried out.

Tensile characteristics: proportionality limit, strength limit, actual strength limit and shrinkage can be calculated using corresponding simple formulas (107) and data recorded with the press in the shearing force = deformation diagram. Checking Cu - Ni, Cu - Zn and Mg alloys (over 100 samples) has shown that for not particularly brittle alloys, the correlation between shearing and tensile strength tests is good, particularly for the strength limit.

Shrinkage values of magnesium alloys brittle at regular temperatures were somewhat low when determined by shearing force tests. For 60 Cu-Zn-Al alloys the correlation coefficient was found to be 0.93 and the average ratio of the strength limit in tensile strength tests and the strength limit in punching tests is 0.63. Values obtained for Cu-Ni alloys which form a continuous series of solid solutions are shown in Fig. 35.

It should be noted, that for determining mechanical properties of 11 Cu-Ni alloys by means of shearing strength tests in the Gagarin press, only 175 gr. net weight samples were needed, whereas standard tensile strength tests require not less than 4 kg. of prepared samples. In addition, the relation between tensile strength limit and Brinell hardness was determined for forged and annealed Cu-Ni alloys. Mean proportionality coefficient in this case was found to be 0.54, being 0.6 for Cu and 0.5 for Ni. Normal elasticity modulus for alloys of this system was determined according to the method of E. M. Rosenberg (105) by pressing a small ball at different loads (Fig. 36). The values were in good agreement with those obtained by standard tensile strength tests.

Fig. 36. Normal elasticity modulus of Cu-Ni alloys. Abscissa: % Ni, Ordinate: E 10^4.kg./mm^2.

The next step of the work was to show the possibility of testing micro samples for breaking in regular testing machines (136). To increase the accuracy of the load calculation it is desirable to use low power machines. If the expansion of the machine can be used only for gripping the micro sample, it is necessary to make special clamps. If it is a compression machine only (such as the Gagarin press) a reverser of the Gagarin type could be used for tensile tests, but it should be reduced to a corresponding size. If testing machines are not available, the load used on the sample can be sand, water or pellets in a special device (Fig. 37). This is feasible as the maximum load for breaking even of a steel micro sample (of 1 mm. diameter) does not exceed 50-60 kg. at room temperatures.

Fig. 37. Schematic presentation of the arrangement to carry out breaking tests with micro samples (E. M. Savitskii and V. P. Lebedev):

1 - cylinder; 2 - punch; 3 - reverser with a sample; 4 - bin.

Fig. 35. Change of temporary resistance to breakage and the transverse shrinkage of alloys of the system Cu - Ni (E. M. Savitskii and N. P. Slavina). Abscissa: % Ni, Ordinate: σ_B.kg./mm^2 and shrinkage in %.

Part II. Apparatus and methods of operation

3. Universal apparatus for micromechanical tests

As the result of much experimental work with microspecimens we were able in the last several years to build, put into practice and improve a simple, but universal apparatus, which permits making micromechanical tests by all of the principal methods of loading an axial force at ordinary, high and low temperatures in the air, in vacuum or in protective media /137, 138/. The apparatus consists of a plate 1 to which is fastened a cylinder with recessed base 2, inside of which are placed a polished cylindrical cushion 3 from tempered steel or plate (?) and a plunger 4 with a changeable tip 5, moving under the action of the particular loading device. The tested microspecimen 6 is placed between the tip and the cushion. The vertical movement of plunger 4 is measured with either an indicator or an optimeter connected to the head of the plunger, with an accuracy of either 0.01 or 0.001 mm., respectively.

To visually observe the deformation of the specimen during testing it is necessary to make the cylinder of the apparatus from transparent material. A ribbed plunger can be used to reduce the friction between the plunger and the cylinder walls. Not only microspecimens, but also specimens of larger dimensions can be tested in the apparatus. The size of the specimen, subjected to testing in the apparatus, is limited only by the dimensions (diameter and height) of the working area in the cylinder of the apparatus and the diameter of the plunger, which, generally speaking, can be made in any size desired, even quite large. Not only specimens of metals and alloys, but also many nonmetallic materials (plastics, etc.) can be tested in the apparatus.

Loading of the Apparatus. We knowingly avoided including in the construction of the apparatus any loading device, since this would have greatly complicated the apparatus and would have made it more expensive. Also there is no great need for this, for the reason that the stock of testing machines, found in plant and institute laboratories, is quite sufficient to run the testing in a wide loading interval. To load the specimen and measure the deformation load during testing it is necessary to place the apparatus between the compression faces of the testing press in such a manner that the head of the plunger is in contact with the top face, while that portion of the plate, to which the cylinder is fastened, should stand on the bottom face. It is desirable to run the testing of microspecimens on a low-capacity machine, since this increases the accuracy of the load readings during testing. In the absence of machines of lower capacity the testing can be done on a Gagarin press or on IM-4A and IM-4P machines. In case the machine operates only for stretching, then it is necessary to place the apparatus in an ordinary reverser, which converts the stretch into compression. In case of need, it is possible from the readings of the force measurement device on the machine and the apparatus indicator to construct in the ordinary manner a working diagram of the testing. In the absence of testing machines the apparatus can be loaded by means of extremely simple devices (see Fig. 37).

The modification shown in Fig. 38 for loading the apparatus is more convenient, especially for the tests that require comparatively large loads (for example, compression tests at ordinary temperatures). The loading is done with screw 7, which is made to move manually, by means of nut 8, conical gear 9 and handle 10. The loading is measured with dynamometer 11, placed between the heel of the screw and the plunger head. Resilient (spring) dynamometers reading 100, 200 and 300 kgs. are most suitable for this purpose. As a result, not only the loads corresponding to the yield strength can be determined, but also those corresponding to the yield point and the breaking point.

Tests on the apparatus can be run not only under the influence of static, but also of impact loads.

Testing With Various Methods of Loading. The proposed apparatus can be used for nearly all of the principal mechanical testing methods (compression, stretch, hardness determination, bending, shear, crumpling, twisting, punching, etc.), and also for some technological tests and the preparation of microspecimens.

The transition from one test method to another is accomplished very simply. For example, to transfer from compression testing to determination of the hardness it is sufficient to replace the flat tip, screwed into the lower end of the plunger, by a tip fitted with a ball (to determine the Brinell hardness), a cone (to determine either the Rockwell or the Kubasov hardness), or a pyramid (Vickers hardness). To run other test methods (for stretch, bending, shear, etc.) it is necessary to place in the working area of the cylinder sundry simple devices for mounting the specimen. In some cases it is also necessary to change the tip of the plunger. A brief description of the manner in which the proposed apparatus can be used to run the various test methods is given below.

Compression Testing. The manner in which the compression tests are run is obvious from the scheme of the apparatus (see Fig. 38). The test specimen 6 is placed in cylinder 2 on the polished cushion 3. The specimen is deformed (compressed) by means of plunger 4 and the degree of deformation is measured with the aid of the indicator. In the given case the plunger tip 5 is a flat polished disk, fabricated from tempered steel. Any of the methods described above can be used to load the specimen and measure the load. To test materials of low plasticity by the method of nonuniform compression in all directions it is first necessary to press the specimen into a collar of a more plastic material /85/.

The specimen taken for compression testing can, generally speaking, be of any shape. It is best to take, as is usually done, cylindrical specimens with a height to diameter ratio equal to 1.5-2.5. Spherical specimens can also be taken, but they are harder to prepare.

A great advantage of compression testing is the fact that a specimen of any dimensions can be taken, since it does not require any special method of mounting (clamping, etc.) and is held between the plunger tip and the cushion by external friction forces. Here it should be

kept in mind that in the case of using very small specimens, due to an increase in the relative surface, the role played by the surface energy shows substantial increase, and the values of the strength and plasticity characteristics, when compared with those obtained for larger specimens, are somewhat high. Consequently, for compression tests it is advisable to use specimens with a diameter of at least 1 mm. The testing is best done up to the point where the first crack appears on the specimen, since this shows the maximum store of strength and plasticity possessed by the material. But such tests require a much larger expenditure of specimens.

Compression tests (or pressing) make it possible to immediately distinguish between a plastic and a brittle material. Specimens of a very brittle material (manganese, quartz, etc.) immediately crumble into a powder when a certain load is reached in the testing process. Here the needle of the force measuring device on the machine and of the indicator return to zero, and at times a snap is heard in the apparatus.

As is known, specimens of less brittle materials (magnesium, cast iron, etc.) shear at an angle of 45° to the vertical axis of the specimen when a certain value of the load and of the deformation is reached during compression. Specimens from plastic materials (copper, aluminum, Armco iron, etc.) are converted into disks during compression. The more plastic the material, the more shrinkage it can stand before cracks appear along the edges of the obtained disk.

The usual formulas are used to calculate the numerical values of the plasticity and strength of microspecimens.

Hardness determination. The proposed apparatus permits determining the hardness of a material by any method that is based on embedding a tip made from a harder material (steel, ? , diamond) into the test specimen.

The most widely used methods to determine the hardness (according to Brinell, Rockwell and Vickers) are all based on this principle. As had already been indicated, modification of the apparatus to determine the hardness reduces to changing the tip of the plunger. Any specimen, having two parallel surfaces (one of them cleaned) and fitting into the working area of the cylinder, can be taken to determine the hardness.

A great disadvantage of all of the existing apparatus for determining the hardness is the fact that the testing can be done only with certain degress of loading for each apparatus. This limitation is not present in the proposed apparatus, and the hardness can be measured with any load placed on the plunger. During testing the depth of penetration of the tip into the specimen can be measured with the aid of the indicator, which to a known degree is a measure of the plasticity of the material under a given load. On conclusion of testing the diameter of the imprint or the length of its diagonals is determined in the usual manner by means of either a Brinell magnifying glass or a measuring microscope. Standard formulas or tables are used to calculate the hardness values of a material, measured by the various methods.

Stretch Testing. The testing of microspecimens for stretch in the universal apparatus (see Fig. 38) is also accomplished very simply by the expedient of using a reverser of the Gagarin type, reduced to suitable dimensions (see Fig. 37). In this case the reverser with contained microspecimen is placed in the working area of the apparatus between the plunger and the cushion. Here a flat plunger tip is used. The testing is done in the usual manner. The magnitude of the deformation force is recorded by the reading of the force measuring device on the machine, while the magnitude of deformation (elongation) is recorded by the reading of the apparatus indicator. In addition, the deformation values (relative elongation of the specimen and the reduction in its cross-sectional area) are calculated by the usual formulas on the basis of measuring the dimensions of the specimen before and after failure. In measuring the microspecimens it is preferable to use a measuring microscope with an accuracy of 0.01 mm. In case of need, the same as for the case of compression, a working diagram of the stretch tests and the curves of the actual stresses can be constructed.

The most satisfactory specimen for microrupture is a specimen with heads, a diameter of 1 mm. for the working part, and a nominal length of 5 mm. In case of need a specimen without heads, in the form of a wire, can also be fastened in the reverser. For this it is necessary to alter in suitable manner the clamping jaws in the reverser, for example, on the type of a drill press chuck, or to make notched jaws.

When tested on steel, copper, aluminum and some nonferrous alloys it was found that the values of the strength and plasticity characteristics for the specimens that had been subjected to microrupture on the universal apparatus were 5-10% higher than those obtained for normal specimens. This is explained by the influence of the scale factor and is customary for micromechanical tests /132/.

Testing for Bending and Shear. Bending tests (on one, as well as on two fulcrums) can easily be run in the described apparatus.

To mount the specimen it is convenient to use a reverser, similar to the Gagarin reverser for flexing, but naturally of a smaller size. It is necessary to install a suitable tip in the plunger of the apparatus, being a flexing plunger for the microspecimen. The needle readings of the apparatus indicator will obviously correspond to the value of the bending deflection. The magnitude of the bending moment can easily be calculated from the readings of the force measuring device on the machine. In case of need, the indicated adaptation in somewhat modified form can be used to slit specimens into sections. To run shear tests on two sides it is necessary to introduce into the working area of the apparatus a suitable attachment with the specimen laid in it. Either a cylindrical or prismatic specimen is used. The plunger of the apparatus should have a tip suitable for the given case.

Hole Cutting and Crumple Testing. For this type of testing a suitable miniature attachment should be installed in the working area of the apparatus. The apparatus can be used to cut holes in sheet material with measurement of the force and deformation, and also to make crumple tests (for the crumple tests the matrix is replaced by a flat cushion).

If necessary, then the obtained data on the stamping properties can be compared with the mechanical characteristics of the material during stretching, as is recommended by some authors /106-109/. In the given case the dimensions of the test specimen depend only on the diameter of the plunger tip and of the matrix, which in turn depend only on the technical possibilities of making a plunger and a matrix with a very small diameter (for example, 0.1 mm.).

It is recommended that the ratio of the plunger diameter to the thickness of the test specimen be taken equal to four.

Determination of the Flow Pressure. The principle of this test is apparent from the scheme (Fig. 39). In case a very small amount of material is available, to reduce the size of the press surface it is expedient to use a detachable matrix and complete the pressing with a conical plunger.

Preparation of Specimens for Microrupture Tests. The apparatus permits obtaining specimens for microrupture tests by the use of a single pressure treatment (pressing). This completely excludes the possibility of obtaining any waste, which is unavoidable when the specimens are prepared by cutting. To prepare the microspecimen it is sufficient to spread both ends of a uniform cylindrical wire, which can then be pressed in the apparatus. Here the contours the dimensions of the stamp should correspond to the shape and dimensions of the heads on the microspecimen. The microspecimen can also be made by several other methods. The necessary amount of material in the form of a powder or as a small ingot is placed in the cylinder (see Fig. 39) and extruded as a wire. The obtained press heel 1 can be one of the heads of the microrupture specimen. To obtain the other head it is sufficient to turn the microspecimen (wire with the press heel) by 180° and then by depressing the plunger 2 to spread the other end of the wire. Prior to this it is expedient to place the wire with the press heel in a suitable die.

Twist Testing. The proposed universal apparatus can also be adapted for running twist tests (Fig. 40).

Specimen 1 is cylindrical in shape, with an indentation on both ends for mounting in cushion 2 and in the tip of plunger 3. Other methods for mounting the specimen can be worked out. To avoid turning the gland together with specimen is slipped on the spindles 5, which are mounted either in the bottom of cylinder 4 or in the lower plate 6 of the apparatus. The specimen is loaded manually by turning the plunger with the aid of handle 7, attached to its head. The deflection angle of the plunger is measured with the aid of pointer 8, attached to the head of the plunger, and reading in angular divisions on scale 9. Unfortunately, measurement of the torque in the given apparatus presents some difficulties. Under these conditions the testing for twist is, essentially, a technological test. Taking into consideration the fact that testing for twist is a quite rare test method, which is used only in special cases, it seems hardly practical to design a special construction for measuring torque, although this can be done if necessary. In this connection the work of P. D. Novokreshchenov and I. E. Markova

should be kept in mind, who used the electromagnetic method to make very precise torque measurements /215/.

Determination of the Pressure in the Compression of Powders. The apparatus can also be used for the compression of powders with measurement of the amount of force needed for this. The need for such a test can arise in the creation of a technology for the fabrication of articles from costly or rare metal powders by the metalloceramic method. The compression testing scheme is used to compress the powders in the apparatus. If the amount of powder is very small, it is not poured directly into the cylinder of the apparatus, but instead it is placed in a small cylinder specially made for this. For convenience in unloading the cylinder it is expedient to make it without a bottom or with a false bottom. It is understood that in this case the tip of the plunger should have a diameter that corresponds to the diameter of the small cylinder. The small cylinder with contained metal powder is placed in the working area of the apparatus on the cushion. The magnitude of the compression force can be determined by reading the force measuring device on the press. To calculate the magnitude of the stresses in the pressed material it is necessary to divide the maximum pressure by the working area of the cylinder in which the powder is contained. Much is also learned from determining the properties, and even a simple examination, of the compressed specimen removed from the cylinder. If the high-temperature modification of the apparatus described below is used, then besides the compression of powders, it can be used to roast (sinter) the obtained conglomerate or to run the pressing at elevated temperatures.

As a result, the indicated apparatus permits determining the optimum technology (temperature, pressure) for the fabrication of articles by the metalloceramic method with a total loss of only several tenths of a gram of powder.

From the given description of the principal methods used to test a material, which can be run on the proposed apparatus, it can be seen that the apparatus is of a universal nature, and in case of need it can be used to run still other test methods, not described here. Substantial changes in the apparatus construction are not needed for this.

Passing over to a description of the apparatus modifications for testing at either elevated or low temperatures, in protective media or in vacuum, it should be mentioned that all that has been said above on the individual test methods at room temperatures also retains its significance here. The fabrication of special tips and attachments is not required.

Modification of the Apparatus for Testing at Elevated Temperatures. Those working in the field of materials testing know how complicated the apparatus becomes when the testing has to be done at elevated temperatures. In general, for some types of testing an apparatus and method for testing at high temperatures (testing of microspecimens, testing for twist, flexing, etc.) has not yet been developed.

A special, very great virtue of the described apparatus is the ease with which tests at elevated temperatures can be run on it. For this it is sufficient to place the cylinder of the apparatus, together with contained sample and the plunger tip, in a suitable furnace. But it is even more practical to design the cylinder in a shape suitable for heater winding, i.e. in the shape of a bobbin. The apparatus modification for testing at elevated temperatures is shown in Fig. 41. To increase the accuracy of measuring the temperature the thermocouple 2 should be inserted in a special opening in the cushion support or in the plunger tip. The water-cooled guide sleeve is necessary to prevent sticking of the plunger in the cylinder when the heating is in an air atmosphere. It is preferable to make the cylinder of the apparatus from stainless steel, and the cushion and plunger tip from ? The permissible upper temperature limit of testing on the apparatus is determined only by the heat strength and heat stability of these parts. The order of testing is as follows. The apparatus is assembled in the usual manner, then the electric heater (furnace) is connected and, after the specimen has been kept at the desired temperature for the necessary length of time, the indicator pointer on the apparatus is set at zero. Then the test is run. The tests themselves, by all of the methods described above, remain exactly the same as when run at room temperature.

It is interesting to mention that when sufficiently large specimens are used this modification of the apparatus can also function as a dilatometer, since changes in the specimen length as a function of the heating or cooling temperature (without loading) can easily be determined by the readings of the indicator pointer (with an accuracy of 0.01 mm. or even 0.001 mm.). In addition, the apparatus permits making measurements, which, in general, have apparently not been made up to now, and specifically, a quantitative measurement of the magnitude of the internal stresses, arising in a material during phase, and in general, any other transformations, which occur with a change in the volume (allotropic and other transformations /216/). For this the apparatus with specimen should be heated on the testing machine with the faces of the latter brought up close to the apparatus. Heating of the specimen, especially after transition through a temperature of some sort of transformation, will cause the specimen to expand. This will be hindered by the plunger, the head of which rests against the upper face of the machine. As a result, the expanding specimen will transmit its pressure through the plunger and faces on the force measuring device of the machine, which will then be deflected in accord with the pressure shown by the specimen. As a result, the apparatus permits studying the influence of one of the most important state-temperature factors, both on the mechanical properties of the material, and on the transformations that take place in it in the solid state. The apparatus can also be used to study the influence of pressure on the transformations taking place in a solid material at various temperatures.

Modification of the Apparatus for Running Tests at Low Temperatures. This modification of the apparatus (Fig. 42) differs from the high-

temperature modification shown in Fig. 41 only in that in the area, surrounding the cylindrical portion of the cylinder bobbin, instead of a heater, dry ice or a cooling liquid 1, for example, liquid nitrogen, is introduced. In accord with the properties of the liquid coolants known up to now it is possible to run tests in the apparatus down to temperatures of the order of -200°.

Modification of the Apparatus for Testing in Protective Liquid Media. Some materials, for example, the alkali and alkaline-earth metals, are rapidly oxidized in the air and consequently cannot be subjected to testing without adopting special protective measures. Based on our experimentation the testing of such materials is conveniently and reliably run in protective media, which can be certain liquids that are both inert toward the given substance and transparent. For example, for the mentioned metals such liquids are toluene, kerosene, etc. The testing of aluminum and copper alloys up to 450° can be run in saltpeter. Many other materials can be protected from oxidation at high temperatures by immersion in a bath composed of molten salt mixtures, representing the chlorides and fluorides of some of the alkali metals.

This modification of the apparatus differs from the main modification only in that the specimen is placed in a small bath with the protective liquid, while the tip of the plunger is taken of such a diameter as to permit its entrance into the bath (Fig. 43).

The placing of the bath in the cylinder and its removal can be easily accomplished with the aid of a special key, which can enter into the slots made for this in the upper part of the bath.

The use of protective media permitted us to determine on this apparatus, apparently for the first time, the mechanical properties of a number of metals, for example, the alkaline-earth metals, and to show that in the order of decreasing strength they can be arranged as follows: Ca, Sr, Ba. As regards plasticity these metals are arranged in the opposite order.

The actual stress curves for the case of compressing these metals at room temperature are shown in Fig. 44.

Cylindrical specimens (1 x 1 mm.) were taken for the compression tests. The experiments were run in toluene. The hardness (using a cone) of calcium is 13.2 kg./sq. mm., while that of barium is 5.5 kg./sq. mm. From calcium in a protective medium at room temperature we were able to extrude a wire, having a diameter of 1 mm. and a length of about 15 mm. The flow pressure at 75% deformation was about 90 kg./sq. mm.

In case it is impossible to find a protective liquid that is completely inert toward the material (it is quite difficult to find such media for high temperatures), then the testing has to be done in an inert gas (for example, argon or helium) or in vacuum.

Modification of the Apparatus for Testing at High Temperatures in Vacuum or in an Inert Gas Atmosphere.

This modification of the apparatus mainly differs from the high-temperature modification (for testing in the air) shown in Fig. 41 only in the fact that the whole working area of the apparatus is found in a hermetically sealed steel jacket (Fig. 45).

Other than the sealing requirements that apply to any vacuum assembly, no essential changes are made in the construction of the apparatus, with the exception of using a sylphon 1 and spring 2. The use of a sylphon (corrugated tube made from either brass or steel) successfully solves the problem of transmitting into the vacuum area the forward movement of the plunger without upsetting the achieved degree of vacuum. Other methods can probably be used to solve this problem, for example, the use of rubber-metal stuffing boxes. But on the basis of the existing experimental work done with the apparatus it may be considered that the problem is best solved by the use of a sylphon. Spring 2 is needed to compensate for atmospheric pressure. If this spring is absent the sylphon, after evacuation, contracts under the influence of atmospheric pressure, and its shrunk corrugations prevent the free movement of the plunger during testing. The introduction of an external cooling jacket is due to the use of rubber seals for bringing out the leads from the furnace and thermocouple. In the absence of cooling the jacket of the apparatus will become hot from the furnace, and the rubber may burn. When operating in vacuum it is best to fabricate the carcass of the electric furnace from quartz, since any ceramic material when heated will evolve gases and reduce the vacuum. In the described apparatus it is comparatively easy to obtain with either a vacuum-force of a diffusion pump a vacuum of the order of either 10^{-4} or 10^{-5} mm. In special cases, for an even greater reduction in the possibility of oxidation, the burning of various materials (strontium, barium, etc.) in the apparatus can be specified.

The described modification of the vacuum apparatus can be used not only at temperatures that it is possible to obtain with ordinary heaters (nichrome, Alloy No. 2), but also for operation at higher temperatures, where as heaters in the electric furnace it is possible to use such metals as, for example, tungsten, molybdenum or tantalum. It is quite obvious that in this case supplemental measures to protect the heaters from oxidation are not required.

When working with ordinary heaters the vacuum area of the apparatus can be reduced due to removal of the heater from it. As a result of this the scheme of the apparatus is greatly simiplified (Fig. 46), and the degree of vacuum is increased.

When the testing is done in vacuum it is necessary to first calibrate the empty movement of the plunger, and the amount of force needed for this is to be substracted from the reading of the machine force measuring device during experiment.

The transition from testing in vacuum to testing in an inert gas substantially reduces the sealing requirements, the cooling of the jacket, etc. In this case the need for spring 2 disappears, but still another opening should be made in the outer jacket of the apparatus for escape of the gas. A reduction in the quality of sealing the system when operating with this modification leads only to some increase in inert gas expenditure due to its escape from the apparatus.

The order of operating the apparatus when using an inert gas or when operating in vacuum is as follows: the specimen, laid in an attachment suitable for the type of test involved, is placed in the working area of the cylinder. The upper part of the apparatus, consisting of the cover with cooling connection and the plunger with sylphon, is fastened to the cylinder by means of bolts. After this the vacuum pumps are started or the inert gas is supplied to the system. Then the electric furnace is turned on, and the sample is heated to the desired temperature. After the lapse of the necessary holding time the specimen and apparatus are finally ready for running the test. The rest of the testing sequence remains exactly the same as had already been described for the case of testing at room temperature.

The general appearance of the vacuum modification of the apparatus with loading device assembly is shown in Fig. 47.

Some Experimental Data. Of the voluminous amount of experimental data, obtained in working with the universal apparatus, in the nature of an example only the results obtained in determining the mechanical properties of copper-nickel alloys can be presented here.

Copper and nickel, as is known, show unlimited solubility in each other in both the liquid and solid states. The data, obtained by us on microspecimens, characterizing the mechanical properties of these alloys are shown in Fig. 48.

In their time N. S. Kurnakov and Ya. Rapke measured the Brinell hardness of these alloys and established that the hardest alloys in this system are found in the region of 40-60 wt. % nickel /10/. Measuring the hardness of these alloys on microspecimens by the method of cone indentation made it possible for us to refine this region and show that the alloy with a 60% nickel content is the hardest. The testing of microspecimens of these alloys for compression shows a similar nature of the curves for resistance to deformation and plasticity. In the given case as a measure of the resistance to deformation we took the amount of load, necessary to compress a cylindrical microspecimen (diameter and height each 1 mm.) to the extent of a 50% reduction in height; the measure of plasticity was taken as the relative amount of contraction shown by the indicated specimen when compressed by a load of 100 kg. It should be mentioned that to test eleven alloys of this system for compression by both modifications required a total pure specimen weight of 0.2 g.

The testing of specimens for microrupture also confirms the nature of the hardness, strength and plasticity curves during compression. The addition of nickel to copper, or the reverse, of copper to nickel,

results in an increase in the strength of the alloys, while the plasticity decreases. The highest yield strength is possessed by the alloy with 60% nickel. The weight of eleven microrupture specimens from various copper-nickel alloys was about 1.5 g. To obtain reliable data on all of the principal mechanical properties (hardness, determination of plasticity, and the strength during compression and stretch) of the whole system required only about 2 g. of pure specimen weight.

Since the universal apparatus in the form described here was developed quite recently, its advantages could not be fully utilized at the time this was written.

FIGURES

Fig. 37. Scheme of the apparatus for the rupture of microspecimens (E. M. Savitskii and V. P. Lebedev):
1 - cylinder; 2 - plunger; 3 - reverser with specimen; 4 - hopper.

Fig. 38. Scheme of the universal apparatus for testing at ordinary temperatures (the arrow points in the direction of the indicator):
1 - plate; 2 - cylinder; 3 - cushion; 4 - plunger; 5 - plunger tip; 6 - specimen; 7-10 - loading device; 11 - dynamometer.

Fig. 39. Scheme of the attachment for determining the flow pressure:
1 - press heel; 2 - plunger.

Fig. 40. Scheme of the apparatus for testing the torque:
1 - specimen; 2 - cushion; 3 - plunger tip;
4 - cylinder; 5 - spindle; 6 - bottom plate;
7 - handle; 8 - pointer; 9 - scale.

Fig. 41. Modification of the apparatus for testing at elevated temperatures:
1 - specimen; 2 - thermocouple; 3 - cylinder;
4 - plunger; 5 - electric furnace; 6 - guide sleeve.

Fig. 42. Scheme of the apparatus modification for testing at low temperatures:
1 - cooling liquid.

Fig. 43. Modification of the apparatus for testing in protective media:

1 - specimen; 2 - bath; 3 - protective liquid.

Fig. 44.

(1) Curves for the actual stresses in the compression of alkaline-earth metals.

(2) Actual stresses, kg./sq. mm. (3) Relative contraction, %

Fig. 45.

(1) Modification of the apparatus for testing at high temperatures in vacuum or in an inert gas atmosphere (E. M. Savitskii).

(2) Water (3) For the inert gas (4) Thermocouple

(5) To pump

Fig. 46.

(1) Another modification of the apparatus for running micromechanical tests in vacuum or in an inert gas atmosphere (E. M. Savitskii).

(2) Water (3) for the gas (4) To pump

Fig. 47. General appearance of the apparatus with loading assembly (vacuum modification).

Fig. 48.

(1) Mechanical properties of alloys of the copper-nickel system: a - hardness: H_K - hardness using a cone, h - the depth of cone indentation; b - mechanical properties when compressed; c - mechanical properties when stretched.

(2) Load, kg. (3) H_K, kg./sq. mm. (4) σ_B, kg./sq. mm.

(5) Contraction, %

LITERATURE CITED

/10/ N. S. Kurnakov, Collection of Selected Works, Vol. I, Moscow-Leningrad, United Sci.-Tech. Press, 1938; Vol. II, Moscow-Leningrad, State United Sci.-Tech. Press, 1939.

/85/ B. D. Grozin, Mechanical Properties of Tempered Steel, Moscow, State Sci.-Tech. Press for Machine Construction Literature, 1951.

/106/ E. M. Shevandin, Factory Lab., 12, No. 7-8 and 9-10 (1946).

/107/ E. M. Savitskii and N. P. Slavina, Bull. Acad. Sci. USSR, Div. Chem. Sci., No. 2 (1943).

/108/ S. M. Golovin, Monograph of Studies on the Treatment of Nonferrous Metals, No. 2, Moscow, Metallurgy Press, 1941.

/109/ A. I. Chipizhenko, Collection of Scientific Papers of the State Institute for the Planning of Nonferrous Metal Processing Plants, Vol. 14, Moscow, Metallurgy Press, 1952.

/132/ I. M. Roitman and Ya. B. Fridman, Micromechanical Method of Metal Testing, Moscow, State Press of the Defense Industry, 1950.

/137/ E. M. Savitskii, Author's Certificate No. 78,001 (1949). Patent Bulletin, 11, 54 (1949).

/138/ E. M. Savitskii, Factory Lab., 16, No. 11 (1950).

/215/ P. D. Novokreshchenov and I. E. Markova, Factory Lab., 14, No. 7 (1948).

/216/ E. M. Savitskii and V. F. Terekhova, Proc. Acad. Sci. USSR, 87, No. 5 (1952).

Part IV. Study of the influence of temperature on the mechanical properties of metal alloys

Chapter I. The mechanical properties of alloys in systems of the eutectic type as a function of the temperature

System Magnesium-Silicon

The alloys based on Mg_2Si bear great interest for the reason that the carrier is a light, very hard, high-melting compound. The alloys, having their composition between Mg_2Si and magnesium, begin to melt at 645°, and those lying between Mg_2Si and silicon begin to melt at 920°, (Fig. 115). Magnesium silicide has a complex cubic face-centered lattice of the fluorite type (Fig. 116). On the

FIGURE 115

(1) Equilibrium diagram, mechanical properties and thermal electromotive force $\frac{\alpha}{Cu}$ of Mg-Si alloys

The additive hardness line is shown by the dotted line

basis of determining the electron density, N. V. Ageev and L. N. Guseva classified Mg_2Si as belonging to the coordination compounds /355b/.

The mechanical properties of the alloys in the region of Mg_2Si had hardly been studied before our investigations. The specimens used in our experiments were prepared by fusion and by the metallo-ceramic method. The fusion was run in a high-frequency furnace in a graphite crucible under a caranallite flux. The cast specimens had many pores. To increase the density they were subjected to a force of 20 tons at 620-630° in a steel cylinder with an internal diameter of 22 mm. Measurement of the microhardness of the magnesium silicide revealed that it was a total of 450 kG./sq. mm., although, considering that this compound is relatively high-melting (about 1200°), a greater hardness value could have been expected. The microhardness of the Mg_2Si + Mg eutectic is about 75 kG./sq. mm., while that of the Mg_2Si + Si eutectic is about 190 kG./sq. mm. The microstructure of a typical cast alloy, composed of crystals of magnesium silicide and eutectic, is shown in Fig. 117, a.

The hardness of the specimens was measured at 20, 300 and 600°. A cone with a load of 30 kg. was used to make the measurements.

To determine the plastic flow under compression the alloys were subjected to a force of 2 tons at the "corresponding" temperatures (563 and 800°), representing 90% of the melting point on the absolute temperature scale.

The testing was done in an argon atmosphere, since the alloys underwent strong oxidation at elevated temperatures.

FIGURE 116

(1) Crystal lattice of Mg_2Si /228/.

After compression in a container the thermal electromotive force of the cast alloys in pair with copper was measured. An apparatus, build by N. Kh. Abrikosova, was used to make the measurements. The difference in the temperatures of the cold and hot junction varied from 20 to 390°. The t.e.m.f. was calculated by the formula: $$\alpha = \frac{\Delta E_{Cu-x}}{\Delta t},$$ where Δt is the temperature difference between the cold and hot junction; E_{Cu-x} is the t.e.m.f. of the specimen in pair with copper; and α is the thermal electromotive force in microv. per 1°.

The experimental data are given in Table 34 and plotted in Fig. 115.

As can be seen, the conclusions, made on the example of the aluminum-silicon alloys relative to the important influence exerted by crystal boundaries on the hardness, also proved to be valid in the present case. On both sides of the compound the linear function rule fails to be observed.

Thus, the hardness of the alloy with 35 wt. % of silicon (containing about 75% magnesium silicide by volume) is only 130 kG./sq. mm. at 20°, instead of the expected 400 kG./sq. mm.

The alloys containing less than 35% Si, for which a comparatively soft magnesium eutectic is located along the grain boundaries of the compound, are characterized by a relatively low hardness at all temperatures (up to 133 kG./sq. mm.). The alloys, in which the eutectic contains free silicon, are characterized by a high hardness.

The comparatively high values of the hardness for the alloys, lying adjacent to the compound, is apparently explained by the fact that in them the eutectic inclusions do not completely fill the crystal boundaries of the compound. The hardness of the alloy containing 36.5% silicon is close to being additive (332 kG./sq. mm.).

When heated the relative reduction in the hardness is greater for Mg_2Si than it is for the alloys, but still the values of the hardness at 600° remain quite high (180 kG./sq. mm.). The alloys with a substantial amount of silicon (40 and 45%) also retain high hardness values at 300 and 600°. The alloys based on Mg_2Si differ by showing a low plastic flow under compression (of the order of 2%). The alloys, containing substantial inclusions of the comparatively soft magnesium eutectic (up to 35% Si inclusions), are much more plastic at elevated temperatures (up to 40% at 600°). As a result, the change in the plasticity of the cast specimens proceeds in the opposite direction to the change in the hardness.

FIGURE 117

(1) Microstructure of magnesium-silicon alloys. X150.

a--30% Si, cast (H_K = 120 kG./sq. mm; b--36.9% Si, cast (H_K = 457 kG./sq. mm.), crystals of magnesium silicide; c--hot-pressed.

In accord with the discussion in Chapter III, Section 3, the resistance of the alloys to compression increases with increase in the temperature; thus, for the alloy with 45% silicon it is 12 kG./sq. mm. at 600°, as compared to 0.3 kG./sq. mm. at 20°. As a result, the specimens when heated become as it were more metallic.

TABLE 34

(1) Hardness, Plasticity and Thermal Electromotive Force of Cast Alloys Based on Mg_2Si
(2) Amount of Si, wt. %
(3) Hardness, H_K, kG./sq. mm. at various temperatures
(4) Relative contraction when compressed $\varepsilon_{cp.}$ (T = 90% of $T_{m.p.}$)
(5) T.e.m.f. in pair with copper, microv./deg.
(6) Microstructure of the alloys
(7) Crystals of Mg_2Si and eutectic Mg + Mg_2Si
(8) Likewise
(9) Crystals of Mg_2Si
(10) Crystals of compound and eutectic Mg_2Si + Si
(11) Crystals of silicon

The alloys based on magnesium silicide have high t.e.m.f. values--of the order of 200 microv./deg. For the alloy with 40% Si, composed of crystals of magnesim silicide and eutectic Mg_2Si + Si, the values of the t.e.m.f. are approximately 50 times greater than for the alloys containing up to 35% silicon (cf. Fig. 115). In general, the t.e.m.f. of the alloys in the given system changes with the composition in the same manner as the hardness. The t.e.m.f. is one of the extremely structure-sensitive characteristics and should be more frequently used in the physicochemical study of alloys. It was established that to a considerable measure the properties of cast magnesium-silicon alloys are determined by the mutual distribution of the structure components. The distribution of the eutectic along the grain boundaries is the reason for the lack of additivity in the change of the properties as a function of the composition. Attempts made to change the distribution of the components by compressing the specimens in a heated container failed to achieve the desired result--the distribution of the components did not change (Fig. 117, c). The same as in the Al-Si system, the reason for the lack of success here was apparently due to the great difference in the hardness and in the melting points of the individual components, characteristic for these alloys.

Appendix 12

It could be postulated that if it were possible to distribute the eutectic uniformly within the grains of the compound, then the hardness of the alloy would be determined in the main by the hardness of the crystals of the compound. It was also of great interest to determine how the alloy hardness would change if along the boundaries of the solid component would lie, not the eutectic mixture, but instead some plastic metal like, for example, aluminum or copper. For this it was decided to resort to metalloceramics. Metalloceramic specimens were prepared from mixtures composed of powdered Mg_2Si with various amounts (up to 20%) of powdered aluminum. Specimens of the indicated compound with the addition of 30% copper were made in a similar manner. To prepare the specimens the pulverized alloy, in composition corresponding to the compound Mg_2Si, was mixed with the proper amount of aluminum or copper powder. Both powders were previously sifted through a sieve with a screen diameter of 0.25 mm. The mixing of the powders was done in a special mixer with an eccentric axis of rotation. Oleic acid was added to the powder (on the basis of 1 mg. per gram of mixture), which functioned as a surface-active lubricant, forming a stable adsorption film on the surface of the powder particles.

FIGURE 118

(1) Microstructure of metalloceramic specimens. X150.

a--Mg_2Si + 5% Al; b--Mg_2Si + 30% Cu.

The mixed powders were sifted into a pressure mold and cold-briquetted. Then in the same mold the briquettes were subjected to a pressure of 3-10 tons/sq. cm. at 500-530°.

The microstructures of the obtained metalloceramic specimens are shown in Fig. 118.

The hardness was measured by the same method that was used for the cast alloys. The obtained data are given in Table 35.

TABLE 35

(1) Hardness of Metalloceramic Alloys Based on Mg_2Si, H_K, kG./sq. mm.
(2) Temperature, °C (3) Addition of aluminum, wt. %
(4) Addition of 30 wt. % Cu
(5) * Cast alloy (Mg_2Si).

As can be seen, here also the presence of the soft alloy components along the grain boundaries of the hard compound sharply lowers the hardness value of the specimens, but the hardness values are close to being additive. This is true for all of the temperatures studied; however, at the higher temperatures an increase in the amount of the soft component causes a somewhat smaller relative reduction in the macrohardness of the specimens. Replacement of the plastic aluminum by the somewhat harder copper, even when the latter is present in an amount of 30%, leads to an increase in the hardness of the specimens.

The relatively high hardness values of the metalloceramic specimens at all of the temperatures also deserve attention. However, when these specimens were tested for compression at 20° they showed a weak resistance and underwent damage because of their brittleness.

Part IV. Study of the influence of temperature on the mechanical properties of metal alloys

Chapter III. The mechanical properties of alloys in systems forming metallic compounds as a function of the temperature

In this section the change in the properties of alloys of three metal systems will be discussed. In all cases one of the components is magnesium. Each of these systems represents a typical example of a definite type of chemical reaction of the components. As had been definitely established, in our investigations the compounds formed in the system magnesium-zinc are of the daltonide type, while in the system magnesium-aluminum they have a berthollide character. Magnesium-cadmium alloys are the classical example of systems in which Kurnakov compounds are formed from solid solutions. A study of these systems, especially the first two, gives basic information as to the structure of many light and ultralight industrial alloys.

System Magnesium-Zinc

This system is characterized by a certain inertness of the diffusion processes and a very slow establishment of the equilibrium. Despite the large number of studies made the phase diagram of these alloys has not yet been firmly established. Differences exist even on the very basic questions: amount and composition of the formed compounds, and also their ability to form solid solutions. According to the data of various authors, metal compounds of the following composition can be formed in the system Mg-Zn: MgZn, Mg_7Zn_3, $MgZn_2$, $MgZn_5$ and Mg_2Zn /391, 394, 399-407/. Here only one compound, namely $MgZn_2$, crystallizing from the liquid state, is acknowledged to be present in this system by all authors without exception. The other compounds, formed in the solid state by peretectic reactions, are shown by some and not established by other authors. Quite contradictory opinions exist in the literature on the ability of these compounds to form solid solutions /401, 402/ (Fig. 151).

Matters are even worse relative to a study of the mechanical properties (over the whole concentration range). The published data of Grube and Burkhardt (hardness), and also of Koster and Rosentahl (modulus of elasticity), relate only to room temperature, contradict eachother, and do not agree with the existing information on the phase diagram /408, 409/.

The compound $MgZn_2$ crystallizes in the hexagonal lattice C_{14}, having the parameters a = 5.15Å; c = 8.48Å; $\frac{c}{a}$ = 1.65. Each cell contains four atoms (Fig. 152). Based on crystallographic data the compound MgZn is very close to the compound $MgZn_2$. The same as $MgZn_2$, MgZn crystallizes in the hexagonal lattice, only with a nearly double increase in the parameters (a = 10.66Å, c = 17.16Å, $\frac{c}{a}$ = 1.61). Here the elementary cell contains 48 atoms /410/. It should be mentioned that also on the basis of microstructural data the compound MgZn is very close to the compound $MgZn_2$, for which reason its discovery was quite recent, only after a special etchant (the

so-called Benedict's solution) had been used. The compound $MgZn_5$ crystallizes in the simple cubic lattice, whose constant is equal to 8.53Å. The number of atoms in the elementary cell is about 32 /411/.

According to Laves /406/, the compound $MgZn_5$ is more accurately described by the formula Mg_2Zn_{11}. However, this statement is apparently incorrect.

There is no definite information in the literature as to the nature of the chemical bond in the indicated compounds.

The contradictory nature of the published data relative to the system Mg-Zn prompted us to attempt an examination of the reasons for the existing discrepancies. In addition, there was another important reason, and namely: all of the previous investigations of alloys rich in metal compounds were made with cast specimens. Because of the great brittleness of such alloys at room temperature nobody has succeeded up to now in obtaining deformed specimens. We studied both cast alloys and those that had been treated under pressure. In the study special attention was given to two problems: 1) the influence of the kinetics of establishing the equilibrium on the shape of the Mg-Zn diagram, and also on the shape of the composition-mechanical properties diagrams, and 2) a study of the influence of temperature on the mechanical properties of alloys rich in metal compounds.

We studied 25 alloys, in which the zinc concentration ranged from 24 to 96 wt. %. The specimens were prepared from MG-1 magnesium (99.9% Mg) and Z-1 zinc (99.94% Zn). The fusions were run in an electric hearth furnace in graphite crucibles under a layer of previously dehydrated carnallite flux. The composition of the alloys was controlled by chemical analysis. The specimens were deformed by hot pressing on the equipment shown in Fig. 27. This task proved to be extremely difficult, since to obtain comparable data all of the alloys of a given system should be treated under identical conditions, which were limited by the plasticity of the most brittle alloy. Consequently, we found it necessary to make a preliminary testing of all of the alloys, find the optimum conditions for the plastic deformation of each alloy, and only after this selecting the general conditions for obtaining and testing all of the specimens. Because of the general complexity of the problem more time was consumed in developing the method and establishing optimum and comparable conditions than was consumed in the actual testing.

As the result of the preliminary experiments it was established that with properly chosen pressing conditions (temperature, velocity, degree of deformation and suitable lubrication) it is possible to obtain all of the cast alloys as high-quality rods. To be sure, despite this some of the cast alloys failed to withstand more than 50% compression. Consequently, to obtain a greater deformation effect we resorted to pressing in two stages. In the first pass the ingot having a diameter of 22 mm. was forced through a matrix with a diameter of 15 mm., i.e. the compression was approximately 50%. In the second pass the obtained alloy rods were pressed in a appa-

ratus, having an opening with an internal diameter of 15 mm., through a matrix with an eye diameter of 10 mm., i.e. the compression was again approximately 50%. A mixture of graphite and machine oil was used as the lubricant during pressing. The obtained specimens were used to determine the hardness and flow pressure of the alloys in the deformed state at various temperatures. The pressing of the specimens and determination of the flow pressure were run at temperatures 15-20° below the melting point. Annealing was used to bring the alloys to the equilibrium state. According to the literature, an extremely long annealing time, up to 90 days, is required for the cast alloys of this system /402/. To accelerate the diffusion processes it is desirable to anneal the alloys at higher temperatures. But, taking into consideration the fact that alloys of the magnesium-zinc system differ greatly in their melting points, to avoid over-annealing they were divided into four groups; each group contained the alloys with close melting points. The alloys were annealed at the temperatures indicated in Table 50.

The specimens were heated under a layer of powdered aluminum oxide; the crevice between the shell and cover of the muffle was cemented with clay. The microstructure method was used to control the degree of equilibrium attainment. The alloy was considered to have reached equilibrium when the microstructure of the specimens ceased to change with further annealing, and when in the number of phases it corresponded to the phase diagram. The control by chemical analysis revealed that the amount of zinc in the specimens did not change when the annealing was under the indicated conditions. The specimens were etched with alcohol solutions of either nitric or hydrochloric acid, and also with meta-nitrobenzoic acid. The hardness of the alloys was measured on a 7- ton machine with a 5-millimeter ball and a load of 125 kg., in the temperature interval 20-365°. In determining the flow pressure the deformation reached 80°. Some examples of the microstructure of the alloys in different states are shown in Fig. 153. Apparently, we were the first to show that a completely one-phase structure exists in the region of the compound MgZn (Fig. 153). For earlier investigators, working with cast specimens, the microphotographs always revealed traces of a second phase. A one-phase structure during annealing is established with great difficulty specifically in the region of this compound. For the deformed specimens this occurs after 10-day annealing. In the region of the compound MgZn Hume-Rothery considers the magnesium:zinc ratio to be equal to 1:1 /402/, while Takei considers it to be 1:1.5 (Mg_2Zn_3) /403/. According to our data (microstructure, hardness) this ratio is equal to 1:1.2, which corresponds to the stoichiometric formula Mg_5Zn_6.

Until the composition of this compound is conclusively established by the x-ray method we will designate it as MgZn in the future.

Some of the basic results of our investigation are given below /335, 337/.

The structure and properties of Mg-Zn alloys depend on the previous thermal and mechanical treatment to a much greater degree than do many other alloys. The reason for this is the slow diffu-

Appendix 12

sion rate, and because of this, the extremely long time required to reach equilibrium. The degree of equilibrium shown by alloys determines: the form of the phase diagrams of alloys after their solidification (the absence or presence of solid solutions based on compounds), the shape of the composition-property isotherms (the absence of presence of particular points, corresponding to chemical compounds), and also the magnitude of the property characteristics. In accord with what has been said as-cast conditions for specimens determines: the press of a gross two-phase and an nonequilibrium three-phase structure (Fig. 153), a greater scattering in the values of the properties, and the absence of individual points on the composition-property isotherms for the alloys, corresponding to chemical compounds in their composition (Fig. 154, Table 51). For the cast alloys the region of solid solutions based on compounds also does not appear. In Fig. 154 the maxima correspond to a coarse-grained structure, while the minima correspond to a fine-grained structure, but this observation requires further refinement. Even after 5-day annealing the hardness of the cast alloys is influenced to a greater extent by a change in the structure (the presence of a coarse or fine grain) than by a change in the composition.

The annealing of cast specimens facilitates the progress of diffusion and creates greater possibilities for the development of chemical reaction between the components in the solid state. But to bring cast Mg-Zn alloys into a state of equilibrium it is necessary to resort to prolonged annealing (measured in months).

In not a single case (from 25 alloys) did annealing of the cast specimens for 20 days lead to establishing a completely one-phase structure in the region of the compounds and their solid solutions (see Fig. 153). This, naturally, was also reflected in the change of the properties as a function of the composition (Table 51). All of the previous investigators of this system (Grube, Chadwick, Hume-Rothery, Takei, Laves, Koster, etc.) worked with cast alloys that had been annealed. Consequently, the presence of sharp discrepancies in the data of the indicated authors is first of all explained by the different degree that the cast alloys approximated the equilibrium state, depending on the conditions and annealing duration chosen by the various investigators.

Hot deformation (pressing) makes the structure much finer (see Fig. 153), creates fresh joints between the grains, and facilitates more rapid equilization of the specimen composition. But despite this, in view of the slow progress of diffusion, especially in the region of the compound MgZn, the deformed unannealed alloys are not completely in equilibrium. In accord with this the microstructures of the alloys, in the region of possible existence of homogeneous regions, still show small inclusions of a second phase (see Fig. 153), while on the composition-mechanical property curves at 20° only the compound $MgZn_5$ shows a singular point--the minimum (Fig. 155, Table 51).

From Fig. 155 and Table 51 it can be seen that in the region of the compound MgZn at ordinary and elevated temperatures the de-

formed alloys are characterized by the magnitude of their hardness and flow pressure. In the deformation or slight heating of these alloys there probably occurs precipitation to form the compound MgZn, and possibly even its separation in a finely dispersed state, which leads to an alteration of the alloy structure and an increase in the hardness to 350 kg./sq. mm. In the process of measuring the hardness above 300° it is already possible for partial "coagulation" of the compound to occur, since here the hardness maxima tend to become smoother. This also applies to the compound $MgZn_2$. In this case the kinetics of the aging processes should be studied in greater detail, since both MgZn and $MgZn_2$ function as strengthening agents for some heat treated alloys of magnesium with aluminum and zinc.

The application of mechanical and heat treatments to the specimens greatly shortens the time required for the alloys to approximate the equilibrium state during annealing, and consequently permits showing to a greater extent the form of the phase diagrams and composition-property diagrams corresponding to a given type of chemical reaction between components. The hardness of the studied alloys depends on the length of annealing (Fig. 156).

Of the studied alloys the ones that had been deformed and then annealed for 20 days proved to be closest to the equilibrium state. A 5-day annealing failed to introduce any important changes in the shape of the hardness isotherms as regards the cast condition, but individual alloys showed an increase in their hardness. Thus, the alloy with 76.8% Zn, corresponding to the compound MgZn, in the deformed state had a hardness of 315 kg./sq. mm., and after annealing for 5 days a hardness of 357 kg./sq. mm. After the deformed alloys of the compound MgZn had been annealed for ten days the hardness isotherms began to be characterized by a deep minimum.

Even a quick glance at the 20° isotherm of the hardness after a 20-day annealing clearly shows that the hardness, disregarding some variations due to structure heterogeneity, is first of all determined by the chemical nature of the alloys. All three metal compounds present in this system are characterized by special points on the hardness isotherms: MgZn and $MgZn_5$ by deep minima, and $MgZn_2$ by a slight maximum. In the region of compounds MgZn and $MgZn_5$ a change in the alloy composition by 1.5-2% can lead to a change of 1.5-2.5 times in the hardness. Thus, for example, the alloy with 76.8% Zn has a hardness of 107 kg./sq. mm., while the alloy with 75.4% Zn has a hardness of 280 kg./sq. mm., or the alloy with 93.1% Zn has a hardness of 85 kg./sq. mm., while the alloy with 92.6% Zn has a hardness of 251 kg./sq. mm. In Fig. 156 we also show the 325° isotherm of the hardness after 20-day annealing and the hardness at 20° of the alloys that had been quenched from 325° in the region of the compound MgZn. For both curves the attention is attracted to the shift in the maximum hardness values of the alloys in the region of the solid solutions based on MgZn in both directions from the composition of the compound when compared with room temperature, which is evidence of the fact that the region of homogeneity expands with elevation of the temperature. The hardness in the quenched state of the alloy, in composition corresponding to the compound MgZn, more accurately

Mg_5Zn_6 (76.8% Zn), is equal to 117 kg./sq. mm., while the alloys with 74.8% Zn and with 80.6% Zn have a hardness of 132 and 159 kg./sq. mm., respectively.

The compound $MgZn_2$ has a much higher melting point (around 590° as compared to 354 and 380° for the neighboring alloys). Consequently, it fails to give a minimum on the usual hardness isotherms. The minimum, and also the presence of solid solution regions, is distinctly shown only when the hardness isotherms are constructed (plotted) in the "homologous" (in equal fractions of the absolute melting point) temperatures (Fig. 157).

The use of the microstructure method on the specimens that had been deformed and annealed for 20 days made it possible to establish the presence of three one-phase regions in the Mg-Zn system, respectively located in the regions for the existence of the compounds $MgZn_2$ and $MgZn_5$ (see Fig. 153).

The hardness method revealed that these regions expand somewhat with elevation of the temperature.

The approximate boundaries of the one-phase regions at 20° are as follows: in the region of compound MgZn--from 75.4 to 77.5 wt. % Zn; in the region of compound $MgZn_2$--from 85.0 to 86.6 wt. % Zn; in the region of compound $MgZn_5$--from 92.7 to 93.1 wt. % Zn.

An exact determination of the boundaries of the one-phase regions and the change in their position with temperature did not enter into the problem of the present study.

The hardness of the alloys, constituting mixtures of solid solutions based on compounds, in general follows the additivity rule, both at ordinary and at high corresponding temperatures.

The three indicated compounds are characterized by the presence of singular minima on the hardness isotherms (see Fig. 156 and 157). These experimental facts testify not only to the existence of the indicated metal compounds, but also to their daltonide nature. As a result, our data refute the statements that the compounds Mg_7Zn_3 (Koster), Mg_2Zn_3 (Takei) and Mg_2Zn (Laves and Werner) exist, and they also refute the statement (Hume-Rothery and Rounsfell) that the compounds in the Mg-Zn system are completely incapable of forming solid solutions. The presence of the compounds MgZn, $MgZn_2$ and $MgZn_5$, established earlier on cast annealed specimens (G. G. Urazov, N. A. Filin, A. V. Shashin, Hume-Rothery, M. I. Zakharova and A. B. Mlodzeevskii, V. I. Mikheeva, F. I. Shamrai, and others), is without dispute. Also without dispute is the formation of solid solutions based on each of these compounds.

We made a detailed study of the influence of temperatue on the mechanical properties of the alloys. It was found that at room temperature the Mg-Zn alloys in the region, rich in compounds, are characterized in all states not only by brittleness, but also by a high hardness (Table 51, Figs. 155-157). The hardness of these alloys is from one to ten times the hardness of either magnesium or zinc. Especially characteristic in this respect are the alloys based on compounds MgZn and $MgZn_2$, the hardness of which at 20° is, on the

average, about 300 kg./sq. mm. After deformation the hardness of the alloys, due to a reduction in grain size, increases even more, and some of them become capable of scratching glass. The flow pressure of these alloys is considerably higher than the values of the flow pressure for the pure metals and reaches a value of 40-60 kg./sq. mm. (Table 51). The flow pressure of magnesium at this temperature is equal to 15 kg./sq. mm., and for zinc it is equal to 17 kg./sq. mm. Attention is attracted to the low (less than unity) value of the ratio of the flow pressure to the hardness of the alloys, rich in compounds (Fig. 158).

With elevation of the temperature the alloys show intense softening (see Table 51, Figs. 155-160). For example, at 325° the magnitude of their hardness is 30-50 kg./sq. mm., i.e. of the order of 10% of their value at room temperatue. Based on an approximate estimate (based on the hardness) the strength limit for the compound $MgZn_5$ at 350° is less than 1 kg./sq. mm. The relative reduction in the hardness when heated is greatest for the alloys, representing a mixture of metal compounds or especially their solid solutions (see Fig. 160). Then follow the alloys, containing substantial eutectic inclusions. Thus, for example, the alloy with 45.6% Zn, in composition close to the eutectic, has a hardness of 109 kg./sq. mm. at 20°, and a hardness of 16 kg./sq. mm. at 325°, i.e. there is approximately a 7-fold reduction in the hardness. The alloy with 80.6% Zn, from its structure being a mixture of solid solutions of compounds $MgZn_2$ and $MgZn_5$, when heated from room temperature to 325° shows a reduction in the hardness from 303 to 31 kg./sq. mm., i.e. approximately a 10-fold decrease. The other alloys of analogous structure show a similar behavior. Such a change in the hardness when heated apparently occurs as the result of a sharp difference in the hardness of the two groups of alloys at room temperature. Consequently the perplexity, expressed by Luori on this behavior, is not justified /341/. Using this system as an example it can be seen that the harder the alloy at ordinary temperature, the greater is its softening when heated. As can be seen from the data in Table 51 and Fig. 161, when compared with the neighboring alloys the pure compounds have minimum temperature coefficients of the hardness in the interval 20-325°, i.e. when heated they show less softening than do their mixtures or the alloys with substantial eutectic inclusions.

The alloys in the region of compound $MgZn_5$ proved to be the most sensitive to the influence of temperature. They show the greatest temperature coefficient of the hardness and are also the softest at 325° (the hardness is less than 10 kg./sq. mm.). From the viewpoint of ease of treatment and substantial increase in the hardness when heat treated the alloys in the region of $MgZn_5$ possess practical interest.

Alloys of the Mg-Zn system, including those rich in metal compounds, show a strong increase in their plasticity when heated. This increase in the plasticity is so great that with a properly selected temperature any alloy of the Mg-Zn system, characterized at room temperature by a great brittleness and hardness, can be pressed through the eye of a cylindrical matrix to yield a high-quality rod, while a

cylinder from such an alloy can be squeezed into a disc with a small thickness. In this connection the alloys withstand 80-90% deformation in one pass. It was specifically this intense softening of the alloys that permitted us to obtain deformed specimens from these compounds, a more detailed discussion of which has already been given in Chapter III of Part III.

At our request, A. P. Obukhov and B. I. Boltaks, in the LFTI of the Academy of Sciences of the USSR, measured in the interval from -170 to +450° the electroconductivity and thermal e.m.f. of the compounds formed in the system Mg-Zn, in the deformed state. The obtained data are given in Table 52. Of interest are the absolute electroconductivity values of the compounds, and also the substantial increase in the electroconductivity with decrease in the temperature.

TABLES AND FIGURES

FIGURE 151

(1) Phase diagram of the magnesium-zinc system:
a--according to Hume-Rothery; b--according to Takei.
(2) Temperature, °C (3) At. % Zn (4) Wt. % Zn

FIGURE 152

(1) Structure of $MgZn_2$ /43/.

TABLE 50

(1) Annealing Conditions for Alloys of the Mg-Zn System
(2) Amount of Zn, wt. % (3) Annealing temperature, °C
(4) Duration of annealing (5) Conditions used to cool the specimens
(6) Cooling together with the furnace for a period of two days

FIGURE 153

(1) Microstructure of Alloys of the Mg-Zn System (in different states) X600.

a--45.6 wt. % Zn

1) Cast (α + eutectic); 2) deformed (α + eutectic); 3) annealed (α + eutectic).

b--76.8 wt. % Zn

1) Cast (MgZn + eutectic); 2) deformed (MgZn + eutectic); 3) annealed (MgZn).

c--85 wt. % Zn

1) Cast ($MgZn_2$ + eutectic); 2) deformed ($MgZn_2$); 3) annealed ($MgZn_2$).

FIGURE 153

(1) Microstructure of Alloys of the Mg-Zn System (in different states) X600.

d--93.1 wt. % Zn

1) Deformed, annealed for 5 days ($MgZn_2$ + $MgZn_5$);
2) deformed, annealed for 10 days ($MgZn_5$);
3) deformed, annealed for 20 days ($MgZn_5$).

e--96.6 wt. % Zn

1) Cast ($MgZn_5$ + eutectic); 2) deformed ($MgZn_5$ + eutectic); 3) annealed ($MgZn_5$ + eutectic).

FIGURES 154 and 155

(1) Flow pressure of cast magnesium-zinc alloys.
(2) Hardness of deformed magnesium-zinc alloys at various temperatures.

TABLE 51

(1) Mechanical Properties of Alloys in the Magnesium-Zinc System
(2) Wt. % Zn (3) Testing temperature, °C (4) Cast alloys
(5) Hardness, H_B, kg./sq. mm. (6) without annealing
(7) after annealing (5 days)
(8) Flow pressure of unannealed alloys, K, kg./sq. mm.
(9) Hardness, H_B, kg./sq. mm. (10) Deformed alloys
(11) after annealing
(12) Temperature coefficient of the hardness for the alloys annealed for 20 days (20-325°)
(13) Flow pressure, K, kg./sq. mm.

FIGURE 156

(1) Hardness of deformed and annealed alloys of the Mg-Zn system: X - · - X - annealed 5 days; Δ - - - Δ - annealed 10 days; o - o - annealed 20 days; · - · - hardness at 325° of deformed and annealed (20 days) alloys.
(2) H_B, kg./sq. mm. (3) Quenched alloys

Appendix 12

FIGURE 157

(1) Hardness of alloys of the magnesium-zinc system at homologous temperatures (50,60 and 75% of the absolute melting point) (E. M. Savitskii and V. V. Baron).

FIGURES 158 and 159

(1) Ratio of the flow pressure to the hardness of alloys of the magnesium-zinc system

(2) Hardness and flow pressure of magnesium-zinc alloys at elevated temperatures (after annealing for 5 days).

FIGURE 160

(1) Relative softening of magnesium-zinc alloys when heated (based on the measurement data at 20 and 325°).

(2) Temperature, °C.

TABLE 52

(1) Specific Conductivity and Thermal E.M.F. of Mg-Zn alloys

(2) Temperature (3) $ohm^{-1} \cdot cm.^{-1}$ (4) α, microvolts/degree

(5) In the limits 5 - 8 (6) In the limits 3 - 6

(7) In the limits 4 - 7

(8) The thermal e.m.f. was measured relative to copper electrodes. At 150°C the thermal e.m.f. of $MgZn_5$ changes sign from + to -.

FIGURE 161

(1) Temperature coefficient of the hardness of magnesium-zinc alloys

(2) Temperature coefficient of the hardness α

LITERATURE CITED

/43/ Ya. S. Umanskii, B. N. Finkel'shtein and M. E. Blanter, Physical Principles of Metal Working, Moscow-Leningrad, Metallurgical Press, 1949.

/335/ E. M. Savitskii, Bull. S.Ph.Kh.A., 19 (1949).

/337/ E. M. Savitskii and V. V. Baron, Proc. Acad. Sci. USSR, 64, No. 5 (1949).

/341/ R. Louri, Problems of Contemporary Metallurgy, No. 5 (1953).

Appendix 12

/391/ G. G. Urazov, I. A. Filin and A. V. Shashin, Metallurgist, No. 6 (1940).

/394/ V. I. Mikheeva, Alloys of Magnesium With Aluminum and Zinc, Moscow, Acad. Sci. USSR Press, 1946.

/399/ M. Khansen, Structure of Binary Alloys, Moscow, Metallurgist Press, 1941.

/400/ Grube, Z. anorg. Chem., 49, 77 (1906).

/401/ Chadwick, J. of Metals, 39, 285 (1928).

/402/ Hume-Rothery and Rounsfell, J. Inst. Metals, 41, 119 (1929).

/403/ Takei, Kinzoku no Kenkyn, 6, 177 (1929).

/404/ A. A. Bochvar and I. P. Velichko, Trans. M.I.Ts. M.Z., No. 1, Studies of the Metallography Laboratory for 1931-1932, Moscow, 1933.

/405/ M. I. Zakharova and A. B. Mlodzeevskii, Bull. S.Ph.Kh.A., 9, (1936).

/406/ Laves and Werner, Z. Kristallogr., 95, 114 (1936).

/407/ Koster, Z. Metallkunde, 41, 78 (1950).

/408/ Grube and Burkhardt, Z. Elektrochem., 35, 315 (1929).

/409/ Koster and Rosentahl, Z. Metallkunde, 6, 163 (1940).

/410/ Tarschisch, Z. Kristallogr., 86, 423 (1933).

/411/ M. S. Mirgalovskaya, Proc. Acad. Sci. USSR, 78, No. 5 (1951).

APP. 12,

еще каким-нибудь способом. Во всяком случае логарифмический анализ характеристик пластичности имеет не меньшие физические обоснования, чем логарифмический анализ характеристик сопротивляемости пластической деформации.

2. РАЗРАБОТКА АППАРАТУРЫ И МЕТОДИКИ МИКРОМЕХАНИЧЕСКИХ ИСПЫТАНИЙ

Наряду с созданием установок для испытания макрообразцов была разработана, освоена и использована специальная аппаратура для микромеханических испытаний. В этом направлении было затрачено много усилий и было найдено достаточно хорошее решение вопроса. В начале работа шла только по линии замены испытаний на растяжение испытаниями на срез, как требующими значительно меньших и более простых в изготовлении об-

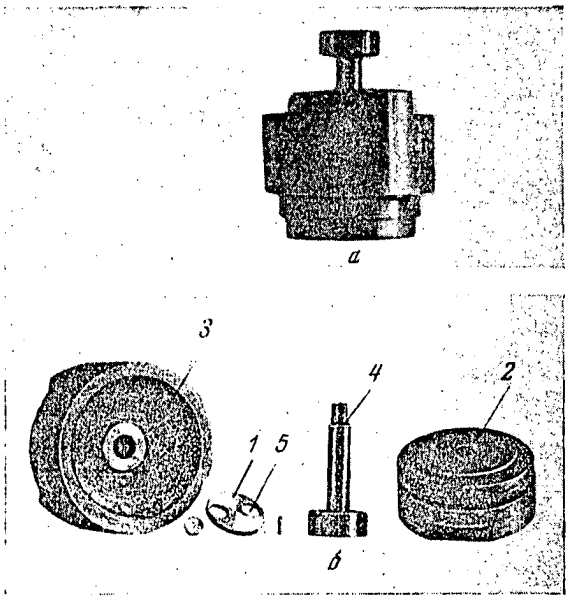

Фиг. 34. Приспособление к прессу Гагарина для испытаний на срез:
а — в собранном состоянии; *б* — в разобранном виде.

разцов. В ЛФТИ АН СССР был создан специальный прибор для высечки отверстий диаметром 2 мм в пластинке толщиной 0,5 мм. Идея прибора заключалась в том, чтобы на основании записи перемещения пуансона в зависимости от нагрузки в процессе высечки строить рабочую диаграмму среза, из данных которой затем вычислить основные характеристики растяжения [106].

Первым этапом нашей работы было исследование возможности применения прибора ЛФТИ АН СССР для целей физико-химического анализа. Проверка на сплавах системы медь — никель и на некоторых магниевых сплавах дала положительные результаты [107]. Но испытание на приборе ЛФТИ АН СССР имеет некоторые существенные недостатки, а именно:

APP. 12.

1) необходимость иметь дополнительно к испытательной машине специальный, сравнительно сложный прибор, который к тому же приспособлен только для одного вида испытаний; 2) наличие весьма малой (3 мм²) площади среза у испытуемого образца, из-за чего незначительные колебания в составе и величине зерен, количестве включений могут дать разброс показаний; 3) необходимость в прерывании опыта во время отсчета нагрузки. Поэтому было решено проводить испытание на срез на прессе Гагарина, причем достигался ряд преимуществ: отпадала необходимость в специальном сложном приборе, образец имел большую площадь среза (50 мм²) и производилась автоматическая запись большой рабочей диаграммы [107]. Для проведения испытаний на срез мы воспользовались приспособлением, изображенным на фиг. 34. Образец *1* толщиной 2 мм помещается на матрицу *2* и прижимается гайкой *3*, которая имеет направляющее отверстие для пуансона *4* диаметром 8 мм. Собранное приспособление ставится на рабочий стол пресса Гагарина, и производится продавливание — выштамповка 8-миллиметрового отверстия *5*.

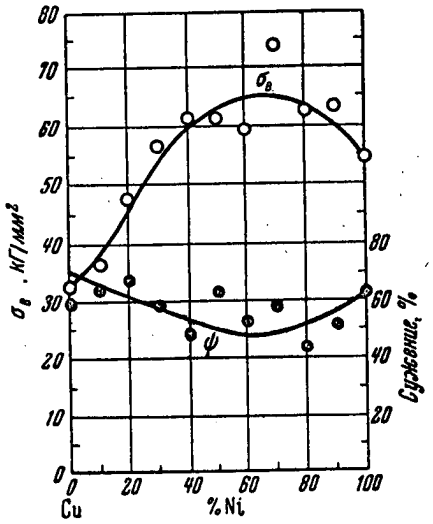

Фиг. 35. Изменение временного сопротивления разрыву и поперечного сужения сплавов в системе медь—никель (Е. М. Савицкий и Н. П. Славина).

Характеристики растяжения: предел пропорциональности, предел прочности, истинный предел прочности и сужение определяются путем пересчета по соответствующим несложным формулам [107] данных записанной на прессе диаграммы усилие среза — деформация. Проверка на медноникелевых, медноцинковых и магниевых сплавах (более сотни образцов) показала, что для не особенно хрупких сплавов соответствие между срезом и растяжением, особенно в отношении предела прочности, получается довольно хорошим.

Значения сужения для магниевых сплавов, обладающих хрупкостью при обычных температурах, при определении путем испытаний на срез оказались несколько заниженными. Для 60 сплавов системы Cu — Zn — Al коэффициент корреляции оказался равным 0,93, а среднее отношение предела прочности при растяжении к пределу прочности при продавливании составило 0,63. Полученные данные для сплавов системы медь — никель, образующей непрерывный ряд твердых растворов, приведены на фиг. 35.

Следует отметить, что для определения механических свойств 11 сплавов системы медь — никель путем испытаний на срез на прессе Гагарина потребовалось всего 175 г чистого веса образцов, тогда как для проведения стандартных опытов на растяжение необходимо иметь не менее 4 кг готовых образцов. Кроме того, для прокованных и отожженных медноникелевых сплавов было определено соотношение между пределом прочности при растяжении и твердостью по Бринеллю. Средний коэффициент пропорциональности в этом случае оказался равным 0,54 при 0,6 для меди и 0,5 для никеля. Для сплавов этой системы был определен также модуль нормальной упругости по методу Е. М. Розенберга [105] путем вдавливания шарика при раз-

APP. 12.

личных нагрузках (фиг. 36). Совпадение с данными, полученными по стандартному способу при испытаниях на растяжение, оказалось довольно хорошим.

На следующем этапе работы была показана возможность испытания микроразрывных образцов на обычных испытательных машинах [136]. Для увеличения точности отсчета нагрузки желательно использовать маломощные машины. В случае, если машина работает только на растяжение для зажима микрообразца необходимо сделать специальные захваты. Если машина работает только на сжатие (например, пресс Гагарина), для испытаний

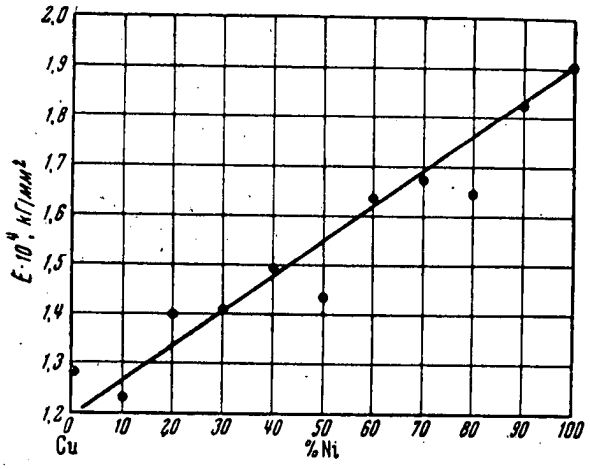

Фиг. 36. Модуль нормальной упругости для сплавов системы медь — никель.

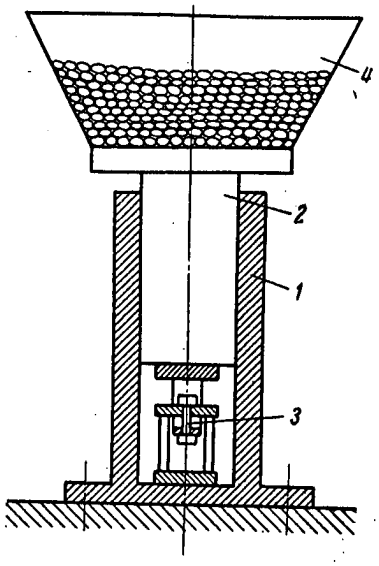

Фиг. 37. Схема установки для разрыва микрообразцов (Е. М. Савицкий и В. П. Лебедев):

1 — цилиндр; *2* — пуансон; *3* — реверсор с образцом; *4* — буннер.

на растяжение можно применить реверсор гагаринского типа, но уменьшенный до соответствующих размеров. Если нет испытательных машин, образец можно нагружать песком, водой или дробью при помощи специального приспособления (фиг. 37). Это вполне допустимо, так как максимальная нагрузка для разрыва даже стального микрообразца (диаметром 1 мм) обычно не превышает 50—60 кг при комнатной температуре.

3. УНИВЕРСАЛЬНЫЙ ПРИБОР ДЛЯ МИКРОМЕХАНИЧЕСКИХ ИСПЫТАНИЙ

В результате накопленного опыта по работе с микрообразцами за последние несколько лет нам удалось сконструировать, осуществить и усовершенствовать простой, но универсальный прибор, позволяющий проводить микромеханические испытания по всем основным способам нагружения осевой силой при обычных, высоких и низких температурах на воздухе, в вакууме или в защитных средах [137, 138]. Прибор (фиг. 38) состоит из закрепленного на плите *1* полого цилиндра *2*, внутри которого помещены шлифован-

APP. 12.

ная цилиндрическая подушка *3* из закаленной стали или победита и пуансон *4* со сменным наконечником *5*, перемещаемый под действием того или иного нагружающего устройства. Испытуемый микрообразец *6* помещается между наконечником и подушкой. Вертикальное перемещение пуансона *4* измеряется при помощи связанных с его головкой индикатора или оптиметра с точностью до 0,01 или до 0,001 мм.

Для визуального наблюдения за деформацией образца в процессе испытания цилиндр прибора необходимо делать из прозрачного материала. Для уменьшения трения между пуансоном и стенками цилиндра пуансон можно делать ребристым. В приборе можно испытывать не только микрообразцы, но и образцы больших размеров. Размер образца, подвергаемого испытанию в приборе, лимитируется только габаритами (диаметром и высотой) рабочего пространства в цилиндре прибора и диаметром пуансона, которые, вообще говоря, могут быть сделаны любых, даже довольно больших размеров. Испытанию в приборе могут быть подвергнуты не только образцы из металлов и сплавов, но и из многих неметаллических материалов (пластмассы и др.).

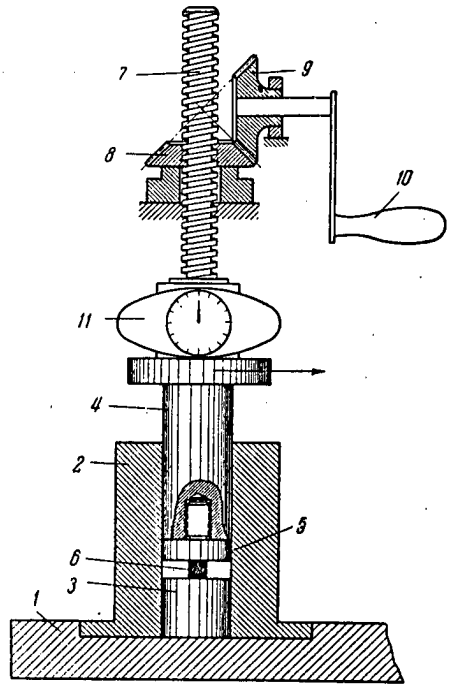

Фиг. 38. Схема универсального прибора для испытаний при обычных температурах (стрелкой показано направление к индикатору):

1 — плита; *2* — цилиндр; *3* — подушка; *4* — пуансон; *5* — наконечник пуансона; *6* — образец; *7—10* — нагружающее устройство; *11* — динамометр.

Нагружение прибора. Мы сознательно отказались от включения в конструкцию прибора какого-либо нагружающего устройства, так как это сильно усложнило бы прибор и сделало бы его более дорогим. В этом нет и большой необходимости, потому что имеющегося в заводских и институтских лабораториях парка испытательных машин вполне достаточно для осуществления испытаний в широком интервале нагрузки. Для нагружения образца и измерения деформирующей нагрузки в процессе испытания прибор необходимо поместить между бойками работающего на сжатие испытательного пресса таким образом, чтобы головка пуансона касалась верхнего бойка, а часть плиты, на которой закреплен цилиндр, стояла на нижнем бойке. Испытания микрообразцов желательно производить на машине малой мощности, так как это увеличивает точность отсчета нагрузки при испытаниях. В случае отсутствия машин меньшей мощности испытания можно производить на прессе Гагарина или на машинах ИМ-4А и ИМ-4Р. В том случае, если машина работает только на растяжение, прибор необходимо поместить в обычный реверсор, превращающий растяжение в сжатие. В случае надобности по показаниям силоизмерителя машины и индикатора прибора обычным способом может быть построена рабочая диаграмма испытания. В случае отсутствия испытательных машин прибор можно нагружать при помощи весьма простых приспособлений (см. фиг. 37).

APP. 12.

и размерам головок микрообразца. Микрообразец можно также изготовить и несколько другим способом. В цилиндр (см. фиг. 39) закладывают необходимое количество материала в виде порошка или маленького слитка и выдавливают проволоку. Получившийся прессостаток *1* может быть одной из головок микроразрывного образца. Для получения другой головки достаточно микрообразец (проволоку с прессостатком) повернуть на 180° и путем нажатия пуансоном *2* расклепать другой конец проволоки. Перед этим целесообразно проволоку с прессостатком заложить в соответствующий штамп.

Испытания на кручение. Предлагаемый универсальный прибор может быть приспособлен и для испытаний на кручение (фиг. 40).

Образец *1* — цилиндрический, с нарезкой на обоих концах для закрепления в подушке *2* и в наконечнике пуансона *3*. Могут быть разработаны и другие варианты крепления образца. Во избежание поворота прокладки она вместе с образцом надевается на шпильки *5*, закрепленные в дне цилиндра *4* или в нижней плите *6* прибора. Образец нагружается вручную путем поворота пуансона при помощи рукоятки *7*, приделанной к его головке. Угол поворота пуансона измеряется при помощи прикрепленной к его головке стрелки *8* и проградуированной в угловых делениях шкалы *9*. К сожалению, в приборе данной конструкции измерение крутящего момента представляет некоторые трудности. В этих условиях испытание на кручение является, в сущности, технологической пробой. Учитывая, что испытания на кручение — довольно редкий вид испытаний, которое применяется только в специальных случаях, вряд ли целесообразно разрабатывать специальную конструкцию для измерения крутящего момента, хотя при необходимости это может быть осуществлено. При этом следует иметь в виду работу П. Д. Новокрещенова и И. Е. Марковой, применявших весьма точное измерение крутящего момента электромагнитным методом [215].

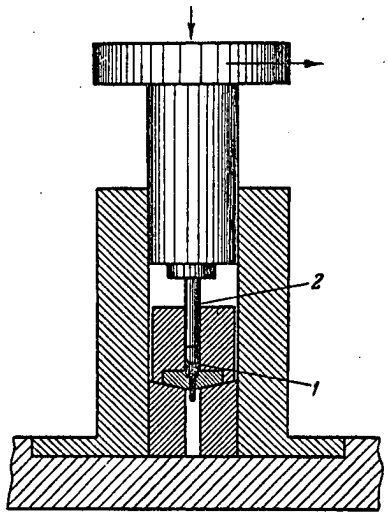

Фиг. 39. Схема приспособления для определения давления истечения:
1 — прессостаток; *2* — пуансон.

Определение давления при прессовании порошков. В приборе можно производить также прессование порошков с замером величины необходимого для этого усилия. Потребность в таком испытании может возникнуть при создании технологии изготовления изделий из порошков дорогих или редких металлов металлокерамическим путем. Прессование порошков в приборе производится по схеме испытаний на сжатие. В случае, если порошка очень мало, он засыпается не непосредственно в цилиндр прибора, а в специально изготовленный для этого маленький цилиндрик. Для удобства разгрузки цилиндрика целесообразно его сделать без дна или со вставным дном. Понятно, что наконечник пуансона в этом случае должен иметь диаметр, соответствующий диаметру маленького цилиндра. Цилиндрик с засыпанным в него металлическим порошком ставится в рабочее пространство прибора на подушку. Величина давления спрессовки может быть определена по показаниям силоизмерителя пресса.

APP 12.

Для подсчета величины напряжений в спрессовываемом материале необходимо максимальное давление разделить на рабочую площадь цилиндра, в который был засыпан порошок. Много также дает определение свойств и даже простой осмотр вынутого из цилиндра спрессованного образца. Если воспользоваться описанным ниже высокотемпературным вариантом прибора, то в нем можно кроме спрессовки порошка, производить также отжиг (спекание) полученного конгломерата или производить прессование при повышенных температурах.

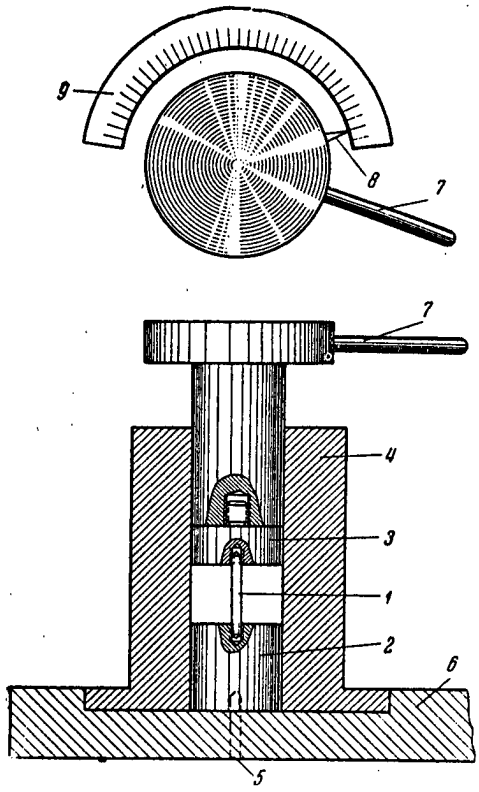

Фиг. 40. Схема прибора для испытаний на кручение:

1— образец; *2* — подушка; *3* — наконечник пуансона; *4* — цилиндр; *5* — шпилька; *6* — нижняя плита; *7* — рукоятка; *8* — стрелка; *9* — шкала.

Таким образом, прибор позволяет выявить оптимальную технологию (температуры, давления) получения изделий металлокерамическим путем с затратой всего нескольких десятых долей грамма порошка.

Из описания основных способов испытаний материала, которые можно осуществить на предлагаемом приборе, видно, что прибор — универсальный, и в случае надобности на нем можно провести испытание еще по другим способам, здесь не описанным. Для этого не потребуется существенных изменений в конструкции прибора.

Переходя к описанию вариантов прибора для испытаний при повышенных или пониженных температурах, в защитных средах или в вакууме, следует указать, что все сказанное об отдельных способах испытаний при комнатных температурах сохраняет и здесь свое значение. Изготовления специальных наконечников и приспособлений не требуется.

Вариант прибора для испытаний при высоких температурах. Работающие в области испытаний материалов знают, насколько усложняется установка, когда испытание надо проводить при высоких температурах. Для некоторых видов испытаний вообще еще не разработана аппаратура и методика для высокотемпературных испытаний (испытания микрообразцов, испытания на кручение, изгиб и т. п.).

Особое, большое достоинство описанного прибора — легкость осуществления на нем испытаний при высоких температурах. Для этого достаточно только поместить цилиндр прибора вместе с находящимися в нем образцом и наконечником пуансона в соответствующую печь. Но более целесообразно сам цилиндр выполнить в форме, удобной для намотки нагревателя, т. е. в виде катушки. Вариант прибора для испытаний при повышенных температурах показан на фиг. 41. Для увеличения точности измерения температуры термопара *2* может быть вставлена в специально сделанное отверстие

APP. 12

в опорной подушке или в наконечнике пуансона. Охлаждаемая водой направляющая втулка необходима для предупреждения заедания пуансона в цилиндре при нагревании в атмосфере воздуха. Цилиндр прибора желательно делать из нержавеющей стали, а подушку и наконечник пуансона — из победита. Верхний допустимый температурный предел испытаний на приборе определяется только жаропрочностью и жаростойкостью этих его частей. Порядок испытания следующий. Прибор собирается обычным способом, затем включается электропечь, и, после необходимой выдержки образца

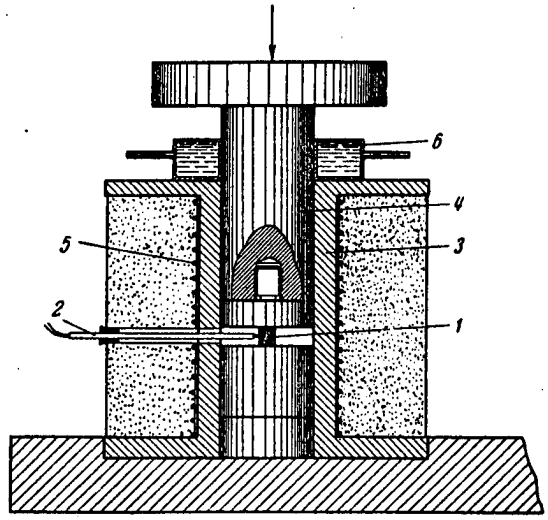

Фиг. 41. Вариант прибора для испытаний при высоких температурах:
1 — образец; *2* — термопара; *3* — цилиндр; *4* — пуансон; *5* — электропечь; *6* — направляющая втулка.

при заданной температуре, стрелка индикатора прибора устанавливается на нуль. Затем производится испытание. Сами испытания по всем описанным выше способам остаются точно такими же, как и при комнатной температуре.

Интересно отметить, что в случае применения образцов достаточного размера этот вариант прибора может работать как дилатомер, так как изменения длины образца в зависимости от температуры нагрева или охлаждения (без нагрузки) могут быть легко определены по показаниям стрелки индикатора (с точностью до 0,01 или даже 0,001 мм). Более того, прибор позволяет производить измерения, которые вообще, по-видимому, не делались до сих пор, а именно количественно измерять величину внутренних давлений, возникающих в материале при фазовых и вообще любых превращениях, которые происходят с изменением объема (аллотропические и другие превращения [216]). Для этого прибор с образцом надо нагревать на испытательной машине при вплотную подведенных к прибору бойках. Нагрев образца, особенно после перехода через температуру какого-либо превращения, будет вызывать его расширение. Этому будет препятствовать пуансон, головка которого упирается в верхний боек машины. Таким образом, расширяющийся образец будет передавать свое давление через пуансон и бойки на силоизмеритель машины, который и будет отклоняться соответственно оказываемому образцом давлению. Таким образом, прибор позволяет исследовать влияние одного из важнейших факторов состояния — темпера-

APP. 12

туры как на механические свойства материала, так и на превращения, происходящие в нем в твердом виде. В приборе можно также исследовать влияние давления на превращения в материале в твердом состоянии при различных температурах.

Вариант прибора для испытаний при низких температурах. Этот вариант прибора (фиг. 42) отличается от изображенного на фиг. 41 высокотемпературного варианта только тем, что в пространство, окружающее цилиндрическую часть катушки цилиндра, вместо нагревателя, вводится сухой лед или охлаждающая жидкость *1*,

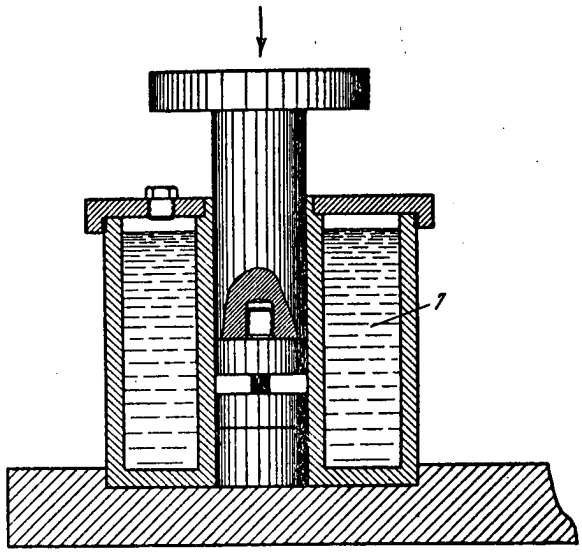

Фиг. 42. Схема варианта прибора для испытаний при низких температурах:
1 — охлаждающая жидкость.

например, жидкий азот. В соответствии со свойствами известных до настоящего времени охлаждающих жидкостей в приборе можно производить испытания до температур порядка —200°.

Вариант прибора для испытания в жидких защитных средах. Некоторые материалы, например, щелочные и щелочно-земельные металлы, быстро окисляются на воздухе и поэтому не могут быть подвергнуты испытанию без принятия специальных защитных мер. По нашему опыту испытания таких материалов удобно и надежно производить в защитных средах, которыми могут быть некоторые нейтральные для данного вещества и прозрачные жидкости. Например, для упомянутых металлов такими жидкостями являются толуол, керосин и др. Испытания алюминиевых и медных сплавов до 450° можно проводить в селитре. Многие другие материалы от окисления при высоких температурах могут быть защищены погружением в ванну из расплавленных солевых смесей, представляющих собой хлориды и фториды некоторых из щелочных металлов.

Этот вариант прибора от основного варианта отличается только тем, что образец помещается в ванночку с защитной жидкостью, а наконечник пуансона выбирается такого диаметра, чтобы он мог войти в ванночку (фиг. 43).

Ставить ванночку в цилиндр и вынимать ее оттуда удобно при помощи

APP. 12.

специального ключа, который может входить в сделанные для этого прорези в верхней части ванночки.

Применение защитных сред позволило нам определить на этом приборе, по-видимому, впервые, механические свойства некоторых металлов, например, щелочно-земельных, и показать, что в отношении убывания прочности

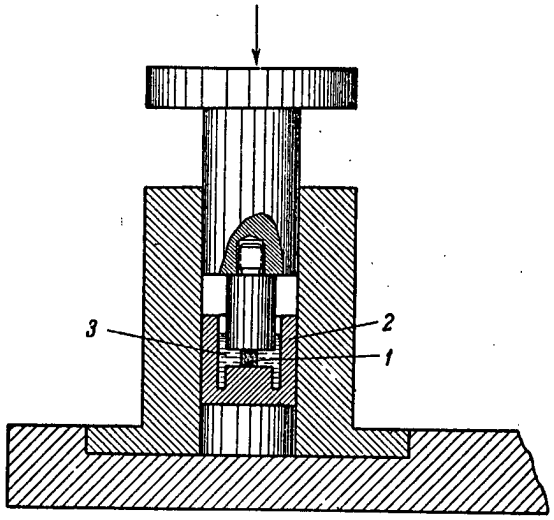

Фиг. 43. Вариант прибора для испытаний в защитных средах;
1 — образец; *2* — ванночка; *3* — защитная жидкость.

они располагаются в следующий ряд: Ca, Sr, Ba. По пластичности эти металлы располагаются в обратном порядке.

На фиг. 44 приведены кривые истинных напряжений для случая сжатия этих металлов при комнатной температуре.

Сжатию подвергались цилиндрические образцы (1 × 1 мм). Опыты проводились в толуоле. Твердость (по конусу) кальция составляет 13,2 кГ/мм², а бария—5,5 кГ/мм².

Из кальция в защитной среде при обычной температуре удалось отпрессовать проволоку диаметром 1 мм, длиной около 15 мм. Давление истечения при степени деформации 75% составило около 90 кГ/мм².

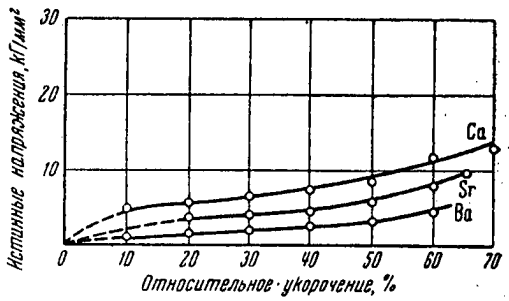

Фиг. 44. Кривые истинных напряжений при сжатии щелочно-земельных металлов.

В случае, если для материала не удается подобрать защитную жидкость, которая бы совершенно не взаимодействовала с ним (такие среды для высоких температур подобрать довольно трудно), испытание приходится проводить в инертном газе (например, аргоне или гелии) или в вакууме.

Вариант прибора для испытаний при высоких температурах в вакууме или в атмосфере инертного газа.

Этот вариант прибора отличается от показанного на фиг. 41 высокотемпературного варианта (для испытаний на воздухе) в основном только тем,

APP. 12.

что все рабочее пространство прибора находится в герметически уплотненном стальном кожухе (фиг. 45).

Кроме требований в отношении уплотнений, предъявляемых ко всякой вакуумной установке, никаких существенных изменений в устройстве прибора не вводится, за исключением применения сильфона *1* и пружины *2*.

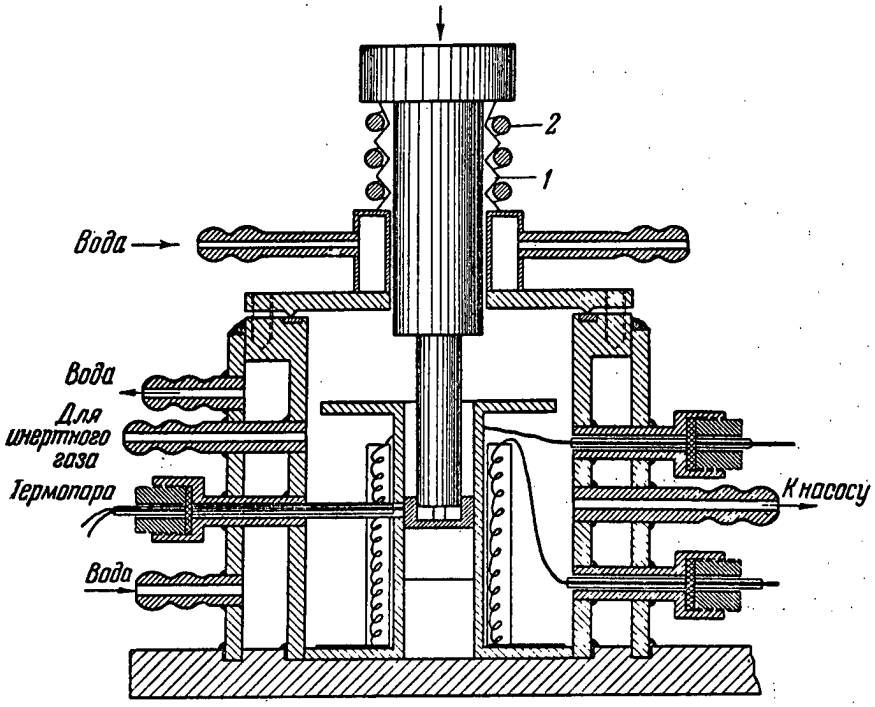

Фиг. 45. Вариант прибора для испытаний при высоких температурах в вакууме или в атмосфере инертного газа (Е. М. Савицкий).

Применением сильфона (гофрированной трубки из латуни или стали) удачно разрешается вопрос о передаче в вакуумное пространство поступательного движения пуансона без уменьшения достигнутой глубины вакуума. Вероятно, могут быть применены и другие способы разрешения этой задачи, например применение резинометаллических сальников. Но на основе имеющегося опыта работы с прибором решение вопроса путем применения сильфона можно считать наилучшим. Пружина *2* необходима для компенсации атмосферного давления. В случае отсутствия этой пружины сильфон после откачки под влиянием атмосферного давления сжимается, а его сошедшиеся вплотную гофры препятствуют свободному ходу пуансона в процессе испытания. Введение наружной рубашки охлаждения вызвано применением резиновых уплотнителей для вывода концов проводов от печи и термопары. При отсутствии охлаждения корпус прибора будет нагреваться от печи, и резина может сгореть. При работе в вакууме каркас электропечи лучше всего изготовлять из кварца, так как всякая керамика при нагреве будет выделять газы и снижать вакуум. В приборе описываемой конструкции при откачке форвакуумным и диффузионным насосами удается сравнительно легко достичь глубины вакуума порядка 10^{-4} или 10^{-5} мм. В особых случаях,

App · 12

для еще большего уменьшения вероятности окисления, в приборе может быть предусмотрено сжигание геттера (стронция, бария и др.).

Описанный вариант вакуумного прибора может быть использован не только при температурах, которые позволяют получить обычные нагреватели (нихром, сплав №2), но и для работы при более высоких температурах, когда в качестве нагревателей в электропечи могут быть применены, например, вольфрам, молибден или тантал. Совершенно очевидно, что в этом случае дополнительных мер по предохранению нагревателей от окисления не потребуется.

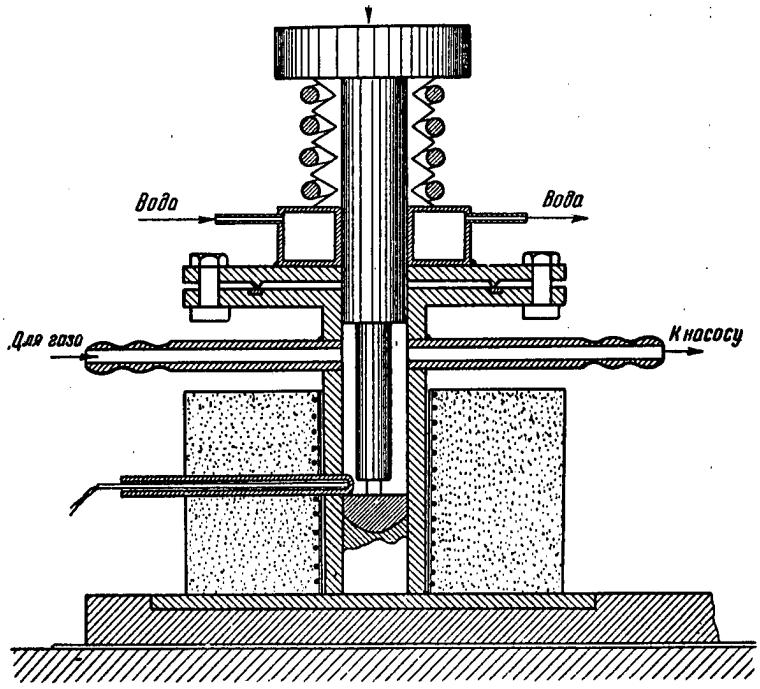

Фиг. 46. Другой вариант прибора для микромеханических испытаний в вакууме или в атмосфере инертного газа (Е. М. Савицкий).

При работе с обычными нагревателями вакуумное пространство прибора может быть уменьшено за счет вывода из него нагревателя. В результате этого схема прибора значительно упрощается (фиг. 46), а глубина вакуума увеличивается.

При испытаниях в вакууме следует предварительно протарировать холостой ход пуансона, и необходимую для этого величину усилия вычитать из показаний силоизмерителя машины во время опыта.

Переход от испытаний в вакууме к испытаниям в инертном газе значительно снижает требования к уплотнениям, охлаждению корпуса прибора и т. д. В этом случае отпадает надобность в пружине *2*, но в наружном кожухе прибора должно быть сделано еще одно отверстие для выхода газа. Снижение качества уплотнения системы при работе по этому варианту приведет лишь к некоторому увеличению расхода инертного газа за счет его утечки из прибора.

Порядок работы на приборе, в случае применения инертного газа или вакуума, следующий: образец, заложенный в соответствующее для того или иного способа испытаний приспособление, вставляется в рабочее пространство цилиндра. К цилиндру при помощи болтов прикрепляется верх-

App. 12

няя часть прибора, состоящая из крышки с охладительной муфтой и пуансона с сильфоном. После этого включаются в работу вакуумные насосы или производится подача инертного газа. Затем включается электропечь, и образец нагревается до заданной температуры. По прошествии необходимого

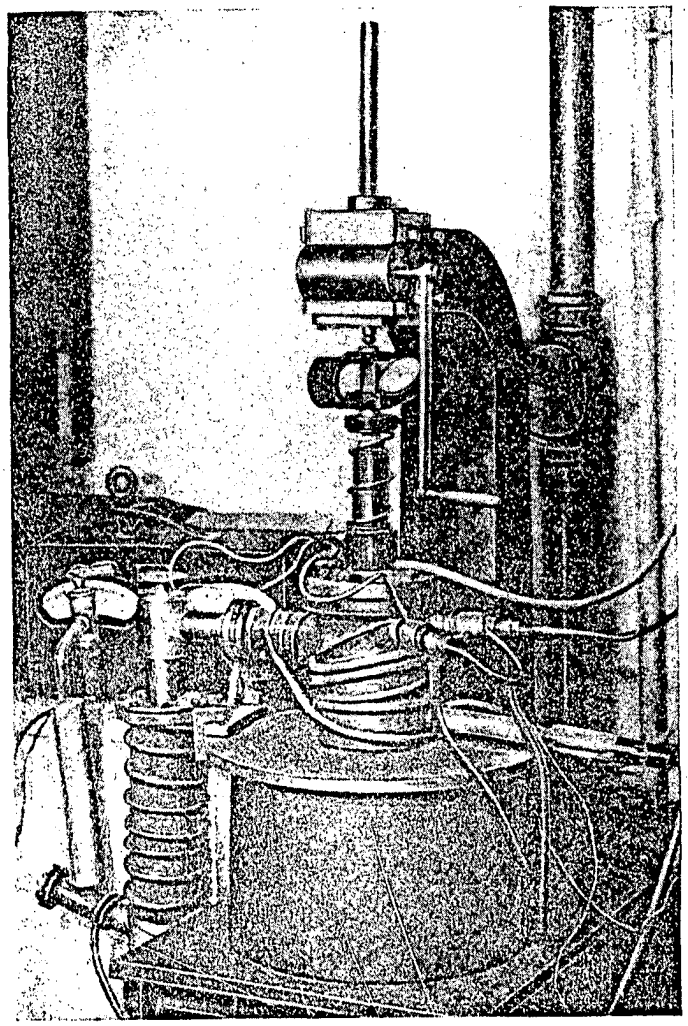

Фиг. 47. Общий вид прибора с нагружающим устройством (вакуумный вариант).

времени выдержки образец и прибор окончательно подготовлены к испытанию. Дальнейший порядок испытания остается точно таким же, каким он был описан для случая испытаний при комнатной температуре.

На фиг. 47 показан общий вид вакуумного варианта прибора с нагружающим устройством в собранном виде.

Некоторые экспериментальные данные. Из большого числа экспериментальных данных, полученных при работе на универсальном приборе, здесь в качестве примера можно привести результаты определений механических свойств сплавов меди с никелем.

Медь и никель, как известно, неограниченно растворимы друг в друге

App. 12

в жидком и твердом состояниях. Полученные нами на микрообразцах данные, характеризующие механические свойства этих сплавов, приведены на фиг. 48.

Н. С. Курнаков и Я. Рапке в свое время измеряли твердость этих сплавов по Бринеллю и установили, что наиболее твердые сплавы в этой системе находятся в области 40—60 вес. % никеля [10]. Проведенное нами измерение

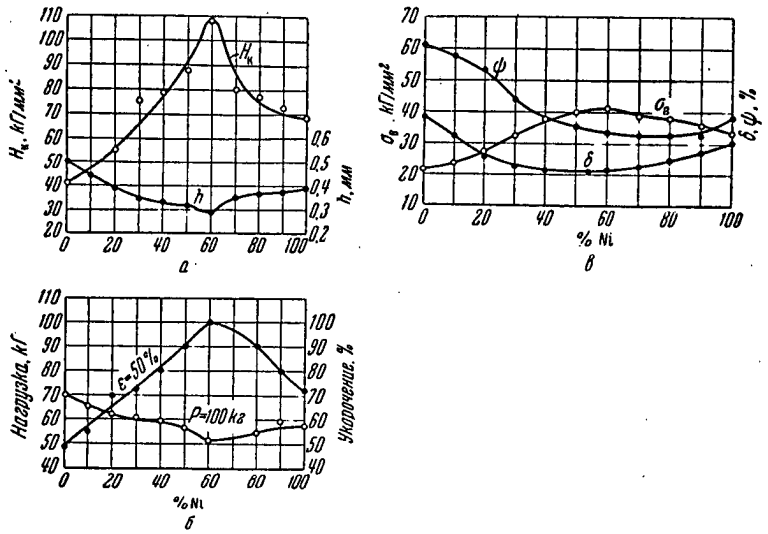

Фиг. 48. Механические свойства сплавов системы медь — никель:

а — твердость: $H_К$ — твердость по конусу, *h* — глубина внедрения конуса; *б* — механические свойства при сжатии; *в* — механические свойства при растяжении.

твердости этих сплавов на микрообразцах путем внедрения конуса позволило уточнить эту область и показать, что наиболее твердым является сплав с 60% никеля. Испытание микрообразцов этих сплавов на сжатие показывает аналогичный ход кривых сопротивляемости деформации и пластичности. В данном случае в качестве меры сопротивляемости деформации нами была взята величина нагрузки, необходимой для сжатия микрообразца цилиндрической формы (диаметром и высотой по 1 мм) на 50% уменьшения высоты; мерой пластичности была взята величина относительного укорочения указанного образца при сжатии нагрузкой в 100 кг. Следует отметить, что для испытаний на сжатие одиннадцати сплавов этой системы по обоим вариантам потребовалось всего 0,2 г чистого веса образцов.

Испытания микроразрывных образцов также подтверждают ход кривых твердости, прочности и пластичности при осаживании. При прибавлении никеля к меди или, наоборот,— меди к никелю прочность сплавов растет, а пластичность падает. Наибольшим пределом прочности обладает сплав с 60% никеля. Вес одиннадцати микроразрывных образцов из различных сплавов меди с никелем составляет около 1,5 г. Для получения достоверных данных о всех основных механических свойствах (твердость, определение характеристик пластичности и прочности при сжатии и растяжении) всей системы потребовалось только около 2 г чистого веса образцов.

Поскольку универсальный прибор в описанной форме был разработан сравнительно недавно, на данной стадии работы его преимущества не могли быть использованы в полном объеме.

App. 12

дования микроструктуры и микротвердости этих образцов показали, что микротвердость твердой и мягкой структурных составляющих совпадает с их микротвердостью в случае литых сплавов, но эвтектика не окружает всех границ кристаллов кремния, а распределяется среди них в виде скоплений (фиг. 114, *б*).

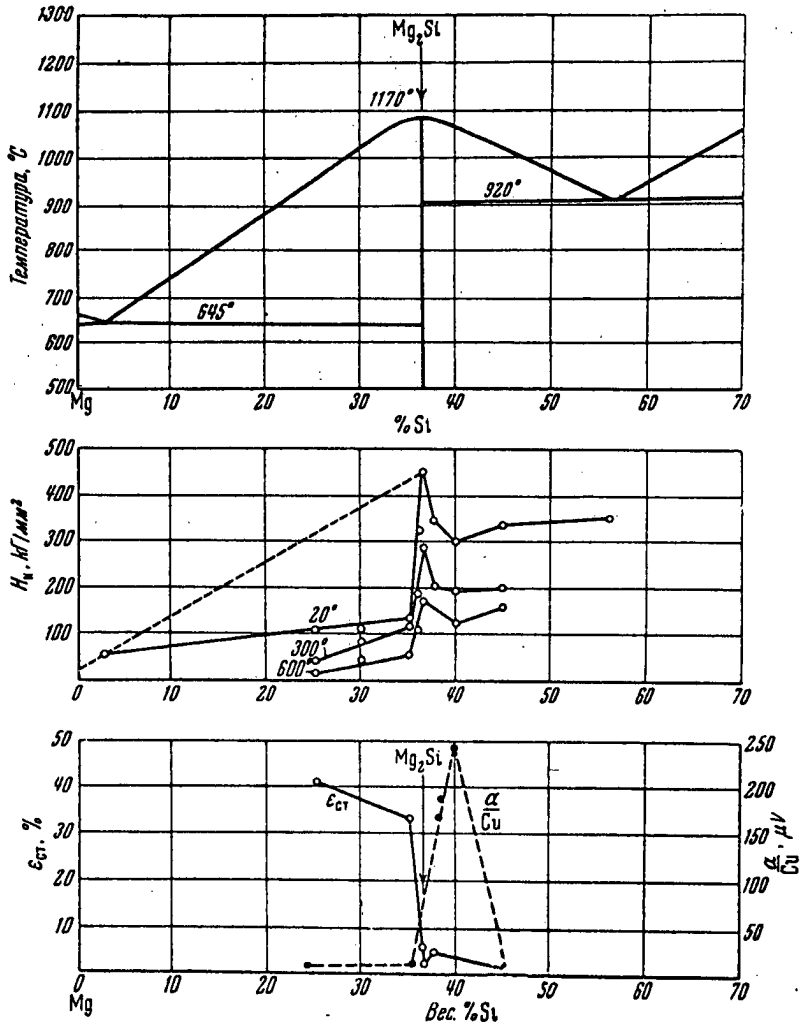

Фиг. 115. Диаграмма состояния, механические свойства и т. э. д. с. $\left(\frac{\alpha}{Cu}\right)$ сплавов Mg—Si.

Пунктиром показана аддитивная прямая твердости.

Система магний — кремний

Сплавы на основе соединения Mg_2Si представляют большой интерес в том отношении, что носитель высокой твердости — тугоплавкое и легкое соединение. Сплавы, расположенные по составу между Mg_2Si и магнием, начинают плавиться при 645°, а между Mg_2Si и кремнием — при 920° (фиг. 115). Силицид магния имеет сложную кубическую гранецентрированную решетку типа плавикового шпата (фиг. 116). Н. В. Агеев и Л. Н. Гусева, на

App. 12

основании определения электронной плотности, отнесли Mg_2Si к координационным соединениям [355б].

Механические свойства сплавов в области соединения Mg_2Si до нас почти не изучались. Образцы для наших опытов изготовлялись сплавлением и металлокерамическим способом. Плавка проводилась в высокочастотной печи в графитовом тигле под карналлитовым флюсом. Отлитые образцы имели много пор. Для увеличения плотности они подвергались осаживанию силой 20 т при 620—630° в стальном цилиндре с внутренним диаметром 22 мм. Измерение микротвердости силицида магния показало, что она составляет всего 450 кГ/мм², хотя, учитывая относительную тугоплавкость этого соединения (около 1200°), можно было ожидать большей величины твердости. Микротвердость эвтектики $Mg + Mg_2Si$ — около 75 кГ/мм², а эвтектики $Mg_2Si + Si$ — около 190 кГ/мм². Микроструктура типичного литого сплава, состоящего из кристаллов силицида магния и эвтектики, показана на фиг. 117, *а*.

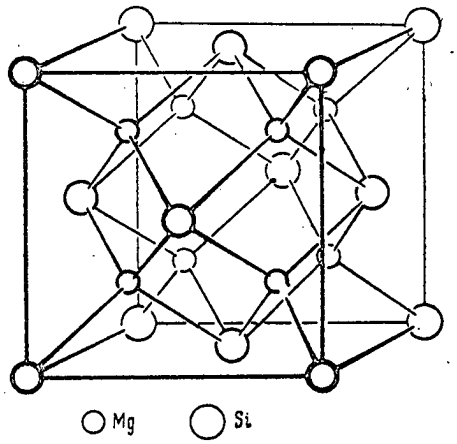

Фиг. 116. Кристаллическая решетка соединения Mg_2Si [228].

Была измерена твердость образцов при 20, 300 и 600°. Испытания производились конусом при нагрузке 30 кг.

Для определения пластичности при сжатии сплавы осаживались силой в 2 т при «соответственных» температурах (563 и 800°), составляющих 90% от температуры плавления по абсолютной шкале температур.

Испытания проводились в атмосфере аргона, так как при повышенных температурах сплавы сильно окислялись.

У литых сплавов после осаживания в контейнере была измерена термоэлектродвижущая сила в паре с медью. Определения производились на установке, сконструированной Н. Х. Абрикосовым. Разность температур холодного и горячего спаев колебалась от 20 до 390°. Т.э.д.с. подсчитывалась по формуле:

$$\alpha = \frac{\Delta E_{Cu-x}}{\Delta t},$$

где Δt — разность температур холодного и горячего спаев; ΔE_{Cu-x} — т. э. д. с. образца в паре с медью; α — термоэлектродвижущая сила в мкв на 1°.

Экспериментальные данные приведены в табл. 34 и на фиг. 115.

Как видно, выводы, сделанные на примере сплавов алюминий — кремний, о решающем влиянии границ кристаллов на величину твердости оказались справедливыми и в данном случае. По обе стороны от соединения правило прямой не соблюдается.

Так, твердость сплава с 35 вес.% кремния (содержащего около 75% силицида магния по объему) составляет при 20° только 130 кГ/мм² вместо ожидаемых 400 кГ/мм².

Содержащие менее 35% Si сплавы, у которых по границам зерен соединения расположена сравнительно мягкая магниевая эвтектика, при всех температурах отличаются относительно небольшой твердостью (до 133 кГ/мм²). Сплавы, у которых в составе эвтектики входит свободный кремний, отличаются высокой твердостью.

Сравнительно высокие значения твердости у сплавов, прилегающих к

App. 12

соединению, объясняются, по-видимому, тем, что у них включения эвтектики не заполняют полностью границ кристаллов соединения. Твердость сплава с 36,5% кремния близка к аддитивной (332 кГ/мм²).

У соединения Mg_2Si относительное падение твердости при нагревании больше, чем у сплавов, но все же значения твердости при 600° остаются

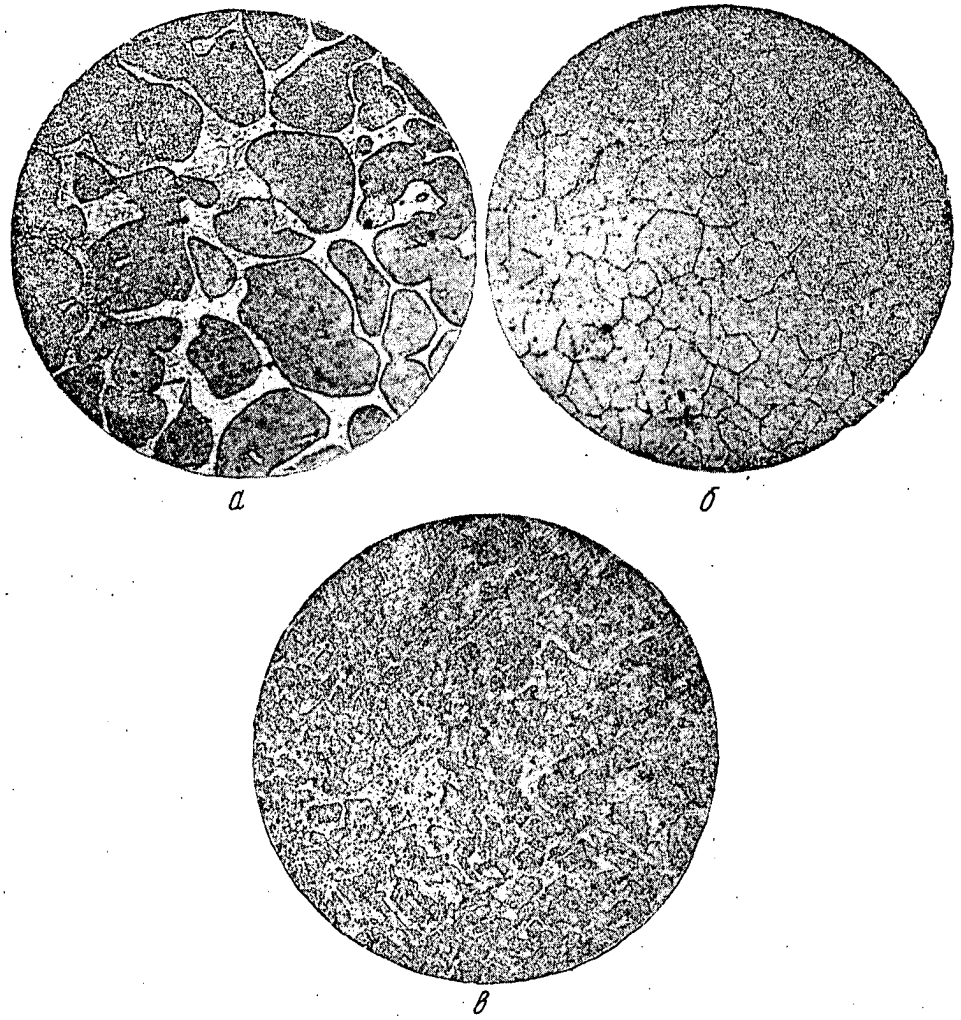

Фиг. 117. Микроструктура магний-кремнистых сплавов. × 150.

а — 30% Si, литой ($H_К$ = 120 кГ/мм²); *б* — 36,9% Si, литой ($H_К$ = 457 кГ/мм²), кристаллы силицида магния; *в* — 30% Si, горячеосажденный.

довольно высокими (180 кГ/мм²). Сплавы со значительным содержанием кремния (40 и 45%) также сохраняют высокие значения твердости при 300 и 600°. Сплавы на основе соединения Mg_2Si отличаются низкой пластичностью при сжатии (порядка 2%). Сплавы, содержащие значительные включения сравнительно мягкой магниевой эвтектики (до 35% Si вкл.), значительно более пластичны при повышенных температурах (до 40% при 600°). Таким образом, пластичность литых образцов изменяется в направлении, обратном изменению твердости.

App. 12

В соответствии с изложенным в главе III, третьей части с повышением температуры прочность на сжатие сплавов возрастает; так, у сплава с 45% кремния она составляет при 600° 12 кГ/мм² по сравнению с 0,3 кГ/мм² при 20°. Таким образом, образцы при нагревании становятся как бы более металлическими.

Таблица 34

Твердость, пластичность и термоэлектродвижущая сила литых сплавов на основе Mg_2Si

Содержание Si, вес.%	Твердость, $H_к$, кГ/мм² при различных температурах			Относительное укорочение при сжатии $\varepsilon_{ст}$ ($T=20°$/ от $T_{пл}$)	Т.э.д.с. в паре с медью, мкв/градус	Микроструктура сплавов
	20°	300°	600°			
3	46	—	—	—	—	Кристаллы соединения Mg_2Si и эвтектика $Mg + Mg_2Si$
15	70	—	—	—	—	То же
25	113	30	14	43,4	4	»
30	120	86	32	—	—	»
35	133	128	40	38,2	6	»
36,5	332	187	108	5,0	—	Кристаллы соединения Mg_2Si
36,9	457	320	180	2,2	180	Кристаллы соединения и эвтектика $Mg_2Si + Si$
37,0	350	200	—	4,4	—	То же
40	308	204	117	2,0	240	»
45	346	200	169	1,6	126	»
57	365	—	—	—	—	Кристаллы кремния
100	1100	—	—	—	150	

Сплавы на основе силицида магния имеют высокие значения т.э.д.с. — порядка 200 мкв/градус. У сплава с 40% Si, состоящего из кристаллов силицида магния и эвтектики $Mg_2Si + Si$, значения т. э. д. с., примерно, в 50 раз больше, чем у сплавов, включающих до 35% кремния (см. фиг. 115). Т.э.д.с. сплавов в данной системе изменяется с составом, в общем, аналогично твердости. Т.э.д.с. является одной из весьма структурно-чувствительных характеристик и должна чаще использоваться при физико-химическом исследовании сплавов. Установлено, что свойства литых магний-кремнистых сплавов в значительной мере определяются взаимным расположением структурных составляющих. Расположение эвтектики по границам зерен —причина нарушения аддитивности в изменении свойств в зависимости от состава. Попытки изменить расположение составляющих при помощи сжатия образцов в нагретом контейнере существенных результатов не дали — расположение составляющих не изменилось (фиг. 117, *в*). Так же как и в системе Al — Si, причиной неудачи здесь, по-видимому, явилась большая разница в твердости и в температурах плавления отдельных составляющих, характерная для этих сплавов.

Можно было предполагать, что в случае, если бы эвтектику удалось распределить равномерно внутри зерен соединения, то твердость сплава определялась бы главным образом твердостью кристаллов соединения. Представляло также большой интерес проследить, как изменится твердость сплава, если по границам твердой составляющей будет залегать не эвтектическая смесь, а какие-либо пластичные металлы, например, алюминий и медь. Для этого было решено прибегнуть к металлокерамике. Были изготовлены

App. 12

металлокерамические образцы из смеси порошков Mg_2Si с различным содержанием алюминия (до 20%). Аналогичным образом были сделаны образцы из указанного соединения с добавкой 30% меди. Для приготовления образцов измельченный сплав, соответствующий по составу соединению Mg_2Si, смешивался с соответствующим количеством алюминиевого или медного порошка. Оба порошка предварительно просеивались через сито с диаметром отверстий 0,25 мм. Смешение порошков производилось в специальном сме-

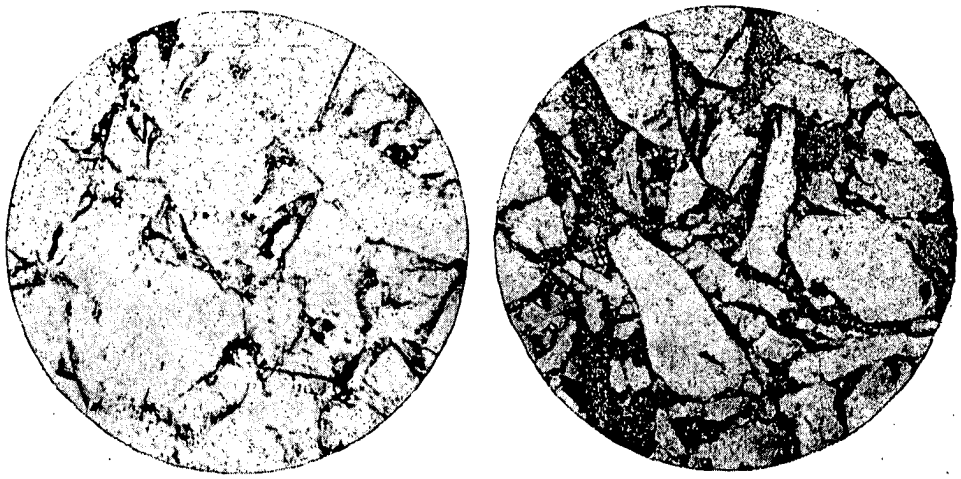

а *б*

Фиг. 118. Микроструктура металлокерамических образцов. × 150.
а — Mg_2Si + 5% Al; *б* — Mg_2Si + 30% Cu.

сителе с эксцентрической осью вращения. К порошкам добавлялась олеиновая кислота (из расчета 1 мг на 1 г смеси), играющая роль поверхностно-активной смазки, образующей прочную адсорбционную пленку на поверхности частиц порошка.

Смешанные порошки засыпались в прессформу и брикетировались вхолодную. Затем в этой же прессформе при 500—530° брикеты подвергались спрессовыванию под давлением 3—10 т/см².

На фиг. 118 приведены микроструктуры полученных металлокерамических образцов.

Методика измерения твердости была такой же, как и для литых сплавов. Полученные данные приведены в табл. 35.

Таблица 35

Твердость металлокерамических сплавов на основе Mg_2Si, $H_к$, кГ/мм²

Температура, °С	Добавка алюминия, вес. %				Добавка 30 вес. % Cu
	0*	5	10	20	
20	457	400	250	180	220
300	320	197	122	117	197
600	180	96	92	54	100

* Литой сплав (Mg_2Si).

App. 12

($a = 10{,}66$Å, $c = 17{,}16$Å, $\frac{c}{a} = 1{,}61$). В элементарной ячейке содержится 48 атомов [410]. Следует отметить, что соединение MgZn и по микроструктурным данным очень похоже на соединение $MgZn_2$, поэтому оно было обнаружено относительно недавно, лишь после применения специального травителя (так называемый раствор Бенедикса). Соединение $MgZn_5$ кристаллизуется в простой кубической решетке, постоянная которой равна 8,53Å. Число атомов в элементарной ячейке около 32 [411].

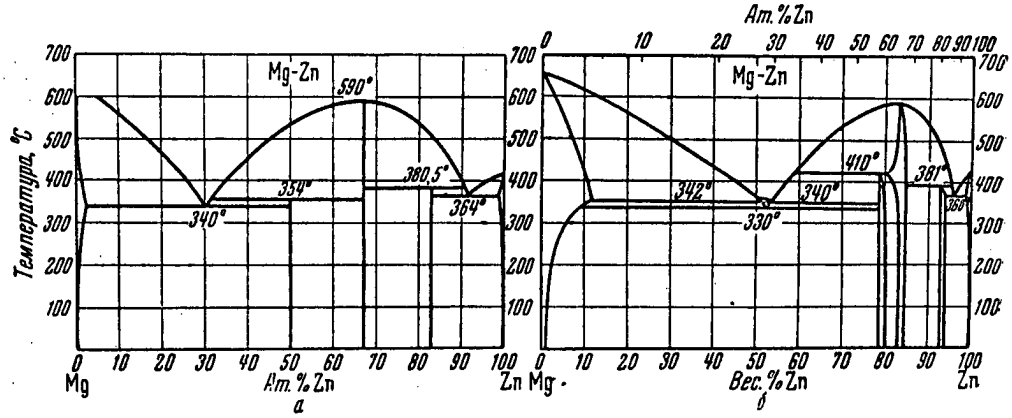

Фиг. 151. Диаграмма состояния системы магний — цинк:
а — по Юм-Розери; *б* — по Такей.

Соединение $MgZn_5$, согласно Лавесу [406], более точно описывается формулой Mg_2Zn_{11}. Однако это утверждение, по-видимому, неверно.

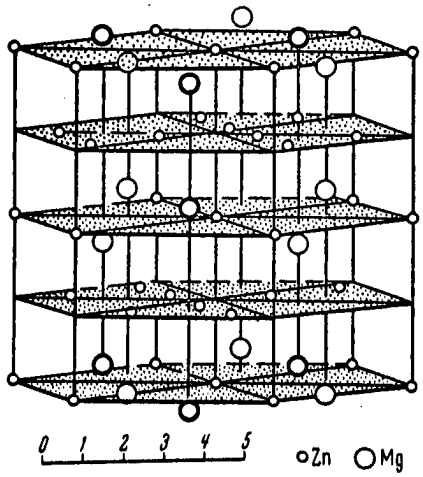

Фиг. 152. Структура $MgZn_2$ [43].

О характере химической связи в указанных соединениях в литературе определенных указаний нет.

Противоречивость опубликованных данных о системе Mg — Zn побудила нас сделать попытку разобраться в причинах имеющихся расхождений. Кроме того, имелось еще одно важное основание к этому, а именно: все предыдущие исследования богатых металлическими соединениями сплавов проводились на литых образцах. Получить деформированные образцы из-за большой хрупкости таких сплавов при комнатной температуре никому до сих пор не удавалось. Мы провели работу на сплавах как в литом, так и в обработанном давлением состояниях. В работе основное внимание было уделено двум вопросам: влиянию кинетики установления равновесия на вид диаграммы Mg — Zn, а также диаграмм состав — механические свойства и изучению влияния температуры на механические свойства богатых металлическими соединениями сплавов.

Исследования проводились на 25 сплавах, расположенных по концентрации цинка в интервале от 24 до 96 вес. % . Образцы изготовлялись из магния

App. 12

марки МГ-1 (99,9% Mg) и цинка марки Ц-1 (99,94% Zn). Плавка велась в тигельной электропечи в графитовых тиглях под покровом предварительно обезвоженного карналлитового флюса. Состав сплавов контролировался химическим анализом. Образцы деформировались путем горячего прессования на установке, показанной на фиг. 27. Задача эта оказалась весьма трудной, так как для получения сравнимых данных все сплавы данной системы должны были быть обработаны в одинаковых условиях, которые лимитировались пластичностью наиболее хрупкого сплава. Поэтому пришлось произвести предварительное опробование всех сплавов, найти оптимальные условия пластического деформирования для каждого и лишь после этого выбрать общие для всех условия получения образцов и их испытаний. На выработку методики и установление оптимальных и сравнимых условий ушло в общей сложности больше времени, чем на испытания.

В результате предварительных опытов было установлено, что при правильно выбранных условиях прессования (температура, скорость, степень деформации и надлежащая смазка) все отлитые сплавы могут быть получены в виде доброкачественных прутков. Правда, все же некоторые литые сплавы не выдерживали больше 50% обжатия. Поэтому для получения большего эффекта от деформации было введено прессование в два приема. В первом переходе слиток диаметром 22 м продавливался через матрицу диаметром 15 мм, т. е. обжимался приблизительно на 50% . Во втором переходе полученные прутки сплава прессовались в приборе с диаметром внутреннего отверстия 15 мм через матрицу с диаметром очка 10 мм, т. е. также на 50%. В качестве смазки при прессовании применялась смесь графита и машинного масла. Полученные образцы использовались для определения твердости и давления истечения сплавов в деформированном состоянии при различных температурах. Прессование образцов и определение давления истечения производились при температурах на 15—20° ниже точки плавления. Для приведения сплавов в равновесное состояние применялся отжиг. По литературным данным, для литых сплавов этой системы требуется очень длительный отжиг — до 90 суток [402]. С целью ускорения процессов диффузии желательно отжигать сплавы при наиболее высоких температурах. Но, учитывая, что сплавы системы магний — цинк значительно различаются по температурам плавления, во избежание пережога они были разбиты на четыре группы; в каждой группе находились сплавы с близкими температурами плавления. Отжиг сплавов производился при температурах, указанных в табл. 50.

Таблица 50

Условия отжига сплавов системы Mg — Zn

Содержание Zn, вес. %	Температура отжига, °С	Продолжительность отжига	Условия охлаждения образцов
От 20 до 72,89 . . .	300	5, 10 и 20 суток	Охлаждение вместе с печью в течение двух суток
От 72,89 до 84,74 . .	320		
От 84,74 до 92,7 . .	340		
От 92,7 до 100 . . .	335		

Образцы нагревались под слоем порошка окиси алюминия; щель между корпусом и крышкой муфеля замазывалась глиной. Степень достижения равновесия контролировалась методом микроструктуры. Сплав считался

App. 12

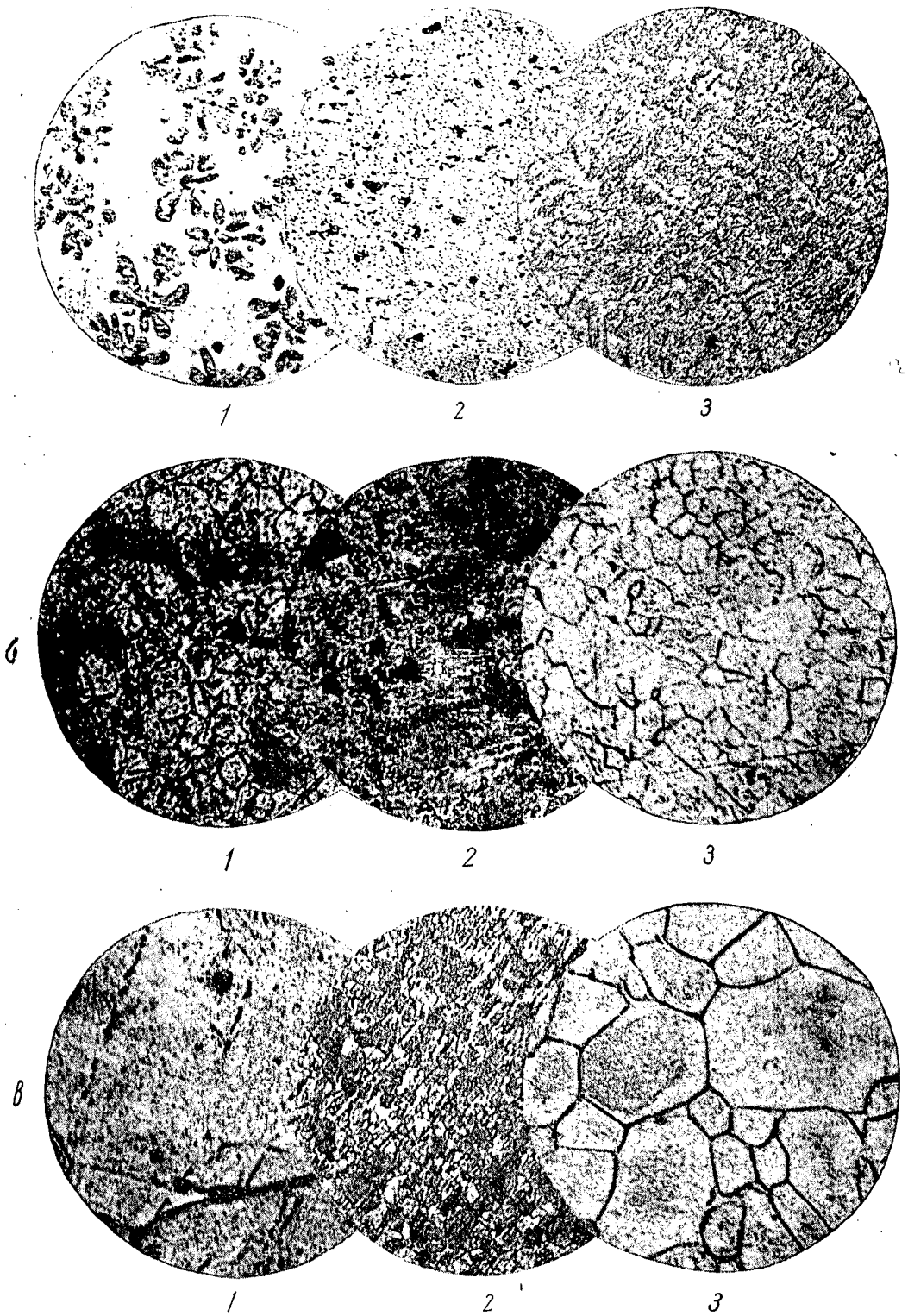

Фиг. 153. Микроструктура сплавов системы Mg—Zn (в различных состояниях)×600.

а — 45,6 вес. % Zn
1) Литой (α + эвтектика); 2) деформированный (α + эвтектика); *3*) отожженный (α + эвтектика).
б — 76,8 вес. % Zn
1) Литой (MgZn + эвтектика); 2) деформированный (MgZn + эвтектика); *3*) отожженный (MgZn).
в — 85 вес. % Zn
1) Литой ($MgZn_2$ + эвтектика); 2) деформированный ($MgZn_2$); *3*) отожженный ($MgZn_2$).

App. 12

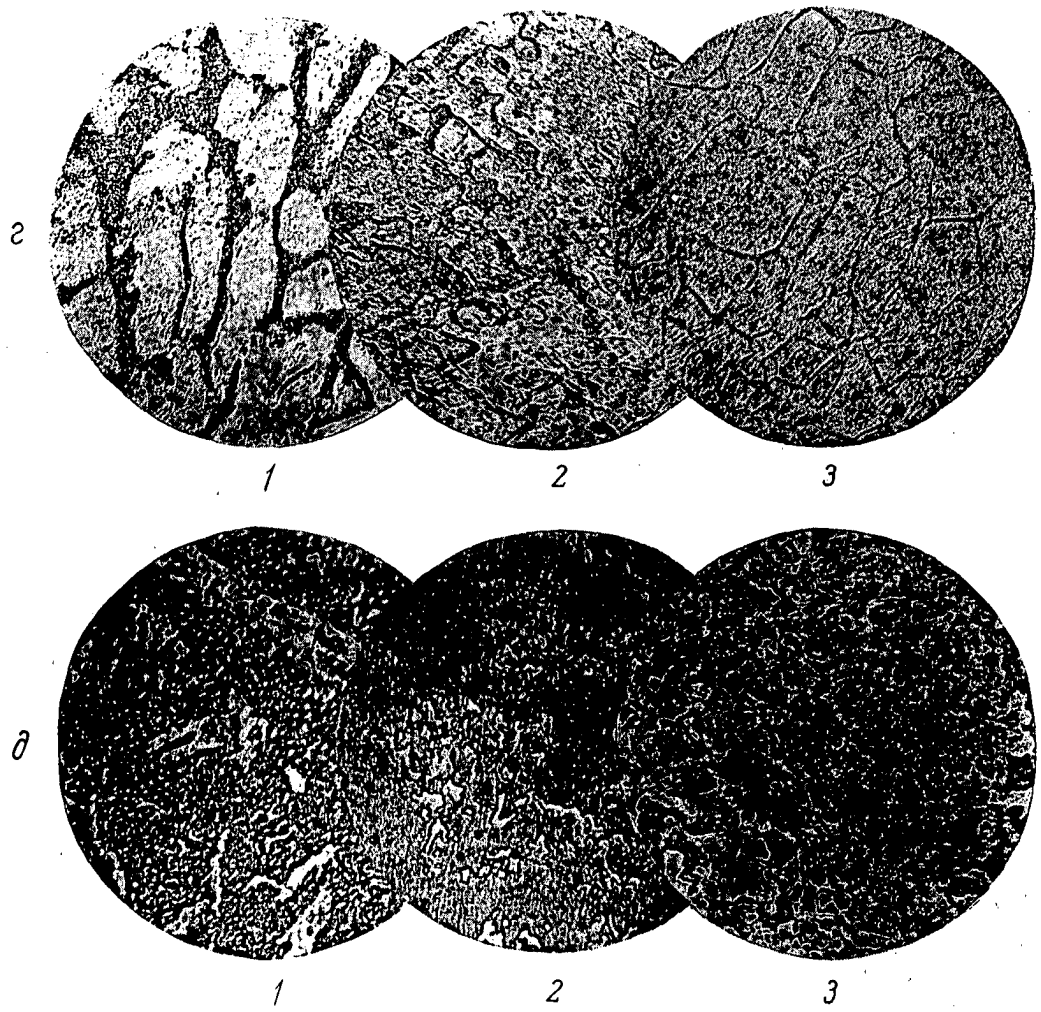

Фиг. 153. Микроструктура сплавов системы Mg — Zn (в различных состояниях) × 600.

г — 93,1 вес. % Zn

1) Деформированный, отожженный 5 суток ($MgZn_2 + MgZn_5$); *2*) деформированный, отожженный 10 суток ($MgZn_5$); *3*) деформированный, отожженный 20 суток ($MgZn_5$).

д — 96,6 вес. % Zn

1) Литой ($MgZn_5$ + эвтектика); *2*) деформированный ($MgZn_5$ + эвтектика); *3*) отожженный ($MgZn_5$ + эвтектика).

Горячая деформация (прессование) резко измельчает структуру (см. фиг. 153), создает свежие стыки между зернами и способствует более быстрому выравниванию состава образцов. Но все же, в силу медленного протекания диффузии, особенно в области соединения MgZn, деформированные неотожженные сплавы не являются полностью равновесными. В соответствии с этим в микроструктуре сплавов, в области возможного существования гомогенных областей, еще содержатся небольшие включения второй фазы (см. фиг. 153), а на кривых состав — механическое свойство при 20° только соединение $MgZn_5$ имеет сингулярную точку—минимум (фиг. 155, табл. 51).

На фиг. 155 и в табл. 51 видно, что деформированные сплавы в области соединения MgZn при обычной и повышенных температурах выделяются величиной своей твердости и давления истечения. Вероятно, в этих сплавах

App. 12

при деформации или небольшом нагреве происходит подготовка к образованию соединения MgZn, а может быть даже его выделение в мелкодисперсной форме, что вызывает искажение основной структуры сплавов и повы-

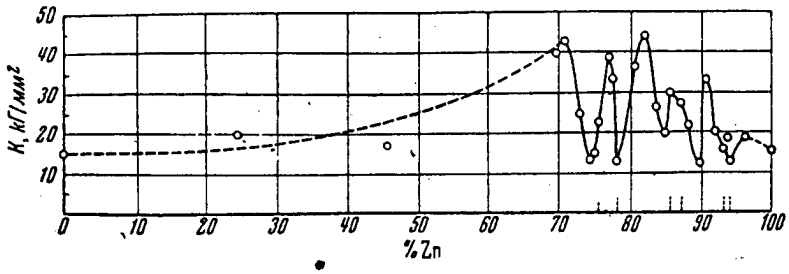

Фиг. 154. Давление истечения литых магний-цинковых сплавов.

шение твердости до 350 кГ/мм². В процессе измерения твердости выше 300° возможно уже происходит частичная «коагуляция» соединения, так как максимумы твердости сглаживаются. Сказанное относится также и к соединению $MgZn_2$. Кинетику процессов старения в этом случае следует изу-

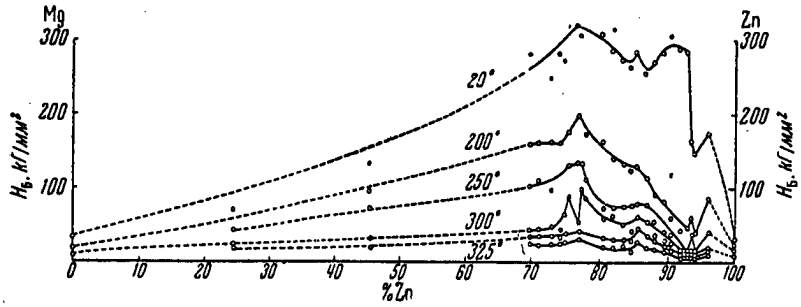

Фиг. 155. Твердость деформированных магний-цинковых сплавов при различных температурах.

чить более подробно, так как MgZn и $MgZn_2$ — упрочнители некоторых термически обрабатываемых сплавов магния с алюминием и цинком.

Применение механической и термической обработки образцов значительно сокращает время приближения сплавов к равновесному состоянию при отжиге и, следовательно, позволяет выявить более соответствующий данному типу химического взаимодействия компонентов вид диаграммы состояния и диаграмм состав — свойство. Твердость изучавшихся сплавов зависит от времени отжига (фиг. 156).

Наиболее равновесными из изучавшихся нами оказались деформированные и отожженные в течение 20 суток сплавы. Пятисуточный отжиг не внес принципиальных изменений в ход изотермы твердости по отношению к литому состоянию, но отдельные сплавы увеличили свою твердость. Так, сплав с 76,8% Zn, соответствующий соединению MgZn, в деформированном виде имел твердость 315 кГ/мм², а после пятисуточного отжига — 357 кГ/мм². После десятисуточного отжига деформированных сплавов соединение MgZn на изотерме твердости стало выделяться глубоким минимумом.

App. 12

Механические свойства

Вес. % Zn	Температура испытания, °С	Литые сплавы				Твер
		Твердость, $H_Б$, кГ/мм²		Давление истечения неотожженных сплавов, K, кГ/мм²		
		без отжига	после отжига (5 суток)			без отжига
24,2	20 325	128	102	20,0		118,0 15,9
45,6	20 325	194	138	17,1		109,0 15,9
69,8	20 325	260	303	40,7		280,0 38,1
70,8	20 325	303		43,7		204,0 25,9
72,9	20 325	297	280	25,0		270,0 31,2
74,3	20 325	260	225	13,1		280,0 31,2
74,8	20 325		242	14,7	335°	270,0 37,0
75,4	20 325	291	373	23,1		315,0 34,4
76,8	20 325	303	342	39,4		315,0 38,1
77,0	20 325	233	315	33,4		303,0 34,4
77,5	20 325	280	315	13,1		303,0 34,4
80,6	20 325	265	260	36,8		303,0 31,2
81,5	20 325	255	280	44,7		280,0 27,5
83,1	20 325	197	225	26,3		270,0 27,0
84,3	20 325	200	208	19,7		260,0 24,8
85,0	20 325	280	170	28,9		280,0 47,5
86,6	20 325	197	208	27,6	365°	251,0 38,0
87,9	20 325	237	251	22,3		265,0 25,9
89,4	20 325	150	242	11,8		280,0 18,5
90,2	20 325	144	260	33,7		303,0 23,8
91,7	20 325	142	225	20,3		285,0 7,0
92,6	20 325	233	260	15,8		280,0 7,0
92,7	20 325	129	242	18,4	345°	159,0 9,1
93,1	20 325	194	121	14,5		146,0 5,6
95,6	20 325	200	218	18,7		74,0 9,1

App. 12

Таблица 51

сплавов системы магний — цинк

Деформированные сплавы						
дость, $H_Б$, кГ/мм²			Температурный коэффициент твердости сплавов, отожженных 20 суток (20—325°)	Давление истечения K, кГ/мм²		
после отжига				без отжига		после отжига (5 суток)
5 суток	10 суток	20 суток				
90,7 18,4		73,2 12,0	$-0,26\cdot10^{-3}$	29,9		17,7
164,0 18,4		126,0 11,0	$-0,35\cdot10^{-3}$	23,0		21,1
233,0 31,2		138,0 25,0	$-0,2\cdot10^{-3}$	57,0		20,4
233,0 28,4	159	242,0 18,9	—	59,8		15,3
280,0 34,4		233,0 45,6	$-0,23\cdot10^{-3}$	45,4		20,7
303,0 31,2		233,0 31,3	$-0,25\cdot10^{-3}$	—		19,9
260,0 34,4	291	270,0 65,0	$-0,2\cdot10^{-3}$	40,8		23,6
280,0 47,5	303	280,0 41,6	$-0,27\cdot10^{-3}$	38,8	335°	26,1
357,0 41,9	150	107,0 37,0	$-0,15\cdot10^{-3}$	63,7		29,3
303,0 38,1	303	246,0 43,9	$-0,25\cdot10^{-3}$	42,0		22,1
315,0 41,9	315	280,0 50,0	$-0,25\cdot10^{-3}$	35,0		23,1
280,0 38,1		260,0 60,4	$-0,21\cdot10^{-3}$	38,7		23,5
342,0 40,0		290,0 50,0	$-0,25\cdot10^{-3}$	40,1		14,5
315,0 38,1		280,0 45,6	$-0,26\cdot10^{-3}$	34,7		22,9
199,0 31,2		246,0 25,2	$-0,33\cdot10^{-3}$	31,5		18,1
290,0 53,1		255,0 45,6	$-0,24\cdot10^{-3}$	42,3		25,1
233,0 28,4		212,0 25,2	$-0,31\cdot10^{-3}$	20,6		21,1
303,0 26,1		251,0 22,4	$-0,35\cdot10^{-3}$	20,4		14,8
270,0 19,3		191,0 15,0	$-0,36\cdot10^{-3}$	24,4		15,3
291,0 20,1		242,0 14,5	$-0,4\cdot10^{-3}$	33,5	365°	15,1
280,0 17,1		242,0 15,7	$-0,39\cdot10^{-3}$	20,4		16,3
303,0 28,4		251,0 28,3	—	14,1		22,9
185,0 15,9		218,0 11,0	$-0,43\cdot10^{-3}$	22,9		15,03
138,0 15,6		84,9 8,0	$-0,33\cdot10^{-3}$	17,2		14,5
179,0 17,1		233,0 16,9	$-0,38\cdot10^{-3}$	23,5	345°	16,9

App. 12

Даже при беглом взгляде на изотерму 20° твердости после 20-суточного отжига становится ясным, что, несмотря на некоторые вызванные неоднородностью структуры колебания, твердость определяется, в первую очередь, химической природой сплавов. Все три имеющихся в этой системе металлических соединения на изотерме твердости выделяются особыми точками: MgZn и $MgZn_5$—глубокими минимумами, $MgZn_2$—небольшим максимумом. В области соединения MgZn и $MgZn_5$ изменение состава сплавов на 1,5—2% может привести к изменению твердости в 1,5—2,5 раза. Так, например, сплав

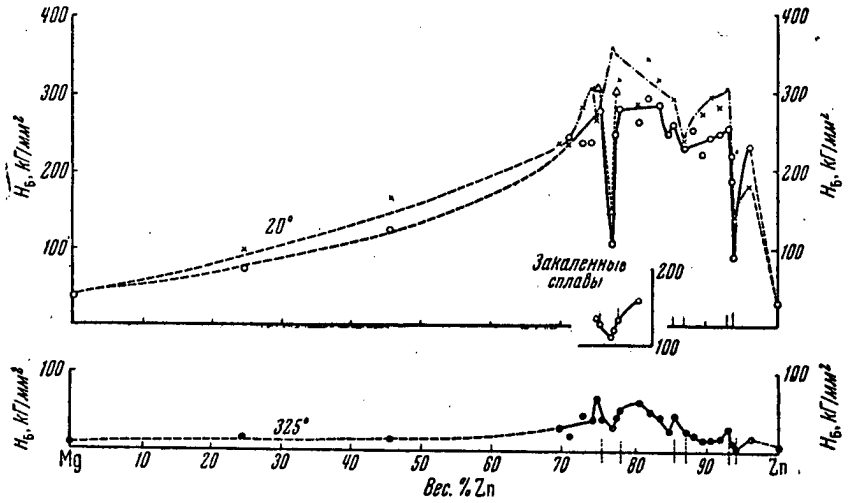

Фиг. 156. Твердость деформированных и отожженных сплавов системы Mg — Zn:

×—•—× — отожженные 5 суток; Δ———Δ—отожженные 10 суток; о—о — отожженные 20 суток; •—•— твердость при 325° деформированных и отожженных (20 суток) сплавов.

с 76,8% Zn имеет твердость 107 кГ/мм², а сплав с 75,4% Zn—280 кГ/мм² или сплав с 93,1% Zn имеет твердость 85 кГ/мм², тогда как сплав с 92,6% Zn—251 кГ/мм². На фиг. 156 показана также изотерма 325° твердости после 20-суточного отжига и твердость закаленных с 325° сплавов при 20° в области соединения MgZn. На обеих кривых обращает на себя внимание смещение максимальных значений твердости сплавов в области твердых растворов на основе MgZn в обе стороны от состава соединения по сравнению с комнатной температурой, что свидетельствует о расширении области однородности с повышением температуры. Твердость сплава в закаленном состоянии, соответствующего по составу соединению MgZn, точнее Mg_5Zn_6 (76,8% Zn), равна 117 кГ/мм², тогда как сплавы с 74,8% Zn и с 80,6% Zn имеют соответственно твердость 132 и 159 кГ/мм².

Соединение $MgZn_2$ имеет значительно более высокую температуру плавления (около 590° против 354 и 380 у соседних сплавов). Поэтому на обычных изотермах твердости оно не дает минимума. Минимум, а также наличие областей твердых растворов, четко выявляется только при построении изотерм твердости в «соответственных» (в равных долях от абсолютной температуры плавления) температурах (фиг. 157).

На деформированных и отожженных в течение 20 суток образцах методом микроструктуры было установлено наличие в системе Mg—Zn трех однофазных областей, соответственно располагающихся в области существования соединений $MgZn_2$ $MgZn_2$ и $MgZn_5$ (см. фиг. 153).

Арр. 12

Метод твердости показал, что эти области несколько расширяются с повышением температуры.

Примерные границы однофазных областей при 20° следующие: в области соединения MgZn—от 75,4 до 77,5 вес.% Zn; в области соединения $MgZn_2$—от 85,0 до 86,6 вес.% Zn; в области соединения $MgZn_5$—от 92,7 до 93,1 вес.% Zn.

Точное установление границ однофазных областей и изменение их положения с температурой не входило в задачу данной работы.

Твердость сплавов, представляющих собой смеси твердых растворов на основе соединений, в общем, следует правилу аддитивности как при обычных, так и при высоких соответственных температурах.

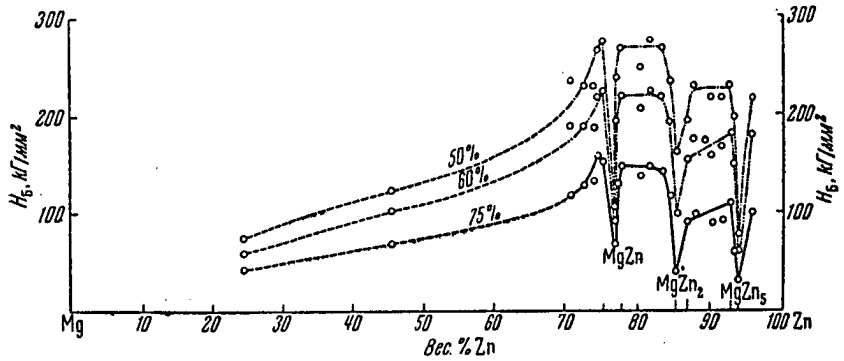

Фиг. 157. Твердость сплавов системы магний — цинк при соответственных температурах (50, 60 и 75% от абсолютной температуры плавления) (Е. М. Савицкий и В. В. Барон).

Указанные три соединения характеризуются наличием сингулярных минимумов на изотермах твердости (см. фиг. 156, 157). Эти экспериментальные факты свидетельствуют не только о существовании указанных металлических соединений, но и об их дальтонидном характере. Таким образом, наши данные опровергают утверждения о существовании соединения Mg_7Zn_3 (Костер), Mg_2Zn_3 (Такей) и Mg_2Zn (Лавес и Вернер), а также о полном отсутствии у соединений системы Mg—Zn способности к образованию твердых растворов (Юм-Розери и Роунсфелл). Установленное ранее на литых отожженных образцах наличие соединений MgZn, $MgZn_2$ и $MgZn_5$ (Г. Г. Уразов, Н. А. Филин, А. В. Шашин, Юм-Розери, М. И. Захарова и А. Б. Млодзеевский, В.И.Михеева, Ф. И. Шамрай и др.) бесспорно. Бесспорно также и образование твердых растворов на основе каждого из этих соединений.

Нами подробно изучалось влияние температуры на механические свойства сплавов. Оказалось, что при комнатной температуре сплавы Mg—Zn в области, богатой соединениями, характеризуются во всех состояниях не только хрупкостью, но и большой твердостью (табл. 51, фиг. 155—157). Твердость этих сплавов раз в десять больше твердости как магния, так и цинка. Особенно в этом отношении выделяются сплавы на основе соединений MgZn и $MgZn_2$, твердость которых при 20°, в среднем, равна около 300 кГ/мм². После деформации твердость сплавов из-за измельчения зерна еще более возрастает, и некоторые из них становятся способными царапать стекло. Давление истечения этих сплавов значительно выше величин давления истечения чистых металлов и достигает 40—60 кГ/мм² (табл. 51). Давление истечения магния при этой температуре равно 15 кГ/мм², а цинка—17 кГ/мм². Обращает на себя внимание низкая (меньше единицы) величина отношения давления истечения к твердости сплавов, богатых соединениями (фиг. 158).

App. 12

С повышением температуры сплавы интенсивно размягчаются (см. табл. 51, фиг 155—160). Например, при 325° величина их твердости составляет 30—50 кГ/мм², т. е. порядка 10% от ее величины при комнатной температуре. По приближенной оценке (по твердости) предел прочности у соединения $MgZn_5$ при 350° меньше 1 кГ/мм². Относительное падение твердости при нагревании наибольшее у сплавов, представляющих смесь металлических соединений

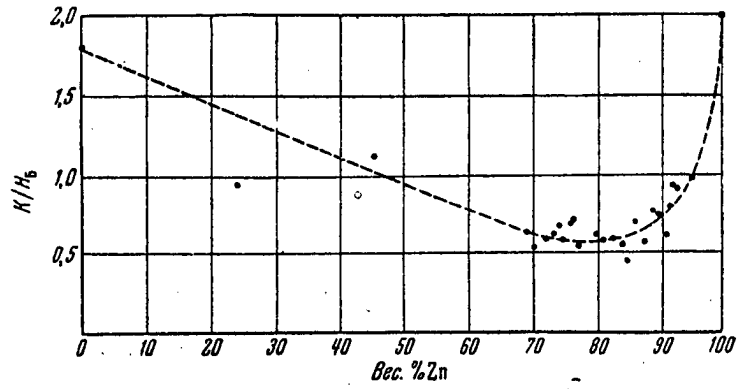

Фиг. 158. Отношение давления истечения к твердости сплавов системы магний — цинк.

или особенно их твердых растворов (см. фиг. 160). Затем следуют сплавы, содержащие значительные включения эвтектик. Так, например, сплав с 45,6% Zn, близкий по составу к эвтектическому, имеет при 20° твердость 109 кГ/мм², а при 325° 16 кГ/мм², т. е. его твердость уменьшается примерно в семь раз. Сплав с 80,6% Zn, являющийся по своей

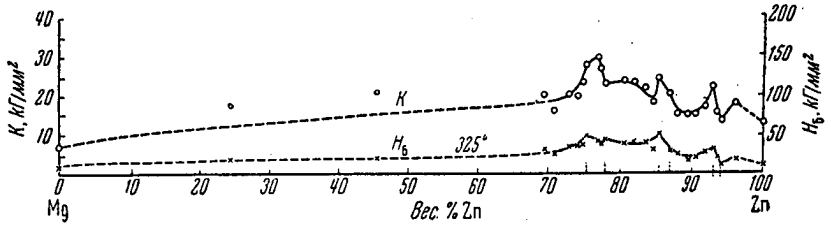

Фиг. 159. Твердость и давление истечения магний-цинковых сплавов при повышенных температурах (после отжига в течение 5 суток).

структуре смесью твердых растворов соединений $MgZn_2$ и $MgZn_5$, при нагреве от комнатной температуры до 325° снижает свою твердость с 303 до 31 кГ/мм², т. е. примерно в десять раз. Таково же поведение других аналогичных по структуре сплавов. Такое изменение твердости при нагревании происходит, по-видимому, из-за резкой разницы в твердости обеих групп сплавов при комнатной температуре. Поэтому недоумение, высказанное Луори по этому поводу, не оправдано [341]. На примере этой системы видно, что чем тверже сплав при обычной температуре, тем сильнее он размягчается при нагревании. Как видно из данных табл. 51 и фиг. 161, чистые соединения по сравнению с соседними сплавами имеют в интервале 20—325° минимальные температурные коэффициенты твердости, т. е. при нагревании размягчаются меньше, чем их смеси или сплавы со значительными включениями эвтектики.

Наиболее чувствительными к воздействию температуры оказались сплавы в области соединения $MgZn_5$. У них наибольший температурный

App. 12

коэффициент твердости и при 325° они наиболее мягкие (твердость менее 10 кГ/мм²). С точки зрения удобства обрабатываемости и значительного увеличения твердости при термической обработке, сплавы в области $MgZn_5$ имеют практический интерес.

Сплавы системы Mg — Zn, в том числе и богатые металлическими соединениями, при нагревании сильно увеличивают свою пластичность. Это увеличение пластичности так велико, что при правильно выбранной температуре любой сплав системы Mg—Zn, отличающийся при комнатной температуре большой хрупкостью и твердостью, может быть продавлен через очко цилиндрической матрицы в виде доброкачественного прутка, а цилиндр из такого сплава может быть сдавлен в диск небольшой толщины. Сплавы при этом выдерживают 80—90% деформации за один прием. Именно интенсивное размягчение сплавов и позволило нам получить деформированные образцы из этих соединений, о чем более подробно уже говорилось в главе III третьей части.

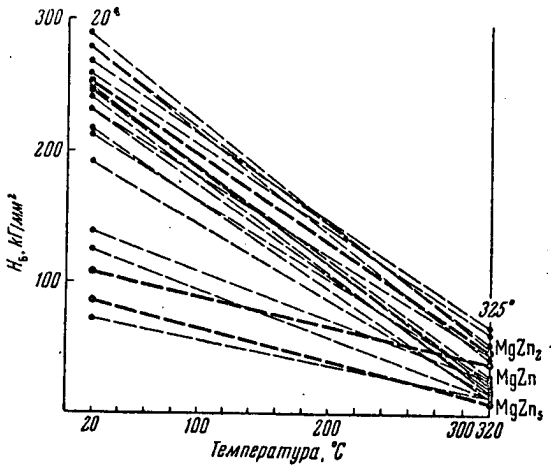

Фиг. 160. Относительное размягчение магний-цинковых сплавов при нагревании (по данным измерений при 20 и 325°).

В ЛФТИ АН СССР А. П. Обухов и Б. И. Болтакс по нашей просьбе измерили в интервале —170+450° электропроводность и т. э. д. с. соединений, образующихся в системе Mg—Zn, в деформированном состоянии. Полученные данные приведены в табл. 52. Представляют интерес абсолютные значения электропроводности соединений, а также ее значительное возрастание с понижением температуры.

Таблица 52

Удельная электропроводность и т. э. д. с. сплавов Mg — Zn

Температура	MgZn		$MgZn_5$		$MgZn_2$		Примечание
	$ом^{-1} \cdot см^{-1}$	α, мкв/градус	$ом^{-1} \cdot см^{-1}$	α, мв/градус	$ом^{-1} \cdot см^{-1}$	α, мкв/градус	
—170	56 000	~5,0	95 000	~3,0	118 000	~4,0	Т. э. д. с. измерялась по отношению к медным электродам. Т. э. д. с. $MgZn_5$ при 150° С меняет знак с + на —
—80	39 000		66 000		79 500		
40	28 500		42 200		52 700		
70	26 700	В пределах 5—8	39 100	В пределах 3—6	47 200	В пределах 4—7	
100	25 700		38 750		44 100		
150	24 500		32 700		41 800		
200	23 800		29 200		40 100		
250	22 800				37 200		
300	22 200		28 900		35 000		
350	21 800		27 900		33 000		
400	—		26 700		32 100		
450	—		25 100		30 100		

App. 12

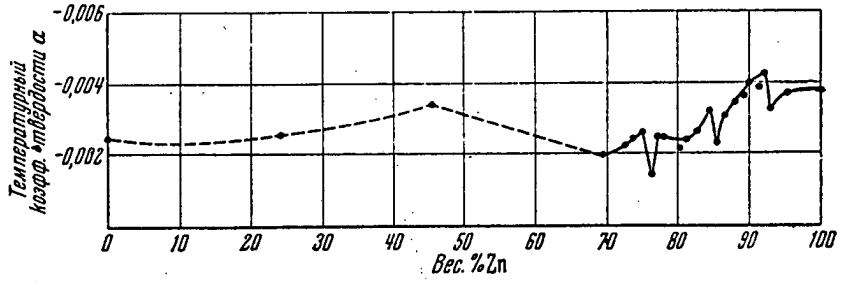

Фиг. 161. Температурный коэффициент твердости сплавов системы магний — цинк.

Система магний—алюминий

Диаграмма состояния системы магний—алюминий представляет особый интерес потому, что она дает основные направляющие сведения о природе и строении многих легких и ультралегких сплавов.

В результате работы ряда исследователей общий вид этой диаграммы, в основном, можно считать установленным, за исключением имеющихся расхождений в толковании средней ее части,т. е. в области концентрации 35—60% Mg [394, 412—421].

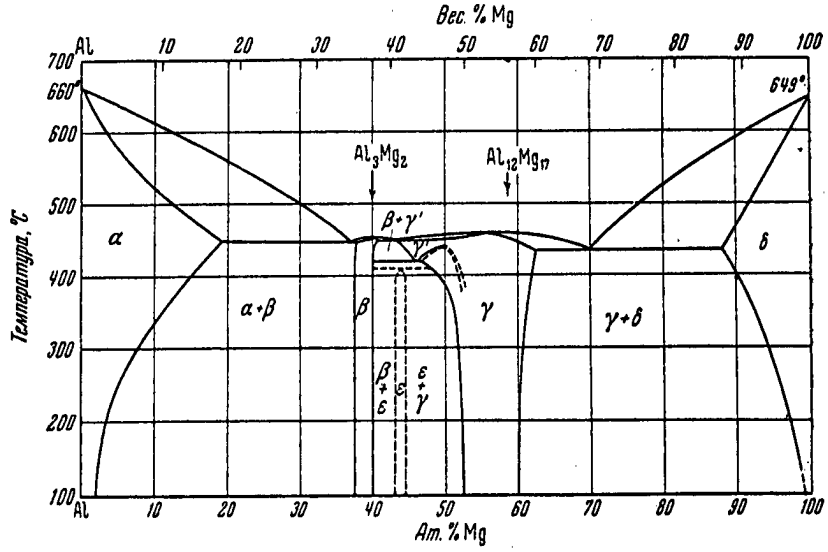

Фиг. 162. Диаграмма состояния системы Al — Mg (по совокупности литературных данных).

В 1953 г. был опубликован подробный разбор многочисленных работ по установлению диаграммы состояния сплавов системы Al—Mg и приведен ее итоговый вариант (фиг. 162) [421]. Мы в своих исследованиях Mg—Al сплавов за основу брали диаграмму состояния по данным Н. С. Курнакова и В. И. Михеевой, приведенную на фиг. 164. Существование межметаллических фаз β и γ признается всеми авторами и сомнений не вызывает, но пределы существования этих фаз указываются несколько различные. Основные разногласия вызывает строение гетерогенной области между фазами β и γ, где многими исследователями обнаружено несколько различных

APPENDIX 13

A. I. Belyaev and E. A. Zhemchuzhina

THE BEHAVIOR OF MAGNESIUM OXIDE IN THE ELECTROLYSIS OF MAGNESIUM CHLORIDE MELTS

(Tsvetnye Metally, ?, No. 1, pp. 50-57, 1956)

In the operation of industrial magnesium electrolyzers the formation of a non-metallic, so-called passivating film on the surface of the iron cathodes is observed, which is accompanied by a substantial reduction in the magnesium yield based on the current. Numerous investigations have established that this film consists essentially of magnesium oxide, a certain amount of other oxides, and iron. The approximate composition of such a film, removed from the cathodes of plant electrolyzers, neglecting the salt portion, is characterized by the following values (mole %): 87-90 MgO; 6-11 Fe; 2-2.5 Al_2O_3; 1.5-2 SiO_2; 1-1.5 CaO. Passivation of the cathodes of magnesium electrolyzers usually occurs when the latter are fed magnesium chloride that had been obtained by the chlorination of caustic magnesite, and much more rarely when synthetic carnallite is used as the feed.

Since the main component of the cathode film is magnesium oxide (up to 90 mole %), it was postulated by the authors that a difference in the character and behavior of the magnesium oxide in the electrolyte is the reason for the passivation of the cathodes in magnesium electrolyzers. The magnesium oxide appears in the electrolyte as the result of the hydrolysis of either magnesium chloride or carnallite, in which connection the formation of the cathode film itself is the result of the direct current carrying the magnesium oxide particles to the surface of the cathode.

Hydrolysis of Magnesium Chloride, Solubility and the Settling of Magnesium Oxide in the Electrolyte

The hydrolysis of magnesium chloride and of carnallite was studied in a potassium-containing electrolyte (containing more than 70% KCl) at 750° as a function of the $MgCl_2$ concentration in the electrolyte, the source of the $MgCl_2$ being either that obtained from the chlorination of magnesite or else it was added as synthetic carnallite. The degree of hydrolysis was characterized by the amount of MgO that was formed in the electrolyte in one hour. The results of these experiments are plotted in Fig. 1, from which it can be seen that the degree of magnesium chloride hydrolysis increases in measure with increase

in its concentration in the melt. Here (for equal $MgCl_2$ concentrations) the greatest degree of hydrolysis is observed for the magnesium chloride that was obtained by the chlorination of magnesite, with the $MgCl_2$ introduced into the melt as synthetic carnallite showing a lesser degree of hydrolysis. This can be explained by the fact that in the case of the former a large number of very fine primary magnesium oxide crystals are introduced into the melt together with the magnesium chloride, thus creating a correspondingly large number of crystallization centers, which facilitate hydrolysis of the $MgCl_2$. In the case of carnallite a smaller number of primary MgO crystals are introduced into the melt, in which connection, as will be shown below, they are much coarser, as a result of which the hydrolysis of the $MgCl_2$ proceeds at a slower rate.

Next we studied the solubility of magnesium oxide in a molten potassium-containing electrolyte, containing 10% $MgCl_2$, and also in melts of pure sodium and potassium chlorides, taken in a 1:10 ratio by weight. For this we used the magnesium oxide that had been obtained by the hydrolysis of magnesium chloride and of carnallite. The indicated potassium-containing electrolyte, even without the addition of magnesium oxide to it, was turbid due to the MgO particles suspended in it, introduced into the melt together with the magnesium chloride.

On the average the magnesium chloride itself contained 0.057% MgO. After adding the $MgCl_2$ to the melt the amount of magnesium oxide in the latter was 0.00518%. Consequently, even in this amount the MgO proved to be insoluble in the given electrolyte.

The oxides of silicon, aluminum, calcium and iron are also practically insoluble in such an electrolyte. A similar picture was also observed when we studied the solubility of magnesium oxide in a melt composed of a mixture of pure potassium and sodium chlorides. After mixing this melt for 2 hours with magnesium oxide at 800° the amount of magnesium oxide in the settled portion of the melt was 0.0044% in the case of the MgO obtained from magnesium chloride, and 0.0013% in the case of the magnesium oxide obtained from carnallite.

As a result, magnesium oxide proves to be practically insoluble in both a molten potassium-containing electrolyte and in pure potassium and sodium chlorides. Consequently, the magnesium oxide present in industrial magnesium cells, found by analysis to usually be of the order of hundredths and tenths of a percent, is mainly present in the suspended state.

In connection with this it was necessary to determine the character and rate of magnesium oxide deposition (settling) in molten electrolytes. In this connection we did not make a special addition of magnesium oxide to the melt. We studied the settling of only that magnesium oxide that was introduced into the melt together with the magnesium chloride or the synthetic carnallite, and that also appeared in the melt as the result of their hydrolysis. In Fig. 2 we show the results

of the experiments on the settling of magnesium oxide in melts that contained either magnesium chloride or carnallite. The degree of magnesium oxide settling was characterized by its amount (in percent) in the upper layer of the melt after a definite time interval. The observations made by us, and also the data in Fig. 2, show that not only the settling rate, but also the very character of this process, depends on whether the magnesium oxide was obtained by the hydrolysis of magnesium chloride or of carnallite. In the first case the magnesium oxide settles at a slower rate and it deposits chiefly on the walls of the melting-pot; in the second case the magnesium oxide settles at a faster rate, and here directly on the bottom of the melting-pot. In addition, as can be seen from Fig. 2, in the melts containing magnesium chloride the $MgCl_2$ hydrolysis rate is already faster than the MgO deposition rate at a concentration of 20% $MgCl_2$ in the melt; in the melts containing magnesium chloride in the form of carnallite the $MgCl_2$ hydrolysis rate begins to exceed the magnesium oxide precipitation rate only at a concentration of 30-40% $MgCl_2$.

Mechanism For the Formation of a Passivating Film on the Cathode

To establish the mechanism for the formation of a passivating film on the cathode surfaces of magnesium electolyzers we studied the adsorption of magnesium oxide on a cathode surface without polarization and with polarization of the electrode by a direct current, i.e. as the result of cataphoresis. It should be mentioned that the phenomenon of cataphoresis--the transfer of positively charged solid particles to the cathode by means of an electric current in an electrolyte medium--has hardly been studied relative to molten layers. Nevertheless, it can be assumed that cataphoresis is specifically one of the more probable processes here, leading to the formation of a film of oxides on the cathodes of a magnesium electrolyzer. The travel rate (v) of spherical solid particles during electrophoresis is determined by the following equation:

$$v = \frac{Z.D.E}{6\pi\eta l},$$

where E is the voltage drop; l is the distance between electrodes; D is the dielectric constant; η is the viscosity of the liquid; and Z is the electrokinetic potential of the disperse phase relative to the dispersion medium, which is found to depend on the nature of the ions, adsorbed by the solid particles, and on their concentration in the electrolyte.

The following basic tenets ensue from this equation: 1) the rate of motion of solid particles during their displacement in an electric

field in a liquid (electrolyte) medium is greater the higher the Z-potential, the greater the value of the dielectric constant of the liquid, and the greater the value of the voltage, i.e. the difference of the potentials at the electrodes; 2) the rate of motion of the particles is slower the greater the viscosity of the liquid and the distance between the electrodes.

Unfortunately, we know nothing about the value of the Z-potential of magnesium oxide particles relative to a medium of molten chlorides. However, studies show that a number of oxides, sulfides and other inorganic compounds are positively charged relative to water and electrolyte solutions, i.e. they adsorb cations from the electrolyte on their surface, becoming positively charged particles (1). Further, encouraging cataphoresis under the conditions of a magnesium electrolyzer will be the low solubility of magnesium oxide and other oxides in molten chlorides, the constant presence of suspended magnesium oxide particles (especially in the case of their fine dispersion) in the electrolyte, the relatively low viscosity of the molten electrolyte, the comparatively small interpolar distance, and also the high voltage at the clamps of the bath.

The studies on the adsorption of magnesium oxide at the cathode with polarization of the electrodes by a direct current were run at a voltage that was below the decomposition potential of $MgCl_2$, so as to avoid the separation of magnesium on the surface of the cathode. As cathode we used a 30x25 mm. iron sheet, while the above indicated potassium-containing electrolyte was used in all cases; the electrolyte temperature was 750°. After electrolysis for 4 hours the cathodes were removed and rinsed with hot water. The water-insoluble deposit obtained here, representing the oxide film on the cathode, was dried, weighed, and analyzed for the amount of MgO.

Hardly any deposit of MgO was formed on the surface of the cathodes when the electrodes were not polarized by a direct current, even when 0.5% of dispersed magnesium oxide was added to the electrolyte. In the experiments with polarization of the electrodes a layer of oxides always deposited on the surface of the cathodes, the density and thickness of which depended on the voltage applied to the electrodes, on the amount of magnesium chloride in the electrolyte, on the amount of magnesium oxide added to the electrolyte, and finally, on the coarseness and shape of the magnesium oxide crystals, appearing in the electrolyte during experiment as the result of magnesium chloride hydrolysis.

Thus, with a voltage of 0.5 and 1 v. we obtained a very thin film of oxides on the cathode; with a voltage of 1.5 v. a denser layer of oxides deposited on the cathodes, in which connection the water-insoluble portion of this film weighed on the average 0.0053 g. With a voltage of 2 v. a layer of oxides deposited over the whole cathode, in which connection the insoluble portion weighed 0.246-0.505 g. As a result, the value of the voltage exerts an influence on the formation

of a passivating film on the surface of the cathode. The higher the voltage, the more intense is the process for the deposition of oxides (MgO) on the surface of the cathodes, which is in agreement with the equation given above.

In Fig. 3 we show the relationship between the amount of magnesium oxide in the cathodic film and the amounts of magnesium oxide and magnesium chloride in the electrolyte in the cataphoresis experiments run at a voltage of 2 v. From Fig. 3 it can be seen that the amount of MgO in the cathodic film increases with increase in the amount of magnesium oxide suspended in the electrolyte; the same also happens in measure with increase in the concentration of magnesium chloride in the electrolyte. In the latter case this is due to an increase in the number of magnesium oxide particles in the electrolyte, formed as the result of $MgCl_2$ hydrolysis in measure with increase in its concentration in the melt. Our experiments also showed that the amount of MgO in the cathodic film was twice as great when the magnesium chloride was introduced into the electrolyte in the form of the magnesium chloride obtained by the chlorination of MgO as when it was introduced in the form of carnallite. This last can be explained by the fact that the magnesium oxide, formed in the hydrolysis of the magnesium chloride, represents very fine, almost amorphous particles, readily adsorbing positive charges (cations) and carrying them to the cathode.

Influence of the Medium on the Coarseness of Magnesium Oxide Crystals

To study the shape and coarseness of the magnesium oxide crystals formed in the hydrolysis of magnesium chloride and of carnallite the molten salt was kept in the air at 750° until the liquid phase was completely removed. The solid residue was leached with water to completely remove chlorine ions and then it was ignited at 800-900°. The magnesium oxide obtained in this manner was examined under a microscope with a magnification of 90 times, using glycerine as the immersion liquid. The microphotographs of the magnesium oxide crystals, obtained from magnesium chloride and from artificial carnallite, are shown in Fig. 4. These photographs show that magnesium oxide crystals obtained from the two sources differ greatly between themselves. The magnesium oxide, obtained from magnesium chloride, has a fine, tiny-grained, almost amorphous structure, while the magnesium oxide crystals, obtained from synthetic carnallite, have a coarse crystal structure and an elongated needlelike shape. The size of the magnesium oxide crystals, obtained from magnesium chloride, is on the average 0.0055 mm., while the length of the needlelike magnesium oxide crystals, obtained from carnallite, on the average is equal to 0.56 mm. This difference in the shape and size of the magnesium oxide crystals

is evidently due to the fact that the magnesium oxide, formed in the hydrolysis of molten carnallite, has more favorable conditions for the crystallization and growth of the crystals than does the magnesium oxide, obtained in the hydrolysis of magnesium chloride. This is explained as follows.

First, as was shown above, the hydrolysis proceeds with much greater intensity when molten magnesium chloride is used than when molten carnallite is used. Consequently, the number of crystallization centers for the magnesium oxide in the magnesium chloride will be considerably greater than for the magnesium oxide in the carnallite, as a result of which the magnesium oxide crystals in the magnesium chloride do not have suitable conditions for growth. Second, the growth of the magnesium oxide crystals in the carnallite can be influenced by the presence of sodium and potassium chlorides, the cations of which can play the role of mineralizing agents in this case (2). However, the mineralizing action exerted by the potassium ion is smaller than that exerted by the sodium ion.

The sodium ion is more mobile than is the potassium ion: its radius (0.98 Å) is smaller than that of the potassium ion (1.33 Å), and at the same time it is close to the value of the radius of the magnesium ion (0.78 Å). It can be postulated that the action of the alkali metal cations as mineralizing agents consists in the fact that they, being transposed into the MgO lattice, approximate the magnesium and oxygen ions, in that way facilitating the phase transformation of the magnesium oxide (transition from the amorphous state to the crystalline) and the growth of its crystals. Consequently, in feeding magnesium chloride into the bath a large number of finely dispersed magnesium oxide particles are introduced into the electrolyte, the growth of which in the medium of a molten potassium-containing electrolyte proceeds with extreme slowness in view of their extremely small dimensions and large number.

The microphotographs of the magnesium oxide crystals, extracted from the electrolytes of operating magnesium electrolyzers, are shown in Fig. 5. When magnesium chloride is fed into the electrolyzers the magnesium oxide in the electrolyte is fine-grained, nearly amorphous, and has an average grain size of about 0.0067 mm. Very rarely are needle-shaped crystals encountered. When carnallite is fed into the bath (the sample was taken from a well operating electrolyzer) the magnesium oxide is found to be present in the electrolyte as coarse needlelike crystals with an average length of up to 0.35 mm.

A microphotograph of the magnesium oxide, contained in the passivating film removed from the cathode of an industrial bath, is shown in Fig. 6. In the microphotograph it can be seen that needle-shaped crystals are absent in the cathodic film, the main portion of the film being fine-grained magnesium oxide. It is evident that this circumstance supports the above expressed postulation that the main reason

for cathodic passivation in magnesium electrolyzers, fed with magnesium chloride, consists in the behavior, unfavorable for the electrolysis process, of the finely crystalline or even amorphous magnesium oxide, which accumulates in the electrolyte, is found present as a suspension, and under the influence of a direct current deposits on the surface of the cathodes. In the electrolyte of baths, fed with snythetic carnallite, the magnesium oxide is mainly present in the form of needle-shaped coarse crystals. These crystals can be carried to the cathode only mechanically, since they are charged differently than are the amorphous magnesium oxide particles, which adsorb only positive ions. Crystals having an elongated needlelike shape are capable of adsorbing both positive and negative ions on opposite ends, as a result of which such crystals as a whole are electroneutral (3); this, in addition to their large size, facilitates better deposition of such crystals in the sludge.

To confirm the possibility of the alkali metal cations functioning as mineralizing agents in the crystallization of MgO we prepared equimolar melts of magnesium chloride with the chlorides of potassium, sodium and lithium, from which we then prepared the magnesium oxide by the method described above. The microphotographs of the magnesium oxide crystals, obtained from equimolar mixtures of magnesium chloride with the different alkali metal chlorides, are shown in Fig. 7. As can be seen from these microphotographs, the magnesium oxide crystals from the melt composed of an equimolar mixture of $MgCl_2$ and KCl are predominantly of a small and medium size. The magnesium oxide, obtained from the melts of equimolar mixtures of $MgCl_2$ with either NaCl or LiCl, consists mainly of coarse, needle-shaped crystals.

As a result, the potassium cation exerts a lesser influence as a mineralizing agent on the growth of crystals in the hydrolysis of magnesium chloride than do the sodium and lithium cations, having smaller dimensions of their radii (0.98 and 0.78 Å, respectively).

Our investigations also revealed that fluorides, introduced as additions into the electrolyte of a magnesium bath, also facilitate the growth of MgO crystals in the hydrolysis of magnesium chloride. In this case the fluoride anion is the mineralizing agent. In Fig. 8 we show the microphotographs of the MgO crystals obtained in the hydrolysis of $MgCl_2$ in the presence of small additions of CaF_2 (2 wt. %), MgF_2 (2 wt. %) and NaF (5 wt. %). As can be seen from these photographs, the fluorides exert considerable influence on the growth of magnesium oxide crystals, in which connection sodium and magnesium fluorides show the greatest degree of influence, with potassium fluoride exerting a smaller influence. This can be explained by the fact that with NaF and MgF_2 a greater amount of fluorine ions is introduced into the melt than in the case of CaF_2. Thus, when CaF_2 (2 wt. %) is introduced into the melt the amount of added fluorine is 0.975% (mole), while for 2% (wt.) MgF_2 and 5% (wt.) NaF the corresponding values are 1.25 and 2.23% (mole) fluorine. From this the influence of adding

MgF_2 and NaF as mineralizing agents for magnesium oxide shows up to a greater degree than does the addition of CaF_2. In Fig. 9 we show a MgO monocrystal (length about 1mm.), obtained in the hydrolysis of $MgCl_2$ in the presence of an equimolar amount of LiF. In this case the mineralizing agents were Li^+ cations and F^- anions.

Influence of the Coarseness of Carnallite Crystals on the Size of Magnesium Oxide Crystals

In conclusion we studied the influence of the coarseness of synthetic carnallite crystals on the size of the magnesium oxide crystals obtained in the hydrolysis of such carnallite. The data on the change in the size of carnallite crystals as a function of their crystallization temperature are shown in Fig. 10. Here we also show the change in the size of the magnesium oxide crystals obtained in the hydrolysis of carnallite with a variable coarseness of the crystals. The coarsest carnallite crystals were obtained at 80 and 60°, and the smallest at room temperature and 95°. At low temperature the process for the creation of carnallite crystallization centers proceeds at a much faster rate than it does at elevated temperatures, as a result of which the crystal growth is retarded. At 95° the solution is very slightly supersaturated, which also does not create conditions suitable for the growth of carnallite crystals. The magnesium oxide crystals, obtained from carnallite with a variable coarseness of the crystals, also had a dissimilar size. In this connection the change in the size of the magnesium oxide crystals varied directly with the coarseness of the carnallite crystals. As was to be expected, the coarsest magnesium oxide crystals with a length of 0.6-0.55 mm. were obtained from the carnallite that had been permitted to crystallize at 80 and 60°, and the smallest crystals were obtained from the carnallite that had been allowed to crystallize at room temperature and at 95°.

The results of this investigation explain the appearance of passivation for the cathodes of industrial magnesium electrolyzers, fed with the melt obtained from a finely crystalline carnallite. In this case also the melt predominantly contains a finely dispersed magnesium oxide, giving a suspension in the electrolyte and capable of being deposited on the cathodes under the action of a direct current.

SUMMARY

1. The hydrolysis of magnesium chloride and of carnallite in a molten potassium-containing electrolyte, accompanied by the formation of magnesium oxide, proceeds at a variable rate--much faster for the magnesium chloride and at a slower rate for the carnallite.

2. As the result of the hydrolysis of magnesium chloride a finely dispersed magnesium oxide (average size of the particles 0.0055 mm.) is formed, giving a suspension in the electrolyte, while in the hydrolysis of carnallite a coarsely crystalling needle-shaped magnesium oxide (average crystal length 0.56 mm.) is obtained, depositing predominantly in the sludge.

3. In the hydrolysis of magnesium chloride a coarsening of the formed magnesium oxide crystals takes place under the influence of the alkali metal chlorides. Here the corresponding cations function as mineralizing agents, in which connection the sodium cation facilitates the coarsening of the magnesium oxide crystals to a much greater degree than does the potassium cation.

4. The metal fluorides exert a similar influence on the coarsening of the magnesium oxide formed in the hydrolysis of magnesium chloride. The extent of this influence is determined by the amount of fluoride ions, introduced by the fluoride in its solution in the electrolyte.

5. In view of the fact that a finely dispersed magnesium oxide is formed in the hydrolysis of magnesium chloride, and consequently it shows a poorer settling from the melt, it is found as a suspension in the electrolyte, in which connection its particles, adsorbing cations, are carried by the direct current to the cathode, where they create a passivating film on the surface.

6. A finely dispersed magnesium oxide is also formed in the molten carnallite, obtained from finely crystalline synthetic carnallite. In the baths, fed with such a melt, passivation of the cathodes can also occur.

Figures

FIGURE 1

(1) Hydrolysis of magnesium chloride and of carnallite in a molten potassium-containing electrolyte:
1--degree of $MgCl_2$ hydrolysis; 2--degree of carnallite hydrolysis

(2) $MgCl_2$, wt. %

(3) Amount of MgO formed in the melt, g./hr.

FIGURE 2

(1) The settling of magnesium oxide in melts containing magnesium chloride and carnallite.

(2) $MgCl_2$ in the melt, wt. %

(3) Amount of MgO in the settled melts, %

(4) _____ MgO in the settled melt containing $MgCl_2$

(5) ---------- MgO in the settled melt containing carnallite

(6) After 30 minutes

(7) After 20 minutes

(8) After 10 minutes

FIGURE 3

(1) Amount of MgO in the cathodic film as a function of the $MgCl_2$ concentration in the electrolyte (1) and the amount of MgO added to the electrolyte (2)

(2) Amount of MgO in the cathodic film, wt. %

(3) Amount of $MgCl_2$ in the electrolyte, wt. %

(4) Amount of MgO added to the electrolyte, wt. %

FIGURES 4, 5, 6 and 9

(1) a--magnesium oxide, obtained by the hydrolysis of $MgCl_2$, X90;
b--the same, obtained by the hydrolysis of carnallite, X90.

(2) a--magnesium oxide from an industrial electrolyte where magnesium chloride was fed to the bath;
b--the same, with carnallite as the bath-feed. X90.

(3) Magnesium oxide from the cathodic (passivating) film of a commercial electrolyzer. X90.

(4) A magnesium oxide monocrystal, obtained from a melt containing $MgCl_2$:LiF = 1:1 (mole). X90.

FIGURES 7 and 8

(1) a--magnesium oxide, obtained from a melt with $MgCl_2$:KCl = 1:1 (mole);
b--the same, from $MgCl_2$:NaCl = 1:1 (mole);
c--the same, from $MgCl_2$:LiCl = 1:1 (mole). X90.

(2) a--magnesium oxide, obtained from an electrolyte containing 2 % CaF_2;
b--the same, in the presence of 2% MgF_2;
c--the same, in the presence of 5% NaF. X90.

FIGURE 10

(1) The size of MgO crystals as a function of the coarseness of carnallite crystals.

(2) Temperature, °C

(3) Size of the carnallite crystals, sq. mm.

(4) Length of the MgO crystals, mm.

LITERATURE CITED

(1) A. N. Brodskii, Physical Chemistry, Volume A, P. 806 (1948). State Chemical Press.

(2) A. I. Avgustinik, The Physical Chemistry of Silicates, P.87 (1947). State Chemical Press.

(3) George Dean, and others, System of Mineralogy, Vol. I (1951). Foreign Literature Press.

Appendix 13

лизеров, без учета солевой части, характеризуется следующими цифрами (мол. %): 87—90 MgO; 6—11 Fe; 2—2,5 Al_2O_3; 1,5—2 SiO_2; 1—1,5 CaO. Пассивирование катодов магниевых электролизеров происходит обычно при питании последних хлористым магнием, получаемым хлорированием каустического магнезита, и значительно реже — в случае питания искусственным карналлитом.

Поскольку основной составляющей катодной пленки является окись магния (до 90 мол. %), авторами было сделано предположение, что причиной пассивирования катодов магниевых электролизеров является различие в характере и поведении в электролите окиси магния. Последняя появляется в нем за счет гидролиза хлористого магния или карналлита, причем образование самой катодной пленки является результатом переноса частиц окиси магния на поверхность катода постоянным током.

Гидролиз хлористого магния, растворимость и отстаивание окиси магния в электролите

Исследование гидролиза хлористого магния и карналлита осуществлялось в среде калиевого электролита (содержащего свыше 70% KCl) при 750° в зависимости от концентрации в электролите $MgCl_2$, который вводился в расплав в виде хлористого магния, полученного хлорированием магнезита, или в виде искусственного карналлита. Степень гидролиза характеризовалась количеством MgO, образовавшейся в электролите в течение часа. Результаты этих исследований графически представлены на рис. 1, из которого видно, что степень гидролиза хлористого магния возрастает по мере увеличения концентрации его в расплаве. При этом (для равных концентраций $MgCl_2$) в большей степени гидролиз протекает в случае применения хлористого магния, полученного хлорированием магнезита, и в меньшей степени — при введении в расплав $MgCl_2$ в форме искусственного карналлита. Последнее может быть объяснено тем, что вместе с хлористым магнием в расплав вносится большое число очень мелких первичных кристаллов окиси магния, создающих соответственно большое число центров кристаллизации, которые ускоряют гидролиз $MgCl_2$. С карналлитом в расплав вносится меньшее количество первичных кристаллов MgO, причем, как будет показано ниже, они значительно крупнее, вследствие чего гидролиз $MgCl_2$ протекает медленнее.

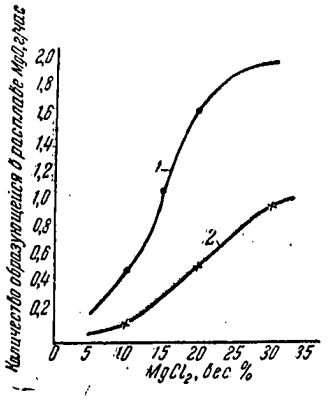

Рис. 1. Гидролиз хлористого магния и карналлита в расплавленном калиевом электролите:
1 — степень гидролиза $MgCl_2$;
2 — степень гидролиза карналлита

Далее была исследована растворимость окиси магния в расплавленном калиевом электролите, содержавшем 10% $MgCl_2$, а также в расплавах чистых хлоридов натрия и калия, взятых в весовом отношении 1 : 10. Для этого была применена окись магния, полученная гидролизом хлористого магния и карналлита. Указанный калиевый электролит, даже без введения в него окиси магния, был мутным вследствие взвешенных в нем частиц MgO, вносимой в расплав с хлористым магнием.

В самом хлористом магнии содержалось в среднем 0,057% MgO. После введения $MgCl_2$ в расплав содержание окиси магния в последнем составляло 0,00518%. Следовательно, даже и это количество MgO оказывалось не растворимым в данном электролите.

Окислы кремния, алюминия, кальция и железа также практически не растворялись в таком электролите. Аналогичная картина наблюда-

Appendix 13

лась и при исследовании растворимости окиси магния в расплаве из смеси чистых хлоридов калия и натрия. После перемешивания этого расплава в течение 2 час. с окисью магния при 800° содержание окиси магния в отстоявшейся части расплава составило в случае MgO, полученной из хлористого магния, 0,0044%, а в случае окиси магния, полученной из карналлита, — 0,0013%.

Таким образом, окись магния оказывается практически не растворимой как в расплавленном калиевом электролите, так и в чистых хлоридах калия и натрия. Поэтому обычно определяемая аналитическим путем в электролитах промышленных магниевых ванн окись магния в количестве сотых и десятых долей процента находится в них в основном во взвешенном состоянии.

В связи с этим было необходимо определить характер и скорость осаждения (отстаивания) окиси магния в расплавленных электролитах. При этом окись магния в расплав специально не вводилась. Исследовалось отстаивание только той окиси магния, которая вносилась в расплав с хлористым магнием или с искусственным карналлитом, а также появлялась в расплаве вследствие их гидролиза. На рис. 2 показаны результаты опытов по отстаиванию окиси магния в расплавах, содержащих хлористый магний или карналлит. Степень отстаивания окиси магния характеризовалась содержанием ее (в процентах) в верхнем слое расплава после определенного промежутка времени. Проведенные наблюдения, а также данные рис. 2 показывают, что не только скорость отстаивания, но и самый характер этого процесса различен для окиси магния, полученной гидролизом хлористого магния, или карналлита. В первом случае окись магния отстаивается медленнее и осаждение ее происходит преимущественно на стенках тигля; во втором случае окись магния отстаивается быстрее, причем непосредственно на дне тигля. Кроме того, как видно из рис. 2, в расплавах, содержащих хлористый магний, превышение скорости гидролиза $MgCl_2$ над скоростью осаждения MgO заметно уже при 20% $MgCl_2$ в расплаве; в расплавах же, содержащих в своем составе хлористый магний в виде карналлита, скорость гидролиза $MgCl_2$ начинает превышать скорость осаждения окиси магния только при концентрации 30—40% $MgCl_2$.

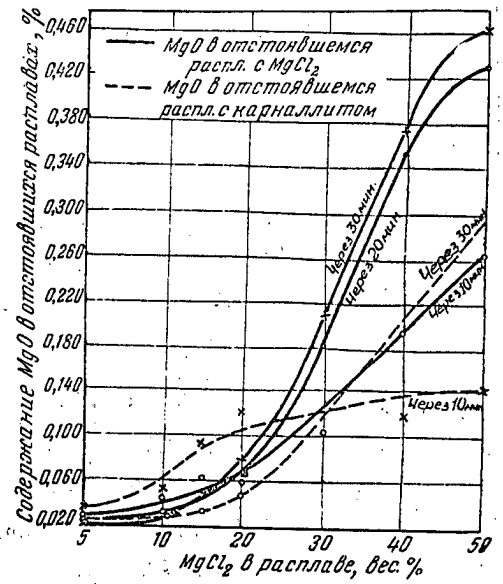

Рис. 2. Отставание окиси магния в расплавах, содержащих хлористый магний и карналлит

Механизм образования пассивирующей пленки на катоде

С целью установления механизма образования пассивирующей пленки на поверхности катодов магниевых электролизеров была исследована адсорбция окиси магния поверхностью катодов без поляризации и с поляризацией электродов постоянным током, т. е. за счет катафореза. Необходимо отметить, что явление катафореза — перенос положительно заряженных твердых частиц на катод с помощью электрического тока в среде электролита — почти не изучено применительно к расплавленным слоям. Тем не менее можно было предположить, что именно катафорез является одним из наиболее вероятных процессов, приводящих к образованию пленки окислов на катодах магниевого электролизера. Скорость движения (v) шарообразных твердых частиц при электрофорезе определяется следую-

Appendix 13

держания окиси магния, взвешенной в электролите; это же происходит и по мере увеличения концентрации хлористого магния в электролите.

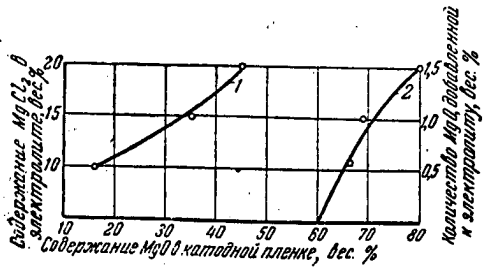

Рис. 3. Содержание MgO в катодной пленке в зависимости от концентрации $MgCl_2$ в электролите (*1*) и величины добавки MgO в электролите (*2*)

Последнее имеет место вследствие возрастания в электролите количества частиц окиси магния, образующихся за счет гидролиза $MgCl_2$ по мере увеличения его концентрации в расплаве. Опыты также показали, что содержание MgO в катодной пленке было в два раза больше тогда, когда хлористый магний вводился в электролит в форме хлористого магния, полученного хлорированием MgO, нежели тогда, когда он вводился в виде карналлита. Последнее может быть объяснено тем, что окись магния, образующаяся при гидролизе хлористого магния, представляет очень тонкие, почти аморфные частицы, легко адсорбирующие положительные заряды (катионы) и переносящие их к катоду.

Влияние среды на крупность кристаллов окиси магния

Для исследования формы и крупности кристаллов окиси магния, образующихся при гидролизе хлористого магния и карналлита, расплавленную соль выдерживали на воздухе при 750° до полного удаления жидкой фазы. Твердый остаток подвергали выщелачиванию водой до полного удаления ионов хлора и прокаливали при 800—900°. Полученный таким образом препарат окиси магния подвергался микроскопическому исследованию при увеличении в 90 раз с применением глицерина в качестве иммерсионной жидкости. На рис. 4 представлены микрофотографии кристаллов окиси магния, полученной из хлористого магния и из искусственного карналлита. Эти фотографии показывают, насколько сильно отличаются кристаллы окиси магния друг от друга. Окись магния, полученная из хлористого магния, имеет тонкую, мелкозернистую, почти аморфную структуру, тогда как кристаллы окиси магния, полученной из искусственного карналлита, имеют крупнокристаллическую структуру и вытянутую игольчатую форму. Величина кристаллов окиси магния, полученной из хлористого магния, в среднем 0,0055 *мм*, протяженность же игольчатых кристаллов окиси магния, полученной из карналлита, в среднем равна 0,56 *мм*. Это различие в форме и величине кристаллов окиси магния происходит, очевидно, потому, что окись магния, образующаяся при гидролизе расплавленного карналлита, имеет более благоприятные условия для кристаллизации и роста кристаллов, нежели окись магния, получающаяся при гидролизе хлористого магния. Это объясняется следующим.

Во-первых, как показано выше, гидролиз протекает значительно интенсивнее при применении расплавленного хлористого магния, чем расплавленного карналлита. Поэтому количество центров кристаллизации для окиси магния в хлористом магнии значительно больше, чем в карналлите, в результате чего кристаллы окиси магния в хлористом магнии не имеют условий для роста. Во-вторых, на рост кристаллов окиси магния в карналлите могут оказывать влияние хлориды натрия и калия, катионы которых в этом случае могут играть роль минерализаторов [2]. Однако ион калия оказывает меньшее влияние как минерализатор, чем ион натрия.

Последний более подвижен, чем ион калия: он имеет радиус (0,98 Å) меньший, чем ион калия (1,33 Å), и близкий по величине к радиусу иона магния (0,78 Å). Можно полагать, что действие катионов щелочных металлов как минерализаторов заключается в том, что они, перемещаясь в решетке MgO, сближают ионы магния и кислорода, облегчая тем самым фазовое превращение

Appendix 13

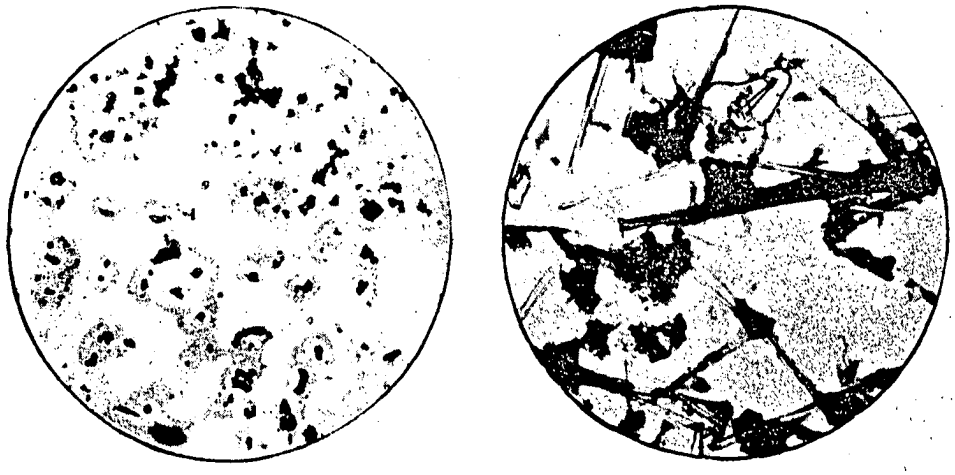

а *б*

Рис. 4.

а — окись магния, полученная гидролизом $MgCl_2$. ×90; *б* — то же, гидролизом карналлита. ×90.

а *б*

Рис. 5.

а — окись магния из промышленного электролита при питании ванны хлористым магнием; *б* — то же, при питании ванны карналлитом. ×90

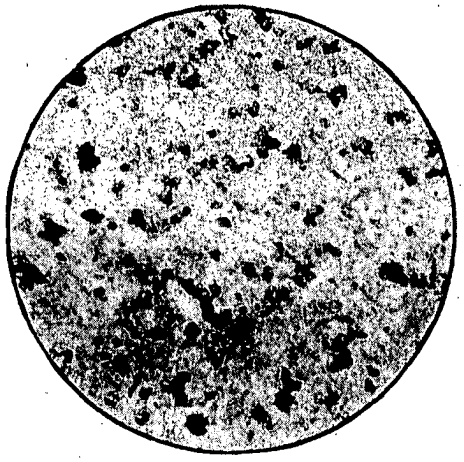

Рис. 6. Окись магния из катодной (пассивирующей) пленки промышленного электролизера. × 90

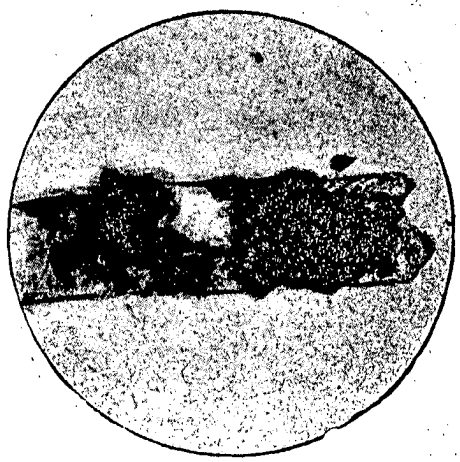

Рис. 9. Монокристалл окиси магния, полученный из расплава $MgCl_2 : LiF = 1 : 1$ (мол.) × 90

Appendix B

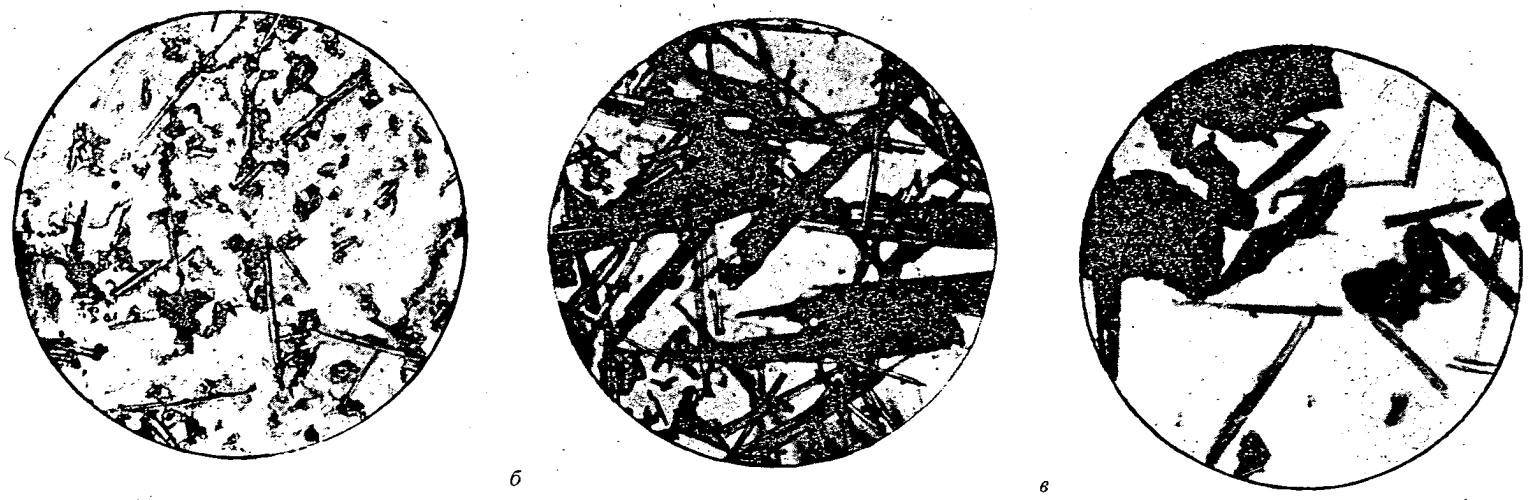

а *б* *в*

Рис. 7.

а — окись магния, полученная из расплава $MgCl_2$: KCl = 1 : 1 (мол); *б* — то же, из $MgCl_2$: NaCl = 1 : 1 (мол); *в* — то же, из $MgCl_2$: LiCl = 1 : 1 (мол). ×90

б *в*

Рис. 8.

а — окись магния, полученная из электролита в присутствии 2% CaF_2; *б* — то же, в присутствии 2% MgF_2; *в* — то же, в присутствии 5% NaF. ×90

Appendix 13

плав вводится большее количество ионов фтора, чем в случае CaF_2. Так, при введении в расплав CaF_2 (2% вес.) количество введенного фтора составляет 0,975% (мол.), а для 2% (вес.) MgF_2 и 5% (вес.) NaF соответственно 1,25 и 2,23% (мол.) фтора. Отсюда влияние добавок NaF и MgF_2 как минерализаторов окиси магния проявляется в большей степени, нежели при добавке CaF_2.

На рис. 9 показан монокристалл MgO (протяженностью около 1 *мм*), полученный при гидролизе $MgCl_2$ в присутствии эквимолярного количества LiF. В этом случае минерализаторами являлись и катионы Li^+ и анионы F^-.

Влияние крупности кристаллов карналлита на величину кристаллов окиси магния

В заключение было исследовано влияние крупности кристаллов искусственного карналлита на величину кристаллов окиси магния, получаемой при гидролизе такого карналлита. На рис. 10 приведены данные по изменению величины кристаллов карналлита в зависимости от температуры их кристаллизации. Здесь же показано изменение величины кристаллов окиси магния, полученной при гидролизе карналлита с различной крупностью кристаллов. Наиболее крупные кристаллы карналлита были получены при 80 и 60°, наиболее мелкие — при комнатной температуре и 95°. При низких температурах процесс зарождения центров кристаллизации карналлита идет значительно быстрее, чем при высоких, в результате чего замедляется рост кристаллов. При 95° раствор очень мало пересыщен, что также не создает условий для роста кристаллов карналлита. Кристаллы окиси магния, полученные из карналлита с различной крупностью кристаллов, также имели неодинаковую величину. При этом соответственно крупности кристаллов карналлита изменялась и величина кристаллов окиси магния. Как и следовало ожидать, наиболее крупные кристаллы окиси магния протяженностью 0,6—0,55 *мм* были получены из карналлита, выкристаллизованного при 80 и 60°, и наиболее мелкие — при комнатной температуре и при 95°.

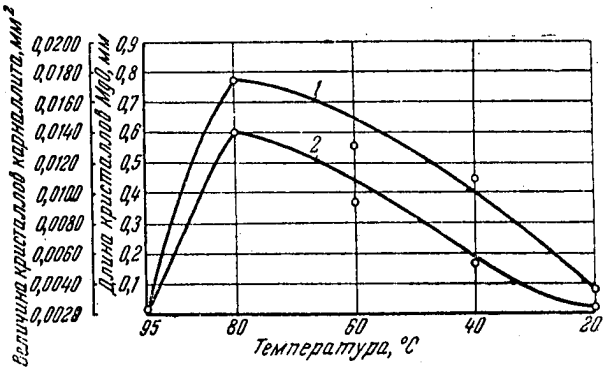

Рис. 10. Зависимость величины кристаллов MgO от крупности кристаллов карналлита

Результаты этого исследования объясняют явление пассивирования катодов промышленных магниевых электролизеров, питаемых расплавом, полученным из мелкокристаллического карналлита. В этом случае в расплаве также содержится преимущественно дисперсная окись магния, дающая в электролите взвесь и способная осаждаться на катодах под действием постоянного тока.

Выводы

1. Гидролиз хлористого магния и карналлита в среде расплавленного калиевого электролита, сопровождающийся образованием окиси магния, протекает с неодинаковой скоростью — значительно большей для хлористого магния и меньшей для карналлита.

2. В результате гидролиза хлористого магния образуется тонкодисперсная окись магния (средний размер частицы 0,0055 *мм*), дающая в электролите взвесь, а при гидролизе карналлита — крупнокристаллическая окись магния игольчатой формы (средняя длина кристалла 0,56 *мм*), осаждающаяся преимущественно в шлам.

3. Под действием хлоридов щелочных металлов происходит укруп-

APPENDIX 14

SURFACE PHENOMENA IN PYRO- AND ELECTROMETALLURGICAL PROCESSES

A. I. Belyaev (Moscow)

(Uspekhi Khim., 25, No. 10, pp. 1282-1293 (1956))

Surface phenomena in the electrolytic preparation of magnesium are associated with such processes as the impregnation of the fire-resistant lining and diaphrams of magnesium baths (cells) by the molten electrolyte, solution of magnesium in the electrolyte, and the coalescence and increase in size of molten magnesium drops in its separation at the cathode (Figure 8).

Studies reveal that in the given case the surface tension of the electrolyte, both at the boundary with the gas phase and at the boundary with either the solid phase or molten metal, increases with increase in the concentration of $MgCl_2$, $CaCl_2$, NaF and CaF_2, but decreases with increase in the concentration of NaCl, and especially of KCl (16). Consequently, the K^+, Na^+ and Cl^- ions are surface-active, while the Mg^{2+}, Ca^{2+} and F^- ions are surface-inactive. The electrolytic separation of magnesium from molten chlorides represents a process for the formation of fine magnesium droplets at the cathode and their coalescence into coarser drops. The latter is a necessary condition for obtaining a high current efficiency. A small value of the interfacial tension of the salt at the boundary with the molten metal, i.e. good wetting of the molten metal by the electrolyte, prevents the coalescence of the individual metal droplets and facilitates the retention of the dispersed magnesium in the molten electrolyte. On the other hand, a high surface tension of the electrolyte at the boundary with the molten metal ($\sigma_{el.-Mg}$) facilitates the separation of the metal from the molten salt and the coalescence of its fine droplets into coarse drops. In this connection the growth of the metal drops directly on the cathode surface possesses great importance.

A drop of molten magnesium, formed on the cathode (Figure 9), is subjected to the action of three different surface tension forces: $\sigma_{1.3}$--between the molten metal and the solid cathode, $\sigma_{2.1}$-- between the molten electrolyte and the molten metal, and $\sigma_{2.3}$ --between the molten electrolyte and the solid cathode. These forces operate in the plane of the phase interfaces, and the direction for $\sigma_{1.3}$ and $\sigma_{2.3}$ coincides with the plane of the cathode. At $\sigma_{1.3} > \sigma_{2.3}$ the force $\sigma_{2.1}$ assumes a direction that is tangential to the surface of the metal. The vertical component of this force is equal to $\sigma_{2.1} \cos (180 - \theta)$, and equilibrium ensues when

$$\sigma_{1.3} = \sigma_{2.3} + \sigma_{2.1} \cos(180 - \theta),$$

whence

$$\cos(180 - \theta) = \frac{\sigma_{1.3} - \sigma_{2.3}}{\sigma_{2.1}} .$$

From this expression it can be seen that an increase in $\sigma_{2.3}$ and $\sigma_{2.1}$ decreases the absolute value of $\cos(180 - \theta)$. This, evidently, takes place when $(180 - \theta)$ increases, which occurs when the contact angle of the molten metal drop decreases.

In other words, an increase in the interfacial tension of the molten electrolyte at the boundary with the solid cathode ($\sigma_{2.3}$) and with the molten magnesium ($\sigma_{2.1}$) under the influence of surface-inactive substances, for example fluorides (F^- ions), should improve wetting of the cathode by molten magnesium, and consequently, in this case conditions are created for the growth of magnesium drops on the cathode surface. On the other hand, the surface-active components of the electrolyte, for example potassium chloride (K^+ ions), prevent the growth of magnesium globules.

In addition, an increase in $\sigma_{2.1}$ under the influence of F ions also creates conditions for the coalescence of fine droplets into coarser drops within the electrolyte mass, which also leads to a reduction in the loss of magnesium, and consequently, to an increase in the current efficiency. As is known, the practicality of adding calcium and sodium fluorides to the electrolyte is supported by many years of practical experience in the electrolytic production of magnesium.

FIGURE 8

(1) Regions where surface forces arise in a magnesium bath (cell)

(2) $$\text{Cos}(180 - \theta) = \frac{\sigma_{\text{Mg-cathode}} - \sigma_{\text{el.-cathode}}}{\sigma_{\text{el.-Mg}}}$$

(3) $$P = \frac{2\sigma_{\text{el.-gas}} \text{Cos}\,\theta}{r}$$

FIGURE 9

(1) Scheme of the surface tension forces, acting on a drop of magnesium at the cathode

Appendix 14

Одним из важных показателей процесса электролиза является выход по току, величина которого зависит от потерь алюминия в электролите. Последние, в частности, определяются растворимостью алюминия за счет химического взаимодействия компонентов электролита и алюминия. Растворимость же металлов в расплавленных солях характеризуется межфазным натяжением этих солей на границе с расплавленным металлом. Поэтому повышение $\sigma_{эл.-Al}$ должно приводить к снижению потерь (растворимости) алюминия в электролите и соответственно к повышению выхода по току. Следовательно, повышение в электролите концентрации поверхностно-активного NaF должно приводить к росту потерь алюминия и снижению выхода по току, а введение в электролит поверхностно-неактивных CaF_2 или MgF_2, напротив,— к уменьшению потерь алюминия в электролите и повышению выхода по току. Это подтверждается экспериментальными исследованиями и практикой электролитического производства алюминия. Присутствие в электролите CaF_2 и MgF_2 (ионов Ca^{2+} и Mg^{2+}), обусловливающих увеличение межфазного натяжения на границе электролит — уголь, облегчает всплывание на поверхность электролита угольных частиц, диспергированных в электролите, что повышает его электропроводность.

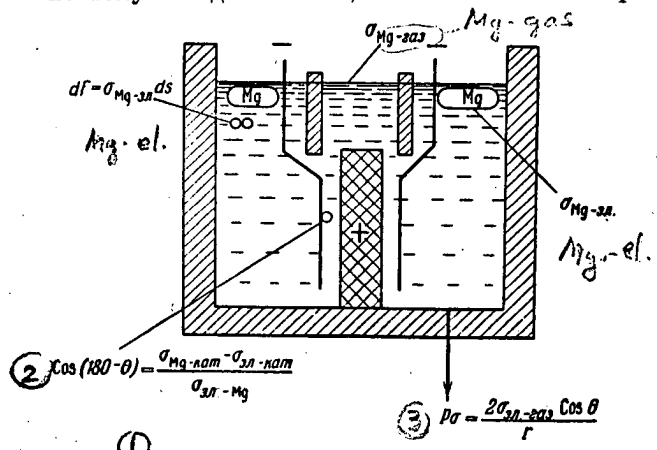

Рис. 8. Области проявления поверхностных сил в магниевой ванне

При электролитическом получении магния с поверхностными явлениями связаны такие процессы, как пропитывание огнеупорной футеровки и диафрагм магниевых ванн расплавленным электролитом, растворение магния в электролите, слияние и рост капель расплавленного магния при выделении его на катоде (рис. 8).

Исследования показывают, что в данном случае поверхностное натяжение электролита как на границе с газовой фазой, так и на границе с твердой фазой или расплавленным металлом увеличивается при повышении концентрации $MgCl_2$, $CaCl_2$, а также NaF и CaF_2, но уменьшается с ростом концентрации NaCl и, особенно KCl [16]. Следовательно, поверхностно-активными являются ионы K^+, Na^+ и Cl^-, а поверхностно-неактивными — Mg^{2+}, C^{2+} и F^-. Электролитическое выделение магния из расплавленных хлоридов представляет собой процесс образования на катоде мелких капель магния и слияния их в более крупные. Последнее является обязательным условием получения высокого выхода по току. Малая величина межфазного натяжения соли на границе с расплавленным металлом, т. е. хорошее смачивание расплавленного металла электролитом, препятствует слиянию отдельных капель металла и способствует удержанию диспергированного магния в среде расплавленного электролита. Наоборот, повышенное поверхностное натяжение электролита на границе с расплавленным металлом ($\sigma_{эл.-Mg}$) облегчает отделение металла от расплавленной соли и слияние его мелких корольков в крупные капли. Большое значение при этом имеет рост капель металла непосредственно на поверхности катода.

Капля расплавленного магния, образующаяся на катоде (рис. 9), подвержена действию трех сил поверхностного натяжения: $\sigma_{1,3}$ — между расплавленным металлом и твердым катодом, $\sigma_{2,1}$ — между расплавлен-

Appendix 14

ным электролитом и расплавленным металлом и $\sigma_{2,3}$ — между расплавленным электролитом и твердым катодом. Силы эти дей[ствуют в плоскости раздела фаз, и направление для $\sigma_{1,3}$ и $\sigma_{2,3}$ совпадает с [плоскостью катода. При $\sigma_{1,3} > \sigma_{2,3}$ сила $\sigma_{2,1}$ примет направление, касател[ьное к поверхности металла. Вертикальная составляющая этой силы равна $\sigma_{2,1}\cos(180-\theta)$, и равновесие наступит при условии, когда

$$\sigma_{1,3} = \sigma_{2,3} + \sigma_{2,1}\cos(180-\theta),$$

откуда

$$\cos(180-\theta) = \frac{\sigma_{1,3}-\sigma_{2,3}}{\sigma_{2,1}}.$$

Из этого выражения видно, что увеличение $\sigma_{2,3}$ и $\sigma_{2,1}$ уменьшает абсолютную величину $\cos(180-\theta)$. Это, очевидно, имеет место при возрастании $(180-\theta)$, что происходит тогда, когда краевой угол капли расплавленного металла θ уменьшается.

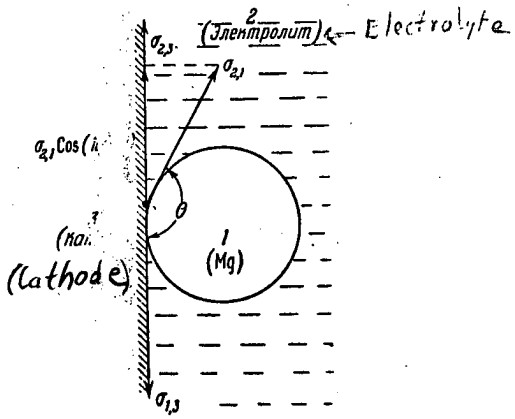

Рис. 9. [Схема сил поверхностного [натяжения, действующих на [каплю магния на катоде

Иными словами, при повышении межфазного натяжения расплавленного электролита на границе с твердым катодом ($\sigma_{2,3}$) и расплавленным магнием ($\sigma_{2,1}$) под влиянием поверхностно-неактивных веществ, например фторидов (ионов F^-), должно улучшаться смачивание катода расплавленным [магнием, а следовательно, в этом случае создаются условия для роста [капель магния на поверхности катода. Наоборот, поверхностно-активные [компоненты электролита, на[пример хлористый калий (ионы [K^+), препятствуют росту капел[ь магния.

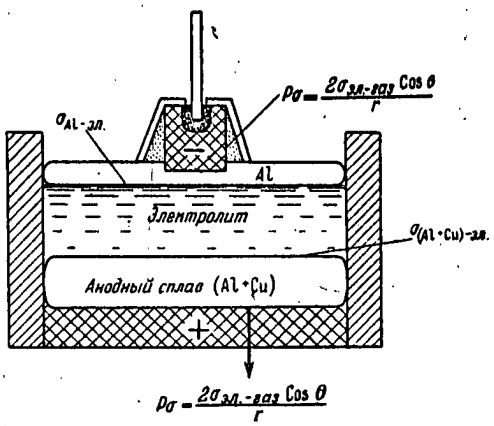

Рис. 10. Области проявления поверхностных сил в ванне для электролитического рафинирования алюминия

Кроме то[го], повышение $\sigma_{2,1}$ под влияние[м] ионов F создает условия для [появления мелких корольков в [более крупные и в массе элект[ролита, что также приведет к [уменьшению потерь магния, а сл[едовательно, и к росту выхода [по току. Целесообразность п[рименения добавок фторидов ка[льция и натрия к электролиту [подтверждена, как известно, м[ноголетней практикой электро[литического производства маг[ния.

В заключ[ение кратко остановимся на р[оли поверхностных явлений в п[роцессе электролитического ра[финирования алюминия. В ванне для электролитического рафинирования [алюминия имеется, как известно, три расплавленных слоя: анодный [сплав (Al + Cu), электролит и чистый катодный алюминий. Поверхностные явления в этом процессе протекают на границе различных фаз, обусл[авливая проникновение солевого расплава в футеровку, потери металла [в электролите и деформацию катодов (рис. 10).

Электролиты современных ванн для электролитиче[ского рафинирования алюминия представляют собой сложные по составу [сплавы из смеси фтористых и хлористых солей. Исследования [17] показы[вают, что смачива-

Appendix 15

SURFACE TENSION OF MOLTEN SALT MIXTURES FOR AN ISOCONCENTRATIONAL SECTION (10% BY WEIGHT OF $MgCl_2$) OF THE SYSTEM $MgCl_2$ — $CaCl_2$ — KCl — NaCl

Kh.L. Strelets and O.G. Desyatnikov

Measurements of the surface tension of molten salts can be carried out most accurately by the maximum bubble pressure method, which permits the use of apparatus made of materials of good resistance to the action of molten salts. Also, in this method it is easy to ensure constancy of temperature in the space in which the measurements are made, since the tip of the capillary at which the gas bubbles are formed is immersed to a depth of only 0.1-0.3 mm.

In its application to molten salts, this method has received its most detailed development in the hands of Jaeger [1].

V. Semenchenko and L. Shikhobalova [2,3] have used the same method for the measurement of the surface tensions of pure salts and binary mixtures of Na, K, and Li chlorides and sulfates, but they have improved it by the use of an electrical contact to determine the moment at which the capillary makes contact with the melt.

RESULTS OF THE MEASUREMENTS

For the measurement of surface tension we used the method based on the maximum pressure developed in a gas bubble.

The accuracy of the method was checked against data for the surface tensions of pure molten KCl, NaCl, $MgCl_2$, and $CaCl_2$ at the interface with the gas phase. In order to check the reproducibility of the results, duplicate measurements were made: the results agreed within 1%.

Figure 1 shows the results of our measurements of surface tensions of pure salts in comparison with those of other authors. For NaCl and KCl there is good agreement with the results of Zhivov [4] and Jaeger [1], and for $CaCl_2$, with the results of Barzakovsky [5].

With respect to the magnitude of the surface tension of the molten salt at its interface with the gas phase, the salts that we have studied may be placed in the following order: $MgCl_2$ → KCl → NaCl → $CaCl_2$, in which $MgCl_2$ has the lowest and $CaCl_2$ the highest surface tension.

Tables 1-7 give the results of the measurements for all compositions.

In Figure 2 a comparison is made of the surface tension isotherms for all sections at 750°. All of the curves are smooth and are convex in the direction of the axis of abscissas. As the KCl content increases this convexity also increases.

From these curves it will be seen that with increase in NaCl content the surface tension increases greatly. Increase in the $CaCl_2$ content from 0% to 30-40% by weight at a constant NaCl : KCl ratio has practically no effect on the value of the surface tension. In the region of 20% $CaCl_2$ there is a poorly defined minimum on all of the curves.

With further increase in the concentration of calcium chloride, a rise in surface tension occurs; this is most marked in the range 70-90%.

Figures 3 and 4 are the concentration triangles for 700° and 750°, and they show the lines of constant surface tension.

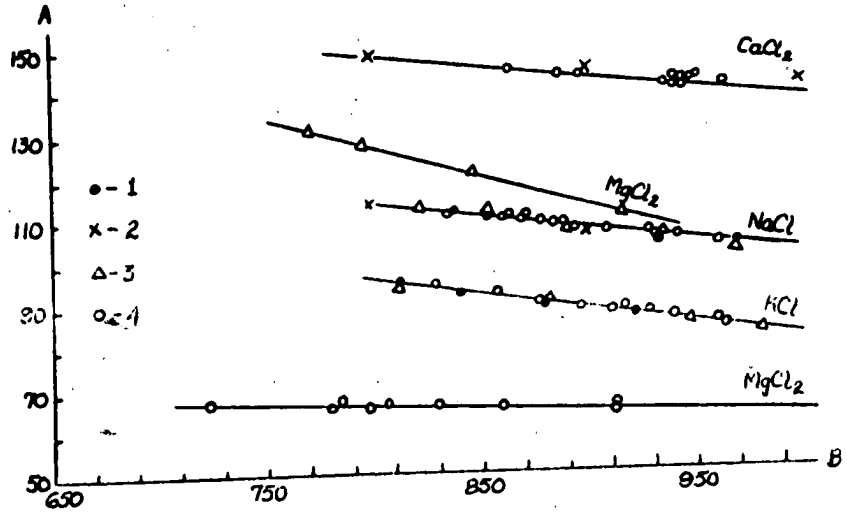

Fig. 1. Surface tensions of pure salts.

A) Surface tension σ (erg/ cm^2). B) temperature (°C).

1)Jaeger's data. 2) Barzakovsky's data. 3) Zhivov's data. 4) our data.

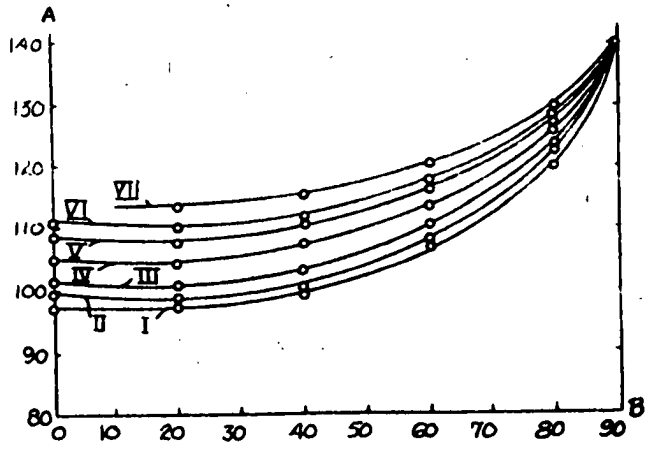

Fig. 2. Surface tension isotherms for compositions in all of the sections studied (750°).

A) Surface tension σ (erg/ cm^2). B) $CaCl_2$ content (% by weight). The Roman numerals correspond to the numbers of the sections.

TABLE 1

Surface Tension σ (erg/ cm^2) for Compositions of Section I (NaCl = 0)

$CaCl_2$ content (% wt.)											
0		20		40		60		80		90	
°C	σ	°C	σ	°C	σ	°C	σ	°C	σ	°C	σ
806	93.3	717	100.5	757	100.00	712	108.9	766	119.0	815	138.5
848	89.9	793	95.2	789	97.8	721	108.6	878	114.2	875	136.9
869	88.6	842	92.0	800	96.6	757	107.5	901	113.8	903	135.2
892	86.6	900	88.0	806	96.5	787	106.1	911	112.3	917	134.8
907	85.8	942	85.0	815	95.9	852	101.0	-	-	952	133.4
914	84.7	963	84.1	877	92.0	892	100.1	-	-	988	132.9

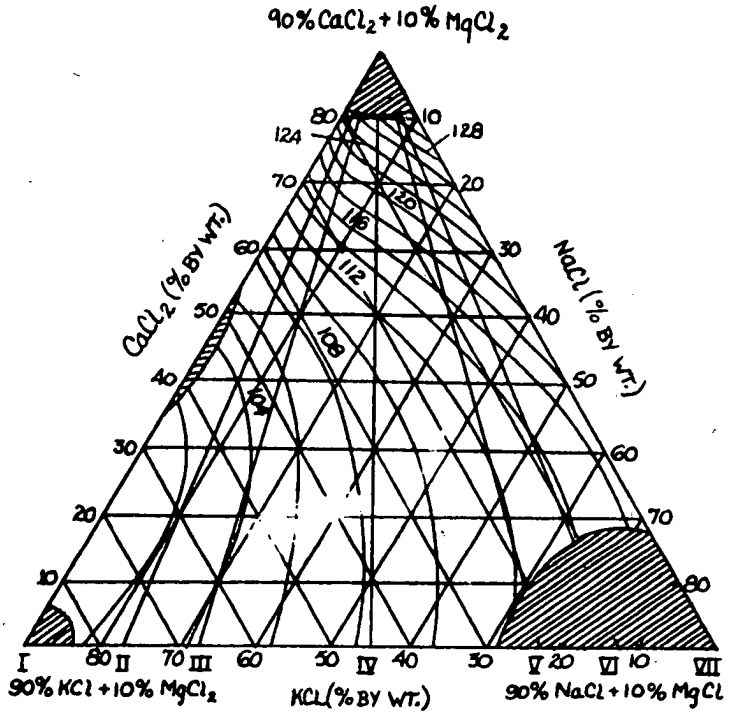

Fig. 3. Concentration triangle for 700°, showing lines of constant surface tension.

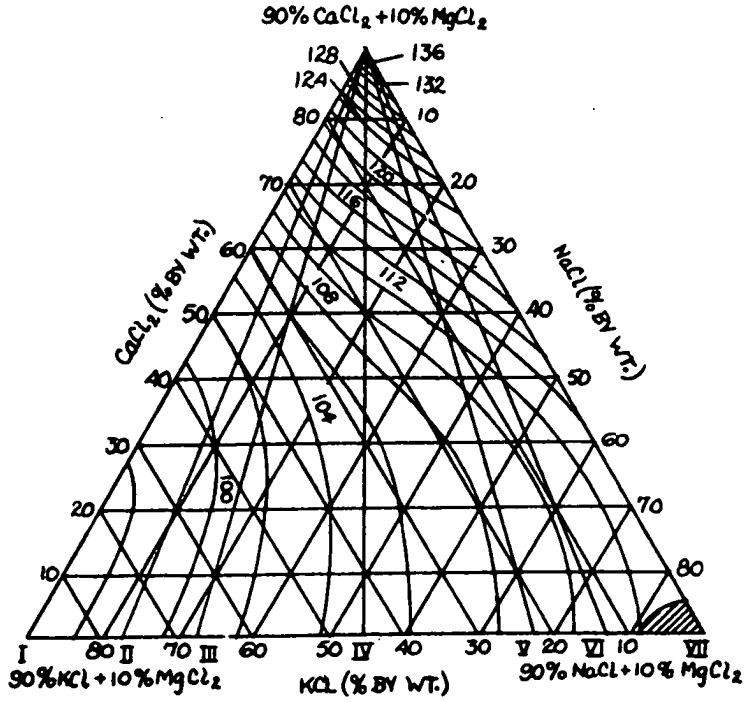

Fig. 4. Concentraton triangle for 750°, showing lines of constant surface tension.

TABLE 2

Surface Tension σ (erg/cm²) for Compositions of Section II $\left(\frac{NaCl}{KCl} = \frac{1}{6}\right)$

$CaCl_2$ content (% by wt.)									
0		20		40		60		80	
°C	σ	°C	σ	°C	σ	°C	σ	°C	σ
697	103.0	695	102.1	709	101.6	672	111.5	732	123.8
758	98.5	705	101.9	722	101.6	685	111.4	802	120.0
768	98.3	763	97.6	758	100.0	734	108.9	808	120.8
826	94.3	838	92.4	795	97.7	760	108.0	836	119.2
887	91.0	865	91.7	895	93.1	827	104.0	895	117.1
954	92.3	900	89.3	907	92.6	875	102.6	901	116.6

TABLE 3

Surface Tension σ (erg/cm²) for Compositions of Section III $\left(\frac{NaCl}{KCl} = \frac{1}{3}\right)$

$CaCl_2$ content (% by wt.)									
0		20		40		60		80	
°C	σ	°C	σ	°C	σ	°C	σ	°C	σ
733	103.0	694	104.1	667	106.9	732	111.6	747	122.9
821	96.8	769	98.7	716	104.9	780	109.5	766	122.6
865	94.9	790	97.6	730	103.9	803	107.0	779	122.0
880	93.1	829	96.2	745	103.1	818	107.1	900	114.2
915	89.8	830	95.3	839	97.4	852	105.1	904	113.9
942	88.9	880	93.2	895	95.4	870	103.9	907	113.3

TABLE 4

Surface Tension σ (erg/cm²) for Compositions of Section IV $\left(\frac{NaCl}{KCl} = \frac{1}{1}\right)$

$CaCl_2$ content (% by wt.)									
0		20		40		60		80	
°C	σ	°C	σ	°C	σ	°C	σ	°C	σ
697	108.1	672	108.5	702	110.2	709	115.0	756	125.9
732	107.1	688	107.8	722	109.2	770	112.5	816	124.0
768	104.2	740	104.0	772	106.4	820	109.6	882	120.3
805	101.6	853	98.8	882	100.9	838	108.9	886	120.7
842	99.4	860	97.9	905	98.9	850	108.4	930	119.1
870	98.0	945	93.4	972	96.9	866	108.2	968	117.4

TABLE 5

Surface Tension σ (erg/cm² for Compositions of Section V $\left(\frac{NaCl}{KCl} = \frac{3}{1}\right)$

CaC_2 content (% by wt.)									
0		20		40		60		80	
°C	σ	°C	σ	°C	σ	°C	σ	°C	σ
805	105.8	739	108.9	700	113.5	685	119.7	734	127.7
865	101.4	744	108.2	735	112.9	740	117.7	749	126.0
917	98.4	758	107.5	760	110.4	750	116.4	793	125.3
936	95.9	819	103.4	815	108.1	768	115.9	890	120.0
966	94.6	826	102.7	833	106.7	887	111.3	893	120.0
1008	92.2	886	98.1	894	102.9	908	109.5	908	119.0

TABLE 6

Surface Tension σ (erg/cm²) for Compositions of Section VI $\left(\frac{NaCl}{KCl} = \frac{6}{1}\right)$

$CaCl_2$ content (% by wt.)									
0		20		40		60		80	
°C	σ	°C	σ	°C	σ	°C	σ	°C	σ
868	103.6	715	112.1	687	114.4	672	120.8	762	128.9
899	101.3	798	106.8	739	112.1	709	118.8	776	127.4
928	99.6	831	105.0	758	110.4	792	116.2	860	125.3
937	99.4	890	100.6	877	105.9	875	112.5	874	123.3
958	97.6			950	103.1	885	111.8	877	124.2
				962	102.6	933	109.2	912	123.1

TABLE 7

Surface Tension σ (erg/cm²) for Compositions of Section VII (KCl = 0)

$CaCl_2$ content (% by wt.)									
0		20		40		60		80	
°C	σ	°C	σ	°C	σ	°C	σ	°C	σ
871	106.9	769	112.2	720	116.7	721	122.2	723	130.7
892	105.0	797	110.9	737	115.7	733	120.8	747	129.5
920	103.5	828	108.9	779	114.5	787	119.4	758	129.2
947	101.5	880	105.8	837	112.0	815	116.9	787	127.2
961	100.5	900	104.0	868	109.1	846	115.6	852	124.2
		922	103.5	905	107.7	877	114.8	900	121.9

LITERATURE CITED

[1] Jaeger, Z. allg. anorg. Chem., 101, 18 (1917).

[2] V. Semenchenko and L. Shikhobalova, J. Phys. Chem., No. 5(1947).

[3] V. Semenchenko and L. Shikhobalova, J. Phys. Chem., No. 6 (1947)

[4] V. Zhivov, Trans. VAMI, No. 11 - 12 (1935).

[5] V. Barzakovsky, J. Appl. Chem., XIII, 8 (1940).

Received October 9, 1953.

Appendix 16

BRIEF COMMUNICATIONS

DENSITY OF FUSED SALTS ALONG ISOCONCENTRATION SECTIONS (10 wt. % $MgCl_2$) IN THE SYSTEM: $MgCl_2 - CaCl_2 - KCl - NaCl$

Kh. L. Strelets and O. G. Desyatnikov

We measured densities for all the compositions by a method of hydrostatic weighing. We maintained an atmosphere of carbon dioxide gas above the melts in order to avoid the action of oxygen or moisture during the time of measurement.

The accuracy of density determination, as dependent on concentration, amounted to 0.3-0.5%.

Densities of these pure salts were determined to check the method: KCl, NaCl, $MgCl_2$, and $CaCl_2$. The data are given in Fig. 1, where they are compared with data from other authors.

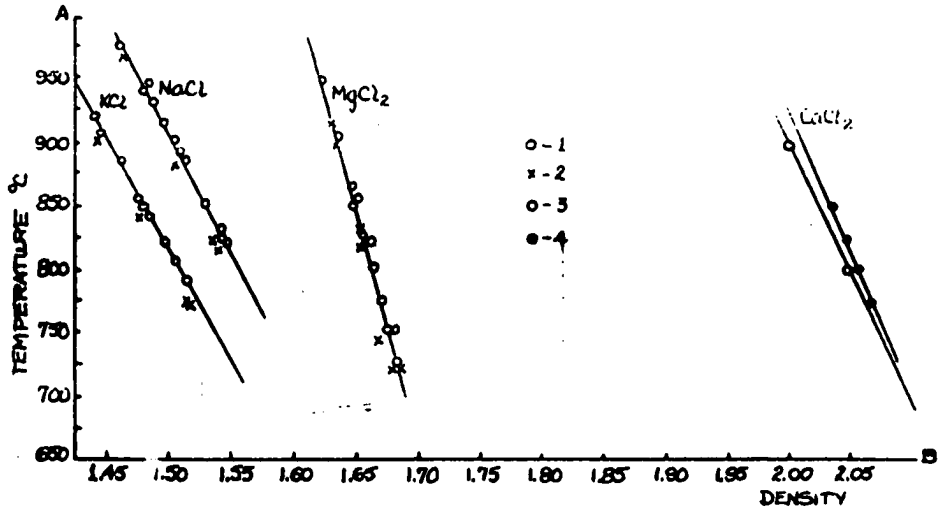

Fig. 1. Densities of KCl, NaCl, $MgCl_2$, and $CaCl_2$, according to various authors. 1) Abramov; 2) Mashovets; 3) Barzakovsky; 4) present authors.

As can be seen from Fig. 1, our data lie between the data of Abramov [1] and Mashovets [2]. The $CaCl_2$ density data are close to the data of Barzakovsky [3]. All of the controlled measurements we made were in good agreement with the above noted limits of error.

Results of Measurements

We studied isoconcentration sections passing through 10 wt. % $MgCl_2$ in the system: $CaCl_2$-$MgCl_2$-NaCl-KCl.

A total of 72 compositions were measured; they were themselves arranged as secondary sections passing through the vertex of the ternary diagram (90 wt. % $CaCl_2$ and 10 wt. % $MgCl_2$).

Compositions which correspond to the same $CaCl_2$ content in these sections differ from one another in their NaCl: KCl ratio.

The results of measuring density for all compositions are given in Table 1.

Density isotherms for five sections at a temperature of 750° C are given in Fig. 2.

APP. 10 - Pg. 2

TABLE 1

Density of Salt Melts

NaCl: KCl ratio	$CaCl_2$ content (wt.%)	Density of salt at indicated temperature: (°C)							
		675	700	725	750	775	800	825	850
KCl—0%	0	—	—	—	—	—	1.555	1.540	1.524
	10	—	—		1.627	1.615	1.603	1.587	1.573
	20	—	—	1.680	1.667	1.654	1.639	1.627	1.610
	30	—	1.748	1.732	1.712	1.701	1.680	1.671	1.656
	40	—	1.789	1.776	1.760	1.745	1.728	1.711	1.696
	50	—	—	1.830	1.816	1.800	1.784	1.768	1.751
	60	1.908	1.891	1.872	1.859	1.846	1.833	1.821	1.806
	70	1.963	1.949	1.936	1.923	1.911	1.897	1.884	1.871
	80	—	—	2.007	1.993	1.978	1.966	1.953	1.939
6:1	0	—	—	—	—	1.567	1.551	1.539	1.526
	10	—	—	1.634	1.618	1.605	1.591	1.580	1.566
	20	—	1.691	1.679	1.614	1.654	1.638	1.623	1.613
	30	1.751	1.739	1.725	1;713	1.700	1.687	1.674	1.661
	35	1.764	1.752	1.740	1.727	1.715	1.703	1.691	1.679
	40	1.790	1.777	1.764	1.751	1.739	1.727	1.714	1.701
	45	1.815	1.801	1.787	1.774	1;761	1.748	1.736	1.724
	50	1.838	1.826	1.813	1.800	1.787	1.774	1.762	1.749
	55	1.868	1.855	1.843	1.830	1.817	1.804	1.792	1.779
	60	1.902	1.890	1.878	1.867	1.855	1.841	1.827	1.815
	70	—	1.961	1.947	1.933	1.918	1.905	1.891	1.878
3:1	0	—	—	1.583	1.570	1.557	1.544	1.530	1.518
	5	—	—	1.605	1.591	1.577	1.564	1.549	1.536
	10	—	1.637	1.623	1.610	1.597	1.584	1.572	1.559
	15	1.673	1.660	1.645	1.631	1.618	1.605	1.592	1.579
	20	1.693	1.678	1.665	1.652	1.640	1.626	1.609	1.600
	30	1.734	1.720	1.706	1.693	1.680	1.667	1.654	1.640
	35	1.755	1.743	1.729	1.716	1.703	1.690	1.677	1.665
	40	1.789	1.776	1.763	1.750	1.737	1.725	1.712	1.700
	45	1.801	1.790	1.778	1.765	1.752	1.739	1.724	1.715
	50	1 839	1.827	1.813	1.800	1.788	1.776	1.763	1.751
	60	1.882	1.869	1.856	1.844	1.832	1.820	1.808	1.795
	70	1.962	1.948	1.935	1.921	1.907	1.893	1.879	1.866
1:1	0	1.602	1.589	1.573	1.561	1.542	1.530	1.518	1.503
	5	1.615	1.601	1.587	1.574	1.559	1.545	1.532	1.520
	10	1.632	1.622	1.608	1.594	1.582	1.568	1.554	1.540
	15	1.665	1.651	1.636	1.622	1.607	1.594	1.580	1.566
	20	1.691	1.678	1.664	1.651	1.636	1.622	1.608	1.594
	25	1.705	1.691	1.675	1.663	1.651	1.637	1.624	1.613
	30	1.729	1.716	1.701	1.690	1.677	1.663	1.650	1.638
	40	1.776	1.762	1.748	1.734	1.721	1.707	1.694	1.680
	45	1.800	1.785	1.773	1.758	1.746	1.732	1.718	1.703
	50	1.820	1 806	1 792	1 778	1 764	1.750	1.738	1.724
	55	1.840	1.828	1.815	1.803	1.792	1.779	1.767	1.754
	60	1.879	1.868	1.856	1.845	1.833	1.821	1.809	1.797
	80	—	—	—	1.991	1.977	1.963	1.950	1.935
1:3	0	1.589	1.576	1.561	1.544	1.528	1.514	1.500	1.485
	10	1.629	1.616	1.602	1.587	1.573	1.559	1.544	1.530
	20	1.669	1.656	1.644	1.629	1.615	1.601	1.588	1.575
	30	1.712	1.700	1.686	1.673	1.659	1.646	1.633	1.619
	40	1.765	1.751	1.737	1.723	2.709	1.695	1.681	1.664
	50	1.822	1.807	1.793	1.779	1.764	1.751	1.739	1.724
	60	1.874	1.861	1.846	1.833	1.819	1.805	1.791	1.777
	70	1.947	1.933	1.920	1.906	1.893	1.897	1.866	1.851

TABLE 1 (Continued)

NaCl: KCl ratio	$CaCl_2$ content (wt.%)	Density of salt at indicated temperature: (°C)							
		675	700	725	750	775	800	825	850
1:6	0	–	1.565	1.551	1.537	1.523	1.510	1.494	1.480
	10	1.622	1.606	1.593	1.578	1.563	1.549	1.532	1.520
	20	1.661	1.646	1.630	1.616	1.603	1.589	1.575	1.561
	30	1.708	1.695	1.681	1.667	1.654	1.640	1.627	1.613
	40	1.755	1.742	1.729	1.715	1.702	1.689	1.675	1.662
	50	1.807	1.793	1.780	1.766	1.753	1.739	1.725	1.711
	60	1.872	1.858	1.844	1.829	1.815	1.802	1.779	1.775
	70	–	1.937	1.923	1.913	1.899	1.883	1.869	1.855
NaCl = 0%	0	–	–	–	–	1.524	1.500	1.490	1.464
	10	–	1.601	1.596	1.578	1.560	1.544	1.527	1.511
	20	1.666	1.652	1.63[illegible]	1.620	1.611	1.585	1.573	1.559
	30	1.706	1.690	1.673	1.660	1.644	1.631	1.618	1.606
	40	–	–	1.722	1.709	1.694	1.680	1.669	1.650
	50	–	1.782	1.774	1.762	1.749	1.729	1.717	1.703
	60	–	1.860	1.845	1.830	1.818	1.805	1.792	1.780
	70	–	–	1.911	1.900	1.887	1.871	1.858	1.847
	80	–	2.011	1.999	1.985	1.969	1.955	1.935	1.924
	90	–	–	–	–	2.058	2.045	2.030	2.016

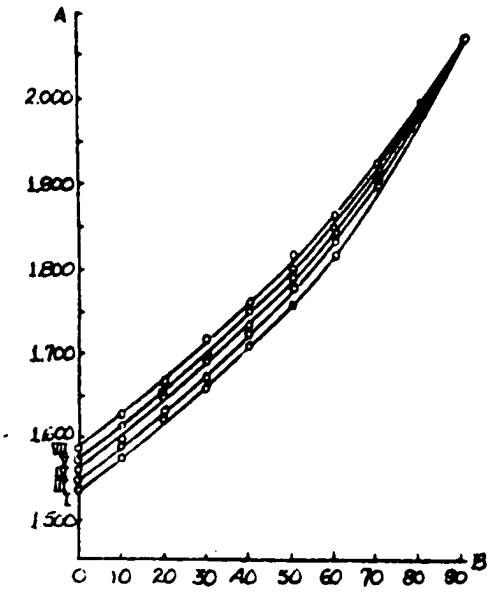

Fig. 2. Density isotherms for sections I, III, IV, V and VII at 750°C. A) Density; B) $CaCl_2$ content (wt. %).

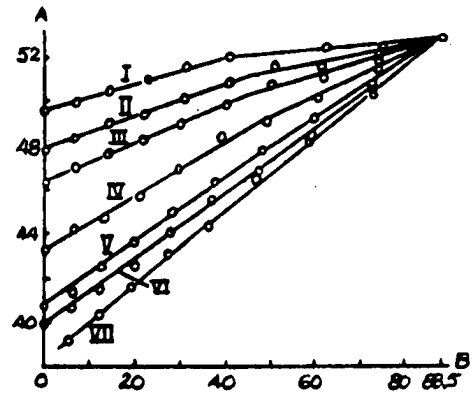

Fig. 3. Isotherm of molecular volume of the composition of all sections studied at 750° C. A) molecular volume; B) content $CaCl_2$ (in mol.-%).

With increased $CaCl_2$ content, the density curves for all sections increase monotonously; the curves are convex to the abscissa axis.

The curvature decreased with increase in sodium chloride content (increase in NaCl: KCl ratio).

It can be seen from considering the data presented that electrolyte density also increases with increased sodium chloride content.

TABLE 2

Temperature Coefficients of Density for Melts in the $MgCl_2 - CaCl_2 - KCl - NaCl$ System.

NaCl:KCl ratio	$CaCl_2$ content (wt. %)	Density at 800° C	$\alpha \cdot 10^5$	Range of measuring temperatures (°C)	NaCl:KCl ratio	$CaCl_2$ content (wt. %)	Density at 800° C	$\alpha \cdot 10^5$	Range of measuring temperatures (°C)
KCl — %	0	1.555	62.5	700-850	1:1	40	1.708	55.0	700-850
	10	1.595	59.0	700-850		45	1.731	55.0	675-850
	20	1.640	56.0	725-850		50	1.751	55.0	700-850
	30	1.685	60.5	700-850		60	1.822	48.5	675-850
	40	1.727	61.5	700-850		80	1.963	55.0	750-850
	50	1.785	60.0	700-850					
	60	1.833	53.0	675-850		0	1.515	60	650-850
	70	1.898	52.0	675-850		10	1.560	57.5	675-850
	80	1.966	54.0	700-850		20	1.602	55	675-850
						30	1.643	53.5	675-850
	0	1.551	49.0	775-850	1;3	40	1.694	57.5	675-850
	10	1.593	52.5	725-850		50	1.752	56	675-850
	20	1.638	55.0	700-850		60	1.805	55.5	675-850
	30	1.688	50.5	675-850		70	1.880	54	675-850
	40	1.726	50.0	700-850					
6:1	45	1.750	51.5	675-850		0	1.510	56.5	675-850
	50	1.775	51.0	700-850		10	1.550	57.5	675-850
	60	1.840	50.0	675-850		20	1.589	57	675-850
	70	1.906	55.0	700-850		30	1.640	54.5	675-850
					1:6	40	1.689	53	675-850
	0	1.544	52.5	725-850		50	1.739	55	675-850
	10	1.584	53.0	700-850		60	1.802	55	675-850
	20	1.626	53.0	675-850		70	1.882	55	675-850
	30	1.667	53.5	675-850					
	40	1.725	51.0	700-850		0	1.502	67.5	700-850
3:1	45	1.740	51.0	675-850		10	1.544	68	700-850
	50	1.776	50.5	700-850		20	1.587	63.5	700-850
	60	1.821	49.5	675-850		30	1.630	60.5	700-850
	70	1.823	55.5	675-850		40	1.680	58	700-850
	0	1.532	56.5	675-850	NaCl = 0%	50	1.731	56	700-850
	10	1.568	54.5	675-850		60	1.805	54.5	725-850
1:1	20	1.623	52.0	675-850		70	1.872	55	700-850
	30	1.662	53.0	675-850		80	1.954	59	700-850
						90	2.044	58	700-850

The nature of the density change is linear for all compositions. Data for density at 800° C and temperature coefficients are given in Table 2.

Considering the molecular volume isotherms (Fig. 3), shows the presence of characteristic points of inflexions on the isotherms at $CaCl_2$ concentrations of 40-45%. The clearest point of inflexion appears on the isotherm for the section from which NaCl is lacking. With further transition to sections corresponding to smaller KCl contents, this point is less readily determined, and it disappears in the section which does not contain KCl. The indicated character of the isotherms may be explained by forming the compound $KCl \cdot CaCl_2$. The characteristic point on the molecular volume isotherms is somewhat shifted to the left from the composition $KCl \cdot CaCl_2$ because of the presence of $MgCl_2$ in the system which also forms a compound with KCl.

LITERATURE CITED

[1] G. Abramov. Metallurgy. No. 8 (1935).
[2] V. Mashovets and Z. Lundina, Trudy Scientific Research Institute of Light Metals, No. 10 (1935).
[3] V. Barnakovsky, J. Appl. Chem., XIII, 8 (1940).

Received October 9, 1953

Appendix 17

CONDUCTANCE OF THE FUSED SALTS OF ISOCONCENTRATED MIXTURES OF THE SYSTEM $MgCl_2 - CaCl_2 - KCl - NaCl$ (10% $MgCl_2$ BY WEIGHT)

Kh. L. Strelets and O. G. Desyatnikov

Many studies have been devoted to determination of the conductance of fused salts. Karpachev, Stromberg and Poltoratskaya [1] have studied the conductance of the system. $KCl - MgCl_2$. They made their measurements in a vessel with a quartz capillary having a constant of 230. A Ruhmkorff coil provided them with alternating current. The vessel was calibrated in terms of fused $CdCl_2$.

Batashev [2] studied the conductivity of mixtures of fused chloride salts of Na, K and Mg. A generator having the frequency of sound was employed in this work. A flat-bottomed cylindrical platinum vessel served both as container and as one of the electrodes. A platinum disc served as the other. The electrolytic capacity of the vessel was 0.322. The accuracy of the measurement was evaluated as being within 3%.

Shcherbakov and Markov [3], measuring the conductance of the same system, developed a more exact method. They used cells with both U-shaped and vertical capillaries. The conductivity of the vessel walls was taken into consideration in making these measurements, and the drop in temperatures through the thickness of the melt was reduced by improving the thermal insulation of the furnace.

Barzakovsky [4] studied the conductance of binary systems of fused salts, including $CaCl_2 - NaCl$.

The present work employs a system of measurement which satisfies to a maximum the conditions resulting from the theory of the alternating current bridge. We have employed vessels with capillaries, capacity being from 100 to 400.

EXPERIMENTAL

Method of measurement. For our measurements, we employed quartz vessels of the vertical type with capillaries 5 to 20 mm long and 1 and 1.5 mm in diameter. Fig. 1 presents a drawing of the vessel.

The electrolytic capacity of the vessels we used varied from 100 to 400 with the diameter and length of the capillaries, and the resistances of the salts from 25 to 250 Ω.

The vessels were calibrated with 30% sulfuric acid.

The use of vessels having capillary portions 5 to 7 mm in length assured that the temperature differential through the thickness of the measured layer of salt would be negligible (about 2 °C); this was confirmed by special readings.

In calculating the conductance we allowed a correction for the conductivity of the walls of the vessel, the value of which was determined for all the vessels over a large temperature interval.

An equimolecular mixture of NaCl and KCl was adopted as the control. An identical level of salt in beaker and vessel was maintained in all experiments.

To make our measurements we employed a bridge supplied with alternating current at the speed of sound (Fig. 2). The theory of systems of measurement has been analyzed in adequate detail by Semenchenko [5], Polyakov and Ivanov [6], and Barzakovsky [4]. Our design made it possible to determine the sound minimum within 1 mm of the rheochord scale. The accuracy of measurements was to 0,5-0.8%.

The reproducibility of the results was verified by measurement of the conductance of the control mixture.

In Fig. 3 we show our data for the conductance of pure salts of KCl, $MgCl_2$, NaCl and $CsCl_2$ in comparison with that of other researchers.

Conductance measurements both of pure salts and of mixtures thereof were taken at a number of temperatures both at heating and cooling. The data was in complete agreement, in both cases.

Results of measurements. Tables 1-7 adduce the data arrived at and Fig. 4 compares the isotherms of specific conductance of all the samples studied, at 750 °C. Gradual elevation of the $CaCl_2$ content from 0 to 90% resulted first in a drop and then in a rise in conductance. The most marked minimum was shown with materials having a composition lacking in NaCl (Mixture 1).

As KCl content rose, the position of the minimum shifted in the direction of lower $CaCl_2$ concentrations. In Mixture I, the minimum was found in the region of $CaCl_2$ concentration of between 48 and 52%, and corresponded approximately to that in which the chemical compound $KCl \cdot CaCl_2$ is formed.

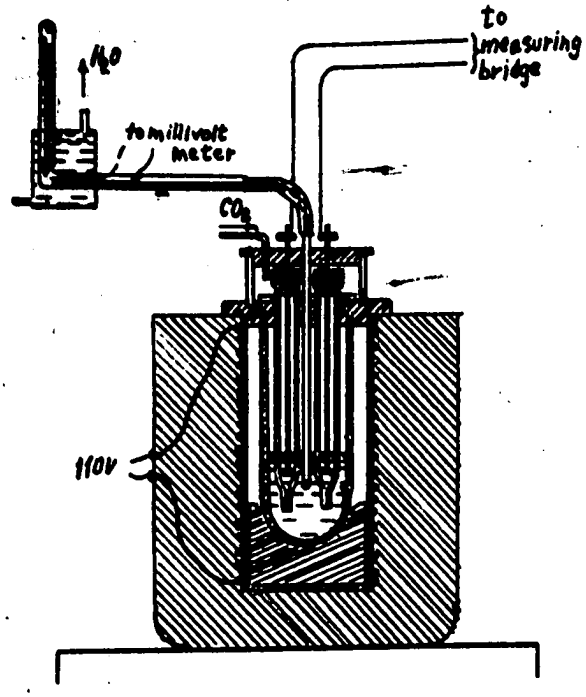

Fig. 1. Position of furnace and vessel at moment of measurement.

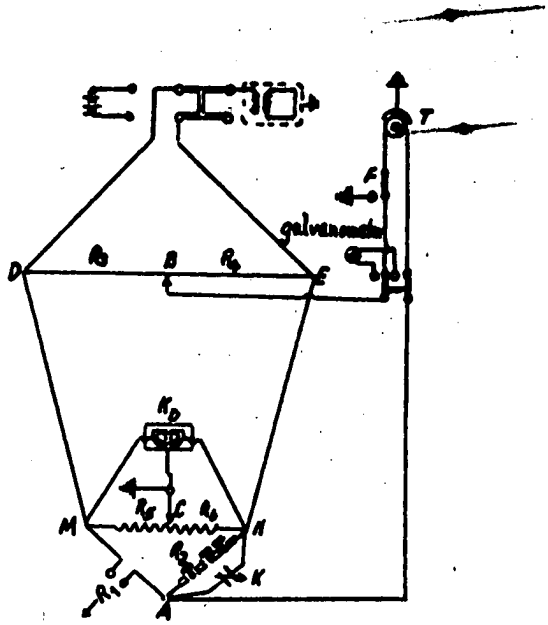

Fig. 2. Electrical circuit of system for determination of conductance.

TABLE 1

Specific Conductance (χ) of Type I Mixtures (NaCl = 0) (in Ω^{-1} cm^{-1})

$CaCl_2$ content (% by weight)																			
0		10		20		30		40		50		60		70		80		90	
°C	χ	°C	χ	°C	χ	°C	χ	°C	χ	°C	χ	°C	χ	°C	χ	°C	χ	°C	χ
780	1.90	757	1.67	687	1.295	717	1.26	715	1.175	708	[illegible]6	686	1.05	686	1.16	722	1.45	758	1.86
810	1.98	783	1.73	718	1.40	740	1.33	759	1.29	744	1.22	709	1.14	715	1.29	757	1.56	775	1.91
817	2.00	796	1.76	777	1.55	778	1.25	798	1.395	767	1.28	726	1.20	748	1.36	787	1.66	795	1.99
853	2.07	824	1.82	798	1.61	788	1.45	825	1.455	790	1.335	809	1.41	767	1.40	821	1.76	824	2.08
877	2.10	865	1.90	818	1.65	860	1.61	870	1.535	823	1.415	832	1.47	826	1.57	860	1.86	850	2.16
887	2.11			860	1.725					857	1.485	868	1.54	868	1.66				

TABLE 2

Specific Conductance (χ) of Type II Mixtures $\left(\frac{NaCl}{KCl} = \frac{1}{6}\right)$ (in $\Omega^{-1} \cdot cm^{-1}$)

$CaCl_2$ content (% by weight)																	
0		10		20		30		40		50		60		70		80	
°C	χ	°C	χ	°C	χ	°C	χ	°C	χ	°C	χ	°C	χ	°C	χ	°C	χ
728	1.83	697	1.60	684	1.37	685	1.26	681	1.17	685	1.15	725	1.24	710	1.33	690	1.41
768	1.94	730	1.69	730	1.52	709	1.34	709	1.24	726	1.26	764	1.39	729	1.39	727	1.54
803	2.03	760	1.78	780	1.60	757	1.46	750	1.36	758	1.36	795	1.47	744	1.44	753	1.61
840	2.09	795	1.86	817	1.72	835	1.66	830	1.56	827	1.53	835	1.57	817	1.63	805	1.75
822	2.16	830	1.93	866	1.80	871	1.73	870	1.64	872	1.65	862	1.64	842	1.69	845	1.84
		864	2.00					880	1.65	890	1.67			875	1.75		

TABLE 3

Specific Conductance (χ) of Type III Mixtures $\left(\frac{NaCl}{KCl} = \frac{1}{3}\right)$ (in $\Omega^{-1} \cdot cm^{-1}$)

$CaCl_2$ content (% by weight)																	
0		10		20		30		40		50		60		70		80	
°C	χ	°C	χ	°C	χ	°C	χ	°C	χ	°C	χ	°C	χ	°C	χ	°C	χ
682	1.795	677	1.62	685	1.47	702	1.41	687	1.24	745	1.37	717	1.31	757	1.5	687	1.44
720	1.91	761	1.87	722	1.59	766	1.57	725	1.35	763	1.42	760	1.44	790	1.61	724	1.56
780	2.06	807	1.97	769	1.72	802	1.66	750	1.44	792	1.51	825	1.61	823	1.72	760	1.67
792	2.09	820	2.00	814	1.74	835	1.73	762	1.47	830	1.58	871	1.73	860	1.77	796	1.77
830	2.17	867	2.08	845	1.90	862	1.79	838	1.65	872	1.67					850	1.89
868	2.22			861	1.92			874	1.74								

TABLE 4

Specific Conductance (χ) of Type IV Mixtures $\left(\frac{NaCl}{KCl} = \frac{1}{1}\right)$ (in $\Omega^{-1} \cdot cm^{-1}$)

$CaCl_2$ content (% by weight)																	
0		10		20		30		40		50		60		70		80	
°C	χ	°C	χ	°C	χ	°C	χ	°C	χ	°C	χ	°C	χ	°C	χ	°C	χ
734	2.27	720	2.03	729	1.85	767	1.84	713	1.57	671	1.37	698	1.42	710	1.46	745	1.66
758	2.33	751	2.14	751	1.96	870	2.07	754	1.72	752	1.62	715	1.48	733	1.55	768	1.725
768	2.36	799	2.27	783	2.02	875	2.08	792	1.83	801	1.76	742	1.57	760	1.63	812	1.85
790	2.40	865	2.39	805	2.11	812	1.96	824	1.90	816	1.805	783	1.69	785	1.71	850	1.94
817	2.45			840	2.19			832	1.91	820	1.82	818	1.78	828	1.82		
828	2.47			875	2.25			862	1.99	853	1.87	860	1.88	860	190		

TABLE 5

Specific Conductance (χ) of Type V Mixtures $\left(\frac{NaCl}{KCl} = \frac{3}{1}\right)$ (in $\Omega^{-1} \cdot cm^{-1}$)

$CaCl_2$ content (% by weight)																	
0		10		20		30		40		50		60		70		80	
°C	χ	°C	χ	°C	χ	°C	χ	°C	χ	°C	χ	°C	χ	°C	χ	°C	χ
731	2.63	710	2.36	672	2.04	688	1.87	710	1.93	722	1.736	697	1.59	718	1.60	749	1.73
825	2 845	722	2.41	700	2.14	708	1.96	722	1.98	755	1.825	723	1.68	731	1.64	786	1.85
830	2.85	750	2.49	754	2.32	747	2.09	752	2.07	788	1.92	755	1.78	766	1.76	830	1.97
860	2.90	768	2.54	780	2.39	788	2.20	770	2.13	838	2.07	800	1.92	797	1.85	869	2.06
		779	2.57	834	2.51	870	2.41	800	2.20	870	2.15	830	2.00	820	1.92	872	2.07
		835	2.68					885	2.39								

TABLE 6

Specific Conductance (χ) of Type VI Mixtures $\left(\frac{NaCl}{KCl} = \frac{6}{1}\right)$ (in $\Omega^{-1} \cdot cm^{-1}$)

$CaCl_2$ content (% by weight)																	
0		10		20		30		40		50		60		70		80	
°C	χ	°C	χ	°C	χ	°C	χ	°C	χ	°C	χ	°C	χ	°C	χ	°C	χ
740	2.72	774	2.69	730	2.34	732	2.19	721	1.96	722	1.83	697	1.63	698	1.56	687	1.53
780	2.94	807	2.79	750	2.42	765	2.28	763	2.07	730	1.85	740	1.76	751	1.75	727	1.66
805	3.00	835	2.85	782	2.50	805	2.39	782	2.12	758	1.94	750	1.81	797	1.89	763	1.78
836	3.07			800	2.53	815	2.42	805	2.19	788	2.05	830	2.03	822	1.98	821	1.95
857	3.11			815	2.56	860	2.55	830	2.26	800	2.07	880	2.16	851	2.06	861	2.07
870	3.13			853	2.65			865	2.34	885	2.27	885	2.17	862	2.08		

TABLE 7

Specific Conductance (χ) of Type VII Mixtures (KCl = 0)(in $\Omega^{-1} \cdot cm^{-1}$)

$CaCl_2$ content (% by weight)																	
0		10		20		30		40		50		60		70		80	
°C	χ	°C	χ	°C	χ	°C	χ	°C	χ	°C	χ	°C	χ	°C	χ	°C	χ
785	3.14	780	2.94	757	2.68	691	2.20	730	2.16	686	1.82	715	1.77	692	1.62	690	1.55
825	3.27	813	3.03	800	2.8	722	2.32	767	2.29	713	1.93	757	1.93	731	1.75	767	1.83
845	3.30	824	3.05	829	2.88	759	2.44	808	2.40	724	1.98	790	2.04	753	1.85	780	1.90
850	3.33	871	3.16	865	2.96	798	2.54	836	2.47	840	2.35	832	2.16	774	1.92	826	2.03
883	3.38					837	2.65	868	2.55	867	2.40			815	2.06	835	2.08
						868	2.72							872	2.20	855	2.13

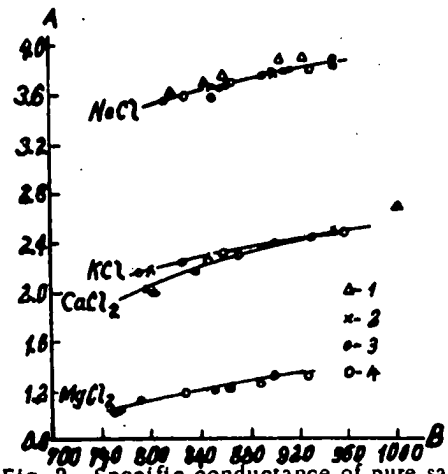

Fig. 3. Specific conductance of pure salts.

A) Specific conductance of salts, χ (in $\Omega^{-1} \cdot cm^{-1}$).
b) temperature, °C
1- According to Varzakovsky; 2-according to Arndt and Gessler; 3- according to Batashev; 4-our findings.

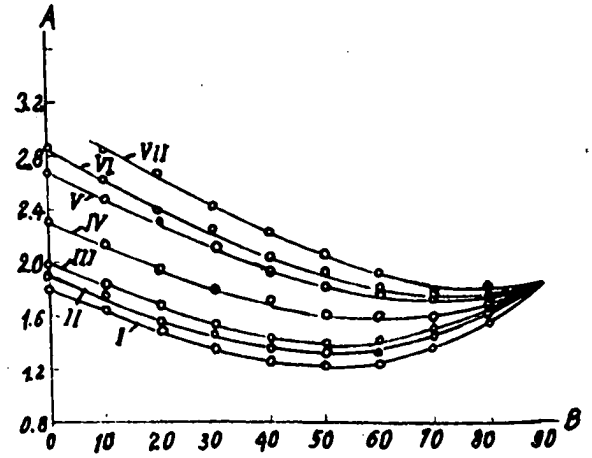

Fig. 4. Isotherms of specific conductance for mixtures of all the types studied, at 750°C.
A) specific conductance, χ (in $\Omega^{-1} \cdot cm^{-1}$), b) $CaCl_2$ content (% by weight). Seven mixtures having constant NaCl : KCl weight ratios. Mixtures I--0, II—1/6, III—1/3, IV—1, V—3, VI—6, VII—KCl = 0.

The complex nature of the relationship between conductance and composition may be explained both by the solvation of ions, and by the appearance of chemical compounds.

Figs. 5 and 6 show concentration triangles with lines for equal specific conductances at 700 and 750 °C.

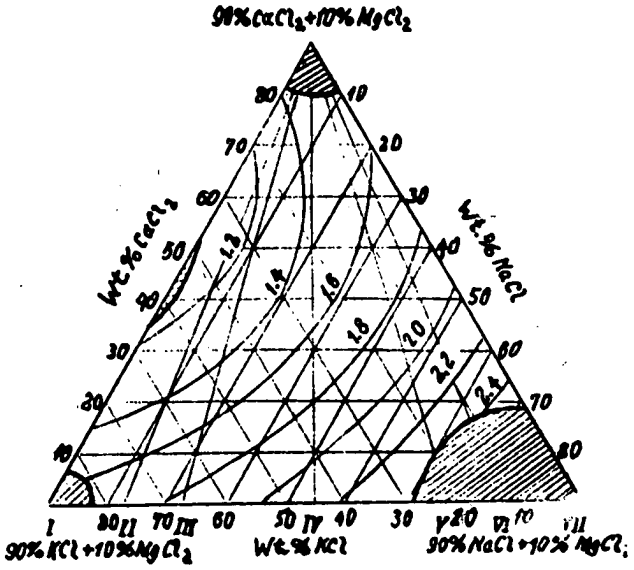

Fig. 5. Concentration triangle with lines showing equal specific conductances at 700 °C.

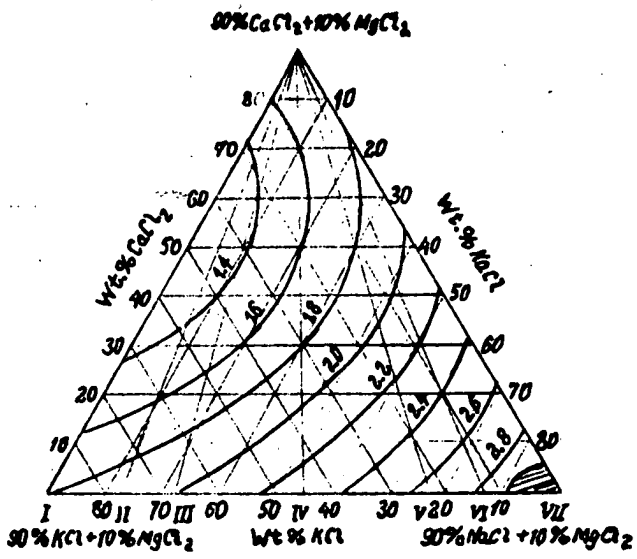

Fig. 6. Concentration traingle with lines showing equal specific conductances at 750°C.

LITERATURE CITED

[1] S. Karpachev, A. Stromberg, and V. Poltoratskaya, J. Gen. Chem., V, 621 (1935).

[2] K. Batashev, The Metallurgist, 7 (1935).

[3] A. Shcherbakov and B. Markov, J. Phys. Chem, XIII, No. 5, 621 (1939).

[4] V. Barzakovsky, Papers on the Electrochemistry of Fused Salts, 1940.

[5] V. Semenchenjo, B. Erofeev and V. Serzhinsky, J. Gen. Chem., II, 10 (1932).

[6] V. Polyakov and A. Ivanov, Bull. USSR Acad. Sci., No. 5-6, 1119 (1938).

Received October 9, 1953.

Appendix 18

VISCOSITY OF FUSED SALTS ALONG AN ISOCONCENTRATION SECTION (10 Wt. % $MgCl_2$) IN THE $MgCl_2$ – $CaCl_2$ – KCl – NaCl SYSTEM

Kh. L. Strelets, V. N. Zhludneva, and I. L. Reznikov

We selected the Kulon method for measuring viscosities since it is most convenient for determining the viscosity of fused salts.

This method is based on observing the damping of harmonic vibrations of a solid of revolution suspended in the liquid by an elastic fiber. By observing a series of successive vibrational amplitudes and calculating the logarithmic decrement of the damping, we can compute the viscosity of the liquid using the following equations given by Fershaffelt:

$$(2 + p)\ \eta + \gamma R \sqrt{d\eta} = \frac{3L}{8\pi R^3},$$

$$\text{where } P = \frac{bR + 1}{b^2R^2 + (bK + 1)^2},\quad b = \sqrt{\frac{\pi d}{\eta T}},\quad L = \frac{2\delta R}{T_0} \text{ and } \gamma = \sqrt{\frac{\pi}{T}}.$$

where η is the viscosity being determined, d the density of the melt under study, δ the decrement in vibrational damping, R the radius of the sphere (the solid of revolution), T the period of vibration of the system in the salt being studied, T_0 the period of vibration of the system in air, and K the moment of inertia of the system.

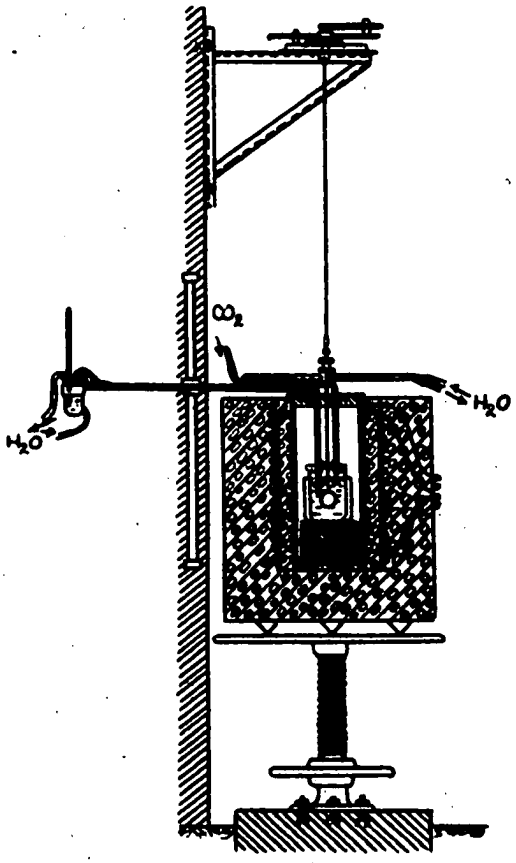

Fig. 1. Arrangement of equipment for viscosity determinations.

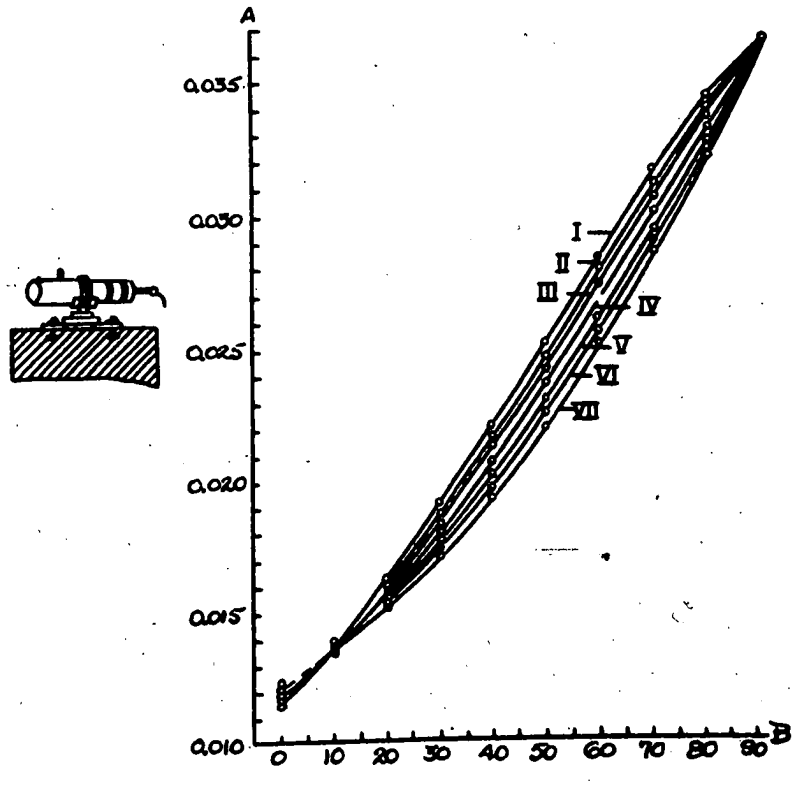

Fig. 2. Viscosity isotherms for compositions along all sections studied at 750°C.
A) Viscosity η (centipoises), B) $CaCl_2$ content (wt. %).

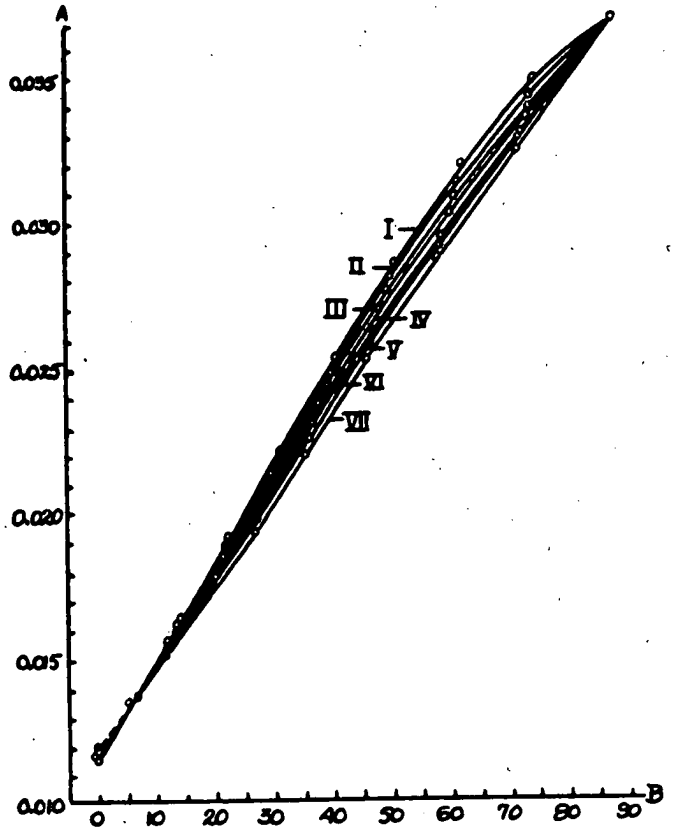

Fig. 3. Viscosity isotherms for compositions along all sections studied at 750°C.
A) Viscosity η (centipoises), B) $CaCl_2$ content (mol. %)

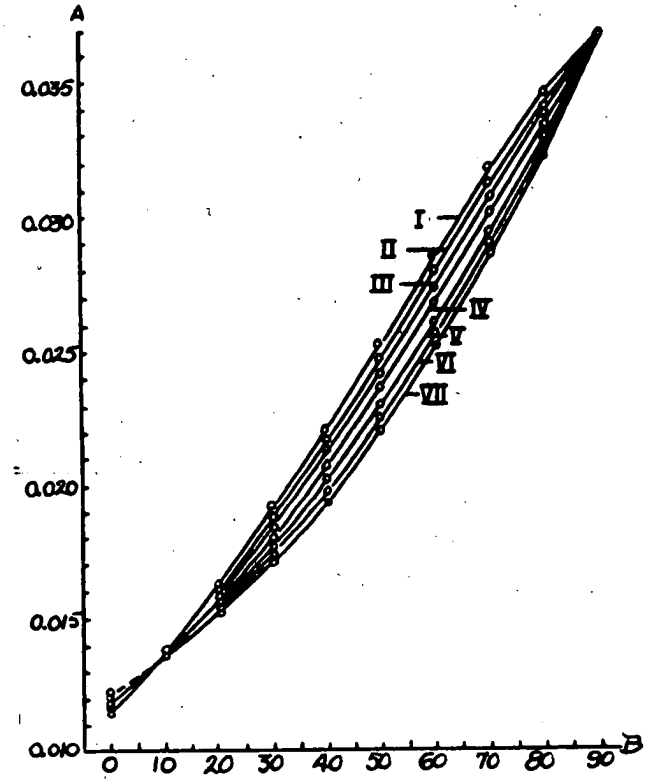

Fig. 4. Viscosity isotherms for compositions along all sections studied at 750°C.
A) Viscosity η (centipoises), B) $CaCl_2$ content (%).

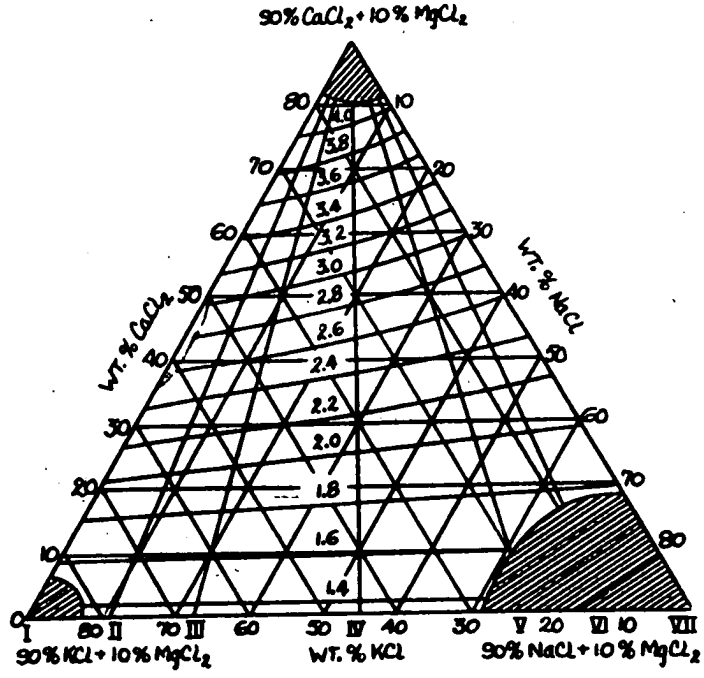

Fig. 5. Triangular concentration diagram with lines of equal viscosity (700°).

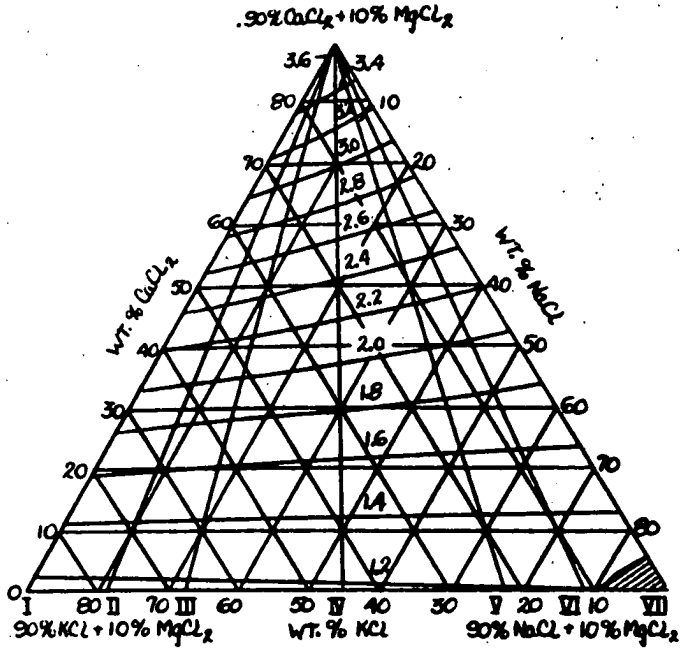

Fig. 6. Triangular concentration diagram with lines of equal viscosity (750°).

pp. 18 - Pg 3

TABLE 1

Viscosity (η) for Compositions along Section I (NaCl = 0) (centipoises)

$CaCl_2$ content (wt. %)																			
0		10		20		30		40		50		60		70		80		90	
°C	η	°C	η	°C	η	°C	η	°C	η	°C	η	°C	η	°C	η	°C	η	°C	η
729	1.24	692	1.70	618	2.83	640	3.12	680	2.96	676	3.37	709	3.34	694	3.94	720	3.83	745	3.74
748	1.17	720	1.48	642	2.51	674	2.71	703	2.65	724	2.74	731	3.05	719	3.63	744	3.52	776	3.20
780	1.05	755	1.36	685	2.11	712	2.22	729	2.37	756	2.44	759	2.73	744	3.32	790	3.03	800	3.02
802	1.00	785	1.29	721	1.77	742	1.97	754	2.15	783	2.25	810	2.28	766	2.99	817	2.77	820	2.91
852	0.85	810	1.16	759	1.54	774	1.75	778	1.96	811	1.98	832	2.11	789	2.75	838	2.59	854	2.60
		833	1.07	793	1.39	814	1.54	800	1.77	833	1.85	854	1.95	809	2.60	856	2.51		
		855	0.99	827	1.27	844	1.41	824	1.67	861	1.73			834	2.36				

TABLE 2

Viscosity (η) for Compositions abng Section II $\left(\frac{NaCl}{KCl} = \frac{1}{6}\right)$ (centipoises)

$CaCl_2$ Content (wt. %)													
0		10		20		30		40		50		60	
°C	η	°C	η	°C	η	°C	η	°C	η	°C	η	°C	η
682	1.44	674	1.74	661	2.23	656	2.64	680	2.85	666	3.47	670	3.93
712	1.28	700	1.59	692	1.97	684	2.37	706	2.56	703	2.87	711	3.28
742	1.19	727	1.50	732	1.72	708	2.16	726	2.34	742	2.56	754	2.71
772	1.09	762	1.32	752	1.56	746	1.89	748	2.16	780	2.22	781	2.43
800	1.05	793	1.24	782	1.46	787	1.67	780	1.96	803	2.12	816	2.24
826	1.00	828	1.06	813	1.32	814	1.57	804	1.84	861	1.78	846	2.06
857	0.88			846	1.25	824	1.39	824	1.72				
								843	1.63				

TABLE 3

Viscosity (η) for Compositions along Section III $\left(\frac{NaCl}{KCl} = \frac{1}{3}\right)$ (centipoises)

$CaCl_2$ Content (wt. %)																	
0		10		20		30		40		50		60		70		80	
°C	η	°C	η	°C	η	°C	η	°C	η	°C	η	°C	η	°C	η	°C	η
660	1.46	666	1.87	667	2.17	660	2.64	680	2.79	666	3.44	689	3.47	683	4.03	720	3.84
690	1.41	710	1.55	690	1.96	708	2.11	710	2.41	717	2.67	720	3.09	700	3.55	753	3.45
730	1.20	752	1.35	718	1.80	745	1.88	744	2.17	764	2.29	748	2.79	731	3.31	786	3.00
761	1.12	816	1.14	748	1.64	792	1.60	777	1.90	804	2.04	779	2.44	754	2.96	810	2.71
796	1.06	849	1.06	784	1.42	816	1.50	809	1.72	827	1.85	813	2.13	778	2.62	824	2.55
822	0.98			820	1.27	857	1.32	833	1.60	852	1.71	849	1.99	822	2.32	845	2.46
852	0.93			856	1.16			855	1.49					844	2.18		

TABLE 4

Viscosity (η) for Compositions along Section IV $\left(\frac{NaCl}{KCl} = \frac{1}{1}\right)$ (centipoises)

$CaCl_2$ Content (wt. %)															
0		10		20		30		40		50		60		70	
°C	η	°C	η	°C	η	°C	η	°C	η	°C	η	°C	η	°C	η
688	1.38	668	1.83	666	2.06	680	2.31	686	2.57	640	3.47	630	4.37	664	4.35
713	1.30	689	1.62	693	1.95	692	2.23	716	2.30	670	3.05	668	3.61	687	3.92
759	1.17	712	1.54	730	1.73	724	1.99	745	2.01	710	2.67	696	3.08	726	3.25
786	1.08	751	1.37	774	1.45	752	1.77	779	1.88	747	2.42	736	2.76	766	2.84
822	0.99	758	1.35	849	1.17	796	1.57	810	1.75	780	2.19	776	2.56	789	2.66
856	0.90	792	1.22			838	1.36	834	1.58	814	1.96	804	2.27	812	2.40
		826	1.14					856	1.52	840	1.76	838	2.02	834	2.28
														855	2.200

APP. 18-Pg 4

TABLE 5

Viscosity (η) for Compositions along Section V $\left(\frac{NaCl}{KCl} = \frac{3}{1}\right)$ (centipoises)

$CaCl_2$ Content (wt. %)																	
0		10		20		30		40		50		60		70		80	
°C	η	°C	η	°C	η	°C	η	°C	η	°C	η	°C	η	°C	η	°C	η
728	1.28	708	1.61	691	1.81	679	2.21	675	2.53	691	2.85	656	3.73	671	4.21	698	4.44
754	1.17	730	1.47	725	1.65	716	1.87	699	2.37	730	2.45	668	3.43	686	3.84	722	3.76
773	1.11	777	1.26	750	1.56	748	1.81	722	2.22	750	2.33	703	3.20	722	3.24	755	3.28
799	1.06	808	1.18	769	1.50	779	1.60	752	1.97	790	1.99	743	2.71	754	2.93	790	2.83
816	1.02			808	1.35	793	1.53	778	1.80	838	1.74	776	2.50	780	2.67	832	2.52
826	1.00							802	1.67			815	2.12	800	2.49	866	2.23
852	0.94							823	1.61			850	1.87	847	2.10		

TABLE 6

Viscosity (η) for Compositions along Section VI $\left(\frac{NaCl}{KCl} = \frac{6}{1}\right)$ (centipoises)

$CaCl_2$ Content (wt. %)															
0		10		20		30		40		50		60		70	
°C	η	°C	η	°C	η	°C	η	°C	η	°C	η	°C	η	°C	η
752	1.18	739	1.42	702	1.81	672	2.21	680	2.53	656	3.26	640	4.09	678	4.25
780	1.11	764	1.31	725	1.69	724	1.94	706	2.30	680	2.98	680	3.37	707	3.61
800	1.08	784	1.25	758	1.48	758	1.71	732	2.05	704	2.56	702	3.04	716	3.39
815	1.03	796	1.23	788	1.35	797	1.51	752	1.94	740	2.31	734	2.75	745	3.00
835	0.99	819	1.19	816	1.31	807	1.48	777	1.77	776	2.08	760	2.47	775	2.65
848	0.95	840	1.09					800	1.69	802	1.96	790	2.23	805	2.46
								824	1.57	840	1.77	818	2.13	832	2.25
								844	1.48			833	2.05	847	2.14

TABLE 7

Viscosity (η) for Compositions along Section VII (KCl = 0) (centipoises).

$CaCl_2$ Content (wt. %)																	
0		10		20		30		40		50		60		70		80	
°C	η	°C	η	°C	η	°C	η	°C	η	°C	η	°C	η	°C	η	°C	η
788	1.13	758	1.34	724	1.69	693	2.09	664	2.67	665	3.02	670	3.33	647	4.26	697	3.88
807	1.04	777	1.26	744	1.59	720	1.91	686	2.42	686	2.76	684	3.20	691	3.59	734	3.42
822	0.98	802	1.18	766	1.49	743	1.75	716	2.20	731	[illegible]	720	2.91	722	3.25	775	2.97
843	0.94	820	1.13	784	1.41	766	1.63	747	1.98	[illegible]	2.09	754	2.53	751	2.87	829	2.58
850	0.93	840	1.05	800	1.35	787	1.52	778	1.77	801	1.85	788	2.29	801	2.53		
865	0.89	861	0.98	840	1.20	811	1.44	802	1.65	836	1.73	811	2.20	830	2.37		
				863	1.17	838	1.35	824	1.55	859	1.62	846	1.98	847	2.26		
						858	1.31	846	1.46								

The method described is suitable for the condition where the solid of revolution vibrates so slowly that turbulent motion is not produced in the liquid.

The Kulon method was developed in detail and improved by Dantuma [1] for measuring the viscosity of fused NaCl.

Karpachev and Stromberg [2] used this method for measuring viscosity in the NaCl-KCl system.

Berenblit [3] studied viscosity in the fused $MgCl_2$-KCl-NaCl System by the same method.

Results of Measurement

The arrangement of our equipment is shown in Fig. 1. The measurements were performed in a porcelain vessel with $\underline{D}$ = 55 mm and $\underline{h}$ = 105 mm. The diameter of the platinum ball was 25 mm.

The results of our measurements are given in Tables 1-7. Isotherms for all sections at 750°C are given in Fig. 2.

It can be seen from Fig. 2, that the viscosity of the quatenary electrolyte studied by us is not an additive function of composition. Electrolyte viscosity sharply increases with increased $CaCl_2$ concentration.

The effect of KCl and NaCl concentrations on viscosity of the electrolytes studied is readily seen in Figs. 3 and 4, on which the viscosity isotherms for all sections at 750°C are compared. Triangular concentration diagrams with lines of constant viscosity are given in Figs. 5 and 6.

It can be seen from Fig. 2 that when calcium chloride is present in the electrolyte, the viscosity increases with increase in the NaCl content in the $MgCl_2$-KCl-NaCl ternary system. In the $MgCl_2$-$CaCl_2$-KCl-NaCl quatenary system with $CaCl_2$ concentration greater than 10 wt. %, the nature of the effect of KCl and NaCl on viscosity changes; in this, the system viscosity increases with increased KCl concentration.

The shape of the viscosity isotherms confirms the fact that the compound $KCl \cdot CaCl_2$ is formed, which leads to increase in the electrolyte viscosity.

LITERATURE CITED

[1] Dantuma, Z. allg. Chem., 1, 175 (1928).

[2] S. Karpachev and A. Stromberg, J. Gen. Chem., 5, 625 (1935).

[3] V. Berenbilt, Trans. All Union Research Institute for Aluminum, Magnesium, No. 14 (1937).

Received October 9, 1953.

APPENDIX 19

"MAGNESIUM CAST IRON"

K. I. Vashchenko and L. Sofroni

State Scientific-Technical Press
of Machine-Construction Literature

Kiev 1957 Moscow

421 Pages.

412 Literature References, of which 184 are Russian.

Table of Contents

INTRODUCTION

Cast iron is one of the most widely used materials in the construction of machines. The weight of cast iron parts of the majority of machines forms 45-85% of the machine weight. Cast iron is used in almost all fields of the national economy. The cast iron castings which are used nowadays are quite complex: Their weight ranges from a few grams to 250 tons; the thickness of the castings varies from 2 to 500 mm. and up (Reference 1).

The widespread use of iron castings is explained by their low cost, good casting properties, and particular properties of the cast iron as a construction material (versatility, high resistance to wear, low sensitivity to concentration of stresses and resistance to vibration).

However, for a long time an important obstacle in the widening of the spread of cast iron parts were the low mechanical properties of the cast iron. This was contrary to the basic tendencies of modern machine construction, which is to lower the machine weight and, in particular, to lower the number of cast parts. The developments in machine construction require castings from alloys which are more stable and have a higher ductility than the regular sulphur-containing cast iron. The production of castings from steel and malleable cast iron is connected with a series of technological difficulties and is less economical than the production of castings from gray cast iron.

Steel as a casting material is not as good as cast iron because it has a high melting temperature, large degree of shrinkage, and low fluidity, and has a tendency to form porosity and internal stresses, which lead to the formation of hot and cold cracks and to liquation. Therefore, the production of formed steel castings is one of the most complicated problems in the castings technology. Castings of steel require a large amount of metal, the castings have to be annealed, cleaned, and there are many losses. All of these operations raise the cost of steel castings and prolong the production cycle.

Cast iron can be looked upon as steel which has graphite inclusions. As is known, the strength of graphite is very low, and, therefore, these graphitic inclusions can be regarded as cavities.

Therefore, the low mechanical properties of cast iron are mainly due to the presence of graphite flakes. Consequently, the casting and metallurgical technician was faced with the problem of increasing the strength of cast iron by lowering the influence of graphite. In principle, the strength of cast iron was increased by changing the shapes, sizes and the distribution of graphite inclusions in the base metal. For this purpose, superheating and holding the liquid cast iron at high temperatures for extended periods of time, the introduction of a large quantity of steel, modification, etc., were used. The application of all these methods allowed us to improve the mechanical properties of cast iron considerably.

There are numerous patents and methods in the literature for the production of cast iron with nodular graphite. Most typical of these are shown in Table 1, in which it can be seen that as modifiers a variety of additives can be used and the nodular shape of graphite can be obtained by treating the cast iron with such elements as magnesium, cerium, calcium, lithium, zinc, barium, potassium, sodium, selenium, tellurium, and thorium.

TABLE I

ADDITIVES AND METHODS OF CAST IRON TREATMENT

Additives and Methods of Cast Iron Treatment	Notes
Magnesium Additives	
Metallic magnesium added in .4 thru 1% (Ref. 8)	Violent reaction; absorption of Mg is not great; it is mostly used for casting of large sections; cast iron is considerably cooled down.
Scrap of magnesium alloys (Elektron) in the amount of .5-1.0% (Ref. 9)	Absorption not large; reaction violent; cast iron is considerably cooled down.
Alloys of magnesium with FeSi, with a higher content of magnesium (over 20%) (Ref. 10 and 11)	Lower absorption of magnesium by cast iron; violent reaction; pyrotechnics increase with increased magnesium content in the alloy.
Alloys of magnesium with FeSi, with a low magnesium content (from 5-15%) (Ref. 12-16)	Good absorption of magnesium by cast iron; quiet reaction.
Alloys:	
Mg Cu (from 15 to 50% Mg) (Ref 17) Mg Ni (from 20 to 50% Mg) (Ref 18-21) Mg-Ni-C (17% Mg, 81% Ni, 2% C) (Ref 22,23) Mg-Ni C (17% Mg, 10 47% Ni, 5% C, remaining Fe) (Ref 22,23)	Specific wt. 7.40) Heavy alloys " " 7.38) good absorption " " 7.45) of Mg
Mg-Cu-Ni-FeSi (33% Cu, 20% Mg, 13% Ni, 26% Si, remaimming Fe) (Ref 22)	Specific wt. 4.20; good absorption and quiet reaction.

TABLE I (CONTINUED)

Additives and Methods of Cast Iron Treatment	Notes
Alloys:	
Mg-Ca (Ref 25) Mg-SiCa (20% Mg) (Ref 26) Mg-Ca-Ni-FeSi (15% Mg, 15% Ca, 15% Ni, 45% Si, 10% Fe) (Ref 22) Mg-Cu-SiCa (12-20% Mg, 20% Cu, 60-68% SiCa) (Ref. 27) Mg-Si-Ca-FeSi (12% Mg, 38% SiCa, 50% FeSi) (Ref 27)	The addition of Ca together with Mg insures stable results; reaction is quiet; the modification of cast iron by FeSi is not necessary; reduction of cementite formation on the surface; minor pyrotechnics.
Mg-Mn-Si (25% Mg, 13% Mn, 55% Si) (Ref 27) Mg-Ca-Si-Al-Mn-Fe (30% Mg, 20% Ca, 39% Si, 2.5% Al, 0.5% Mn, 7% Fe) (Ref 24)	Mn from the alloy removes sulphur from the cast iron, partially replacing Mg.
Alloys:	
Mg-Li (Ref 28, 55)	Reaction is quiet; the ratio of Li to Mg equals 1:30 up to 1:3.
Finer-sized mixture of Mg and Zr (10-30% Mg, 5-45% Fe, 10 30% Zr, 1-45% Si) (Ref. 62)	The quantity of the introduced mixture is calculated from the remaining Mg content in the cast iron which is in the range of 0.01 to 0.1%, Zr from 0.03 to 0.3%.
Mg-Bi (Ref 28,29) Mg-Al (15% Mg) (Ref 17) Mg-Cu-Al (15% Mg) (Ref 17) Mg (2-20%), Ca, Ba, Sr, Li (2-15%, each one or the sum of it) Si (5-50%), Cu (3-50%), Fe (5-65%) (Ref 29)	Alloys of Mg and Cu and Al are not recommended because Cu (more than 3%) and Al (more than 0.3%) have an antimodifying effect.
Mg together with Ce (Ref. 30, 31, 32, 33)	Mg and Ce have a combined effect; modification results are stable; the detrimental effect of elements with anti-modifying effects is neutralized; spherical graphite is formed at 0.005% Mg and at 0.001% Ce.
Mixture of 10% magnesium chips and 90% reduced in size ferrosilicon (Ref 12, 13)	High absorption of magnesium by cast iron; quiet reaction.

TABLE I (CONTINUED)

Additives and Methods of Cast Iron Treatment	Notes
Mixture of calcium cyanamid and the alloy of (10% Mg) and Ni, Cu, and Si. Weight ratio of calcium cyanamid and the alloy is 0.5:1 or 6:1 (Ref 35)	Calcium removes the sulphur from the cast iron and replaces magnesium partially.
Mixture of Mg and MgO (3-10% Mg) with liquid glass (Ref 34)	Quiet reaction; natural MgO can be used.
Briquettes made from 34% Mg, 33% cast iron chips and 33% FeSi (which itself is 75%) (Ref 36, 37)	Compressed at pressures of 40 tons, the briquette diameter is 40 mm.; its height is 120 mm. (Ural-Zis).
Briquettes made from Mg, Si, and MgO (1:4:0.6 and 1.3) (Ref 38) Briquettes made from Mg, Si and graphite (?) (1:4:1) (Ref 39) Briquettes made from Mg, Si, and CaC_2 (1:4:0.6 and 2.5) (Ref 39) Briquettes made from Mg powder (Ref 39)	Reaction quiet; small magnesium losses; absorb magnesium up to 80%.
Melting under a layer of MgO or dolomite (2 MgO. CaO) (Ref 30)	At high temperatures (1700 deg.) Mg and Ca are introduced in the cast iron during the melting.
Gaseous magnesium alone or together with an inert gas (Ref 40)	Introduced through a tube into the ladle or into the furnace.
Magnesium powder together with an inert gas such as nitrogen or argon (Ref 41)	Introduced into the ladle by means of feeders; good absorption of magnesium.
<u>Calcium Additives</u>	
Ca (Ref 42, 43) Ca together with Ce (Ref 22, 51) Ca-Cu (10% Ca) (Ref 42) Ca-Si (20-25% Ca) (Ref 42) Ca-Si (Ref 44)	Amount of Ca introduced is 0.125 to 0.650%; reaction is quiet; cast iron has to be hot. Is introduced in the amount of 3-5% as a powder into the ladle or into the mold.
CaC_2 (Ref 45, 46, 49) Nitride, Cyanamid and calcium hydride (Ref 49) CaF_2 (Ref 47)	Blow into the cast iron together with nitrogen and try to avoid the formation of CaO.

TABLE I (CONTINUED)

Additives and Methods of Cast Iron Treatment	Notes
MgO. CaO (fired dolomite) (Ref. 48) CaO (lime) (Ref 48)	Mg and Ca are introduced into the cast iron from the slag, from the lining, or from the flux cover.
Alloys: Ca-Si-Cu (24% Ca, 56% Si, 20% Cu) (Ref. 43) Ca-Si-Cu-Ni (20-26% Ca, 46-59% Si, 20% Cu, 14-5% Ni) (Ref 43) Ca-Si-Mg-Cu-Ni (10-35% Ca, 40-65% Si, 1-5% Mg, 0-50% Cu, 0-30% Ni) (Ref 43) Ca-Si-Li-Mg-Cu-Ni (20-22% Ca, 40-50% Si, 6-15% Li, 2-4% Mg, 12-20% Cu, 13-20% Ni) (Ref 43)	The addition of Ca together with Mg insures stable results.
1.5% SiCa; 2% CaF_2 0.5% Zr (as a mixture or separately) (Ref 50)	Calcium fluoride is added as a flux reagent; zirconium for the increased strength and obtaining of spherical graphite.
Other Additives	
Cerium alloys (mischmetal) 45-52% Ce, 45-48% rare earth (La, Pr, and ?) 0.5-4% Fe, up to 1.6% Mn, up to 3% Si, Cu, Al (Ref 51)	Is usually applied for modification of hyper-eutectic cast irons.
Metallic Bi (Ref 52)	Is added to the ladle in the amount of 0.2-0.3%.
Te, B (Ref 22)	Reaction products of TeS, TeO and BS are difficult to remove from the cast iron.
K, Na (Ref 22, 53)	Violent reaction; absorption very low; sodium vapors are toxic; alloys based on K and Na are difficult to make.
Li (Ref 54,55)	Spherical graphite is obtained if Li from 0.005 to 0.1%. Sulphur content has to be higher than 0.08%.

TABLE I (CONTINUED)

Additives and Methods of Cast Iron Treatment	Notes
Zn (Ref 56)	Mn content in the cast iron should be less than 0.1%, carbon less than 2.6%; under these conditions spherical graphite is obtained at 0.44% sulphur.
Blowing of gases through cast iron such as: Argon, chlorine, nitrogen and hydrogen (Ref 56, 57)	Spherical graphite is obtained only in part.
Superheating of cast iron in the furnace, melting under vacuum and high-speed of cooling (Ref 57)	Superheating at 1600-1700 deg.; vacuum 5.10^{-4} atmospheres; when casting the iron into the shell mold, the formation of spherical graphite can be observed.
Pre-Treatment of Cast Iron before the Introduction of Magnesium	
Preliminary removal of sulphur, Ca, Ce, or CaC_2 (Ref 58, 59)	The content of sulphur is lowered and less Mg and Ce is used. The amount of introduced Mg can be lowered down to 0.005%. The increase of the range of the composition of the charge as far as sulphur is concerned. Calcium carbide is introduced into the receiver of the cupola by means of a gas (N_2, CO_2, Ar, but not in air or O_2) through a graphite tube. For 1 kg. S, 10 kg. of CaC_2 are introduced.
Preliminary oxidation of cast iron by _____(forging ?) annealing. (Ref 60)	Absorption of Mg by cast iron is increased.
Blowing oxygen or air through cast iron (Ref 61)	Magnesium absorption is increased; the amount of non-metallics is decreased.

The name for this cast iron has not yet been defined in literature. It is called either "Cast Iron with Spherical Graphite", "High Strength Cast Iron", "Super Strong Cast Iron", "Cast Iron with Nodular Graphite", "Cast Iron with Plastic Properties", "Malleable Cast Iron with Spherical Graphite in the Cast Structure", "Ductile Cast Iron", "Magnesium

Cast Iron", "Cast Iron Treated with Magnesium", "Cast Iron Modified by Magnesium", etc.

In order to differentiate between the lamellar form of graphite in the regular gray cast iron and the flake graphite in malleable cast iron, the graphite in cast iron treated with magnesium is called "globular", "round","spheroidal", "spherical", "granular", etc.

According to GOST 7293-54, in castings made from high strength cast iron the graphite is called "spherical" and the cast iron is called "high strength". However, the term "high strength cast iron" is too general and can refer to different cast irons; therefore, in the present work the term "magnesium cast iron" and the term "spherical graphite" are used as the shortest and because they most completely reflect the technology of the product of cast iron and the shape of the graphite.

The mechanical properties of the magnesium cast iron, due to the spherical form of graphite, differ very much from the starting gray cast iron. In Table 2 the properties of cast steel, and magnesium, gray and malleable iron are shown. From this table it can be seen that the range of tensile strength of magnesium cast iron is close to that of carbon steel (70-80% of the steel strength) and is considerably higher than the strength of the gray and the malleable cast irons. The ductility or plasticity of magnesium cast iron is much higher (5-15 times) than the plasticity of the gray iron and is close to that of steel and malleable cast iron. Impact toughness of magnesium cast iron is higher than that of gray and malleable cast iron, but is lower than that of steel, but as we are going to see in the following, it depends to a higher degree on the chemical composition and the conditions of the cast iron cooling, in particular on the phosphorus content. As to the casting properties of magnesium cast iron (Table 3), they represent a peculiar combination of properties of regular gray cast iron (good fluidity, small linear shrinkage, no tendency for the formation of hot cracks), properties of steel (the tendency to form shrink cavities) and the properties of the white cast iron (tendency to form cold cracks).

TABLE 2

Properties	Steel Castings GOST 977-53	Gray Cast Iron GOST 1412-48	Malleable Cast Iron GOST 1215-41	Magnesium Cast Iron GOST 7293-54
Limit of Tensile Strength in kg./mm.^{2}	40-60	12-38	30-40	40-60
Elongation in % ...	10-28	(to 0.5)	3-12 (to 20%)	1.5-10 (to 20%)
Limit of Bending in kg./mm.^{2}	-	28-60	-	(70-110)
Amount of Deflection at Fracture in mm. ..				(3.5-30)

TABLE 2 (CONTINUED)

Properties	Steel Castings GOST 977-53	Gray Cast Iron GOST 1412-48	Malleable Cast Iron GOST 1215-41	Magnesium Cast Iron GOST 7293-54
Impact Toughness in kgm/cm.^{2}	2.5-5	(to 0.5)	0.5-3.0	1.5-3.0 (to 10)
Brinell Hardness ..	-	143-262	149-201	156-269

TABLE 3

Properties	Steel	Gray Cast Iron	Malleable Cast Iron	Magnesium Cast Iron
Linear Shrinkage in %	2.0-2.2	0.8-1.2	1.5-2.2	0.8-1.4
Tendency to Form Shrinkage Cavities	Large	Small	Large	Large
Tendency to Form Stresses	"	"	"	"
Liquid Fluidity	Satis.	Good	Satis.	Good

From the economic point of view, the use of magnesium cast iron is very satisfactory. If the basic cost of the regular cast iron casting is considered to be 100%, then the corresponding basic cost of magnesium cast iron castings equals 130% and of steel castings 160% (Reference 63).

Thus, the high mechanical properties and the good casting properties of magnesium cast iron, the lower cost and the possibility of producing it by way of the regular casting process make it possible to consider it as a new construction material. From this cast iron, in many cases, products can be cast which have a great industrial and economic effect which usually are made from steel, malleable cast iron, bronze, or other nonferrous metals. The use of magnesium cast iron makes it possible to reduce the weight of iron castings and increases their service properties and strength.

The widening of the range is noticeable at the present time in the use of magnesium cast iron in various branches of machine construction such as Diesel construction, compressor construction, ships, auto and tractor construction, etc. Rolling mill rolls made from magnesium cast iron have 2-3 times greater strength than those made from lamellar graphite. Magnesium

cast iron can be used advantageously in several fields as a heat and corrosion resistant material. Great possibilities are open for magnesium alloy cast iron of the austenitic type, "Nirezist", which have high mechanical properties and are resistant to heat and corrosion (Reference 64, 65).

In spite of this and all of the advantages of magnesium cast iron, there has been only limited application in the foundries of the USSR as well as abroad. For instance, in the United States the production of castings from magnesium cast iron in 1951 was only as high as 100,000 tons per year, which is only 0.77% of the gray cast iron output and 11% of the malleable cast iron production (Reference 66); however, at the present time the production of magnesium cast iron castings is increasing rapidly and in 1955 magnesium cast iron was produced in 334 foundries in various countries (Reference 412). This can be explained by the lack of systematic data on properties, production and application fields for magnesium cast iron, as well as by some particularities of the process for its production and casting which remain either unclear or unfinished. The following problems are still open:

(a) The method of introducing magnesium, as well as the introduction of other additives and, in connection with this, the determination of the amount of these additives which would be sufficient to obtain stable results;

(b) Chemical composition of the cast iron and, in particular, the influence of the alloying additives on the structure, mechanical and other properties of magnesium cast iron;

(c) Mechanism of structure formation and occurrences during the modification;

(d) Investigation of other additives besides magnesium which favor the production of spherical graphite;

(e) Studying the mechanical, physical and casting properties of this cast iron from all viewpoints;

(f) Study service of the castings at normal conditions of use;

(g) Improvement of the technology of good quality castings from magnesium cast iron;

(h) Rationalization and economic conditions of the thermal treatment and other treatments.

There are many publications on the theory and the practice of casting production from magnesium cast iron in the USSR as well as abroad.

For further development and improvement of the production of castings, of great importance will be the general and scientific analysis of the experimental and theoretical material collected.

The scope of the present publication is to give a generalization and a systemization of the basic parts in the composition, the properties, the production and the fields of application of the castings based on our own investigations as well as on the literature.

The authors hope that their modest work will contribute to wider introduction in industry of this new construction material.

The authors will be happy for some notes or corrections. Please address to: Kiev_____.

CHAPTER XI

THE FIELDS OF APPLICATION AND THE RESULTS OF THE EXPLOITATION OF MAGNESIUM CAST IRON CASTINGS

Magnesium cast iron possesses high mechanical properties, for which reason castings made from it will be stronger and more durable than the castings made from gray cast iron, or they can have a smaller wall thickness than the castings made from gray cast iron. In other words, the use of magnesium cast iron in place of the gray form is one of the decisive ways to reduce the weight of cast articles and increase their length of service.

Magnesium cast iron on a ferrite base also possesses high plastic properties, which are absent for the ordinary gray and modified cast irons. Nearly all of the exploitation properties of magnesium cast iron are considerably higher than for the gray and modified cast irons. The alloying of magnesium cast iron leads to obtaining new types of cast irons, possessing high service properties, which substantially exceed the properties of the alloyed gray and modified cast irons.

When compared with wrought iron, ferritic magnesium cast iron, with similar values for the elongation and toughness, shows higher strength properties and especially the elastic limit. In addition, the dimensions of the castings from magnesium cast iron and their thickness do not possess the limitations inherent to wrought cast iron.

Magnesium cast iron, having nearly the same strength as cast steel, shows better casting properties, which facilitates obtaining sound castings. Together with this, magnesium cast iron retains the good service properties inherent to gray cast iron (high abrasion resistance, high cyclic tenacity, low sensitivity to the influence of stress concentrations, good workability, etc.).

Magnesium cast iron can be used to cast a series of complicated articles (crankshafts, cam shafts, etc.) instead of their being forged or stamped out.

It should be mentioned again that in recent years the criteria used to evaluate the strength of cast irons and steels have been changed. In order to correctly evaluate the durability it is necessary to take local stress concentrations into consideration. Practice shows that the failure of parts during operation bears in most cases a fatigue character and is associated to less degree with elongation. Consequently, a small elongation for cast iron, when compared to steel, in most cases is not a disadvantage. For this reason machine builders should turn their attention mainly to the resistance offered by the fatigue limit to factors that reduce its value, producing local stress concentrations. In this respect magnesium cast iron differs but slightly from wrought steel.

Some orienting data are given in Table 112 on the cost of articles made from cast iron and steel prior to mechanical treatment, relating to plants building medium machines and to those with assembly line production (the cost of a ton of cast iron articles from gray iron is taken as 100%). The cost of casting, heat treatment and supplementary equipment enters into the cost of the castings made from magnesium cast iron. From Table 112 it can be seen that magnesium cast iron is cheaper than either wrought iron or steel.

TABLE 112

Metal Article	Cost of the article in %
Cast from gray cast iron	100
Cast from modified gray cast iron	110
Cast from magnesium cast iron	130
Steel forgings	185
Wrought iron	226
Steel casting	252

According to the data of the Syzran hydroturbine plant (Russian Ref., 1955), the manufacturing cost of a ton of cast iron castings, prepared from magnesium cast iron, is approximately 2.5 times cheaper than the cost of a ton of steel castings of the same degree of complexity, while according to the orienting data of the Novo-Kramatorsk machine-construction plant it is cheaper by only 25% (Russian Ref., 1955). The cost of manufacturing castings from magnesium cast iron depends to a considerable degree on the scale of production. It is quite obvious that after becoming familiar with the technology of preparing castings from magnesium cast iron the cost of their manufacture will be only slightly above the cost of manufacturing the castings from gray iron.

A comparison of the mechanical, casting and exploitation properties of cast irons and steel permits explaining the exceedingly great interest shown in cast iron containing spherical graphite and visualizing the broad perspectives for its use in machine construction.

We will present some examples of the practical application of magnesium cast iron, proceeding from those requirements as apply to the conditions for the exploitation of various parts.

Crankshafts. In recent years magnesium cast iron has been used to replace wrought steel in the manufacture of crankshafts for stationary ship, automobile and tractor engines and compressors.

Crankshafts can be fabricated either by casting, hot stamping or forging. For technical reasons, the stamping of fabricates is possible only for comparatively small shafts and is practical only for the mass production of the same type of shafts. Of these methods for the fabrication of crankshafts that of casting shows an advantage, since here there is a substantial reduction in the amount of metal loss and in the time of subsequent mechanical treatment. In addition, the employment of special and general equipment for the mechanical treatment of the shafts is reduced, the output of the forge press equipment is set free, the need for cooperation of the plants without forge press equipment is eliminated, etc.

Cast iron is the material usually used for cast shafts, since their casting from steel, due to the much poorer casting properties of the latter, requires extremely complex technology.

Gray cast iron, due to its low mechanical properties and associated inadequate reliability during operation, has failed to find extensive use in the casting of crankshafts. From literature data it is known (Russian Ref., 1953; Russian Ref., 1954; French Ref., 1951; and German Ref., 1955) that the casting of crankshafts from magnesium cast iron is both most progressive and expedient.

To obtain the least amount of wear during use a magnesium cast iron with a pearlitic structure (VH 60-2) is usually used for the casting of crankshafts.

Some comparative technical-economic data are given in Table 113 on the production of forged shafts from 30 XM steel and of shafts from magnesium cast iron for diesels, relating to the tested portions of the castings (Russian Ref., 1953).

TABLE 113

Designation	Forged Steel Shaft	Cast Cast-Iron Shaft
Weight of ingot in tons	12	--
Weight of blank in tons	6.3	2.7
Pure weight in tons	1.9	1.7
Work load in norm-hours	1495	694
Included in this:		
Preparation of the blanks	439	480
Heat treatment	15	6
Mechanical treatment	1050	208
Length of the fabrication cycle in days	60	20

It should be mentioned that in the transition to serial production both the work load and the cost of the cast shaft from magnesium cast iron will be reduced by 25-30%. In addition to effecting a three- to four-fold reduction in the cost, the replacement of wrought steel by magnesium cast iron in the fabrication of crankshafts permits replacing the molybdenum steel alloy by a cheaper and more abundant material (with a simultaneous saving of more than 4 tons of metal), results in a smaller load through the special annealing machines for mechanical treatment (approximately a 5-fold decrease), etc.

As had already been mentioned (see p. 357), a three-year testing of magnesium cast iron crankshafts for D-54 engines, operating on tractors in the MTS, revealed that the average wear of the shaft journals made from magnesium cast iron was one-half that shown by steel journals, while the average total wear of the shaft journals and bushings was 35-40% less than that shown by the steel shafts.

For crankshafts, operating at high speeds, the fatigue endurance is of extreme importance. Actual tests made on shafts (Russian Ref., 1954) with alternate symmetrical flexing reveal that the fatigue endurance of shafts, cast from magnesium cast iron, and the fatigue endurance of shafts, fabricated from steel 45, are practically the same and approximately twice as great as that of shafts fabricated from gray cast iron CH 21-40.

According to the data of Kudryavtseva (Russian Ref., 1954), the fatigue cracks in magnesium cast iron spread from one graphite inclusion to another, and chiefly permeate the graphite inclusions having the least roundness and substantial size. Consequently, in fabricating shafts from magnesium cast iron much attention should be given to the structure of the metal base and the form of the graphite.

Gamma rays are used to control the casting density, while control of the mechanical properties is run on the cast specimens.

As a result, from the presented data it can be seen that magnesium cast iron is a very valuable substitute for wrought steel in the fabrication of crankshafts.

Articles of the Piston Group. Magnesium cast iron is successfully used for the fabrication of such parts as the crankgear and gas distribution mechanism of engines, connecting rods, connecting rod covers, crossheads, pistons, piston rings, sleeves, camshafts, plunger, etc. These articles are usually fabricated from pearlitic magnesium cast iron and are cast in dry molds. The transition in the fabrication of this group of parts to their casting from magnesium cast iron is accompanied by a substantial reduction in the amount of work required for their fabrication and leads to a saving in the consumption of rolled steel and nonferrous alloys (Russian Ref., 1953).

The piston is one of the important parts of the connecting rod-piston group that is exposed to wear, corrosion, action of high temperatures, etc. The pistons of the YAZ-204 engine, fabricated from pearlitic gray iron, have a short life span (on the average a mileage of 15-30 thousand kilometers) due to the appearance of cracks, scorching of the bottoms, and also wear of the piston grooves (Russian Ref., 1953). When these pistons are fabricated from magnesium cast iron with a pearlitic ferrite structure for the base metal their length of service is sharply increased. Most of the tested pistons looked well after being run 65 thousand kilometers: The pistons failed to show cracks, scorching of the bottoms or wear of the piston grooves. In addition, the piston pin operated without bronze bushings on the cast iron, and showed less wear (0.03 mm.) than is customary for a bronze bushing in the upper head of the pitman (0.11 mm.).

Pistons, cast from magnesium cast iron, are long-lived, and their service life is three to four times that of pistons fabricated from wrought iron with a granular pearlite.

As regards piston rings, fabricated from magnesium cast iron, then, as had already been mentioned (see Figure 240), their wear, as tested in the performance of automobile engines GAZ-AA and ZIS-5 (Russian), is considerably less than that shown by rings made from gray and alloyed cast irons.

The installation of a top compression ring from magnesium cast iron on the piston of diesel engine YAZ-204 assured reliable performance of the diesel engine during operation, which could not be obtained with rings fabricated from alloyed gray cast iron.

The wear resistance and reliability of operation of camshafts and plungers, fabricated from modified gray cast iron, and even more so when fabricated from magnesium cast iron, is considerably greater than that shown by the same parts when fabricated from steel (Russian Ref., 1955). And here also magnesium cast iron proves to be a complete substitute for steel with a substantial economic advantage.

Tractor and Automobile Parts. Magnesium cast iron is also successfully used in the fabrication of other tractor and automobile parts: Differential crankcase, front and rear wheel hubs, brake shoes, brake system supports, spring supports, rear transmission housing, armature, jack parts (American, 1952), etc.

According to the data of Gosteva and others (Russian Ref., 1951), the casings for the divided axles of tractors U-1 and U-2, tested under conditions more drastic than the usual field conditions, showed adequate strength and reliability.

The sockets of tractor cross arms are also fabricated from magnesium cast iron, replacing Bronze OCS 5-5-5 (Russian Ref., 1951). As is known, the cross arm sockets operate under conditions of inadequate lubrication and abrasive wear. The results obtained in the testing

of cross arm sockets under exploitation conditions on DT-54 tractors for two seasons of field operation reveal that the wear of sockets made from magnesium cast iron is approximately 30-40% less than the wear shown by serial sockets, fabricated from bronze Br. OCS 5-5-5.

Bearing Separators. As the data of Belkova and Kaminarskii show (Russian Ref., 1955), magnesium cast iron can be recommended as a substitute for brass LS 54-1 in the fabrication of massive separators for roller bearings.

The roller bearing separators, cast from magnesium cast iron by the centrifugal method and heat treated on ferrite and pearlite (20% sorbitic pearlite), were tested under the conditions operating in medium sized section mills and in the machine assemblies used in the coal, lumber and machinery construction industries. All of the bearings with cast iron separators operated satisfactorily, and destruction of the separators and escape of the bearings from the machine assembly was not observed.

Metallurgical Equipment Parts. Magnesium cast iron is successfully used for the fabrication of many metallurgical equipment parts: Rollers, roller conveyor and rolling mill frames, casting molds, gear casings of rolling mills, hammer presses, anvils, frames, boxes, wheels of casting machines, etc. (French Ref., 1951 and German Ref., 1955).

According to the data of Ezerskii (Russian Ref., 1954), Balle (American Ref., 1955) and others (Japanese), the durability of rollers, cast from magnesium cast iron, exceeds the durability of ordinary rollers by 2.5-3 times.

Magnesium cast iron is also successfully used for the rollers of blooming mills in the production of rails, and also in the mills for the production of sheet steel (American Ref., 1955).

As Pisarenko indicates (Russian Ref., 1955), for the production of molds with a wall thickness of 100-150 mm. the composition of the cast iron after its treatment with magnesium is taken as the following: 3.1-3.6% C; 2.2-2.8% Si; 0.3-0.9% Mn; 0.1-0.18% P and up to 0.02% S. To remove the internal casting stresses and impart plastic properties to the cast iron the molds are subjected to graphitization annealing (heating to 910-930° at a rate not exceeding 150° per hour, holding at this temperature for 6-10 hours, cooling to 650° at a rate not exceeding 25° per hour, and further cooling with the furnace).

The average durability of molds made from magnesium cast iron for small and medium sized ingots as 2-2.5 times greater than the durability of molds made from ordinary gray cast iron. The introduction of magnesium cast iron into the production of molds made it possible to reduce their consumption from 12-14 to 5-6 kg. per ton of steel. The use of magnesium cast iron for molds also made it possible to cast them in metal molds, which led to a simplification in the fabrication technology and to a substantial improvement in the mechanical properties when compared to casting in sand molds. It should be

mentioned that attempts to use metal molds for the casting of molds from ordinary gray cast iron have been unsuccessful. The high durability possessed by molds cast from magnesium cast iron is also indicated by other investigators (American Ref., 1951 and American Ref., 1951).

Machine Construction Parts. Mounts, carriages, drums, the casing of hydraulic pumps, gears, shafts, chucks and other parts, cast from magnesium cast iron, have recommended themselves well in use (Polish Ref., 1953).

Agricultural Machinery Parts. Rollers of harvesting machines, conical and cylindrical gear wheels and gears of various sizes with cast teeth, sprocket wheels, plowshares, harrow teeth, harrow disks and other parts can be successfully fabricated from magnesium cast iron instead of steel (Japanese Ref., 1953).

As Nikolaenko indicates (Russian Ref., 1954), plowshares that had been cast from magnesium cast iron are in no way inferior in use to plowshares that had been fabricated from steel L65 and L53. The plowshares are chill-cast, after which they are subjected to graphitizing normalization. To temper the cutting edges the plowshares are heated in a salt bath of 920 and 950° and then quenched in water. The annealing temperature is 240-280°. That plowshares made from magnesium cast iron possess good durability is also indicated by other investigators (French Ref., 1953).

"Zigzag" harrow teeth, cast from magnesium cast iron instead of being forged from rolled structural steel, when tested under field conditions, showed a durability that was on a par with that shown by steel teeth.

Harrow disks, cast from magnesium cast iron, can also be successfully used instead of stamped steel disks. Magnesium cast iron can also be used in the fabrication of cultivator blades, levers and frames for the tractors, etc. (French Ref., 1953).

Use of Magnesium Cast Iron in Other Branches of Machinery Construction. Magnesium cast iron can be successfully used in the fabrication of various equipment parts in the petroleum industry (parts of drilling machines, valves and fittings of cracking installations, etc.); in the fabrication of parts for hoisting and moving equipment (the wheels of overhead cranes and cars, pulleys, flywheels, drums, etc.); locomotive parts (valve sleeves, parts for the steam-distribution assembly, etc.); parts for steam turbines (diaphragms, condensate drains, separator valve boxes, rotors, etc.); parts for compressors and pumps (housing for compressors and pumps, propellers, etc.); parts for hydroelectric turbines (vanes, controls and regulating links of the distributor, etc.); pile-driver heads; vises, anvils, etc. (American Ref., 1955 and French Ref., 1953).

The condensate drains for steam turbines, fabricated from magnesium cast iron instead of the earlier used L30 steel, consist of a float chamber and cantilever, have a rough weight of 450 kg., a shell

thickness of 20 mm, are tested for a pressure of 28 kg./sq. cm., operate in a hot medium under a pressure of 16 kg./sq. cm., and fully justify themselves in use.

The hydroelectric turbine vanes consist of a streamlined portion (fins), cast as one piece with the top and bottom trunnions, the overall length of the vanes is about 3 meters, the weight is about 1.8 tons, the greatest thickness in the trunnions is 240 mm., and the wall thickness of the fins is 40 mm. One hydroelectric turbine requires 24 such vanes with a total weight of 43.2 tons. During operation the vane is loaded by hydrostatic pressure and the power transmitted from the servomotor (relay) through the distributor winding mechanism. Vanes, fabricated from magnesium cast iron, have been installed as replacements in several of the water turbines in one of the hydroelectric stations (Russian Ref., 1955).

Pile-driver hammers, manufactured from magnesium cast iron and weighing 1.8 and 3 tons, after two years of operation, with the hammer falling a distance of 16 meters, fail to show even a single crack or chip (Russian Ref., 1955).

Anchors for river vessels, cast from magnesium cast iron instead of being fabricated from wrought steel, showed excellent results when tested for dropping a distance of 8 meters.

Magnesium cast iron is successfully used in the fabrication of parts that operate under high temperature conditions and in corrosive media.

According to the data of Girshovicha and others (Russian Ref., 1954), armature parts, cast from magnesium cast iron (flange ventilators), are extremely close to cast carbon steel in their properties. Consequently, magnesium cast iron with a ferritic base is fully suitable for armatures, operating at temperatures up to 425° and pressures up to 40 kg./sq. cm.

Parts made from cast iron with a ferrito-pearlitic or pearlitic base are completely graphitized with an increase in volume when heated for extremely long periods of time, and consequently rapidly escape from the assembly. Thus, the valve seats in a tractor head, operating at a temperature of up to 350-450° and fabricated from pearlitic magnesium cast iron, escaped from the system after 100 hours of engine operation.

Since magnesium cast iron operates better than steel in various corrosive media, and has a high strength and plasticity, it is used to fabricate pipes for sewer systems, the transfer of petroleum, etc. (American Ref., 1955; Indian Ref., 1953). The pipes are cast by the centrifugal method. The pressure in pipes made from magnesium cast iron can be increased two-fold when compared with pipes made from ordinary gray cast iron.

As had already been indicated, the austenitic class of magnesium cast iron alloys possesses wide utilization perspectives for the manufacture of parts that operate at high temperatures and in corrosive media.

Magnesium cast iron can be successfully chill-cast, which makes it possible to expand the nomenclature for the parts that lend themselves to serial production. In chill-casting the outer zones and even the whole cross-section of the casting are obtained with a white color; by means of graphitizing annealing and subsequent heat treatment it is possible to obtain any desired structure, and consequently, the desired mechanical properties. Chill-cast parts, operating under rubbing conditions (bearing separators, sockets, etc.), showed better antifriction properties than did the corresponding parts when cast in sand molds, due to the more homogeneous surface structure (Indian Ref., 1954).

It should be mentioned that at the present time magnesium cast iron is used to produce castings of different configuration, varying in thickness from 3 mm. to 1 meter, and weighing from several grams to tens of tons. The variety of parts, being transferred to castings of magnesium cast iron, is constantly expanding.

At the present time the production of castings from magnesium cast iron is utilized by many plants of individual and small serial manufacture. However, the question of this cast iron finding broad acceptance in the casting sections of massive manufacture, and foremost as a substitute for wrought iron and steel, is of greater importance.

From the presented data it can be seen that the broad introduction of magnesium cast iron in machinery construction, as a substitute for cast, wrought and rolled steel, and also for wrought iron and the nonferrous metals, can result in a substantial saving of metal and in a reduction of the work load and cost.

APPENDIX 20

"USE OF RADIOGRAPHIC METHOD IN INVESTIGATING

THE STRUCTURE OF MAGNESIUM ALLOYS"

By M. E. Drits, Z. A. Sviderskaya and E.S. Kadaner
Zavodskaya Laboratoriya (Industrial Laboratory, 1955, #7, 831-833.

"Application of the (contact auto-) radiographic method to the study of structural Mg alloys"

Usual metallographic etching methods are not useful in bringing out the segregation of an alloying element in the inter-dendritic interstices of magnesium alloys. However, if the intercrystalline distribution of Ca is being studied, radioactive Ca (Ca^{45}) may be used in conjunction with an autoradio-graphic technique. The radio-active Ca is used as an alloying material, and, if the macro-distribution is being studied, x-ray film is placed in contact with a polished surface of the cast alloy and exposed for several days. For a study of the micro-distribution, a highly polished surface is put in contact with a fine-grained nuclear emulsion and exposed 10-15 days. The resulting film is enlarged in the microscope and photographed by transmitted light.

Fig. 1 - Slices of a sand-cast billet containing varying percentages of Ca show changes in the distribution of Ca. The most uniform distribution is obtained with the concentration in the range of hundredths of a percent (1a). The dendritic growth of segregation of the Ca in the dendritic interstices is clearly shown as the Ca is raised to the level of tenths of a percent (1b). Segregation toward the center of the billet is shown as the Ca is raised to one or more percent (1c).

In a ternary alloy of Mg-Mn-Ca, etching shows very little (2b) of the Ca distribution. However, contact auto-radiography of a slice (2a) clearly shows the segregation. The cone of segregation is particularly interesting.

The effect of cooling conditions and Ca content can be shown by micro-contact autoradiography. The clearest dendrites are formed in the region of tenths of a percent Ca. (Fig. 3A - tenths of percent Ca. 3b - higher Ca content) In a Mg-Ca-Mn ternary, the Ca distribution varies with position in the casting. Fig. 4a shows a spot from the upper section of a casting and 4b from the lower section.

If a 4-component alloy is cast in a heated mold instead of a sand mold, different segregation patterns are present (6a,b). 6a is from the center and shows grains that have grown practically equiaxially from the liquid. These grains are fairly uniform in Ca distribution but are surrounded by material richer in Ca; but this Ca-rich material

is also non-uniformly distributed, as can be seen from the Fig. 6b taken at higher magnification.

Contact auto-radiography may also be used to study the effect of heat treatment on the Ca distribution. Fig. 7a shows the cast state, and Fig. 7b after heat treating 24 hours at 600C. The Ca is somewhat equalized by the heat treatment.

Figure Captions

Fig. 1 - Autoradiograph (macro) of a binary Mg-Ca alloy (X 3/4)

Fig. 2 - Autoradiograph (macro) of a ternary Mg-Mn-Ca alloy X 3/4

Fig. 3 - Micro-autoradiographs from a binary Mg-Ca alloy X9

Fig. 4 - Autoradiographs of different spots from a sand-cast ingot of a ternary Mg-Mn-Ca alloy X8

a - top
b - lower part

Fig. 5 - Micro-autoradiograph of a 4-component alloy

Fig. 6 - Micro-autoradiograph of the center of a special 4-component magnesium alloy

a - enlarged 25 times
b - enlarged 750 times

Fig. 7 - Micro-autoradiographs of magnesium alloys

a - as cast
b - heat treated 24 hours at 600C

Note: In the radiographs, the Ca is in the light regions for the macrographs, but is in the dark regions for the micro-graphs.

(For the micrographs, the surfaces of the alloys were protected from corrosion by coating with a 3% solution of Japan lacquer in amyl acetate.)

Appendix 20

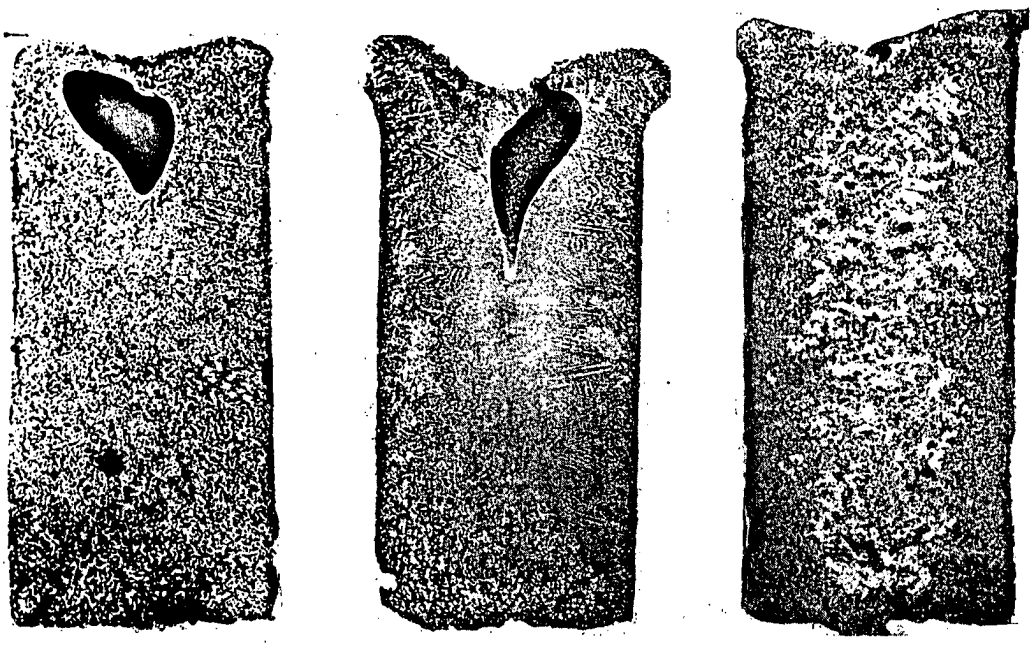

а *б* *в*

Рис. 1. Макрорадиограммы двойных сплавов Mg—Ca, ×⅝

а *б*

Рис. 2. Макроструктура слитка тройного сплава Mg—Mn—Ca; ×⅜

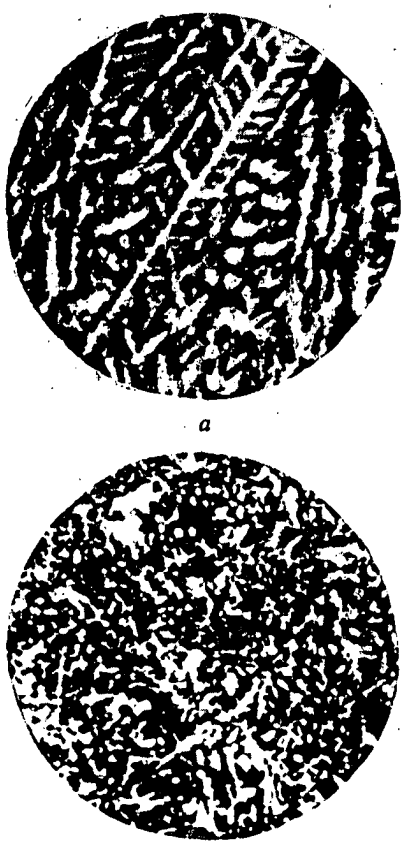

а *б*

Рис. 3. Микрорадиограммы двойных сплавов Mg—Ca

Appendix 20

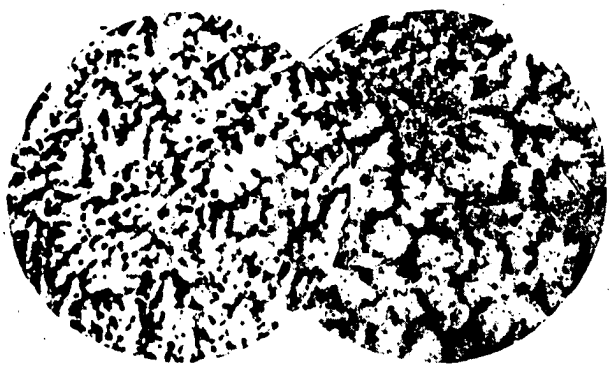

а *б*

Рис. 4. Микрорадиограммы различных мест слитка тройного сплава Mg—Mn—Ca:
а – верхняя зона слитка, *б* – нижняя зона слитка; ×8

Рис. 5. Микрорадиограмма четырехкомпонентного магниевого сплава; ×8

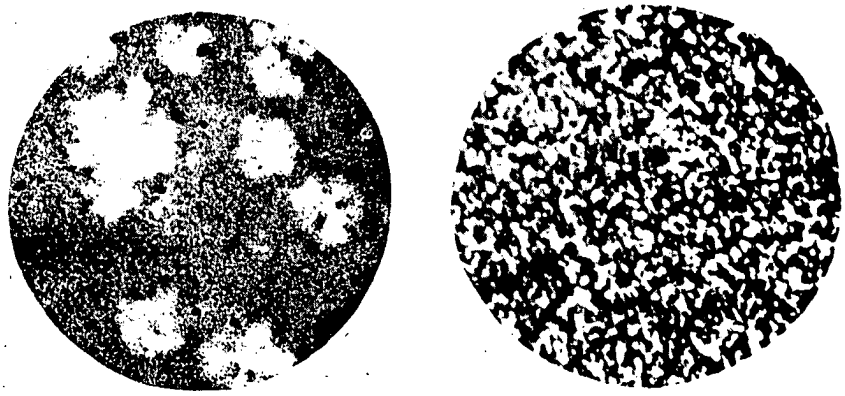

а *б*

Рис. 6. Микрорадиограммы центральной части слитка четырехкомпонентного магниевого сплава:
а — при увеличении 25, *б* — при увеличении 750

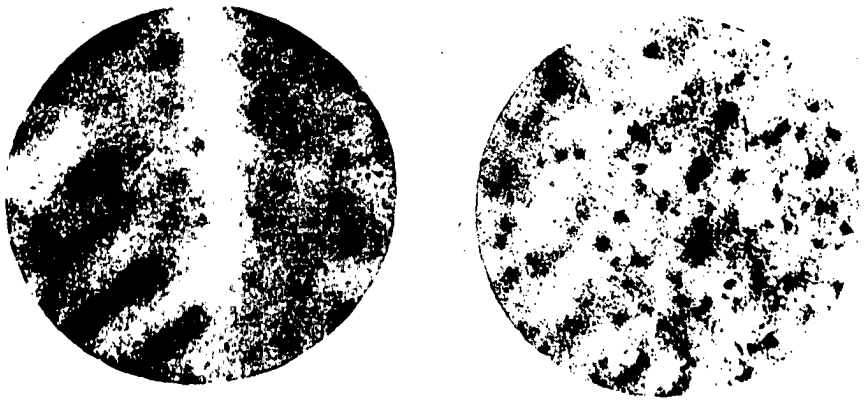

а *б*

Рис. 7. Микрорадиограммы магниевого сплава:
а – литое состояние, *б* – после отжига при 600° в течение 24 час.; ×56

APPENDIX 21

INFLUENCE OF CRYSTALLIZATION RATE ON THE MICROHETEROGENEITY OF MAGNESIUM ALLOYS

Technical Science Candidates Z. A. Sviderskaya and M. E. Drits
and Engineer E. S. Kadaner

The A. A. Baikov Institute of Metallurgy
of the Academy of Sciences of the USSR

Metalloved. i Obrabotka Metal. (Metallography and Metal Working), No. 5, pp. 23-29 (1957).

Many investigators (/1/-/5/) indicate that the physical and mechanical properties of alloys depend to a considerable degree on the microheterogeneity, observed in the structure of the cast material. A. A. Bochvar /1/ indicates that a change in the cooling rate of alloys leads to a change in the degree of intradendritic liquation, which is associated with diffusion of the alloying elements in the liquid and solid states.

Very high cooling rates (for example, at the points of contact of the metal with the cold mold) do not permit passing through primary diffusion in the liquid phase and the structure of the metal is obtained more or less homogeneous. At some average cooling rate, the progress of diffusion processes is facilitated, creating a difference in the composition of the solid and liquid solution, and here the intracrystalline heterogeneity reaches some sort of maximum value.

Further reduction in the cooling rate facilitates secondary diffusion in the already hardened metal, which leads to some smoothing out of the microheterogeneity. However, up to now a similar character of the rule for change in the degree of intracrystalline liquation with change in the cooling rate has failed to receive sufficiently clear experimental confirmation.

Olsen and Hultgren /6/ believe that a reduction in the microheterogeneity of alloys with increases in the cooling rate also facilitates supercooling, which retards the formation of crystalline centers and reduces the degree of liquation. Using the x-ray analysis method, these authors were able to show a regularity in the change of the microheterogeneity as a function of the rate of cooling for the copper-gold system of continuous solid solutions, depicted as a curve with a maximum.

However, they failed to establish a similar relationship for the copper-nickel alloys.

To experimentally prove the existence of a curve with a maximum in the change of the intracrystalline heterogeneity with change in the rate

of cooling N. E. Bolotov, M. I. Gol'dshtein and others /7/ made an attempt to use the autoradiography method, which in recent years is finding constantly increasing use in metallurgy and metallography.

These authors studied the distribution of phosphorus, sulfur, and tungsten in steel with different rates of cooling, but failed to confirm the existence of a curve with a maximum.

On the basis of analyzing the data obtained in studying the dendritic heterogeneity of a steel casting I. N. Golikov /8/ expressed the theory that the reason for the observed divergence in the opinions of different investigators on the question of the existence of a maximum on the curve "degree of microheterogeneity - rate of crystallization" is the fact that in practice cases are considered where the rate of cooling changes on different sides of the maximum. Here to the right of the maximum an increase in the rate of cooling should cause a reduction in the microheterogeneity, while on the other hand, to the left of the maximum an increase in the rate of cooling should cause an increase in the microheterogeneity.

To study the structure heterogeneity of magnesium alloys, containing calcium, we used the radioactive calcium isotope, which permitted us to follow the change in the character of the micro-heterogeneity observed in these alloys as a function of a number of factors.

We observed (/9/,/10/) that a change in the conditions of cooling the alloys during their hardening exerted a sharp influence on the distribution of calcium in the micropores (microspaces). A rapid cooling of the alloys when cast in a metal mold led to a very uniform calcium distribution when compared with the sand-cast specimens, where substantial intradendritic heterogeneity was observed. To establish the relationship between the rate of cooling magnesium alloys and intradendritic liquation we used the quantitative autoradiography method, based on determining the amount of elements contained in a micropore (microspace) of the alloy by the method of photometric examination of the radioautograms (/11/-12/).

First we constructed the characteristic curves, expressing the relationship between the intensity of radioactive radiation and the density of blackening of the photoemulsion. With the assistance of these curves we determined the region of blackening, within the limits of which there existed a direct relationship between the density of blackening and the radioactive calcium concentration. An MF-2 microphotometer with a square slit having an area of 1 sq. mm. was used in the photometric examination of the radiograms at a magnification of 24X, on a 5 mm. portion of the autograph.

The blackening density was measured at 0.01 mm. intervals, i.e. 500 determinations were made.

For studying the microheterogeneity we took three series of castings, the variation in the cooling rate of which was achieved by different

methods. In the first case the binary alloys of magnesium with calcium were cast in a metal mold, heated to different temperatures. The second and third series of castings represented quaternary alloys of the system magnesium-manganese-aluminum-calcium. In this case a change in the cooling rate was achieved by using different types of casting molds (copper, steel with immersion in water, cast-iron with heating to 530°, and dry sand molds), while in the last series of alloys a difference in the cooling rate was created by using sand molds of variable cross section--having a diameter of 11, 30, 50 and 80 mm. respectively.

Curves, showing the change in the blackening density along the length of the photometered portion of the structure, were constructed for all of the alloys studied by us. The curves for the binary magnesium-calcium alloys, cast in molds that had been heated to different temperatures, are shown in Fig. 1. The character of the blackening curves clearly shows the calcium distribution in the microspaces of the alloy as a function of the rate of cooling.

When cast in a cold metal mold at 20° the calcium is distributed very uniformly and the blackening curve has a monotonic shape (Fig. 1). With increase in the temperature of the mold the intracrystalline heterogeneity increases, and large fluctuations in the blackening values, i.e. in the calcium concentration are observed on the blackening curves. By making a statistical analysis of the photometric results it was possible to estimate the degree of microheterogeneity present in the structure of the studied alloys. For this the blackening density values were converted into concentration values, and then the distribution frequency curves were constructed. The frequency curves, corresponding to all three cases of varying the cooling rate of the alloys, are shown in Fig. 2. The maximum on the frequency curves corresponds to the average amount of calcium in the given series of alloys and determines the number of microspaces found in the photometered portions with an average concentration. The higher the maximum on the frequency curve and the smaller the distance between its branches, the more sharply expressed is the intracrystalline heterogeneity in the structure of the alloys. The frequency curves, corresponding to the binary alloys of magnesium with calcium (Fig. 2,a), show that with decrease in the mold temperature, i.e. with increase in the cooling rate of the alloy during its crystallization the liquational microheterogeneity decreases. When the alloy is cast in a cold mold, having a temperature ranging from 20° to 200°, the amount of microspaces with an average calcium concentration is 80-90%. With retarded cooling, when the mold is heated to 600-675°, only 35-38% of the alloy microspaces have an average calcium content (for the given series of alloys 0.06%).

On the whole, the curves shown in Fig. 2b for alloys of the magnesium-manganese-aluminum-calcium system confirm the rule established for

binary alloys relative to the change in the microheterogeneity as a function of the rate of cooling.

An increase in the cooling rate when casting the alloy in either a copper or water-cooled steel mold results in substantially less microheterogeneity than when cast in a sand mold or a heated cast-iron pot. In the first case the amount of microspaces with an average calcium content (equal to 0.13% for this series of castings) is 70-88%, while in the second case this value is reduced to less than 30%. However, it should be mentioned that for slow cooling rates the maxima on the frequency curves for the discussed series of castings lie extremely close to each other. With casting in a sand mold the maximum is even situated somewhat above that obtained when the casting is in a cast-iron pot, heated to 530°, although the cooling rate in the sand mold was minimum. Evidently, a deviation from the direct relationship between the cooling rate and the degree of microheterogeneity shown by a cast material is observed here. This deviation is shown more clearly in the frequency curves (Fig. 2c), which relate to the four-component magnesium alloy, cast in sand molds of different cross-section.

The maximum degree of microheterogeneity is obtained with the smallest and largest diameters of the castings. The castings with average diameter dimensions, and consequently with average cooling rates, show a greater intracrystalline heterogeneity.

For the rods with a diameter of 11 mm. the amount of alloy microspaces, having an average concentration, is 55%. With increase in the casting diameter from 30 to 50 mm. this value shows a corresponding reduction to 32-27%, but then when the diameter of the casting is increased to 80 mm. it again rises to 41%, which is evidence that a more homogeneous structure is again being obtained. The microradiograms of an alloy, taken with specimen diameters of 11, 50 and 80 mm., and at the same magnification as was used in making the photometric measurements, are shown in Fig. 3. With increase in the diameter of the casting from 11 to 50 mm. the intracrystalline heterogeneity becomes more sharply expressed. The interaxial layers, in which the calcium concentrates, become thicker and the branching of the dendrites increases. Further increase in the diameter of the casting to 80 mm. leads to redistribution of the calcium in the alloy structure, conditioned by a quite slow crystallization and the possibility of diffusion processes prevailing in the grain body. From the microradiogram shown in Fig. 3c, it can be seen that the calcium is concentrated in the intergrain boundary zones, while inside the grain the structure becomes more uniform.

As a result, the study made by us shows that a more uniform distribution of calcium in the microstructure of magnesium alloys can be obtained either in the case of high cooling rates or, on the contrary, with a sufficiently slow crystallization.

An intermediate cooling rate determines a large degree of intracrystalline heterogeneity for the calcium distribution. To generalize the

obtained data the results of the statistical analysis of the curves for calcium distribution were depicted in the form of two coefficients K and C. Coefficient K characterizes the degree of microheterogeneity shown by an alloy structure and is determined by the formula

$$K = \frac{100 - n}{100},$$

where n corresponds to the maximum on the frequency curve and represents the number of microspaces with an average concentration, while the 100 represents the number of microspaces in which the calcium content had been measured. Coefficient C is the ratio of the maximum calcium concentration C_{max} to its minimum concentration C_{min} in the individual microspaces found on the investigated portion of the structure:

$$C = \frac{C_{max}}{C_{min}}.$$

In Table 1 we give the values of the coefficients K and C for all of the alloys studied by us, with the different cooling rates that were employed by us in the present investigation. The cooling rate was calculated as the quotient of dividing the temperature difference of the start and end of alloy hardening by the cooling time. The curves showing the relationship between the cooling rate and the microheterogeneity of the alloys studied by us, constructed from the data given in Table 1, are plotted in Fig. 4. As an analysis of these curves shows, in two cases (Fig. 4b and c) the relationship between the coefficents K and C and the cooling rate is expressed by curves with a maximum.

It should be mentioned that for the series of castings, relating to the binary alloys of magnesium with calcium, the curves do not pass through a maximum, i.e. the microheterogeneity of the structure constantly decreases in measure with increase in the cooling rate. Evidently, the curves obtained by us with a maximum correspond to the more general case of a relationship existing between the cooling rate and intracrystalline dendritic heterogeneity, arising in the crystallization of alloys of the solid solution type.

A study of the microstructure of the alloys cast by us reveals that in all cases the amount of a second phase were very small, and consequently in their structure the investigated alloys were extremely close to one-phase solid solutions.

If here it is considered that the photometric measurements of the microradiograms were made at comparatively low magnifications, and that the inclusions of the manganese component in the Mg-Mn-Al-Ca alloys

do not give a blackening on the microradiograms, then evidently it is possible to assume that the obtained rules reflect the character of the calcium distribution, conditioned by intracrystalline liquation during crystallization of a solid solution.

As a result, the use of the quantitative radiography method permitted not only estimating the magnitude of the observed microheterogeneity in the casting of magnesium alloys with calcium, but also permitted obtaining experimental verification of the general character of the change in the microheterogeneity with change in the cooling rate, systematically mentioned by A. A. Bochvar /1/. As regards the deviations (including the curve obtained by us and shown in Fig. 4a) from this rule, observed under actual conditions, then, in addition to the above indicated reasons /8/, other no less important factors, such as, for example, the physicochemical properties of the alloy itself, should show influence here. It is probable that for the same diapason of change in the cooling rate different materials will be differently inclined to show more or less developed dendritic crystallization, which cannot fail to be without influence on the extent of microheterogeneity arising during freezing. There is no doubt as to the importance of establishing a relationship between the degree of microheterogeneity and the cooling rate of alloys for solving individual practical problems.

Many of the physical and mechanical properties of alloys depend on the change in their structure heterogeneity. As is known the heat resistance is one of the properties that belongs here. We determined the heat resistance (endurance limit) of a number of alloy specimens that had been cast in molds of variable cross-section. The structure microheterogeneity of the tested specimens is clearly seen when the microradiograms shown in Fig. 3 are examined. The conditions of casting the specimens, the value of the microheterogeneity coefficient and the values obtained for the endurance limit at 250° are presented in Table 2.

As can be seen from the data in this table, the heat resistance of the investigated alloy shows substantial change with change in the cooling rate. Here the highest values of the endurance limit are obtained with average values of the cooling rate, i.e. with the greatest degree of heterogeneity for the structure of the cast alloy. Evidently, at high cooling rates, the same as with extremely slow cooling, a more uniform distribution of the structure components facilitates the progress of diffusion processes and to a certain degree lowers the heat resistance.

LITERATURE CITED

/1/ Bochvar, A.A., Principles of the Heat Treatment of Alloys, Metallurgy Press, 1934.

/2/ Petrov, D. A., Problems in the Theory of Aluminum Alloys, Metallurgy Press, 1951.

/3/ Dobatkin, V. I., Continuous Casting and Casting Properties of Alloy, State Press of the Defense Industry, 1948.

/4/ Livanov, V. A., Metallurgical Principles of Continuous Casting, Transactions First Technological Conference, State Press of the Defense Industry, 1945.

/5/ Fridlyander, N. N., Transactions MAI, No. 95, 1949.

/6/ Olsen, W. T., and Hultgren, R., Journal of Metals, Sect. 1, 1950.

/7/ Bolotov, N.E., Goldshtein, M.L., Popov, A.A., and Fedorov, A.B., Zavodskaya Lab., No. 6, 1956.

/8/ Golikov, I.N., Monograph "Heat Treatment of Metals", State Press of Literature on Machine Building, 1952.

/9/ Drits, M. E., Sviderskaya, Z. A., and Kadaner, E.S., Zavodskaya Lab., No. 7, 1955.

/10/ Drits, M.E., Sviderskaya, Z. A., and Kadaner, E.S., Investigation of Heat Resistant Alloys, Academy of Science USSR Press, 1956.

/11/ Studnits, M. A., and Malyuchkov, O.T., Metalloved. i Obrabotka Metal, No. 6, 1955.

/12/ Bokshtein, C. Z. Gudkova, T. I., Kishkin, S.T., and Moroz, L. M., Zavodskaya Lab., No. 4, 1955.

TABLES AND FIGURES

FIGURE 1

(1) Blackening curves for magnesium-calcium alloys:

1--320°/min; 2--160°/min.; 3--105°/min.; 4--47°/min.; 5--20°/min.

(2) Density of blackening

FIGURE 2

(1) Calcium distribution with variation in the cooling rate:

a--as the result of differences in the mold temperature (binary magnesium-calcium alloys); 1--320°/min.; 2--160°/min.; 3--105°/min.; 4--47°/min.; 5--20°/min.; b--as the result of using different types of casting molds (Mg-Mn-Al-Ca alloys); 1--1000°/min.; 2--500°/min.; 3--45°/min.; 4--160°/min.; c--as the result of varying the diameter of the sand mold (Mg-Mn-Al-Ca alloys); 1--120°/min.; 2--4°/min.; 3--45°/min.; 4--22°/min.

(2) Relative frequency

FIGURE 3

(1) Microradiograms of Mg-Mn-Al-Ca alloys, cast in sand molds with different cross-sections. x25:

a--diameter of the mold 11 mm; b--50 mm.; c--80 mm.

FIGURE 4

(1) Relationship between the microheterogeneity and the cooling rate:

a--with different mold temperatures (Mg-Ca alloys);
b--with different methods of casting (Mg-Mn-Al-Ca alloys);
c--with different diameters of the sand molds (Mg-Mn-Al-Ca alloys).

(2) Rate of cooling

TABLE 1

(1) Alloy (2) Average calcium content in %

(3) Rate of cooling in °/min. (4) Coefficient of microheterogeneity K

(5) Ratio of the maximum concentration to the minimum C

(6) Casting conditions (7) Remarks (8) Temperature of the mold in °

(9) The cooling rate was varied by varying the temperature of the mold

(10) Sand mold (11) Cast-iron mold 530°

(12) Steel mold with immersion in water (13) Copper mold

(14) The cooling rate was varied by using different types of molds

(15) Diameter of the mold in mm.

(16) The cooling rate was varied by changing the diameter of the sand mold

TABLE 2

(1) Alloy casting conditions (2) Rate of cooling in °/min.

(3) Heat endurance limit $\sigma - \frac{250}{100}$ kg./sq. mm.

(4) Coefficient of microheterogeneity K

(5) Cast in sand d = 80 mm.

(6) Cast in sand d = 50 mm.

(7) Cast in sand d = 11 mm.

температуры изложницы внутрикристаллическая неоднородность возрастает, и на кривых почернения наблюдаются большие колебания в величинах почернения, т. е. в концентрации кальция.

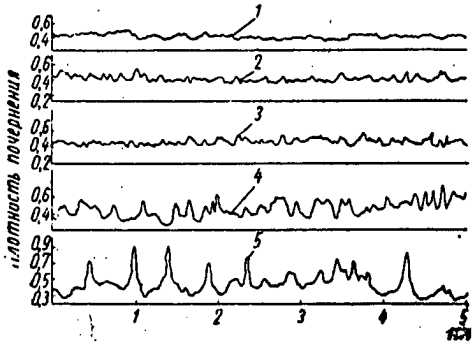

Фиг. 1. Кривые почернения для сплавов магний—кальций:
1 — 320 град/мин; *2* — 160 град/мин; *3* — 105 град/мин; *4* — 47 град/мин; *5* — 20 град/мин.

Проведя статистическую обработку результатов фотометрирования, можно было оценить степень микронеоднородности в структуре исследуемых сплавов. Для этой цели значения плотности почернения пересчитывались в концентрации, и строились частотные кривые распределения. На фиг. 2 представлены частотные кривые, соответствующие всем трем случаям изменения скорости охлаждения сплавов. Максимум частотных кривых отвечает среднему содержанию кальция в сплавах данной серии и определяет количество микрообъемов на фотометрируемых участках, обладающих средней концентрацией. Чем выше лежит максимум частотной кривой и чем меньше расстояние между ее ветвями, тем менее резко выражена в структуре сплавов внутрикристаллическая неоднородность. Частотные кривые, отвечающие двойным сплавам магния с кальцием (фиг. 2, *а*), показывают, что с понижением температуры изложницы, т. е. с увеличением скорости охлаждения сплава при его кристаллизации, уменьшается ликвационная микронеоднородность. При отливке сплава в холодную форму, имеющую температуру от 20 до 200°, количество микрообъемов со средней концентрацией кальция составляет 80—90%. При замедленном охлаждении, когда изложница нагрета до 600—675°, только 35—38% микрообъемов сплава имеют среднее содержание кальция (для данной серии сплавов 0,06%).

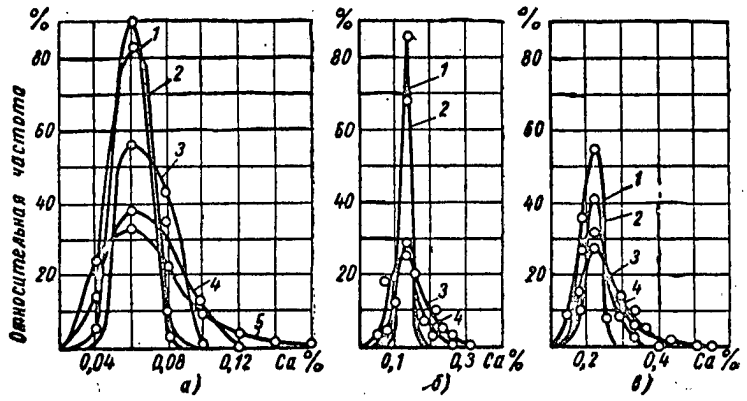

Фиг. 2. Распределение кальция при изменении скорости охлаждения:
а—за счет различия в температуре изложницы (двойные сплавы магний—кальций); *1* — 320 град/мин; *2* — 160 град/мин; *3* — 105 град/мин; *4* — 47 град/мин; *5* — 20 град/мин; *б* — за счет использования различных литейных форм (сплавы Mg — Mn — Al — Ca); *1* — 1000 град/мин; *2* — 500 град/мин; *3* — 45 град/мин; *4* — 160 град/мин; *в* — за счет диаметра земляной формы (сплавы Mg—Mn—Al—Ca); *1* — 120 град/мин; *2* — 4 град/мин; *3* — 45 град/мин; *4* — 22 град/мин.

Кривые, показанные на фиг. 2, *б*,

APP. 21.

для сплава системы магний—марганец—алюминий—кальций, в основном, подтверждают закономерность изменения микронеоднородности в зависимости от скорости охлаждения, установленную для двойных сплавов.

Повышение скорости охлаждения при отливке сплава в медную или стальную водоохлаждаемую изложницы обусловливает значительно меньшую микронеоднородность по сравнению с отливкой в земляную форму или нагретую чугунную изложницу. В первом случае количество микрообъемов со средней концентрацией кальция (равной 0,13% для этой серии отливок) составляет 70—88%, а во втором случае эта величина снижается до значений менее 30%. Однако следует заметить, что для малых скоростей охлаждения максимумы частотных кривых для рассматриваемой серии отливок лежат очень близко друг к другу. При отливке в земляную форму максимум расположен даже несколько выше чем при литье в чугунную изложницу, нагретую до 530°, хотя в земляной форме скорость охлаждения была минимальной. Очевидно здесь наблюдается отклонение от прямой связи между скоростью охлаждения и степенью микронеоднородности литого материала. Это отклонение выражено более заметно в частотных кривых (фиг. 2, *в*), которые относятся к четырехкомпонентному магниевому сплаву, отлитому в земляные формы разного сечения.

Максимальная степень микронеоднородности достигается при наименьшем и наибольшем диаметрах отливки. Средние размеры сечений, а следовательно и средние скорости охлаждения, обусловливают бо́льшую внутрикристаллическую неоднородность.

Количество микрообъемов сплава, обладающих средней концентрацией для стержня диаметром 11 *мм*, соответствует 55%. С увеличением диаметра отливки до 30 и 50 *мм* эта величина снижается соответственно до 32—27%, но затем с увеличением диаметра слитка до 80 *мм* снова возрастает до 41%, что свидетельствует о получении вновь более однородной структуры. На фиг. 3 представлены микрорадиограммы сплава, снятые со слитков диаметром 11, 50 и 80 *мм*, при том же увеличении, при котором производилось фотометрирование. С возрастанием диаметра отливки от 11 до 50 *мм* внутрикристаллическая неоднородность становится более резко выраженной. Междуосные прослойки, в которых сосредоточивается кальций, утолщаются и возрастает разветвленность дендритов. При дальнейшем увеличении диаметра отливки до 80 *мм* происходит перераспределение кальция в структуре сплава, обусловленное достаточно медленной кристаллизацией и возможностью протекания диффузионных процессов в объеме зерна. Из приведенной на фиг. 3, *в* микрорадиограммы видно, что кальций сосре-

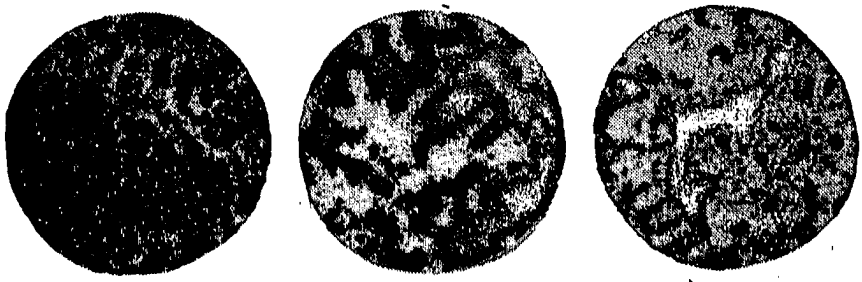

а) *б)* *в)*

Фиг. 3. Микрорадиограммы сплавов Mg—Mn—Al—Ca, отлитых в земляные формы разных сечений. ×25:
а — диаметр формы 11 *мм*; *б* — 50 *мм*; *в* — 80 *мм*.

APP. 21.

доточен в пограничных межзеренных зонах, а внутри зерна структура становится более однородной.

Таким образом, выполненное нами исследование показывает, что более однородное распределение кальция в микроструктуре магниевых сплавов можно получить или в случае высоких скоростей охлаждения или, наоборот, при достаточно медленной кристаллизации.

Промежуточное значение скорости охлаждения обусловливает большую внутрикристаллическую неоднородность в распределении кальция. Для обобщения полученных данных результаты статистической обработки кривых распределения кальция были представлены в виде двух коэффициентов K и C. Коэффициент K характеризует степень микронеоднородности структуры сплава и определяется по формуле

$$K = \frac{100 - n}{100},$$

где n соответствует максимуму частотной кривой и отвечает количеству микрообъемов, имеющих среднюю концентрацию, а число 100 представляет собой количество микрообъемов, в которых измерялось содержание кальция. Коэффициент C является отношением максимальной концентрации кальция C_{max} к минимальной его концентрации C_{min} в отдельных микрообъемах на исследуемом участке структуры:

$$C = \frac{C_{max}}{C_{min}}.$$

В табл. 1 приведены значения коэффициентов K и C для всех изученных нами сплавов при различных скоростях охлаждения, которые осуществлялись в условиях данного исследования. Скорость охлаждения вычислялась как частное от деления разности температур начала и конца затвердевания сплава на время охлаждения. Кривые, выражающие связь между скоростью охлаждения и микронеоднородностью исследованных нами сплавов, построенные по данным табл. 1, изображены на фиг. 4. Как показывает анализ этих кривых в двух случаях (фиг. 4, *б* и *в*), зависимость коэффициентов K и C от скорости охлаждения выражается кривыми с максимумом.

Фиг. 4. Зависимость микронеоднородности от скорости охлаждения:
а — при различных температурах изложницы (сплавы Mg — Ca); *б* — при различных способах отливки (сплавы Mg — Mn — Al — Ca); *в* — при различных диаметрах земляных форм (сплавы Mg — Mn — Al — Ca).

Следует отметить, что для серии отливок, относящихся к двойным сплавам магния с кальцием, кривые не проходят через максимум, т. е. микронеоднородность структуры непрерывно снижается по мере увеличения скорости охлаждения. Полученные нами кривые с максимумом, очевидно, отвечают наиболее общему случаю связи между скоростью охлаждения и внутрикристаллической дендритной неоднородностью, возникающей при кристаллизации сплавов типа твердых растворов.

Исследование микроструктуры отлитых нами сплавов показывает, что во всех случаях количество второй фазы было очень мало и, следовательно, изучаемые сплавы по своей

APP. 21

Таблица 1

Сплав	Среднее содержание кальция в %	Скорость охлаждения в град/мин	Коэффициент микронеоднородности K	Отношение максимальной концентрации к минимальной C	Условия литья	Примечания
					Температура изложницы в °	
Mg—Ca	0,06	20	0,66	4,0	675	Изменение скорости охлаждения за счет различия в температуре изложниц
		47	0,62	3,0	600	
		105	0,43	1,6	400	
		160	0,16	2,0	200	
		320	0,09	2,0	20	
Mg—Mn—Al—Ca	0,13	45	0,72	4,0	Земляная форма	Изменение скорости охлаждения за счет различия в литейной форме
		160	0,75	5,0	Чугунная изложница 530°	
		500	0,32	1,5	Стальная изложница с погружением в воду	
		1000	0,13	1,25	Медная изложница	
					Диаметр формы в *мм*	
Mg—Mn—Al—Ca	0,22	4	0,58	2,9	80	Изменение скорости охлаждения за счет изменения диаметра земляной формы
		22	0,73	3,2	50	
		45	0,68	2,2	30	
		200	0,45	1,7	11	

структуре были весьма близки к однофазным твердым растворам.

Если при этом учесть, что фотометрирование микрорадиограмм производилось при сравнительно небольших увеличениях и что включения марганцовистой составляющей в сплавах Mg—Mn—Al—Ca не дают на микрорадиограммах почернения, то можно, очевидно, полагать, что полученные закономерности отражают характер распределения кальция, обусловленный внутрикристаллической ликвацией при кристаллизации твердого раствора.

Таким образом, применение метода количественной радиографии позволило не только оценить масштабы наблюдающейся микронеоднородности при отливке магниевых сплавов с кальцием, но и подтвердить экспериментально общий характер изменения микронеоднородности с изменением скорости охлаждения, намеченный схематически А. А. Бочваром [1]. Что касается наблюдаемых в реальных условиях отклонений от этой закономерности (включая и полученную нами кривую на фиг. 4, *а*), то, помимо указанных выше причин [8], должны иметь влияние и другие не менее важные факторы, такие, как например, физико-химические свойства самого сплава. Вероятно, для одного и того же диапазона изменения скоростей охлаждения разные материалы будут в различной степени склонны к более или менее развитой дендритной кристаллизации, что не может не сказаться на масштабах возникающей при затвердевании микронеоднородности. Не вызывает сомнения важность установления связи между степенью микронеоднородности и скоростью охлаждения сплавов для решения отдельных практических вопросов.

Многие физические и механические свойства сплавов зависят от изменения их структурной неоднородности. К числу таких свойств относится, как известно, и жаропрочность. Мы определили жаропрочность (предел длительной прочности) на образцах

APP. 21

из отливок одного и того же сплава, полученных в формах разного сечения. Микронеоднородность структуры испытывавшихся образцов хорошо видна из рассмотрения микрорадиограмм, представленных на фиг. 3. Условия отливки образцов, величина коэффициента микронеоднородности и полученные значения предела длительной прочности при 250° приведены в табл. 2.

Как видно, с изменением скорости охлаждения жаропрочность изучаемого сплава заметно меняется. При этом наивысшие значения предела длительной прочности получаются при средних значениях скоростей охлаждения, т. е. при наибольшей степени гетерогенизации структуры литого сплава. Очевидно, при больших скоростях охлаждения, так же, как и при очень медленном охлаждении, более равномерное распределение структурных составляющих облегчает протекание диффузионных процессов и до известной степени снижает жаропрочность.

Таблица 2

Условия отливки сплава	Скорость охлаждения в град/мин	Предел длительной прочности σ^{250}_{100} кг/мм²	Коэффициент микронеоднородности K
Отливка в землю $d = 80$ мм	4	4,0	0,58
Отливка в землю $d = 50$ мм	22	5,0	0,73
Отливка в землю $d = 11$ мм	200	4,2	0,45

Литература

1. Бочвар А. А., Основы термической обработки сплавов, Металлургиздат, 1934.
2. Петров Д. А., Вопросы теории сплавов алюминия, Металлургиздат, 1951.
3. Добаткин В. И., Непрерывное литье и литейные свойства сплавов, Оборонгиз, 1948.
4. Ливанов В. А., Металлургические основы непрерывного литья, Труды I. технологич. конференции, Оборонгиз, 1945.
5. Фридляндер Н. Н., Труды МАИ, вып. 95, 1949.
6. Olsen W. T., Hultgren R., «Journal of Metals», sect. 1, 1950.
7. Болотов Н. Е., Гольдштейн М. И., Попов А. А., Федоров А. Б., «Заводская лаборатория» № 6, 1956.
8. Голиков И. Н., Сб. «Термическая обработка металлов», Машгиз, 1952.
9. Дриц М. Е., Свидерская З. А., Каданер Э. С., «Заводская лаборатория» № 7, 1955.
10. Дриц М. Е., Свидерская З. А., Каданер Э. С., Исследования по жаропрочным сплавам, изд. АН СССР, 1956.
11. Студниц М. А. и Малючков О. Т., «Металловедение и обработка металлов» № 6, 1955.
12. Бокштейн С. З., Гудкова Т. И., Кишкин С. Т., Мороз Л. М., «Заводская лаборатория» № 4, 1955.

ОСТАТОЧНЫЕ НАПРЯЖЕНИЯ В ПОВЕРХНОСТНО-ЗАКАЛЕННЫХ ИЗДЕЛИЯХ ПОСЛЕ ОТПУСКА ПРИ ТЕМПЕРАТУРАХ РАСПАДА МАРТЕНСИТА

Канд. техн. наук М. М. КОБРИН и инж. К. В. ШИШОКИНА
ЦНИИТМАШ

Свойства, сообщаемые изделию поверхностной закалкой (усталостная прочность и др.), связаны с наличием остаточных напряжений, их величиной и распределением [1]. Хотя этот вопрос широко изучался, все же осталось мало исследованным распределение остаточных напряжений в поверхностно-закаленных изделиях, подвергаемых отпуску при температурах интенсивного распада мартенсита.

Эта проблема привлекла к себе внимание в связи с тем, что в поверхностно-закаленном слое изделий среднеуглеродистой стали при отпу-

Appendix 22

ИЗВЕСТИЯ АКАДЕМИИ НАУК СССР
ОТДЕЛЕНИЕ ТЕХНИЧЕСКИХ НАУК

№ 6 1957

ИЗУЧЕНИЕ РАСПРЕДЕЛЕНИЯ ЖЕЛЕЗА В АЛЮМИНИИ МЕТОДОМ АВТОРАДИОГРАФИИ

М. Е. ДРИЦ, Э. С. КАДАНЕР, З. А. СВИДЕРСКАЯ, Е. Л. ЩЕРБИНИНА

(Москва)

Железо является основной примесью алюминия и содержится в различных промышленных марках алюминия в количествах от тысячных и сотых долей до целых процентов.

Повышая прочность и твердость алюминия, оно резко снижает его пластичность и коррозионную стойкость, ухудшая условия обработки давлением [1]. В сплавах алюминия с медью присутствие железа сказывается отрицательно на величине эффекта упрочнения при термической обработке, что приводит к снижению прочностных характеристик этих сплавов, наряду с ухудшением их технологичности. Однако в условиях работы при повышенных температурах железо оказывает положительное влияние, способствуя торможению диффузионных процессов ползучести в алюминии и его сплавах. В работе А. А. Бочвара и др. [2] это положительное действие железа связывается с повышением температуры рекристаллизации алюминия благодаря выделению интерметаллического соединения $FeAl_3$ на поверхности раздела между зернами и внутри зерен.

На развитие или торможение диффузионных механизмов пластичности, наряду с основными легирующими компонентами, вводимыми в сплав в качестве упрочнителей, весьма заметное влияние могут оказывать десятые, сотые или даже тысячные доли процента примесей, содержащихся в исходных материалах. Подобное действие небольшого количества примесей, очевидно, связано с характером их распределения в основе, т. е. с тем влиянием, которое они оказывают на структурное состояние основы сплавов, на степень гетерогенизации, а также на характер взаимодействия отдельных составляющих сплавов [3].

В литых и деформируемых сплавах на алюминиевой основе, предназначенных для работы при повышенных температурах, допускают присутствие железа в количествах, превышающих 0.8—1%. При этом, хотя и создаются определенные затруднения в отношении их обработки, но зато обеспечивается бóльшая надежность материала в эксплуатации. Положительная роль железа в обеспечении жаропрочности алюминиевых сплавов должна рассматриваться, с одной стороны, в связи с его распределением в основе, т. е. в алюминии и, с другой стороны, в связи с теми изменениями, которые вносит железо в фазовый состав сплавов.

Ниже приводятся результаты исследования, наглядно показывающие распределение железа в чистом алюминии, а также перераспределение его под влиянием нагрева. Применение метода количественной авторадиографии [4,5] позволило оценить изменение микронеоднородности в структуре алюминия по мере увеличения содержания в нем железа.

В чистейший алюминий марки АВООО (99.985% Al) вводился радиоизотоп железа Fe^{59} с таким расчетом, чтобы обеспечить активность образцов 6 mCu на 1 *кг* сплава. Слитки алюминия с различным содержанием железа отливались в земляную форму диаметром 30 *мм* и высотой 60 *мм*.

Для наиболее полного растворения железа в алюминии оно запрессовывалось в алюминиевые стаканчики, которые вводились в перегретый до 900° алюминий. Истинное содержание железа в полученных отливках вычислялось из соотношения

$$C = \alpha C' \qquad (1)$$

где α — коэффициент усвояемости, C' — содержание железа в слитке по шихте (в %).

Коэффициент усвояемости определялся радиометрически, как отношение общей активности полученного сплава к активности элемента, введенного в сплав радиоактивным препаратом.

Расчет производился по формуле

$$\alpha = \frac{aQ}{a'q} 100\% \qquad (2)$$

где a — удельная активность сплава [*имп/мин. г*], a' — удельная активность радиоизотопа [*имп/мин*], Q — вес сплава [*г*], q — вес радиоизотопа, введенного в сплав [*г*].

Методика измерения удельной активности состояла в следующем. Стружка сплава, заранее взвешенная (с точностью до 0.0002 *г*), растворялась в определенном объеме 50%-ного раствора соляной кислоты. Затем раствор нейтрализовался аммиаком для устранения вредного действия паров кислоты на работу счетчика. Измерение активности производилось на установке (*Б*) с торцевым счетчиком. Для этой цели из полученного раствора посредством бюретки отбирался строго определенный объем (1.5 *см*^{3}) в стеклянную кювету, которая устанавливалась под окошком счетчика. Вес радиоактивного препарата и объем раствора подбирались таким образом, чтобы скорость счета во всех случаях не превышала 3000 *имп/мин*. Уровень фона при измерениях колебался в пределах 40—45 *имп/мин*.

Определение удельной активности сплавов и самого препарата производилось по формулам

$$a = \frac{NV}{kk_1P}, \qquad a' = \frac{N'V'}{kk_1P'} \qquad (3)$$

где N — скорость счета раствора сплава [*имп/мин*], N' — скорость счета раствора препарата [*имп/мин*], P — навеска растворенного сплава [*г*], P' — навеска растворенного радиоактивного препарата [*г*], V — объем раствора, в котором растворен сплав [*см*^{3}], V' — объем раствора, в котором растворен препарат [*см*^{3}], k — коэффициент, учитывающий распад изотопа, k_1 — коэффициент, учитывающий особенности измерения активности.

Так как при соблюдении постоянных условий опыта коэффициент k_1 был во всех случаях одинаковым, то его можно не учитывать. Подсчитанные по формулам (3) величины удельной активности a и a' подставлялись в формулу (2) для определения коэффициента усвояемости.

Таблица 1

Содержание железа по шихте, %	Коэффициент усвояемости α (%)	Содержание железа по данным радиометрич. анализа, %
0.01	85	0.0085
0.10	63.5	0.0635
0.2	96.8	0.194
1.0	41.9	0.419
0.8	92.5	0.74

В табл. 1 приведены значения коэффициента усвояемости α и истинное содержание железа в полученных образцах, рассчитанное с учетом этого коэффициента.

Чтобы получить достаточно четкие микрорадиограммы, изготовлялись тонкие образцы толщиной 60—70 *м*, которые экспонировались на высокочувствительной пленке МР (НИКФИ) в течение 5—7 суток. Для предохранения от коррозии на поверхность образцов наносилось покры-

тие, состоящее из 1.5%-ного раствора оргстекла в дихлорэтане. Перед тем как производить фотометрирование, при помощи характеристических кривых была определена область почернения (до 1.3), в пределах которой существовала прямая зависимость между плотностью почернения и концентрацией радиоактивного железа. Фотометрирование микрорадиограмм производилось на микрофотометре МФ-2, с квадратной щелью в 1 *мм*^{2} при увеличении (×24).

а *б* *в*

Фиг. 1. Микрорадиограммы (× 25) литых сплавов Al-Fe; *а*) Al + 0.0085% Fe; *б*) Al + 0.0085% Fe; *в*) Al + 0.194% Fe

Фотометрировался участок автографа, равный 4 *мм*. Плотность почернения измерялась через 0.01 *мм*, т. е. в 400 точках автографа. На фиг. 1 (*а*, *б*, *в*) приведены микрорадиограммы алюминия, содержащего тысяч-

а *б*

Фиг. 2. Микроструктуры (× 25) литых сплавов Al-Fe *а*) Al + 0.0085% Fe; *б*) Al + 0.194% Fe

ные (*а*, *б*) и десятые (*в*) доли процента железа. Темные участки микрорадиограмм соответствуют местам, обогащенным железом. Как видно, при введении очень малых количеств железа в алюминий, на одном и том же образце могут наблюдаться весьма различные по своему характеру участки структуры (фиг. 1 *а*, *б*). По-видимому, это связано с большой величиной зерен, которые видны на плоскости шлифа в различных сечениях. Железо концентрируется не только по границам зерен, но располагается и внутри зерна. Введение железа в алюминий в бо́льших количествах, до десятых долей процента, приводит к измельчению зерна и к созданию четкой дендритной структуры с расположением железа в междуосных пространствах (фиг. 1, *в*). На фиг. 2 для сравнения приведена микроструктура тех же самых сплавов, выявленная обычным травлением. В соответствии с практически полным отсутствием области твердых растворов в системе алюминий — железо, выделения интерметаллического соединения $FeAl_3$ можно наблюдать в литых сплавах, начиная уже с тысячных долей процента.

Для количественной оценки микронеоднородности сплавов, обусловленной присутствием в них железа, были построены кривые изменения плотности почернения по длине фотометрируемого участка радиограммы. Полученные данные после статистической обработки были представлены в виде частотных кривых распределения, характеризующих наблюдаемые в каждом случае отклонения по концентрации железа от его среднего содержания в сплаве.

Подобные кривые для некоторых из исследуемых нами сплавов изображены на фиг. 3. По изменению вида кривых распределения можно судить об изменении микронеоднородности в структуре алюминия по мере увеличения в нем железа. Чем выше лежит максимум частотной кривой и чем ближе по горизонтальной оси лежат конечные точки кривой, тем меньше выражена микронеоднородность в распределении железа. Однако наиболее четкое представление об изменении масштабов микронеоднородности в зависимости от состава можно получить, пользуясь определенными коэффициентами.

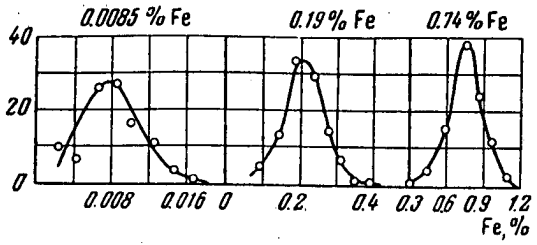

Фиг. 3

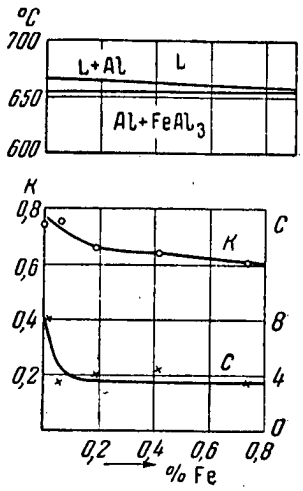

Фиг. 4

Фиг. 3. Статистические кривые распределения литых сплавов Al-Fe; по оси ординат отложена частота в %

Фиг. 4. Зависимость коэффициентов микронеоднородности K и C для литых сплавов Al-Fe от состава

Мы представили данные, полученные после статистической обработки кривых фотометрирования, в виде двух коэффициентов

$$K = \frac{100 - n}{100}, \qquad C = \frac{C_{max}}{C_{min}} \tag{4}$$

Коэффициент K выражает собой степень микронеоднородности структуры фотометрируемого участка. В выражении K за 100 принято количество всех микрообъемов, где измерялось содержание железа, а n отвечает максимуму частотной кривой и соответствует количеству микрообъемов, обладающих средней концентрацией железа. Коэффициент C вычисляется как отношение максимальной концентрации железа к минимальной концентрации его в отдельных микрообъемах на исследуемом участке структуры. Значения коэффициентов K и C для разных содержаний железа в алюминии приведены в табл. 2, а на фиг. 4 графически изображена зависимость микронеоднородности от состава исследованных сплавов.

Таблица 2

Состав сплава	Микронеоднородность	
	K	C
Al+0.0085% Fe	0.73	7.7
Al+0.0635% Fe	0.75	3.3
Al+0.194% Fe	0.66	4.0
Al+0.419% Fe	0.645	4.5
Al+0.74% Fe	0.61	3.4

Результаты исследования показывают, что присутствие железа в алюминии вызывает весьма значительную микронеоднородность в структуре литых сплавов. На это указывают большие абсолютные значения обо-

их коэффициентов. Характер кривых (фиг. 4) говорит о том, что микронеоднородность сначала заметно падает при увеличении железа с тысячных и сотых до десятых долей процента, а затем меняется незначительно по мере дальнейшего возрастания количества железа. Особенно четкий перегиб заметен на кривой, отвечающей коэффициенту C. Следует отметить, что в структурном отношении этот перегиб отвечает изменению характера распределения железа в алюминии, т. е. образованию мелкой дендритной структуры с локализацией железистой составляющей в междендритных пространствах, что видно из сопоставления фигур 1*в*, и 1*а*, *б*. Если выразить величину отклонений по концентрации железа, наблюдаемую в различных микрообъемах одного и того же сплава, как разность между максимальной и минимальной концентрацией железа, отнесенную к средней концентрации, то можно видеть, что эти отклонения в исследованных нами сплавах будут колебаться в пределах 100—170%. Следовательно

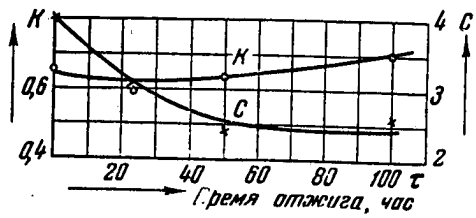

Фиг. 5. Влияние времени отжига на микронеоднородность сплава Al+0.194% Fe

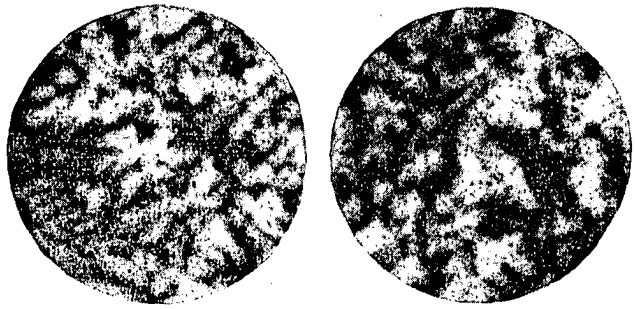

а *б*

Фиг. 6. Микрорадиограммы (×25) сплава Al + 0.194% Fe после отжига при температуре 605° С; *а* — время отжига 50 час.; *б* — время отжига 100 час.

гетерогенность структуры сплавов алюминия с железом весьма велика. Кинетика перераспределения железа в алюминиевых сплавах исследовалась нами в процессе гомогенизирующего отжига при температуре на 50° ниже солидуса (605°). При этом, учитывая имеющиеся данные [6] о малой скорости процессов выравнивания структуры в этих сплавах, продолжительность выдержки образцов в печи достигала 100 часов. В табл. 3 приведены значения коэффициентов K и C при различном времени отжига одного из отлитых сплавов. Для сравнения здесь же помещены данные, характеризующие микронеоднородность этого сплава в литом состоянии.

Таблица 3

Состояние сплава	Микронеоднородность	
	K	C
Литой	.66	4.0
Отжиг 605°—24 час.	.59	3.0
Отжиг 605°—50 час.	.64	2.4
Отжиг 605°—100 час.	0.71	2.6

Кривые, построенные по данным этой таблицы, даны на фиг. 5. По мере увеличения времени выдержки в печи значение коэффициента K почти не меняется, а при сточасовой выдержке несколько даже растет, что отвечает некоторому подъему кривой. Величина коэффициента C, наоборот, плавно снижается с увеличением времени отжига, хотя по сравнению с литым состоянием это снижение нельзя считать очень значительным. Раз-

личие в изменении коэффициентов K и C с увеличением продолжительности гомогенизирующего отжига следует, очевидно, рассматривать, исходя из структурных изменений сплава, происходящих под влиянием нагрева. Соответствующие микрорадиограммы приведены на фиг. 6. Сравнение их с микрорадиограммой литого сплава (фиг. 1 *в*) показывает, что, несмотря на длительность нагрева в печи, дендритный характер структуры сплава хорошо сохраняется. Это указывает на весьма малую подвижность атомов железа в данных условиях, т. е. на сравнительно медленное протекание диффузионных процессов, приводящих к перераспределению железа в алюминии. Некоторое увеличение коэффициента K при больших выдержках связано, по-видимому, с наблюдающимся огрублением структуры, т. е. с ростом самих дендритов, что видно из сопоставления фигур 1 *в* и 6 *б*. Падение значений коэффициента C может быть объяснено меньшей четкостью радиограмм, т. е. процессами выравнивания концентрации железа в алюминии под влиянием нагрева.

Полученные нами данные показывают, что микронеоднородность в распределении железа в алюминии, создающаяся в процессе кристаллизации, весьма устойчива и плохо поддается гомогенизирующей обработке. Большая протяженность поверхностей раздела, на которых происходит выделение интерметаллического соединения $FeAl_3$, создает благоприятные условия для блокировки сдвиговых процессов, развивающихся в результате пластической деформации, что, по-видимому, и оказывает благоприятное влияние на сопротивляемость ползучести алюминия и алюминиевых сплавов в присутствии железа.

Поступило 26 II 1957

ЛИТЕРАТУРА

1. Бочвар А. А. Металловедение. Металлургиздат, 1956.
2. Бочвар А. А., Свидерская З. А., Кычакова Л. М. Влияние примесей на жаропрочность алюминия. Изв. АН СССР, ОТН, № 2, 1954.
3. Бочвар А. А. О разных механизмах пластичности в металлических сплавах. Изв. АН СССР, ОТН, № 5, 1948.
4. Студниц М. А., Малючков О. Т. Авторадиографический метод исследования металлов и сплавов с помощью радиоактивных изотопов. Металловедение и обработка металлов, № 6, 1955.
5. Бокштейн С. З., Гудкова Т. И., Кишкин С. Т., Мороз Л. М. Изучение однородности сплавов и подвижности по границам зерен с помощью радиоизотопов. Заводская лаборатория, № 4, 1955.
6. Kato M., Kobayashi. Study on the behaviour of iron in aluminium of high purity by the use of Fe-59. Journ. Japan, Jnst. Metals № 10, 1955.

APPENDIX 23

"PLASTIC DEFORMATION OF MAGNESIUM ALLOYS"

by
S. I. Gubkin, L. N. Moguchii and M. I. Zatulovskii

Academy of Sciences of the USSR

The A. A. Baikov Institute of Metallurgy

Academy of Sciences of the USSR Press
Moscow 1955

45 Literature References, of which 40 are Russian

TABLE OF CONTENTS

APPENDIX 24

THE I. V. STALIN INSTITUTE OF STEEL
MOSCOW ORDER OF DISTINGUISHED RED LABOR

USE OF RADIOACTIVE ISOTOPES IN METALLURGY

Monograph XXXIV

Editor-in-Chief
I. N. Kidin

State Scientific-Research Press of
Literature on Ferrous and Nonferrous Metallurgy

Moscow 1955

(358 pages - 110 references of which 77 are Russian)

ANNOTATION

In this monograph are published a number of scientific-research studies using radioactive isotopes, made by the scientific personnel of the I. V. Stalin Institute of Steel in Moscow.

Some of the theoretical papers are devoted to a study of the phenomena of diffusion and autodiffusion in alloys, the mechanism of oxidation, the kinetics and equilibrium distribution of various elements between phases, the thermodynamic characterization of components in liquid and solid solutions, etc.

In the monograph are presented papers on establishing methods for studying the change in diffusion and thermodynamic properties and determination of the vapor pressure, and also studies on the use of labeled atoms for the analysis of alloys.

The remaining papers contain data on the results of studying the operation of metallurgical aggregates (blast, open-hearth and electric furnaces) using labeled atoms.

The monograph is designed for research and industrial engineering and technical workers: Metallurgists, physical chemists, physicists, metal workers and metallographers.

The monograph can also be useful to upper class students in the higher educational institutions.

TABLE OF CONTENTS

TABLE OF CONTENTS (Continued)

FOREWORD

In recent years the method of labeled atoms has found broad use in metallurgy and in a short time has become one of the principal study methods.

A large number of papers are given in this monograph, devoted to methods of measuring diffusion coefficients, a method of measuring the vapor pressure, a method of determining thermodynamic constants, a study of the thermodynamic activity, and a study of surface layers on the basis of measuring the repulsion effect of electrons.

The use of the method of labeled atoms in metallurgy is of great interest in connection with the possibility of elucidating the formation sources of nonmetallic inclusions, the sources for the penetration of undesirable components (for example, tin and sulfur) into an alloy, etc. To this group belong the papers published in this monograph on a study of the reasons for flaws in steel tubes and the quality of ball bearing steel.

Of especial interests to metallurgists are the problems associated with determining the distribution of various elements between phases and within individual phases. To this group belong the papers on a study of the penetration of titanium into graphite, the distribution of carbon in steel after high-frequency tempering, the distribution of sulfur, tungsten, etc.

Labeled atoms permit elucidating the mechanism of a process. A series of papers, contained in this monograph, for example, the studies devoted to an examination of the mechanism for the oxidation of iron and the passivity of metals, etc., belong to this group.

As the result of using labeled atoms it was possible to determine the velocity of the processes that take place in production units. The velocity of a gas in a blast furnace was studied, the processes for exchange between the metal and the slag in open-hearth furnaces, the kinetics of iron burning during bessemerization, etc.

A number of papers are devoted to a study of autodiffusion. A study of this most important process became possible only as the result of developing the labeled atom method. The new method permits determining the thermodynamic properties of the components of a solution, which is especially important to metallurgists.

In the monograph are placed papers on determining the various thermochemical and thermodynamic properties of liquid and solid systems, typical for metallurgical studies.

The method of labeled atoms uncovers new possibilities for the analytical determination of the composition, either average or local, and in general. In other papers of the monograph the use of radioactive phosphorus for the analysis of ferrous alloys and the use of the phenomenon of electron repulsion for the analysis of surface layers is discussed.

As a result, the papers published in this monograph deal with various ways of using the method of labeled atoms in metallurgy and with various measurement methods. These studies touch on both theoretical problems (for example, on the theory of diffusion and of autodiffusion, the theory of oxidation, etc.) and on a characterization of the operation of metallurgical aggregates, blast, open-hearth and electric furnaces, and converters.

The studies are associated with a development of the problems, directly characterizing the basic metallurgical processes (distribution of sulfur and tungsten, velocity of a gas in the blast furnace, etc.) or the quality of production (distribution of carbon after high-frequency tempering, the reasons for flaws in tubes, etc.)

In most of the studies the method of counting the emanations was used; in some of the studies different types of ionization chambers and the autoradiography method were also used.

The radioactive isotopes used, besides radon, include iron, cobalt, carbon, silver, calcium, phosphorus, sulfur, copper, tungsten, thallium, etc.

To be sure, the published papers do not embrace all of the possible ways of using the method of labeled atoms in metallurgy.

Despite the fact that the new method has greatly expanded study possibilities and has already led to a number of valuable results, there still remains a greater task ahead on the further development and expansion of its range of application.

A. A. Zhukhovitskii
I. N. Kidin
K. G. Trubin

APPENDIX 25

THE M. I. KALININ MOSCOW INSTITUTE OF NONFERROUS METALS AND GOLD

and

THE ALL-UNION SCIENTIFIC ENGINEERING-TECHNICAL SOCIETY OF NONFERROUS METALLURGY

METALLURGY OF NONFERROUS METALS

Monograph of Scientific Papers

No. 26

State Scientific-Technical Press of Literature on Ferrous and Nonferrous Metallurgy

Moscow 1957

Table of Contents

APPENDIX 26

THE M. I. KALININ MOSCOW INSTITUTE
OF NONFERROUS METALS AND GOLD

METALLURGY OF NONFERROUS METALS

Monograph of Scientific Papers

No. 24

State Scientific-Technical Press of Literature
on Ferrous and Nonferrous Metallurgy

Moscow 1954

Table of Contents